NOTICE

THIS DOCUMENT HAS BEEN REPRODUCED FROM MICROFICHE. ALTHOUGH IT IS RECOGNIZED THAT CERTAIN PORTIONS ARE ILLEGIBLE, IT IS BEING RELEASED IN THE INTEREST OF MAKING AVAILABLE AS MUCH INFORMATION AS POSSIBLE

9950-491

LOW COST SOLAR ARRAY PROJECT

SILICON MATERIALS TASK

DEVELOPMENT OF A PROCESS FOR HIGH CAPACITY
ARC HEATER PRODUCTION OF SILICON FOR SOLAR ARRAYS

CONTRACT No. 954589

Final Technical Report

FEB 1981
RECEIVED
NASA STI FACILITY
ACCESS DEPT.

Maurice G. Fey, Program Manager

Westinghouse Electric Corporation
Power Circuit Breaker Division
Trafford, Pennsylvania 15085

LOW COST SOLAR ARRAY PROJECT

SILICON MATERIALS TASK

DEVELOPMENT OF A PROCESS FOR HIGH CAPACITY

ARC HEATER PRODUCTION OF SILICON FOR SOLAR ARRAYS

Contract No. 954589

Final Technical Report

Maurice G. Fey, Program Manager

Westinghouse Electric Corporation
Power Circuit Breaker Division
Trafford, Pennsylvania 15085

Prepared by: Approved:

Thomas N. Meyer   _Maurice G. Fey_
Thomas N. Meyer   Maurice G. Fey
Arc Heater Project   Program Manager

TABLE OF CONTENTS

LIST OF FIGURES

LIST OF FIGURES (Continued)

LIST OF FIGURES (Continued)

LIST OF TABLES

1. INTRODUCTION

1.1 Program Description

A program sponsored by JPL was established at Westinghouse to develop a high temperature silicon production process using existing electric arc heater technology. Silicon tetrachloride and a reductant, liquid sodium, were injected into an arc heated mixture of hydrogen and argon. Under these high temperature conditions, a very rapid reaction occurred and proceeded essentially to completion, yielding silicon and gaseous sodium chloride. Techniques for high temperature separation and collection of the molten silicon were developed using standard engineering approaches. Although the desired degree of separation was not achieved, it has been determined that higher wall temperatures via more insulation will improve separation significantly. Preliminary technical evaluations and economic projections indicate not only that this process is feasible, but that it also has the advantages of rapid, high capacity production of good quality molten silicon at a nominal cost.[1-4]

The Westinghouse program consists of a four-phase effort directed to the development and implementation of this technology. The initial phase of the program, Phase I, was an eleven-month study funded by JPL which was completed in September, 1977. While the overall JPL program objective is to produce 1000 metric tons of high quality silicon per year on a continuous basis, Phase I was defined as a comprehensive feasibility and engineering review of the reaction process, and a formulation of the design for a test system to experimentally verify the high temperature reaction.

Phase II involved a multi-task approach including (1) a detailed engineering analysis of the entire process (2) design, fabrication, and assembly of the experimental system (3) experimental

testing of the reduction reaction to produce silicon and (4) complementary research programs to augment the experimental system design. The Phase II effort was initiated in October, 1977, and completed in December, 1979.

Although only Phase I and II of the program were funded, Phase III is defined as the design, construction and operation of a pilot plant for the process. This phase would optimize both the product silicon and process parameters.

Phase IV is defined as design and construction of a full scale commercial plant for the production of 1000 metric tons of silicon per year.

2. SUMMARY

During the performance of the program, the experimental verification system for the production of silicon via the arc heater-sodium reduction of $SiCl_4$ was designed, fabricated, installed, and operated. Each of the attendant subsystems was checked out and operated to insure performance requirements. These subsystems included: the arc heaters/reactor, cooling water system, gas system, power system, Control & Instrumentation system, Na injection system, $SiCl_4$ injection system, effluent disposal system ar.' gas burnoff system.

Prior to introducing the reactants (Na and $SiCl_4$) to the arc heater/reactor, a series of gas only-power tests was conducted to establish the operating parameters of the three arc heaters of the system. Following the successful completion of the gas only-power tests and the readiness tests of the sodium and $SiCl_4$ injection systems, a shakedown test of the complete experimental verification system was conducted.

On December 8, 1979 the initial shakedown test was conducted wit'. full reactant injection into the reactor to produce the initial silicon product. Both sodium and $SiCl_4$ were injected into the arc heated reactor with ease and the system operational capability was confirmed. A total of 160 lbs. of sodium and 346 lbs. of $SiCl_4$ were injected during the test and a total of 482 lbs. of products produced were obtained (i.e., a mass balance error of approximately 5%). Of the material produced during the test, the silicon content ranged from 8% to 97% by weight of silicon. The concentration of silicon in the material produced was less than expected due to the presence of NaCl mixed with the product silicon. The NaCl content is attributed to an insufficiently high wall temperature. Thus, the NaCl was condensed on the reactor walls with the silicon, instead of

remaining as NaCl vapor and exiting with the gas stream. However, the condensation technique for silicon collection on a skull wall was verified, i.e., a skull wall of increasing thickness was formed and the reaction kinetics were confirmed (i.e., the reaction of Na and $SiCl_4$ proceeds essentially to completion very rapidly). This lower temperature of the gas stream results mainly from the arc heater thermal input being approximately 1000 kW compared to the anticipated 1500 kW used in the design calculations. This lower power capability was the unexpected result of derating the motor/generator set. With the addition of increased insulation to the reactor walls, it is believed that proper separation of the silicon and NaCl will be achieved, resulting in a silicon product of high purity (see Section 3 - Conclusions and Recommendations). This lower temperature condition was also experienced in the bench scale kinetics experiment (see Appendix G). Changing the tube size enabled the tube wall temperature to increase to a value sufficient to prohibit NaCl condensation over a significant length. It should be further noted that the product separation analysis described in Appendix A was supported by the silicon product separation observed in the Kinetics experiment.

3. CONCLUSIONS AND RECOMMENDATIONS

The following conclusions are made as a result of this program:

- Westinghouse has designed, built and operated a high temperature experimental silicon production apparatus utilizing arc heater technology.

- Controlled the reduction of $SiCl_4$ with sodium to produce silicon at high temperatures.

- Achieved the design production rate of silicon of 45.4 kg/hr.

- Demonstrated that a plasma reactor of high reliability and integrity can be built and operated.

- Demonstrated that the experimental system can be started and stopped as required without the need for extensive disassembly and decontamination.

- Demonstrated that the reaction between $SiCl_4$ and Na within a plasma reactor goes essentially to completion.

- Demonstrated that the products of reaction can be recovered by condensation on the reactor walls.

- Demonstrated the potential of producing high purity silicon via the reduction of $SiCl_4$ with sodium at high temperature.

It is recommended that additional experimental tests on the Westinghouse program for "Development Of A Process for High Capacity Arc Heater Production Of Silicon For Solar Arrays" be undertaken.

The test conducted on December 8, 1979 demonstrates that
the Westinghouse proposed production process for producing
silicon via the reduction of $SiCl_4$ with sodium at high temperature
is viable. Although complete separation of the products was not
achieved, only minor modifications to the reactor are required to
attain separation. The addition of thermal insulation between
the graphite liners and the reactor shell wall will reduce the
heat loss from the liner to the cooling wa·er, thereby increasing
the wall temperature of the liner. The increased wall temperature
will promote separation of silicon from the product stream.

Purity of the silicon product was not a primary concern during
the initial testing and, therefore, is not reported on in detail.
However, the program should be continued to optimize the operating
parameters of the process and to establish the ultimate product
purity.

4. TEST SYSTEM DESIGN AND INSTALLATION

The following sections (4.1-4.11) describe the design requirements, and installation sequences completed for each of the subsystems which collectively formed the experimental verification unit for arc heater-silicon production.

4.1 Electrical System

To meet the electrical needs of the Westinghouse high temperature silicon production process the electrical system in the Arc Heater Laboratory had to be modified and expanded. The following objectives were established:

- Extend existing high current A.C. supply to Silicon Test Cell.

- Expand and distribute the D.C. field supply to Silicon Test Cell.

- Modify existing auxiliary power system and expand it to supply additional equipment.

- Supply heating/cooling system with normal and emergency ventilation equipment.

- Control the power equipment and include necessary interlocks.

To meet these objectives the layout shown in Figure (ES-1) was developed to establish the locational requirements for electrical power and controls. With the development of the new Silicon Test Cell it became necessary to supply high current A.C. power to that cell. Figure (ES-2) shows schematically how the A.C. system is interconnected with the Westinghouse High Power Laboratory generator at Station #1. Also shown in Figure (ES-2) is the D.C. power supply schematic. Figure (ES-3) is a photograph of the four D.C. welders used for the arc heater-D.C. power supply. To satisfy the remaining objectives a schematic for the A.C. low voltage supply (see Figure (ES-4)) was developed from the requirements for auxiliary power, heating/cooling equipment, normal and emergency ventilation equipment, and
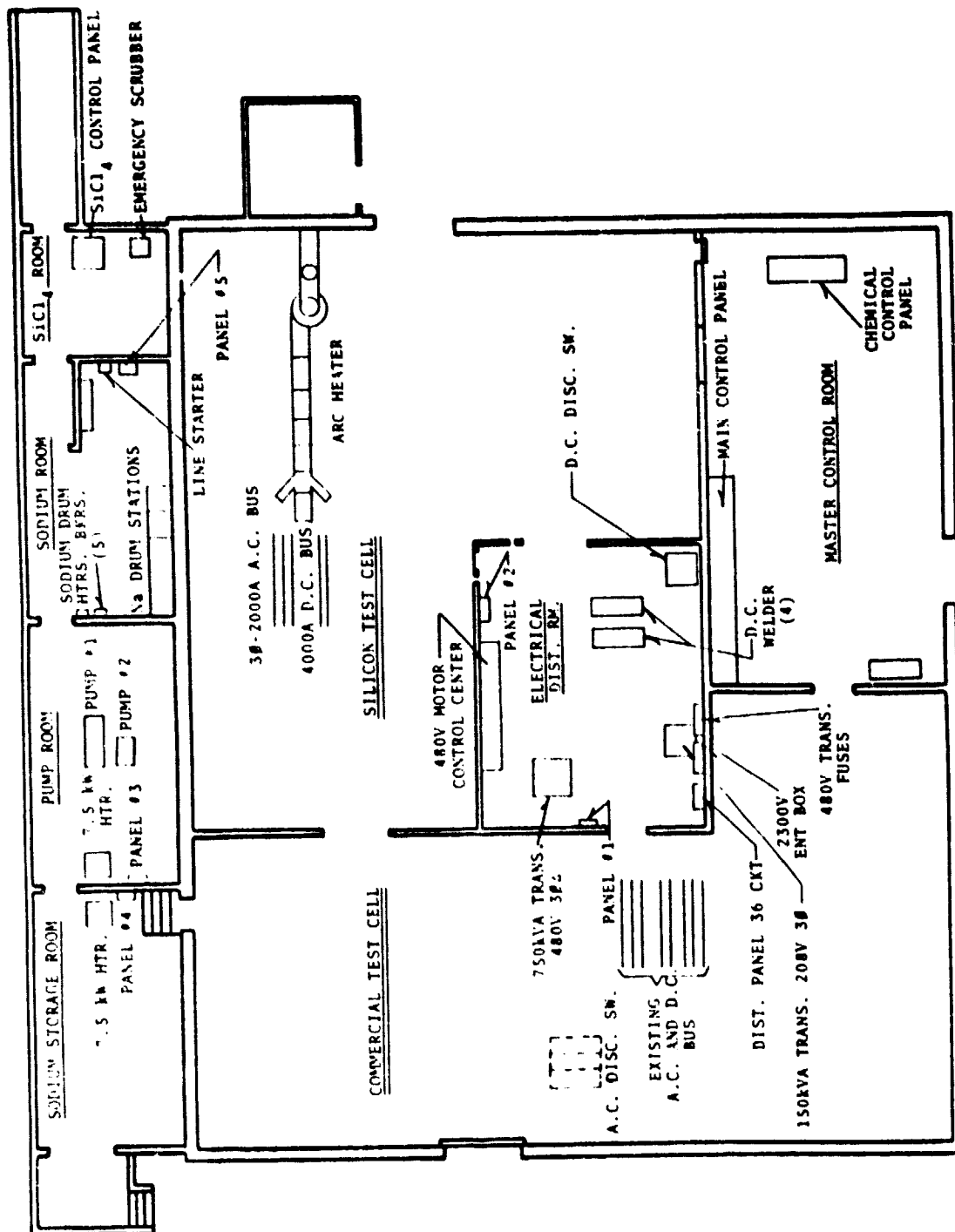
Figure ES-1 – Electrical Distribution Layout

A.C.

TEST CELL
EXISTING
A.C. BUS 2000 AMP

EXISTING
(3) 1200/5 CT'S
(3) 20/1 PT'S

3∅ 1 POLE
DOUBLE THROW
2000A SW.

(3) 800/5 CT'S
(3) 20/1 PT'S

SILICON
TEST CELL
A.C. BUS 2000A

FROM HIGH
POWER LAB
STATION #1
1.6 MVA

TEST CELL
EXISTING
D.C. BUS 4000A

TWO SINGLE
POLE DOUBLE THROW
4000 AMP SWITCHES

SILICON
TEST CELL
D.C. BUS 4000A

4 WSH 650
WELDERS IN
PARALLEL WITH
50MV SHUNT

D.C.

480V 3∅

FROM MOTOR
CONTROL CENTER

Figure ES-2 – Arc Heater Reactor A.C. And D.C. Supply

Figure ES-3 - Photograph Of The dc Welder Units Which Supply Arc Heater Field Coil Power
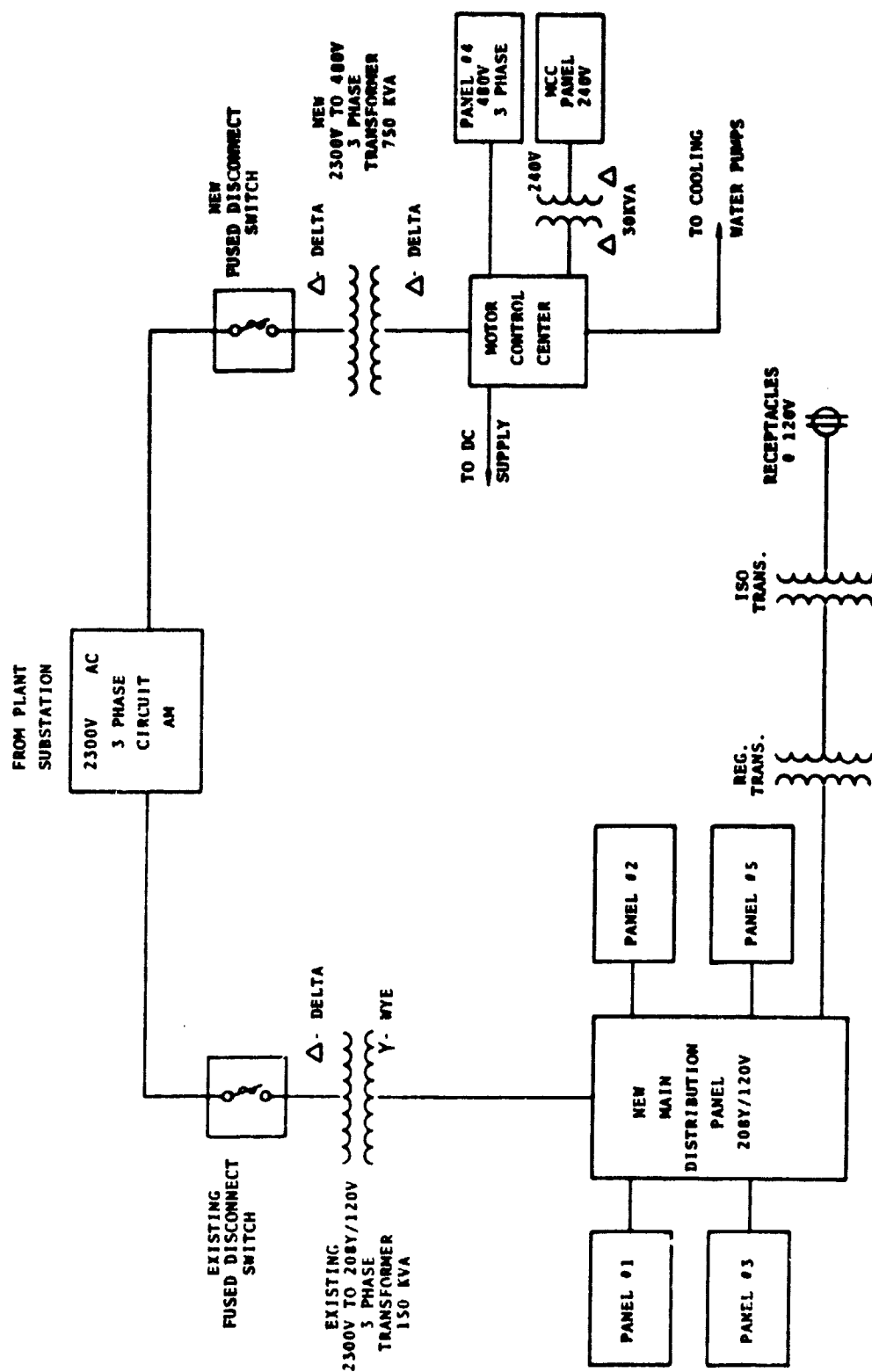
Figure ES-4 - Arc Heater Laboratory Low Voltage A.C. Supply

power equipment controls. Figure (ES-5) is a photograph of the
motor control center located in the electrical distribution room
at the Arc Heater Laboratory.

The installation and debugging of the electrical system
was completed in October, 1979. During the reactant test
conducted on December 8, 1979 the electrical system functioned
as required with the arc heaters operating at a power level of
1500 kW.
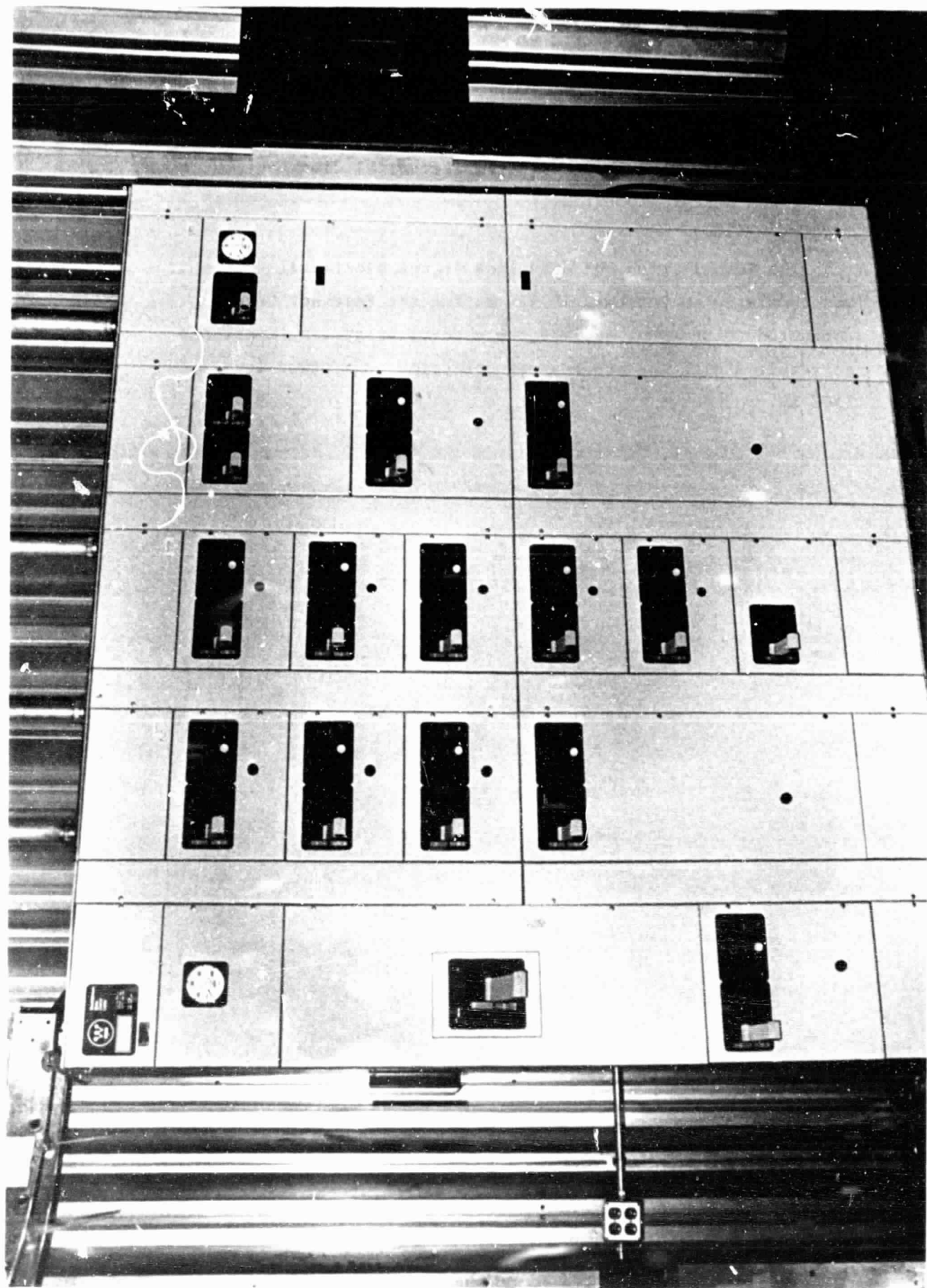
Figure ES-5 - Photograph Of The Motor Control Center At The Arc Heater Laboratory

4.2 Control & Instrumentation

The objective of the Control & Instrumentation task is to
control the production of silicon at 100 lbs./hr. (45 kg/hr.)
and to gather pertinent data relative to that production. Because
of high level electrical noise generated by the arc heaters during
operation, all controls and instrumentation have to be shielded
or be of a design not affected by the noise. Also, the controls
have to be remotely operable and explosion proof or intrinsically
safe because of the potential explosion hazard related to the
presence of hydrogen. In addition, the controls and instrumentation
have to be state-of-the-art and provide maximum flexibility due
to the experimental nature of the project. To meet the above
objective and design requirements, pneumatic type controls and
instrumentation were used where applicable. All cooling water
flow rates were determined by measuring the pressure drop across
an orifice plate and converting this measurement to a proportional
3-15 psig signal that is transmitted to a remote control point.
The 3-15 psig signal is then converted to a proportional electrical
signal (4-20 mA) that can be recorded by a data logger. Similar
devices were used to measure and control the flow of argon and
hydrogen gases to the arc heaters. Likewise, to record the data
all pneumatic signals are converted at the control panel to
proportional electrical signals.

The sodium and silicon tetrachloride flows were controlled
pneumatically. However, in the case of sodium the electromagnetic
flow meter generates an electrical signal that is converted to
a proportional 3 to 15 psig pneumatic signal. This signal is
used to control a pneumatically operated variable transformer
(power stat) that supplies power to the electromagnetic pump
that pumps the liquid sodium. The converted pneumatic signal
from the flow meter is also transmitted to the main process
control panel where it is reconverted back to a proportional

electrical signal for data logging. The flow of sodium can be controlled from either the sodium panel or the main process control panel. Flow of silicon tetrachloride is measured and controlled by using a flow-thru type differential pressure cell and a pneumatically operated flow control valve. Again the pneumatic flow signal is converted to an electrical signal for recording. The ratio of these two reactants is maintained by comparing the pneumatic signals from the respective flow meters. Figure (CI-1) is a schematic of the Na-SiCl$_4$ flow and ratio control system described above.

Temperature measurements are made via platinum resistance temperature devices (RTD) in locations where the temperature is expected to be less than 750°C. RTD's were chosen because (1) RTD's are considered to be immune to electrical noise and (2) their high electrical output provides an accurate input to a datalogger. RTD's are used to measure the temperature of all the cooling water and the incoming gas temperatures. In locations where the temperature is expected to exceed 750°C, chromel-alumel thermocouples are used along with shielded thermocouple extension wire. The temperatures of the graphite liners in the reactor are measured using thermocouples because the temperature is expected to exceed 800°C. The millivolt signal from the thermocouples are converted to a 0-5V signal for data logging.

To record the data generated during testing, a datalogger with one hundred channels (expandable to 1,000 channels) was chosen. To store the data, the datalogger is equipped with a paper tape print-out that records all data in sequence as each of the channels is scanned. In addition, the datalogger is interfaced with a 9-track magnetic tape deck that can store all the data generated during a test on magnetic tape. To achieve maximum flexibility all data is converted to and stored as millivolts. Converting the
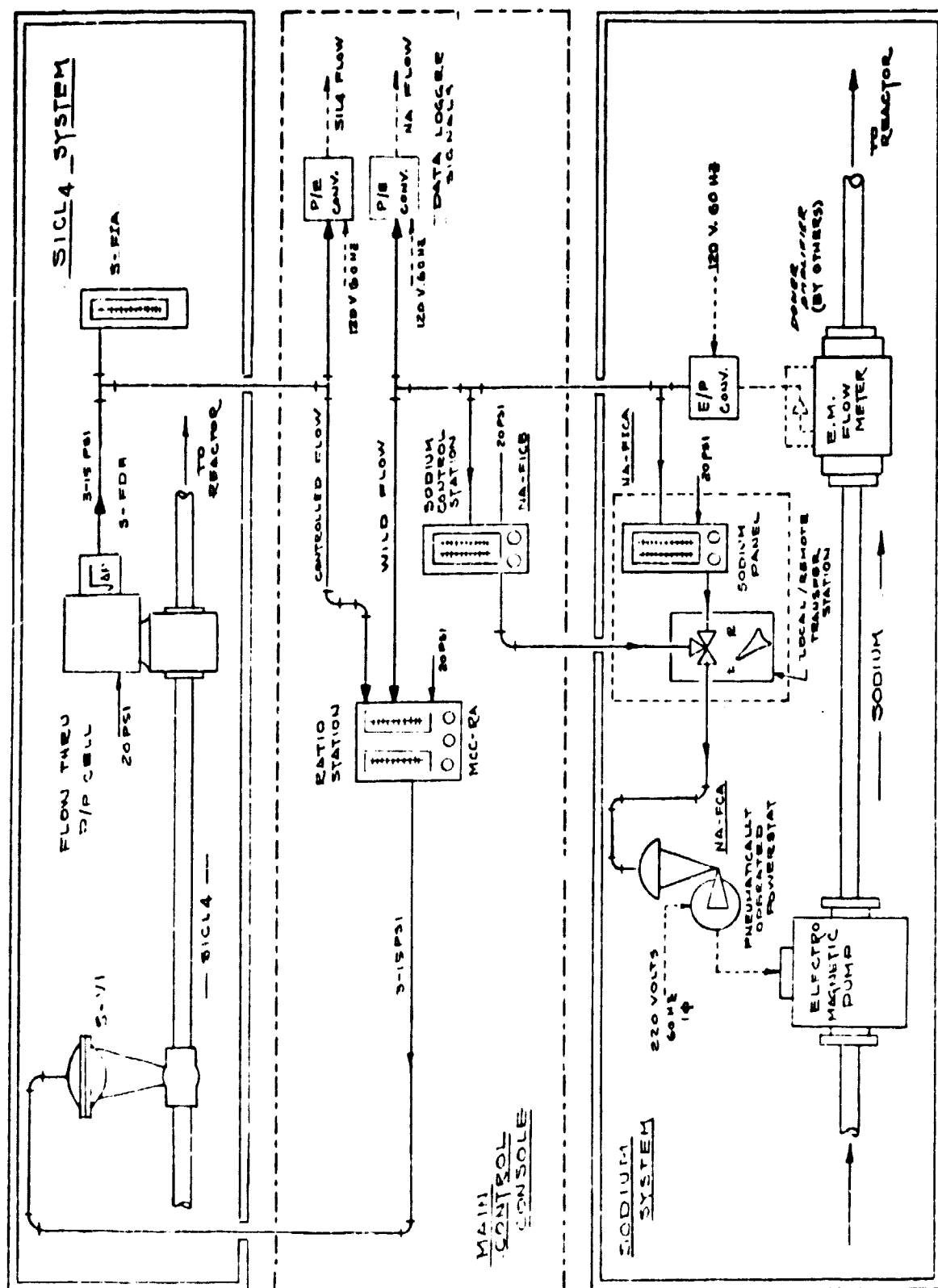
Figure CI-1 – Schematic Of The Na To SiCl₄ Feed Rate-Ratio Controller

millivolts to engineering units is done by a computer program which allows for changing of scaling factors at a minimum expense. In addition to the datalogger, each point that is recorded also has a visual readout device for real time monitoring during testing. Figure (CI-2) is a photograph of the arc heater control and alarm panel. It contains the arc current, voltage and power meters and all interlocks for starting and stopping the arc heaters. It also contains the start-stop controls for the cooling water pumps, the open and close controls for the gas (argon, hydrogen) valves, and the controls for the burnoff stack igniter. Figure (CI-3) is a photograph of the Main Process Control Panel. It contains the datalogger, tape deck, cooling water temperature readout, and cooling water flow readout. Additionally, it contains the ratio controller for Na and $SiCl_4$, the $SiCl_4$ flow controller, the valve controls for injecting Na and $SiCl_4$ and the flow controls for argon and hydrogen to the arc heaters. Also mounted on this panel is the temperature readout for the reactor liner and the pH control instruments for the effluent treatment tank.

The assembly and installation activity for the C&I task was completed during November, 1979.
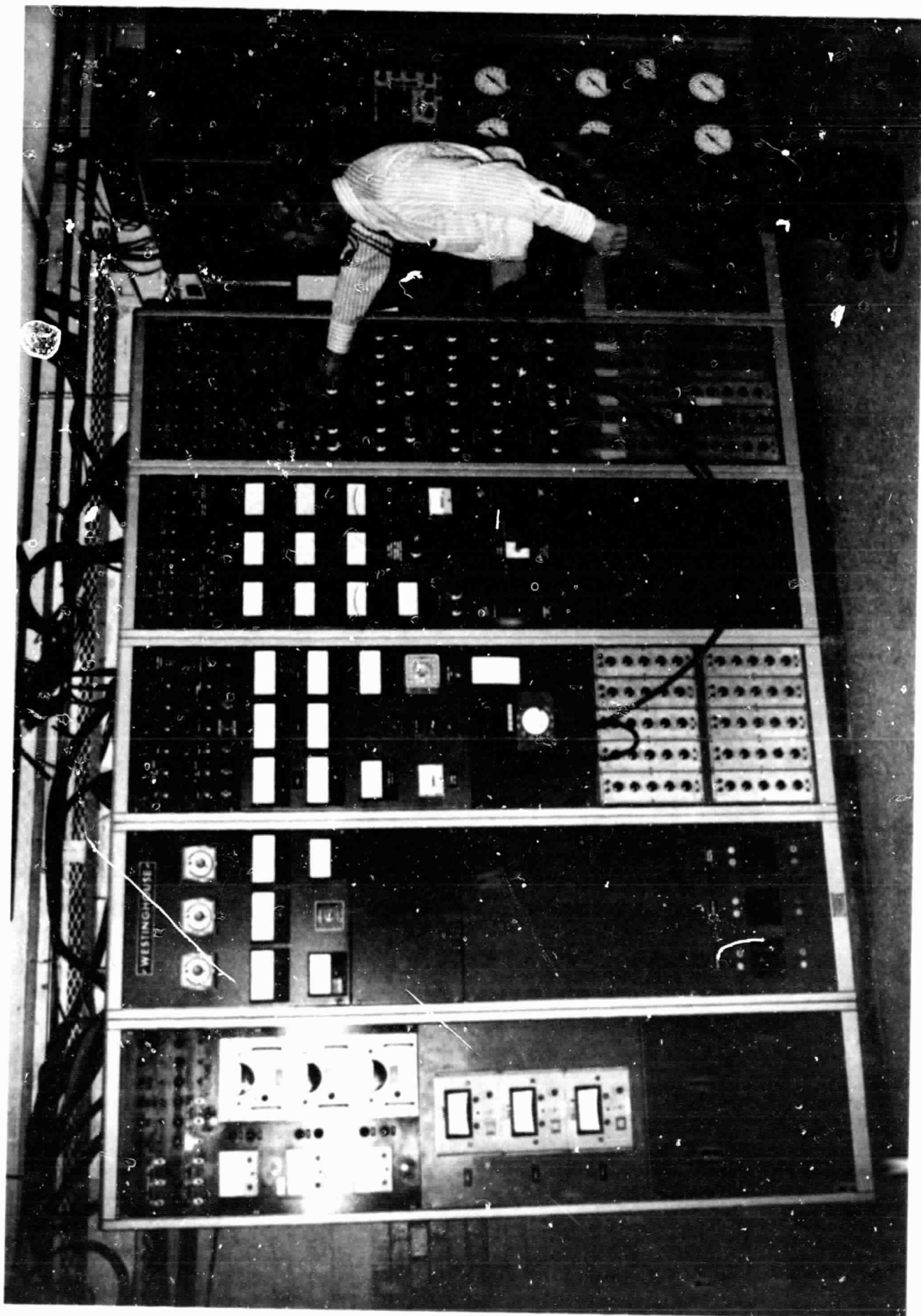
Figure CI-2 - Photograph Of The Arc Heater Control Panel

Figure CI-3 - Photograph Of The Process Control Panel

4.3 Cooling Water System

Arc heaters and their auxiliaries require substantial cooling water systems because of the high temperatures and high internal heat fluxes involved. Therefore, the cooling water system had to:

- Provide closed loop (high pressure) cooling water for the arc heaters.

- Provide closed loop (low pressure) cooling water for the reactor sections, Si collector, effluent system, and burnoff stack.

- Provide effluent cooling water capability.

A piping schematic of the cooling water system as installed is presented in Figure (CW-1).

The cooling water system has two closed-loops with a common line consisting of a surge tank, strainer, filter, and demineralizer. The water from the demineralizer flows to two pumps: one at 800 TDH and 250 gpm feeding the arc heater electrodes and coils; and the other, at 250 TDH and 600 gpm feeding the reactor sections, silicon collector and effluent separation system.

Each loop is equipped with a heat exchanger requiring 75 to 100 gpm of cooling water, thus reducing the circulating water temperature by about 15°F in the range of 120 to 140°F. This moderately elevated temperature minimizes the amount of raw cooling water required.

The demineralizer is provided in order to minimize scale build up and corrosion. It is preferred over the water softener and water conditioner types when concerned with scale or corrosion,

Figure CW-1 - Piping Drawing Of The Cooling Water System

4-16

and especially suitable for high voltage systems where leakage currents through the water are possible.

The filter will remove unwanted particles over 5 microns, while the strainer removes the coarser particles.

The materials of construction for the system are copper and carbon steel.

The cooling water for the effluent scrubber is provided by the outlet water from the heat exchangers for the two closed loop systems. Figure (CW-2) is a photograph of the water pump room components which include the two pumps, surge tank, heat exchangers and demineralizer. A photograph of the cooling water distribution piping is shown in Figure (CW-3).

The cooling water system installation was completed during February, 1979 and functioned well during the reactant tests on December 8, 1979.
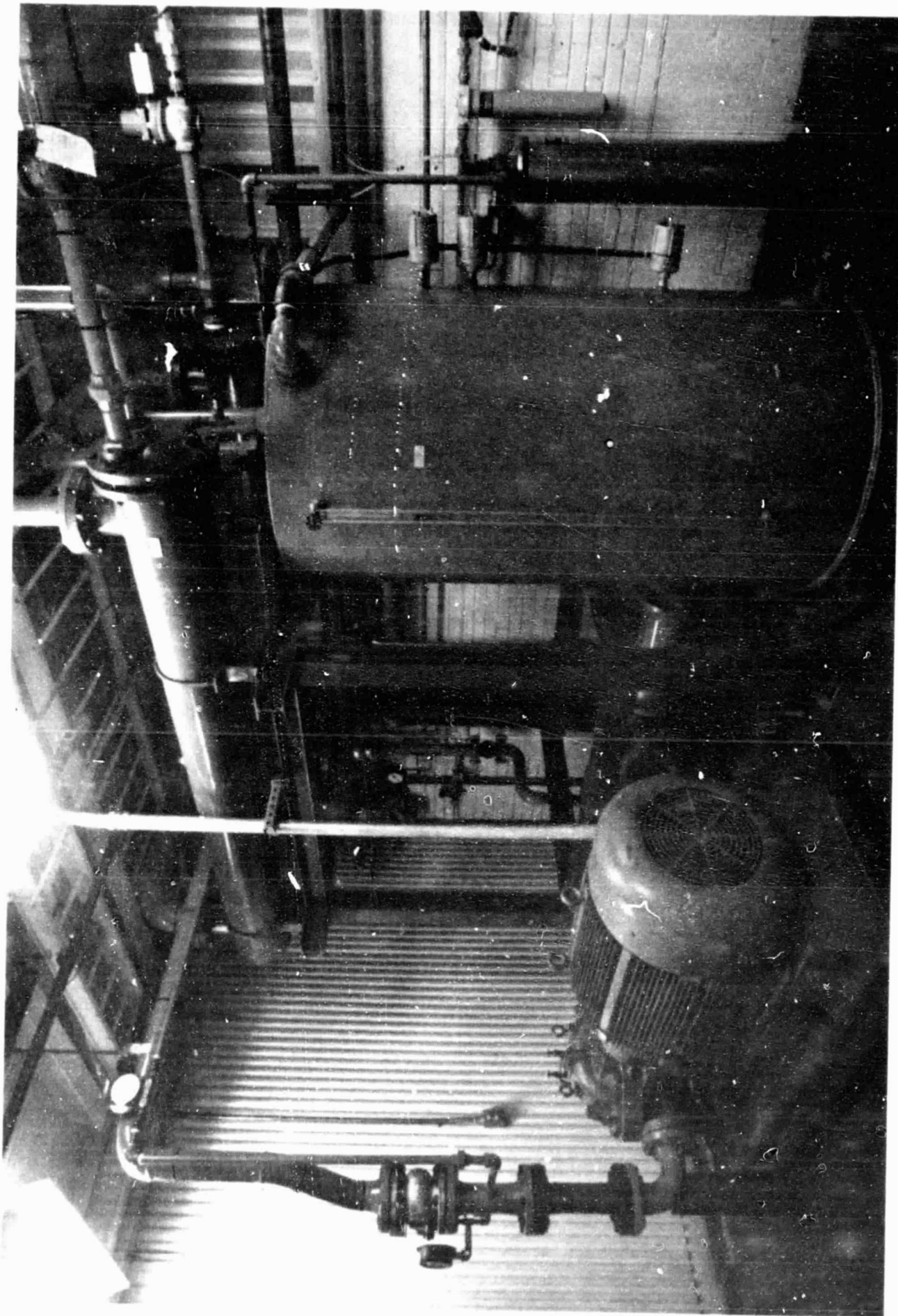
Figure CW-2 – Photograph Of The Cooling Water System Main Components
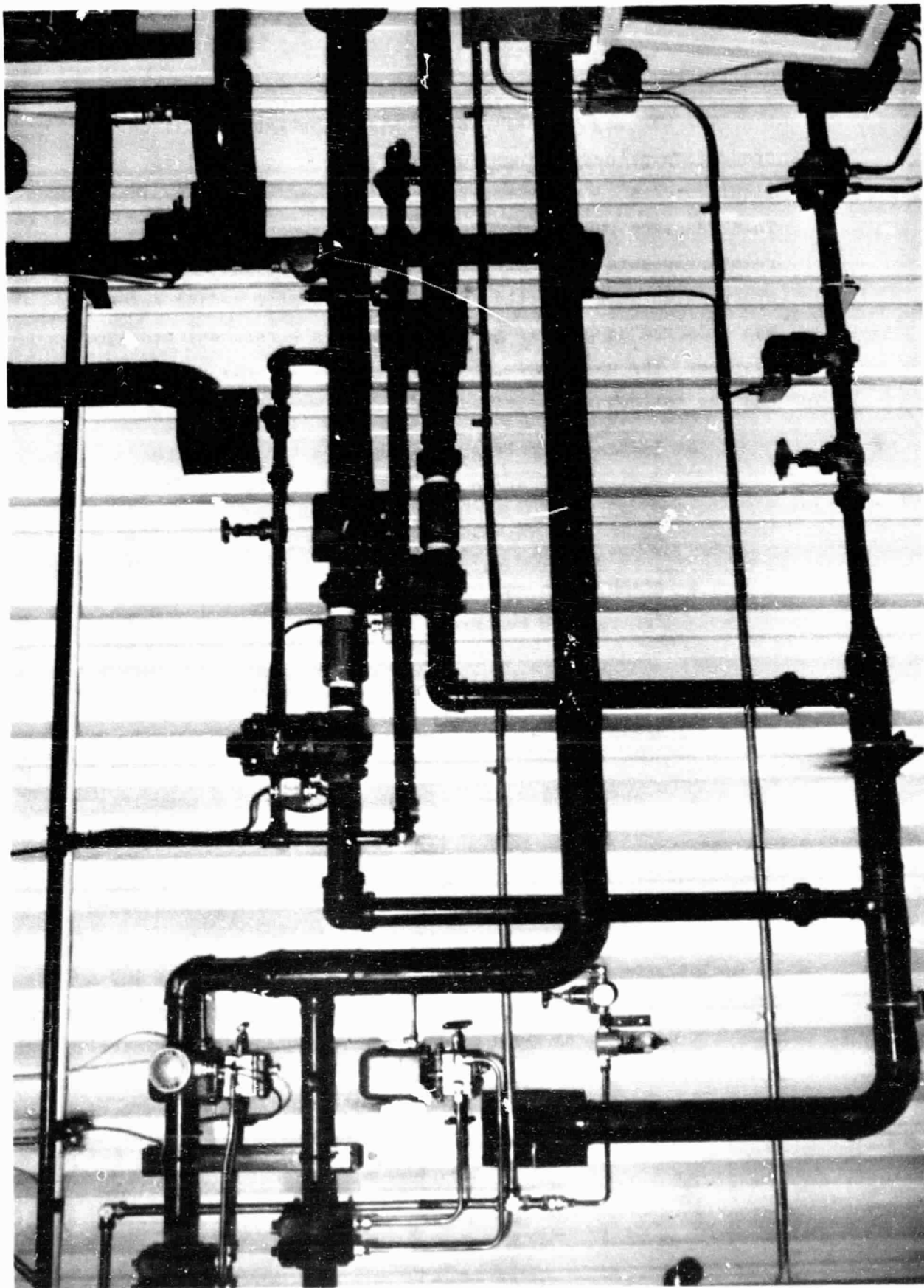
Figure CW-3 - Photograph Of The Distribution Piping For The Cooling Water System

4-19

4.4 Gas System

The Westinghouse Arc Heater high temperature silicon
production process brings together silicon tetrachloride and
liquid sodium to react and form silicon and sodium chloride.
This reaction must take place at a high temperature in a
relatively pure and inert atmosphere. Therefore, hydrogen and
argon gases were selected as the heat transfer medium and argon
was selected as a cover gas for each of the reactant storage
systems. The gas system designed for use in this process
had the following objectives:

- Indicate, monitor, and regulate the individual
  supplies of argon and hydrogen gas to the arc
  heaters.

- Blend argon and hydrogen in the appropriate ratios
  for the arc heaters.

- Supply argon as a cover gas for the Na and $SiCl_4$
  systems.

- Provide instrument air to subsystems for pneumatic
  control and monitoring.

To meet these objectives a system was designed and sized
to provide hydrogen and argon in a ratio of 4 to 1 from 65 scfm
up to 350 scfm and to provide argon injection gas up to 100 scfm.
(Figure (GS-1) presents the conceptual design for the gas
system.) Hydrogen is stored in a tube trailer at approximately
2500 psig and is supplied to a blend panel through a regulating
panel at 150 psig. Argon is stored as a liquid in a 500 gallon
vessel and is supplied as a gas at 150 psig to the blend panel,
the $SiCl_4$ storage system, the sodium storage system and the
injection systems for both reactants.
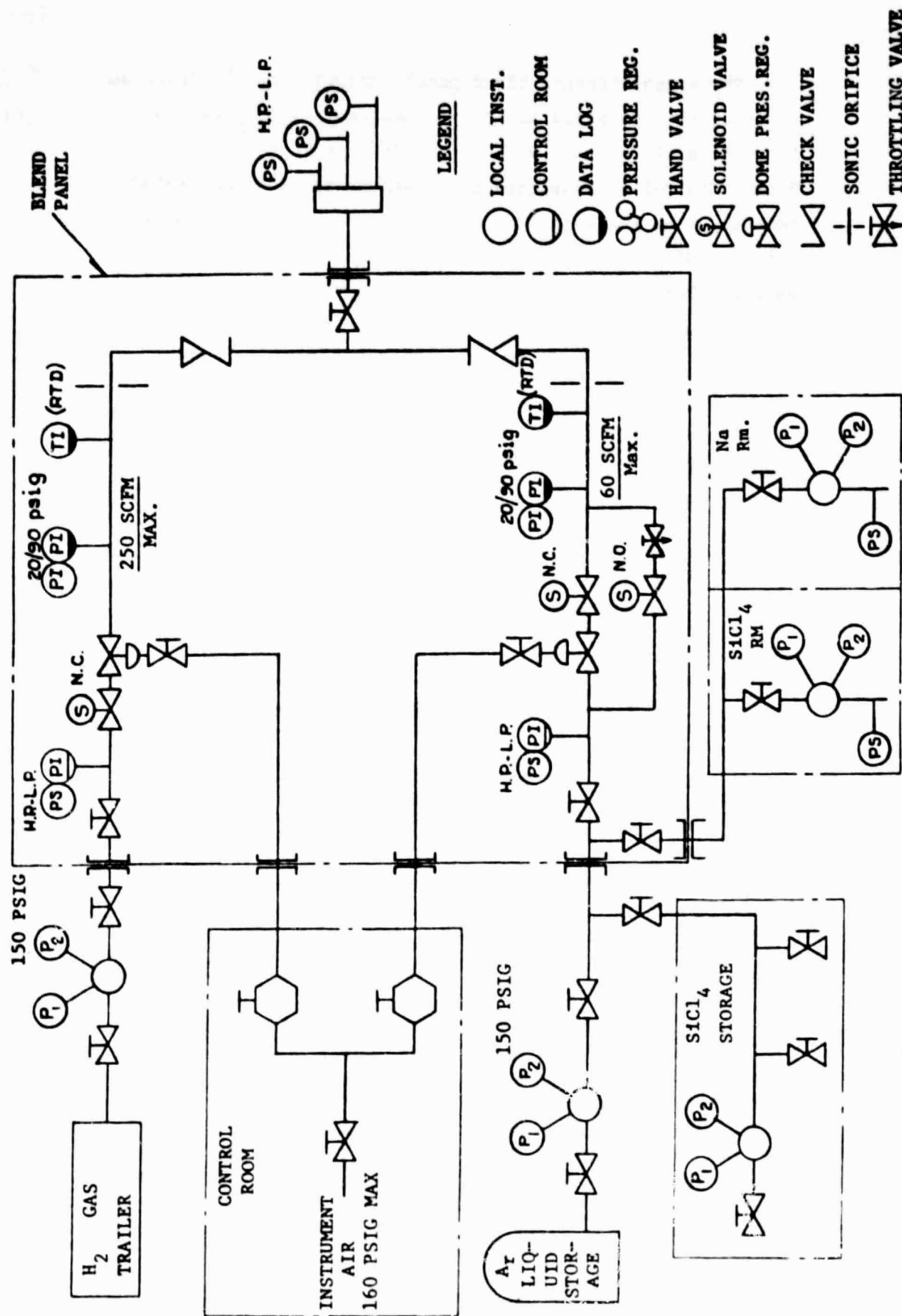
Figure GS-1 - Schematic Of The Ar-H$_2$ Gas System

The argon-hydrogen blend panel controls the flow rate and ratio of the two gases to the arc heaters. This panel is located on the outside wall of the Silicon Tetrachloride Pump Room. Control of flow thru the blend panel is accomplished remotely from the Main Process Control Panel via two pneumatic valve loading stations that open and close the flow control valves. Readout of the flow is also at the Main Control Panel. Pressure upstream of each sonic orifice and temperature of the gases are also read out at the main panel.

Figure (GS-2) is a photograph of the gas blend panel and Figure (GS-3) is a photograph showing the hydrogen and argon storage facilities.

The instrument air for pneumatic controls is provided for by a 27 scfm, 5 horsepower compressor equipped with a dryer that furnishes air with a dew point of 32°F. Instrument air supplied to the gas blend panel located outside the arc heater laboratory is further dried to a dew point temperature of -10°F.

The gas system functioned successfully during the reactant test on December 8, 1979.
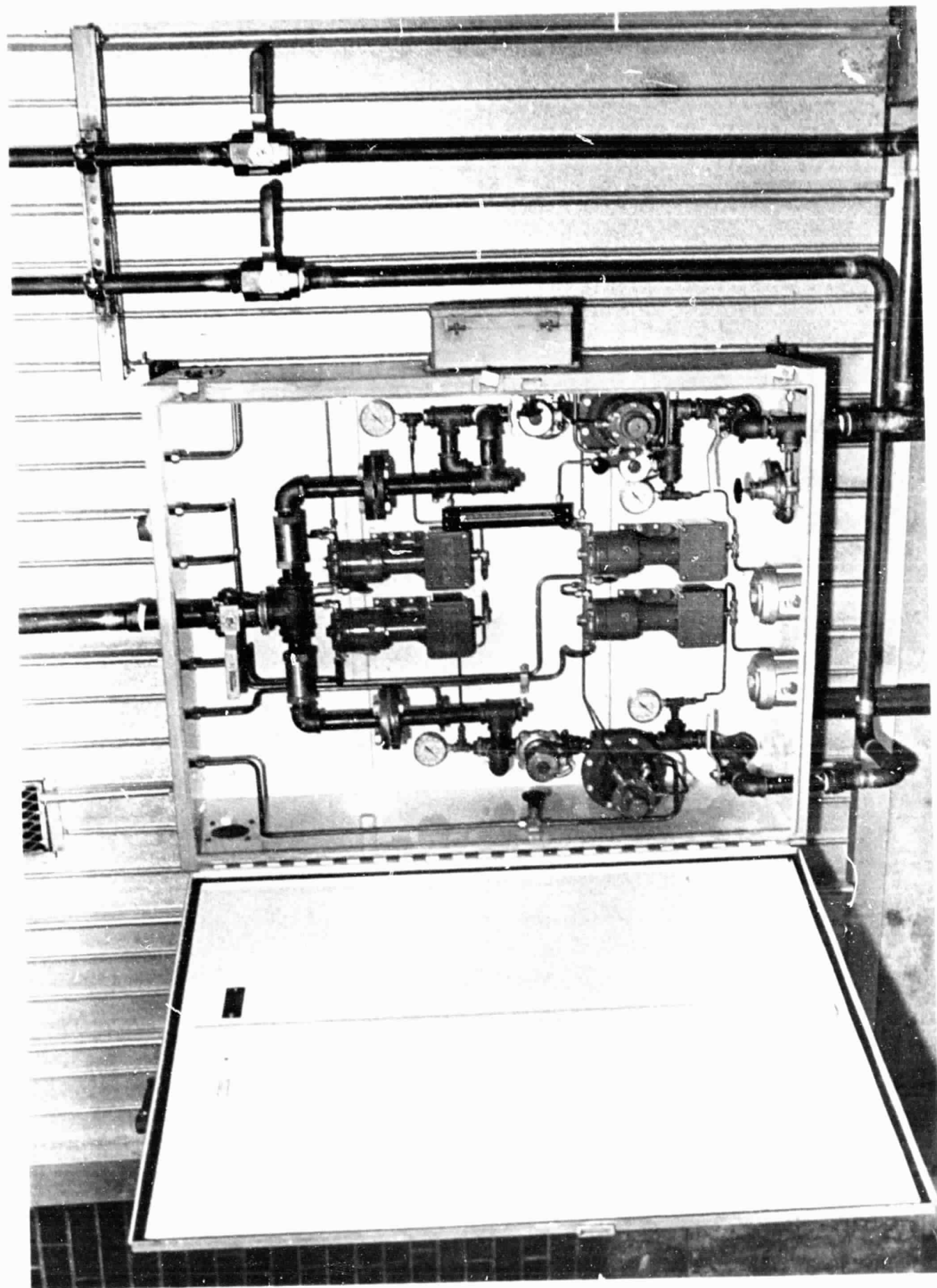
Figure GS-2 - Photograph Of The Ar-H₂ Gas Blend Panel (Mounted Outside At The Arc Heater Laboratory)

Figure GS-3 - Installation Of The Liquid Ar And The H_2 Tube Trailer Supply Facilities

4.5 Plasma Reactor-Separator (0616)

Design of the reactor components is based on the results of the Product Separation Analysis (see Appendix A). Results of the analysis indicate that a reactor length of 5 meters is adequate for silicon collection by condensation. The reactor bore diameter is approximately 19 centimeters.

For silicon separation via condensation within the tubular reactor, a cyclone is not absolutely necessary for product separation. However, to maximize the particulate or droplet collection efficiency, a cyclone has been included in the system. The cyclone design analysis indicates that higher inlet velocities and reduced body diameters will collect higher percentages of small diameter particles, but will have a higher overall pressure drop. The design selected is approximately 52 cm inside diameter of liner with an inlet velocity greater than 100 m/s. Collection efficiency will be nearly 100% for all particles exceeding 4μm diameter. The pressure drop will be less than 0.1 atm. Based on heat transfer rates predicted for the condensation method of silicon collection (see Appendix A), a stress analysis was conducted for candidate materials. A final selection of the reactor shell material was based upon stress and chemical compatibility considerations. Detailed stress analysis of the various sections indicated that high strength carbon steel provides a reasonable safety factor for the high heat transfer rates predicted and, therefore, the high thermal stresses encountered. For maximum corrosion resistance the internal surface of the carbon steel was nickel coated to a thickness of about .25mm (.010 inch).

Table PR-1 presents a summary of the results of the analysis for candidate materials of construction. As indicated in the table, aluminum would appear to be the most likely

Table PR-1 – Material Properties, Dimensions, And Heat Transfer Rates For Reactor Section Analysis

Mechanical Properties

Material	Yield Str kpsi	k Btu/hr ft °F	$\alpha \times 10^6$ ft/ft °F	ν, Poisson's Ratio	E, Young's Mod psi $\times 10^{-6}$
Inconel 625	60	6.67	7.1	.31	30
Monel 400	40	12.58	7.7	.32	26
316 St. Stl.	30	9.4	8.9	.3	28
Carbon Stl. A242	42	27	8.4	.3	29.5
Aluminum 6061-T6	40	99	13.0	.3	10.0
Nickel 200	15	37.5	7.4	.26	29.6

Dimensions And Heat Transfer Rate (At Wall)

Section Name	Inside Dia.	$\bar{Q}$, W/cm^2 (max)
Arc Heater Plenum	406 mm (16 in)	32.3
Reducer Section	356 mm (14 in) Ave	32.3, 50
Reactor Section	305 mm (12 in)	50
Cyclone Inlet	305 mm (12 in)	17.3
Cyclone	771 mm (28 in)	33.3

candidate material provided that it could be completely isolated
from the corrosive (HCl or Na) environment. Carbon steel was
selected over aluminum because it is more corrosion resistant.
Other candidate materials considered have more corrosion
resistance than carbon steel, but do not qualify because thermal
stresses are higher.

Table PR-2 is a compilation of material properties and
section dimensions used for the stress analysis. The basic
reactor vessel design which was analyzed for thermal stresses
is shown in Figure PR-1. The highest stress occurs on the
inside diameter of the inner shell. The maximum stress is
a result of combined compressive loads due to temperature
gradients through the inner shell material and axial
differential thermal expansion between the inner shell and
outer shell. The equation for this combined stress is given
as:

$$\sigma_1 = \frac{\overline{Q} \, t_1 \, \alpha \, E}{2k \, (1-\gamma)} + \frac{\Delta T_{1,o} \, \alpha \, E}{\left[1 + \dfrac{A_o}{A_1} \right]}$$

σ = compressive stress (maximum)

$\overline{Q}$ = heat transfer rate

t = shell thickness

A = shell cross sectional area

E = Young's modulus

α = linear expansion coefficient

k = thermal conductivity

γ = Poisson's ratio

Table PR-2

MATERIAL COMPARISON CHART

MATERIAL	CHEMICAL COMPATABILITY	MAX. STRESS YIELD STRESS (50 WATTS/CM²)	BUCKLING PRESSURE (PSI)	WELDABILITY	AVAILABILITY	SHELL THICKNESS (MM)
INCONEL 625	VERY GOOD	0.7	339	FEW SUPPLIERS STANDARD TECHNIQUES	MILL RUNS ONLY	3.2
MONEL 400	GOOD	0.8	294	FEW SUPPLIERS STANDARD TECHNIQUES	STOCKED MATERIAL	3.2
316 STAINLESS STEEL	GOOD	1.3	313	GOOD	STOCKED MATERIAL	3.2
CARBON STEEL (Ni PLATED)	GOOD	0.6	313	GOOD	STOCKED MATERIAL	3.2
ALUMINUM 6061-T6 (Ni PLATED)	POOR	0.3	397	GOOD	STOCKED MATERIAL	4.8
NICKEL 200	GOOD	1.0	314	FEW SUPPLIERS STANDARD TECHNIQUES	STOCKED MATERIAL	3.2

VESSEL IS 305 MM INNER DIAMETER, DOUBLE WALL WATER COOLED DESIGN. MAXIMUM STRESS IS AXIAL STRESS ON THE INNER WALL SURFACE; ALL ABOVE STRESSES ARE COMPRESSIVE.
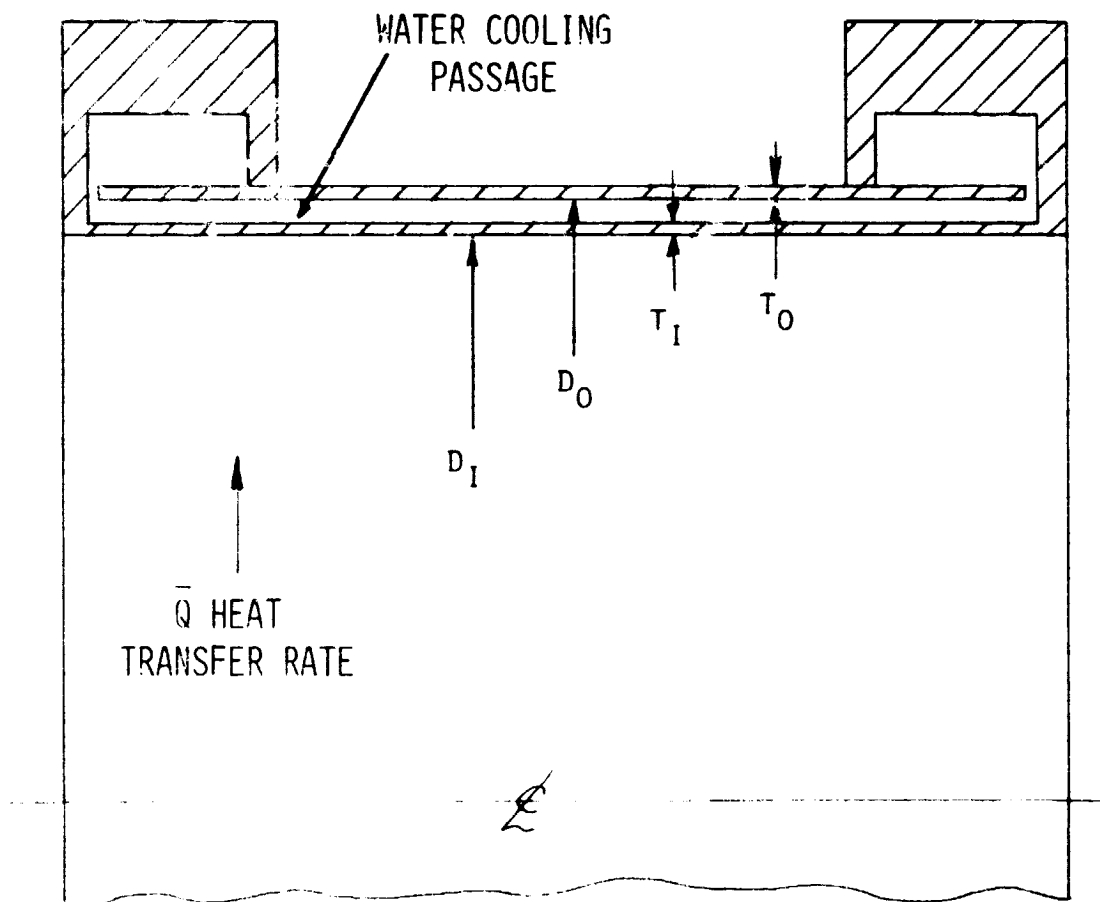
Figure PR-1 - Basic Vessel Parameters For Thermal Stress Analysis

ΔT = temperature difference

i = inner shell subscript

o = outer shell subscript

The outer shell is assumed to be at the same temperature as the cooling water. ΔT is a sum of the temperature gradient of the cooling water film and the mean temperature of the inner shell due to heat transfer.

Table PR-1 shows a ratio of the maximum stress as calculated in Equation (1) to the yie d strength of the candidate material. A reduced inner shell thickness results in lower thermal stress, but decreases the safety factor for inner shell buckling pressure. Wall thickness was selected by evaluating the minimum standard material thickness which yielded a buckling pressure safety factor of three or greater. On this basis, a wall thickness of 3.2mm (0.125 inch) was selected for the reactor sections. The larger diameter bore of both the arc heater plenum and cyclone requires material thickness of 4.8mm (.1875 inch) and 6.4mm (.250 inch), respectively.

Reactor Liners. The straight section of the reactor and the cyclone are lined with high purity graphite. The internal surfaces of the graphite are sealed with pyrolytic graphite. The heat flow, which is required to insure a skull wall, is very high, especially near the reaction zone, and requires a close fit of the graphite liner within the water-cooled jacket. Hence, both the water-cooled jacket and the graphite liner are machined to close tolerances.

Pyrolytic graphite was chosen for coating the internal surfaces of the graphite liners for the following reasons:

a. Pyrolytic graphite forms a good seal having total impurity levels as low as 10 to 30 ppm.

b. In the application of a pyrolytic graphite coating to the graphite, fabrication advantages are realized. The furnace is run up to a high temperature for purification of the graphite. The temperature is lowered and the pyrolytic coating is applied. During the run, the graphite is stress relieved due to the high temperature. Final machining of high accuracy is performed after the furnace operation on the stabilized parts.

The cyclone outlet was lined with both graphite and a refractory insulation. The purpose of the liners is to maintain the gas temperature high enough to prevent condensation of NaCl.

A typical joint between sections is shown in Figure PR-2. It is a slip joint with the liner sections positioned axially by a seal ring. One or two turns of thin pyrolytic graphite foil can be used for better sealing. Where the steel flanges add the most stiffness, relief cuts in the graphite as shown in Figure PR-2 prevent higher stresses in the graphite.

Heat Flow And Temperature Distribution. One of the objects of the reactor wall design is to create the amount of cooling needed to maintain the thickness of the silicon skull wall reasonably close to the desired value of 2 cm. The expected heat transfer rate has been determined in the condensation calculations (see Appendix A) and are plotted as a function of reactor axial position in Figure PR-3. The zero length point has been estimated to fall approximately

Reactor
Flange

Seal
Ring

Reactor
Flange

Water
Manifold

Water
Manifold

Relief
Cut

Graphite

Graphite

Pyrolytic
Graphite

Expansion
Space

Graphite Foil
Joint Seal
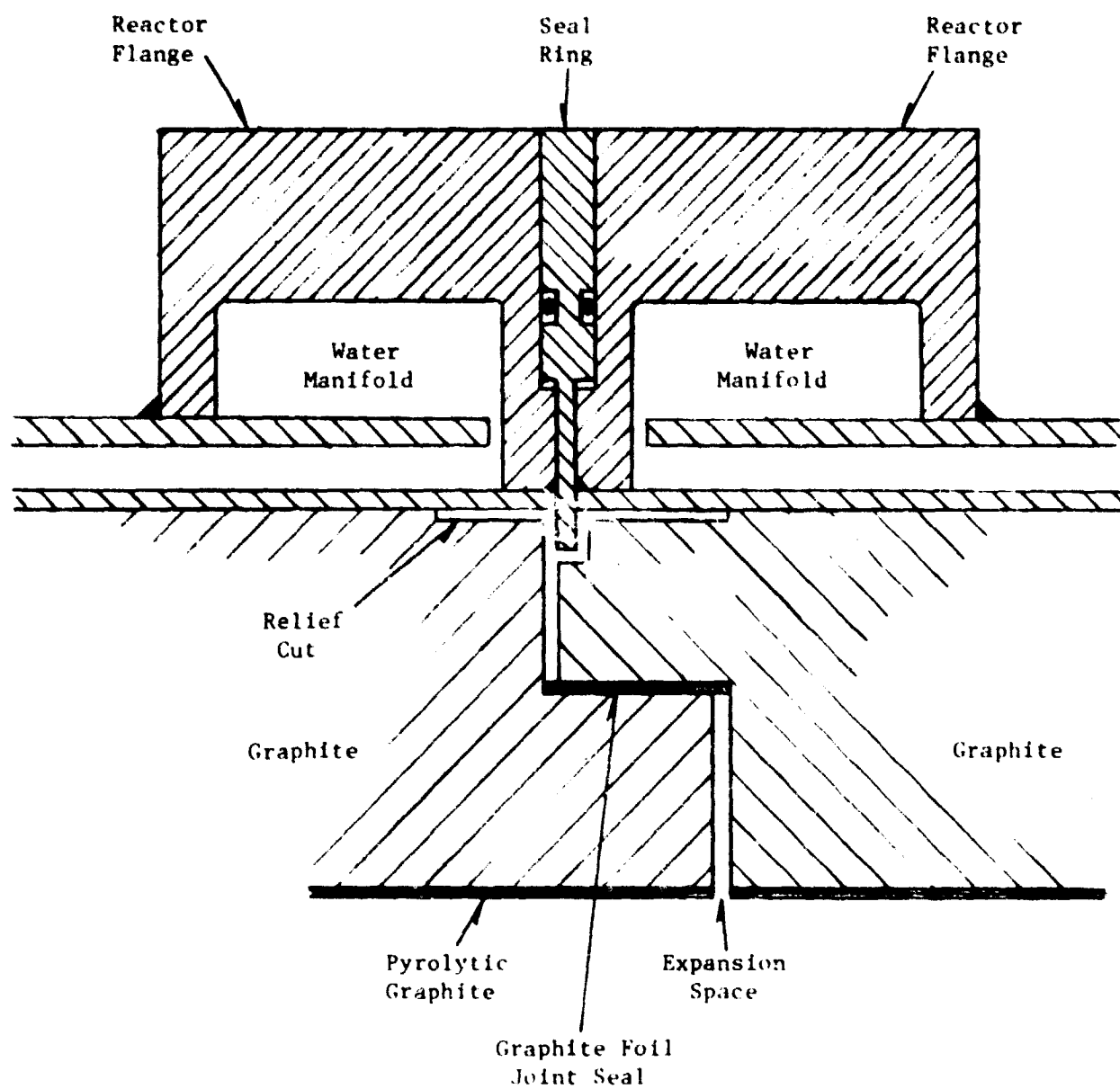
Figure PR-2 – Typical Reactor Section Joint

Reactor Assembly
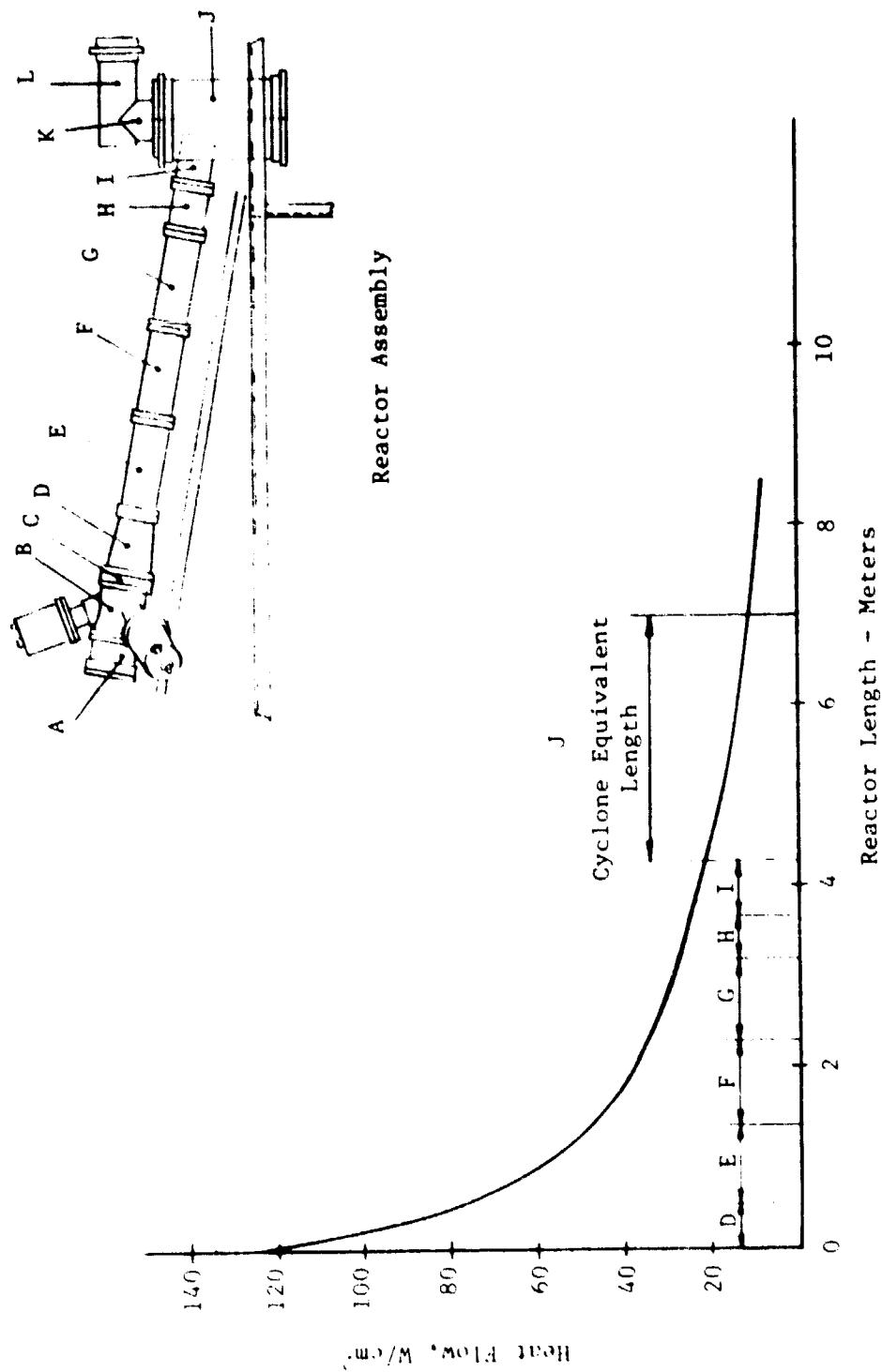
Figure PR-3 – Heat Flow vs. Reactor Length

six inches into the tapered section following the SiCl$_4$ injection. The average heat flow for each reactor section as determined from this graph is shown in Table PR-3 and is the basis for the wall design. The section designations are shown in Figure PR-3.

As the condensation calculations do not apply directly to the cyclone conditions, it was necessary to make some assumptions regarding an "equivalent length". This was done by simply treating the cyclone as a reactor length having the same wall area as the cyclone. The entrance to the cyclone has a smaller diameter, 10 cm, than the reactor, 15 cm, and the heat transfer coefficient was adjusted for the increased gas velocity according to the expression:

$$\frac{h_2}{h_1} = \left(\frac{d_1}{d_2}\right)^{1.8} = \left(\frac{15}{10}\right)^{1.8} = 2.07$$

The average heat flow for the cyclone equivalent length in Figure PR-3 was, therefore, multiplied by 2.07. The resulting value was rounded to 30 W/cm^2.

The wall composition is obtained by an iterative cal- culation. The end result of one such series is shown in Figure PR-4. It indicates the wall geometry and the temperature distribution. This figure applies to Section G (see Figure PR-3), with the results based upon the following assumptions:

    a. The heat flow is 31 W/cm^2 at the gas-silicon interface.

    b. The silicon skull is 3.7 cm thick and the bore diameter is 11.6 cm.

Table PR-3 – Nominal Heat Flux At The Wall For A 15 cm Bore Reactor

Section	Axial Extension	Average Heat Flow
D	0. – 0.46 m	100* W/cm^2
E	0.46 – 1.37	63
F	1.37 – 2.29	41
G	2.29 – 3.20	31
H	3.20 – 3.66	25*
I	3.66 – 4.29	23*
Cyclone	4.29 – 7.50	30

*Not Corrected For Diameter Deviation

Figure PR-4 – Reactor Section Geometry And Temperature Profile
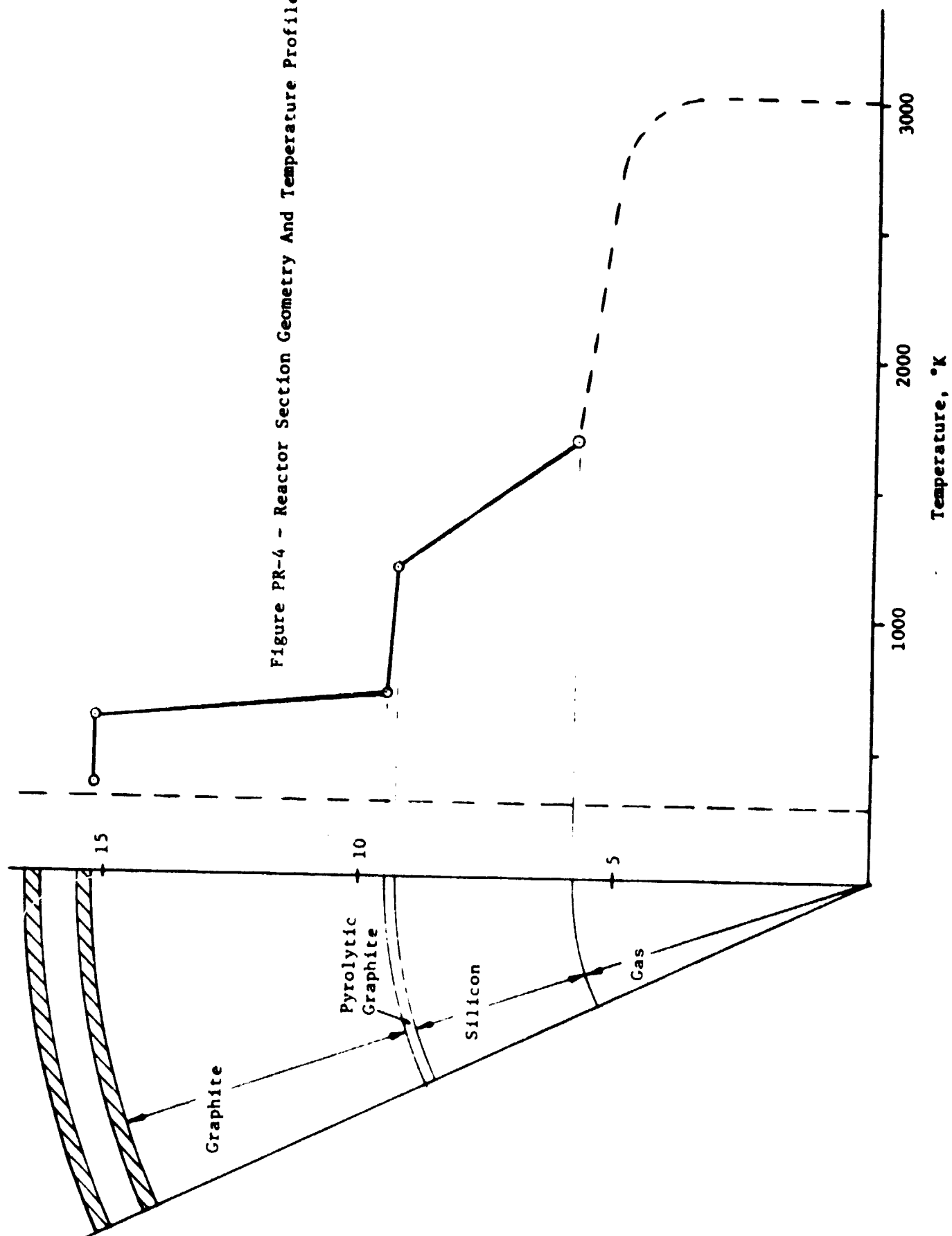
c. The liner consists of Stackpole 2128 graphite with
a 0.07 inch thick pyrolytic graphite coating on the
inner surface. The liner is of one piece construction
with a close fit in the steel shell.

d. The temperature drop in the graphite/steel interface
is equivalent to a 0.010 inch gap filled with
carrier gas (i.e., $4H_2$:1Ar). The thickness of
the silicon skull layer will vary with the gap
and it is, therefore, in part, determined by
component tolerances.

Material Data. As various sources do not agree on the
material properties, the following listing shows data which
has been used for the liner calculations.

Silicon

Thermal conductivity: The graph in Figure PR-5
has been derived from a curve given by Ho & Powell.[5]
The curve is a recommended average of a large number
of curves from different sources. Above room
temperatures the various investigators agree fairly
well.

Thermal Expansion

$$\alpha_{Si} = 2.33 \times 10^{-6} + 4.1 \times 10^{-9} \times t$$

(the temperature t is in °C; valid 0-650°C)

This expression is a straight line fit to the
graph given by Runyan.[6] Above 650°C silicon exhibits
plastic flow and does not normally develop large
stresses.
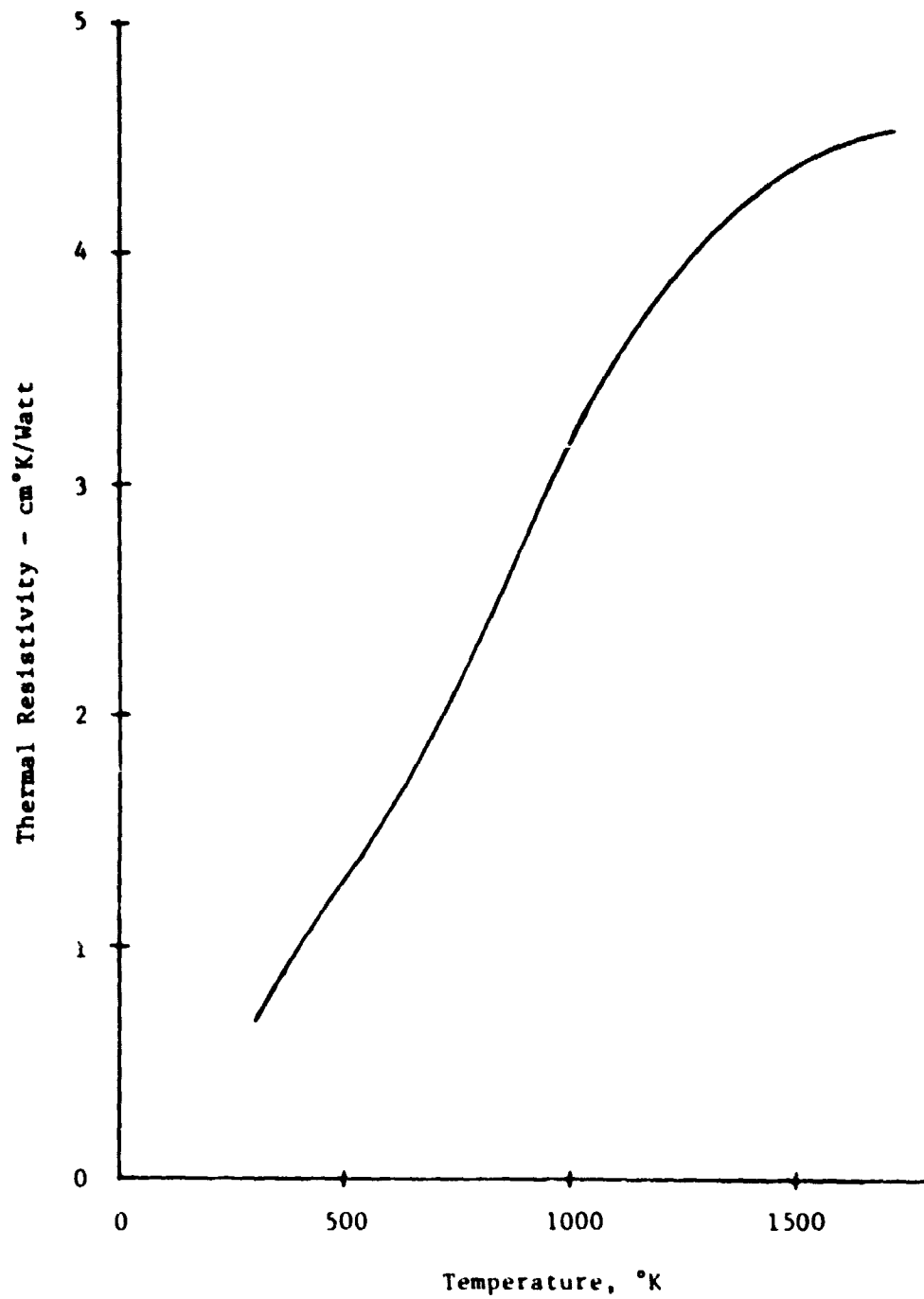
Figure PK-5- Thermal Resistivity vs. Temperature For High Purity Silicon (From Reference 5)

Graphite Liners

The materials selected are Stackpole's grade 2020 and Great Lakes Carbon grade HLM. The variations in properties are attributable mainly to manufacturing methods such as isostatic pressing, molding, and extrusion. Typical thermal properties as shown in Table PR-4 illustrate these variations and the similarity to grade 2128 for which the previous calculations were performed.

Grade HLM has the advantages that it is less expensive and is available in large sizes. The disadvantages are that less data is available and the ash content (impurity level) is somewhat higher. Thus, the HLM grade material is used in the areas where heat transfer is lower and dimensions are not as critical.

Pyrolytic Graphite

Thermal conductivity: Figure PR-6 has been used for this analysis.[7] It has been supported by data from one supplier, Pfizer Inc. Pyrolytic graphite properties vary strongly depending on the conditions at the time of deposition.

Drawings which depict the assembly of the reactor shells and respective liners are presented in Figures PR-7 - PR-11.

Figure PR-12 presents a view of the arc heater-reactor assembly mounted on the frame within the test cell. Key reactor system components are labeled on the figure. One of the three-phase arc heaters from the reactor is presented in Figure PR-13 along with its protective outer cover shown in the left background.

Table PR-4

Thermal Properties Of Candidate Graphites

Graphite Type	Temp. (°C)	Coefficient Of Thermal Expansion		Thermal Conductivity
		Axial (1/°C)	Radial (1/°C)	Watts/cm °C
Stackpole 2128 (Isostatic Pressed)	25	4.1×10^{-6}	4.1×10^{-6}	.63
	600	5.3×10^{-6}	5.3×10^{-6}	1.11
	1000	5.8×10^{-6}	5.8×10^{-6}	.78
	1500	6.6×10^{-6}	6.6×10^{-6}	.38
Stackpole 2020 (Molded)	25	3.3×10^{-6}	2.5×10^{-6}	.61
	600	3.8×10^{-6}	3.3×10^{-6}	.45
	1000	4.2×10^{-6}	3.7×10^{-6}	.35
	1500	4.6×10^{-6}	4.1×10^{-6}	.26
Great Lakes Carbon HLM (Extruded)	25	2.7×10^{-6}	2.7×10^{-6}	1.38 (With Grain)
	600	*	*	*
	1000	*	*	*
	1500	*	*	*

*Data Not Available
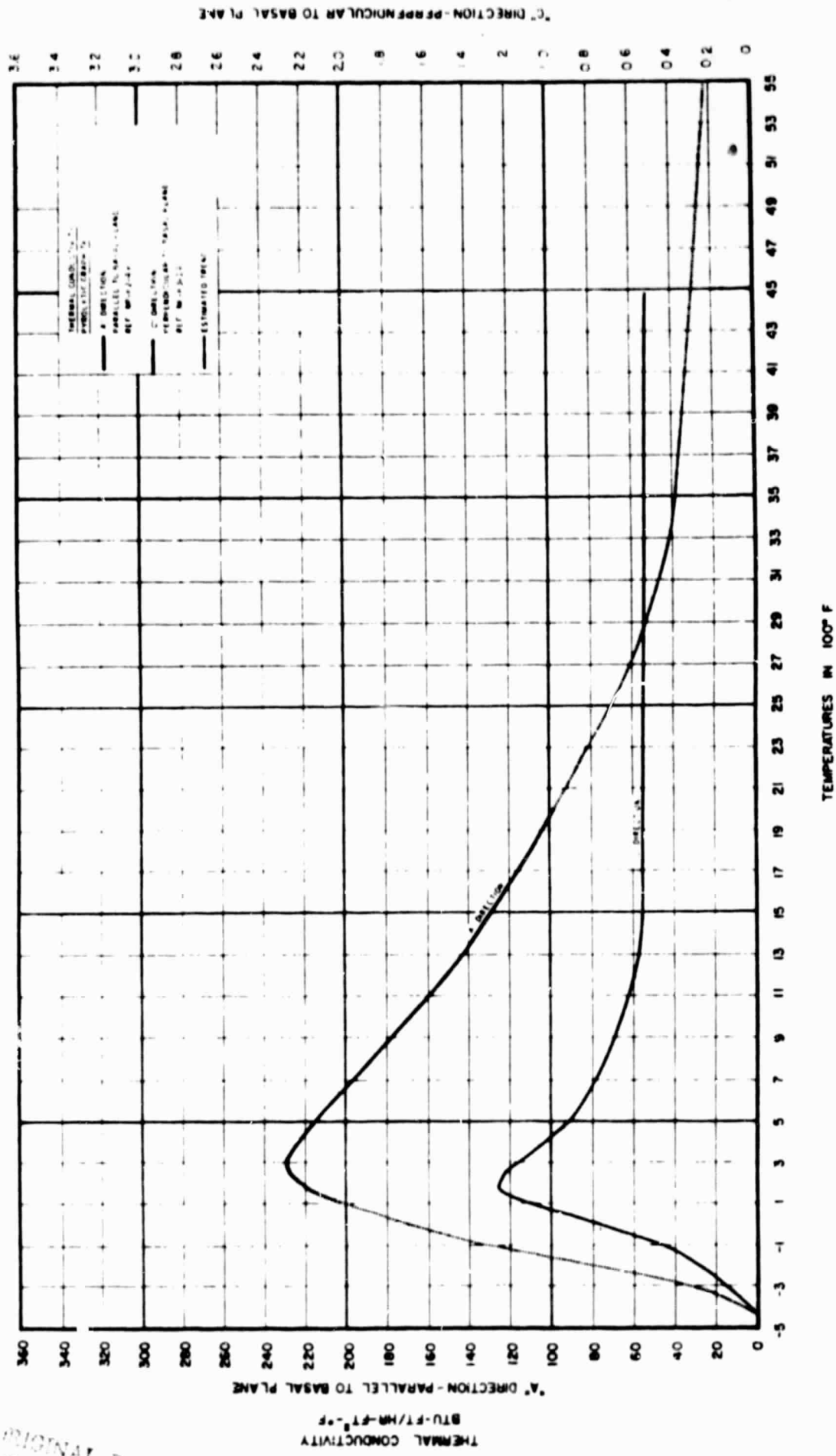
Figure PR-6 – Thermal Conductivity Of Pyrolytic Graphite (From Reference 7)

4-41

Figure PR-7 - Assembly Drawing Of Na Injector And Arc Heater Plenum Sections

4-42
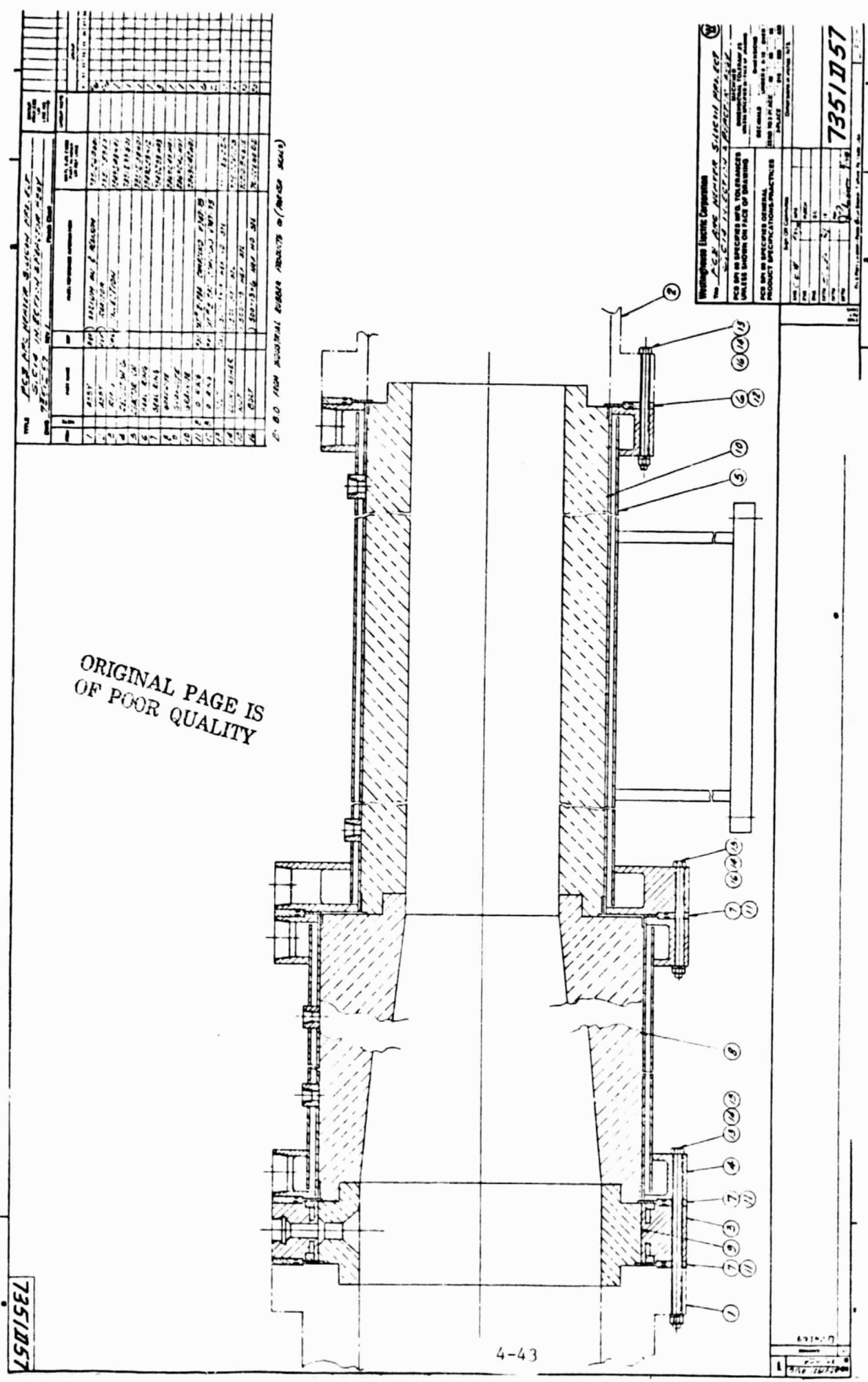
Figure PR-8 - Assembly Drawing Of The SiCl₄ Injector Ring And Reactor Sections

4-43

Figure PR-9 - Assembly Drawing Of Reactor Sections

4-45
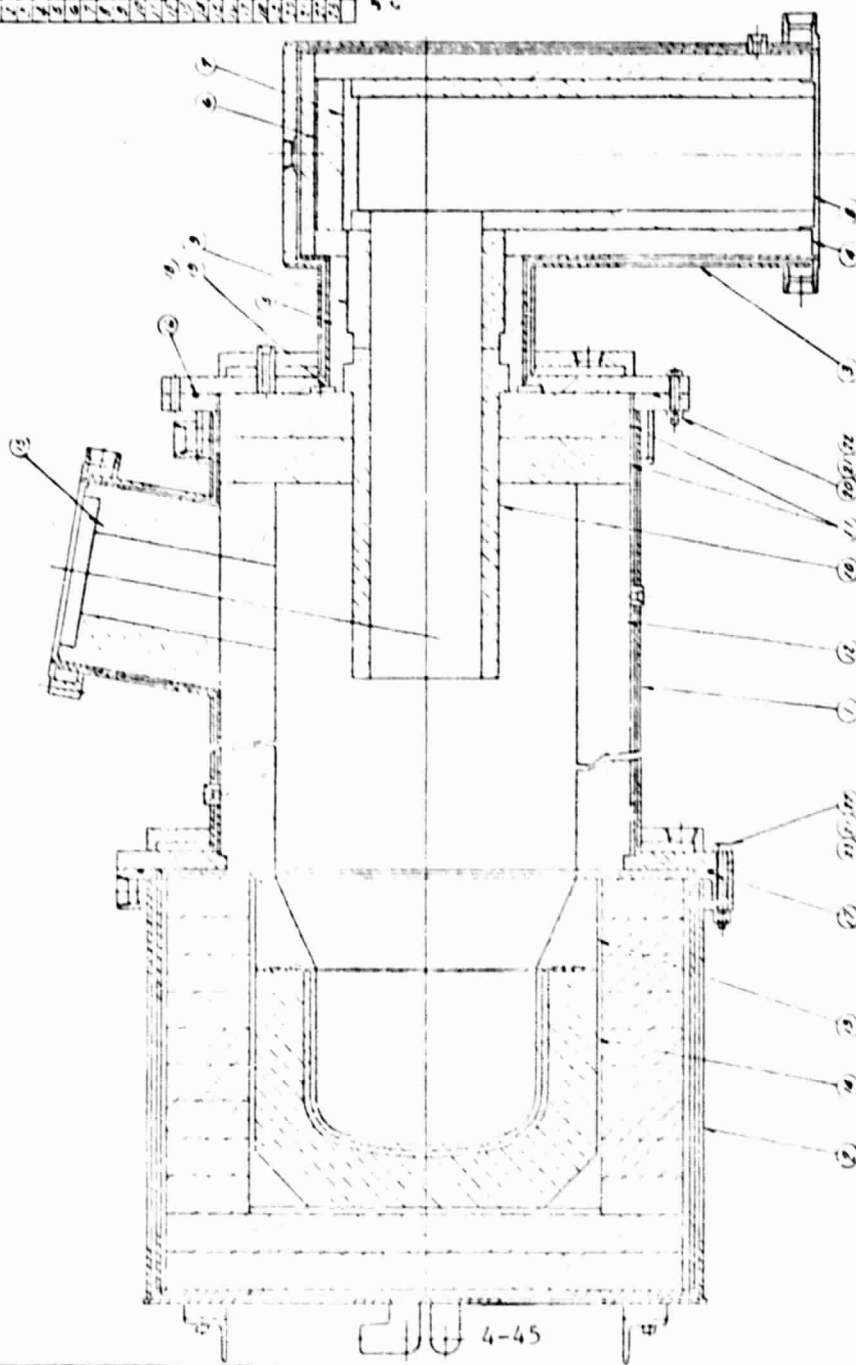
Figure PR-10 - Assembly Drawing Of Silicon Cyclone And Collector
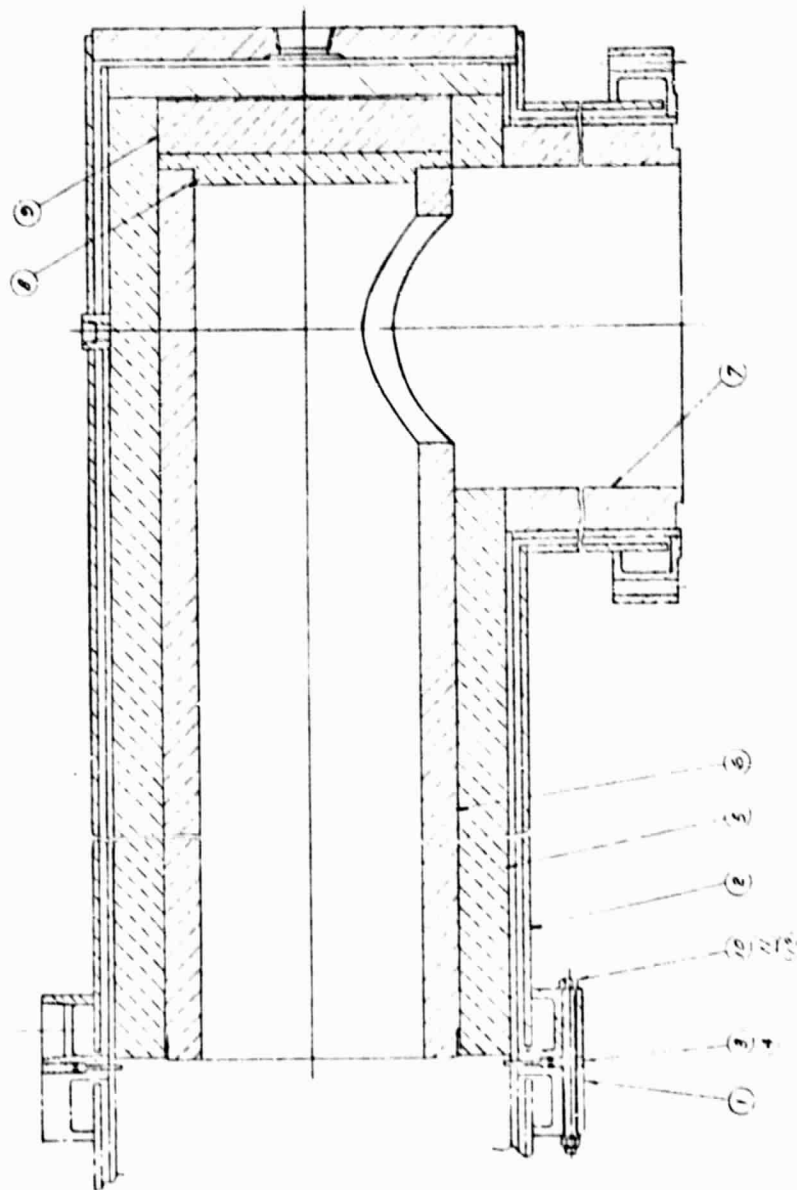
Figure PR-11 - Assembly Drawing Of Gas Scrubber Inlet Section

SCRUBBER

S1 CYCLONE/ COLLECTOR

REACTOR

SiCl$_4$ INJECTION

ARC HEATER

ARC HEATER

SODIUM INJECTION
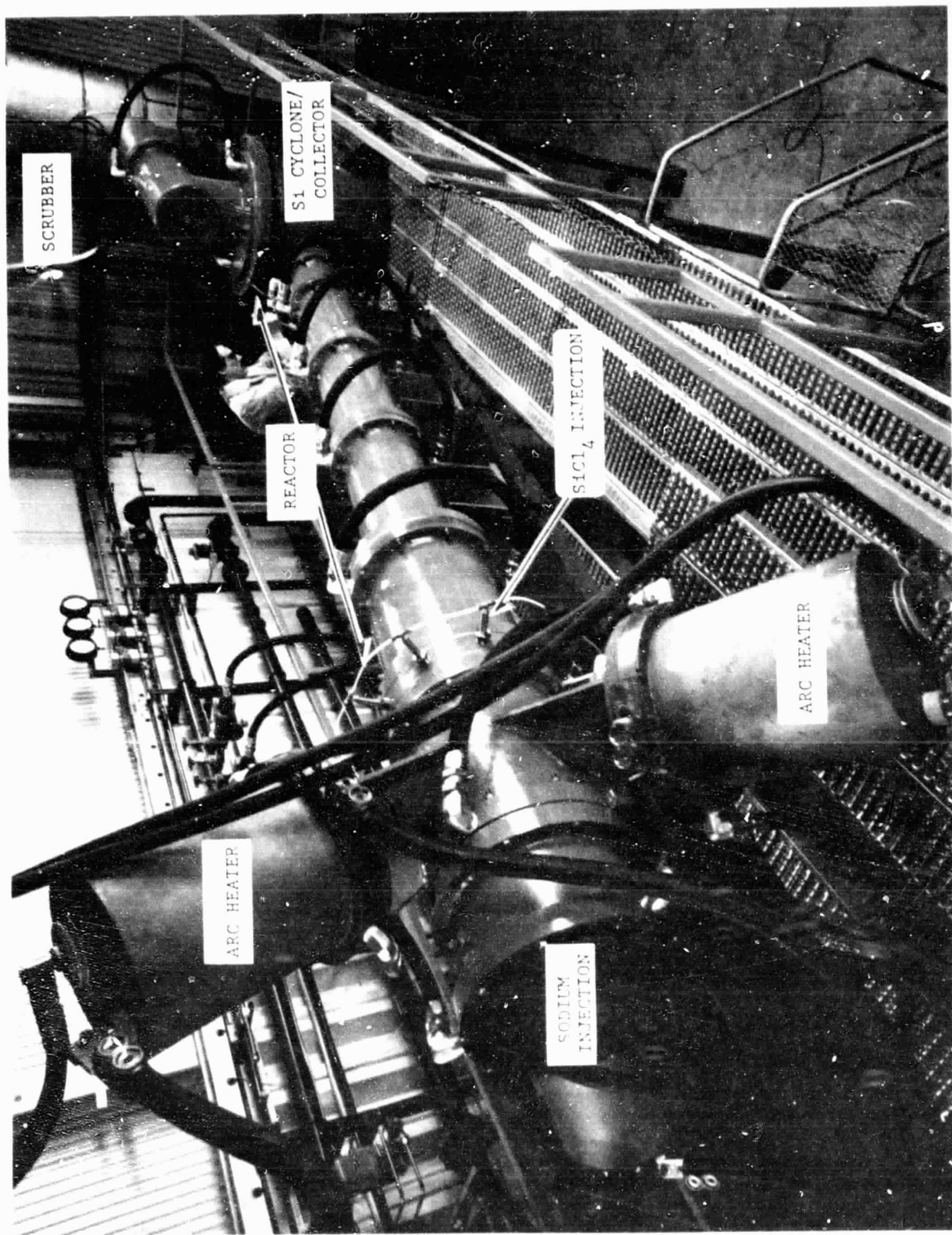
Figure PR-12 - Photograph Of The Arc Heater-Reactor For Experimental Silicon Production.
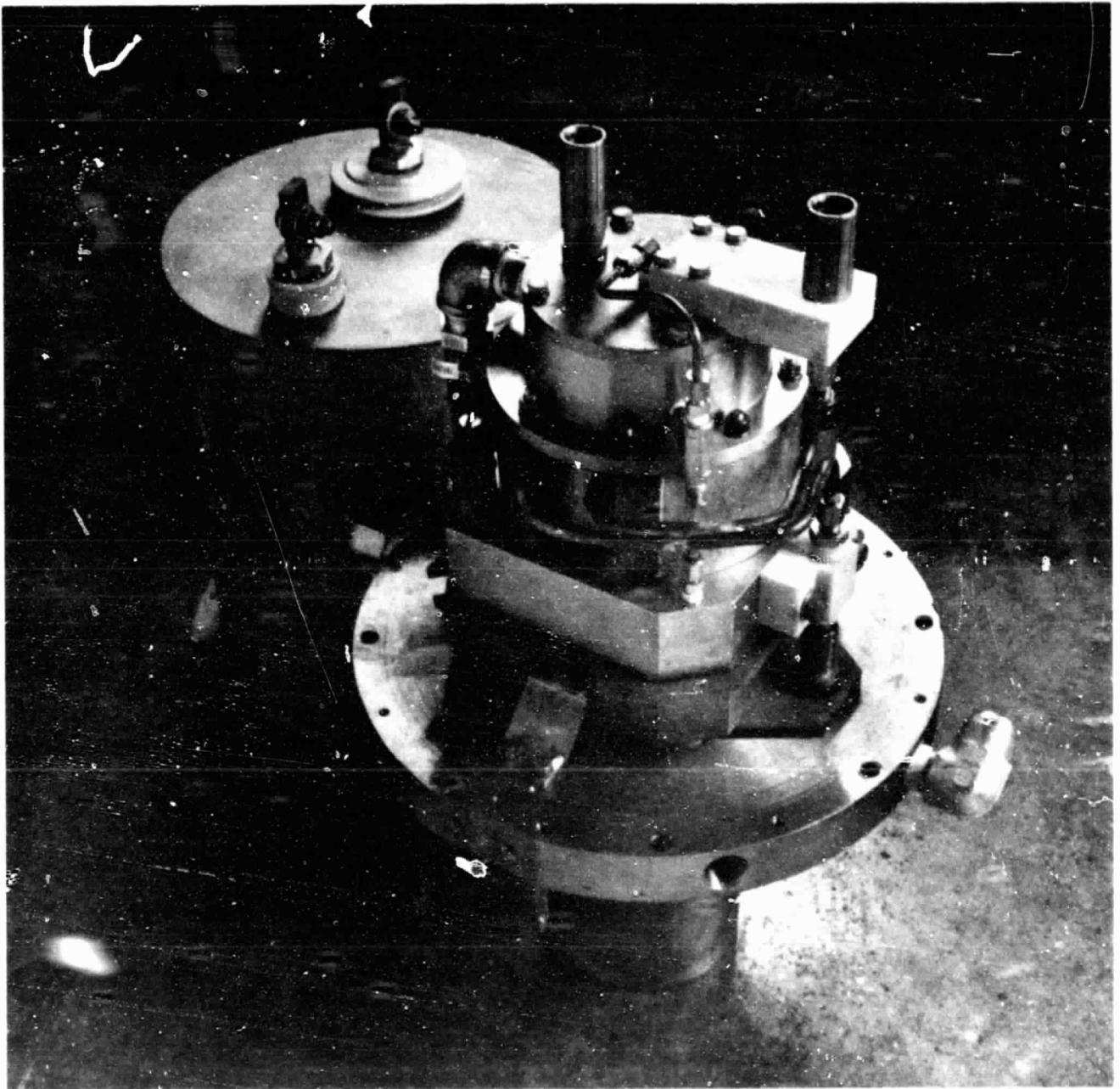
Figure PR-13 - Photograph Of The Westinghouse Arc Heater Used For The
Silicon Process Experimental Verification Unit

4.6 $SiCl_4$ Storage and Feed System

The Westinghouse Arc Heater process reduces silicon
tetrachloride with sodium at a high temperature to form silicon
and a by-product sodium chloride. The objective of the $SiCl_4$
system is to supply $SiCl_4$ of known purity to the reactor at a
rate equivalent to the production of 45.36 kg (100 lbs.) per
hour of silicon. The rate of flow must be variable and
proportional to the sodium flow. The system must be capable
of operating for short runs (1 to 2 hrs.) and for continuous
running. The purity of the $SiCl_4$ must be preserved and
monitored and there must be a method for venting and
recycling it.

A schematic of the designed system is shown in Figure (STC-1)
and the component identification for this system is itemized
in Table STC-1. This design provides for a large storage
tank (4,000 gal.) where the $SiCl_4$ is stored as received from
a supplier and a smaller 2C0 gal. storage or "day" tank where
material for a specific test run is stored. Thus, should
material being used during a test become contaminated, only
the quantity in the "day" tank need be discarded. As part
of the injecting system, a recirculating loop has been included
to allow the $SiCl_4$ to be pumped thru the flow meter and
returned to the "day" tank. This allows for adjusting the
flow rate prior to directing the $SiCl_4$ to the reactor.

Because of the reactive nature of $SiCl_4$ with the normal
atmosphere, a method for providing argon as a cover gas to
the storage tanks and as a purge gas for cleaning the lines of
air and/or $SiCl_4$ was incorporated into the system design. The
argon gas is also used for cooling the injection nozzles
located in the reactor when $SiCl_4$ is not being injected. An
H_2O analyzer and an O_2 monitor are included in the argon
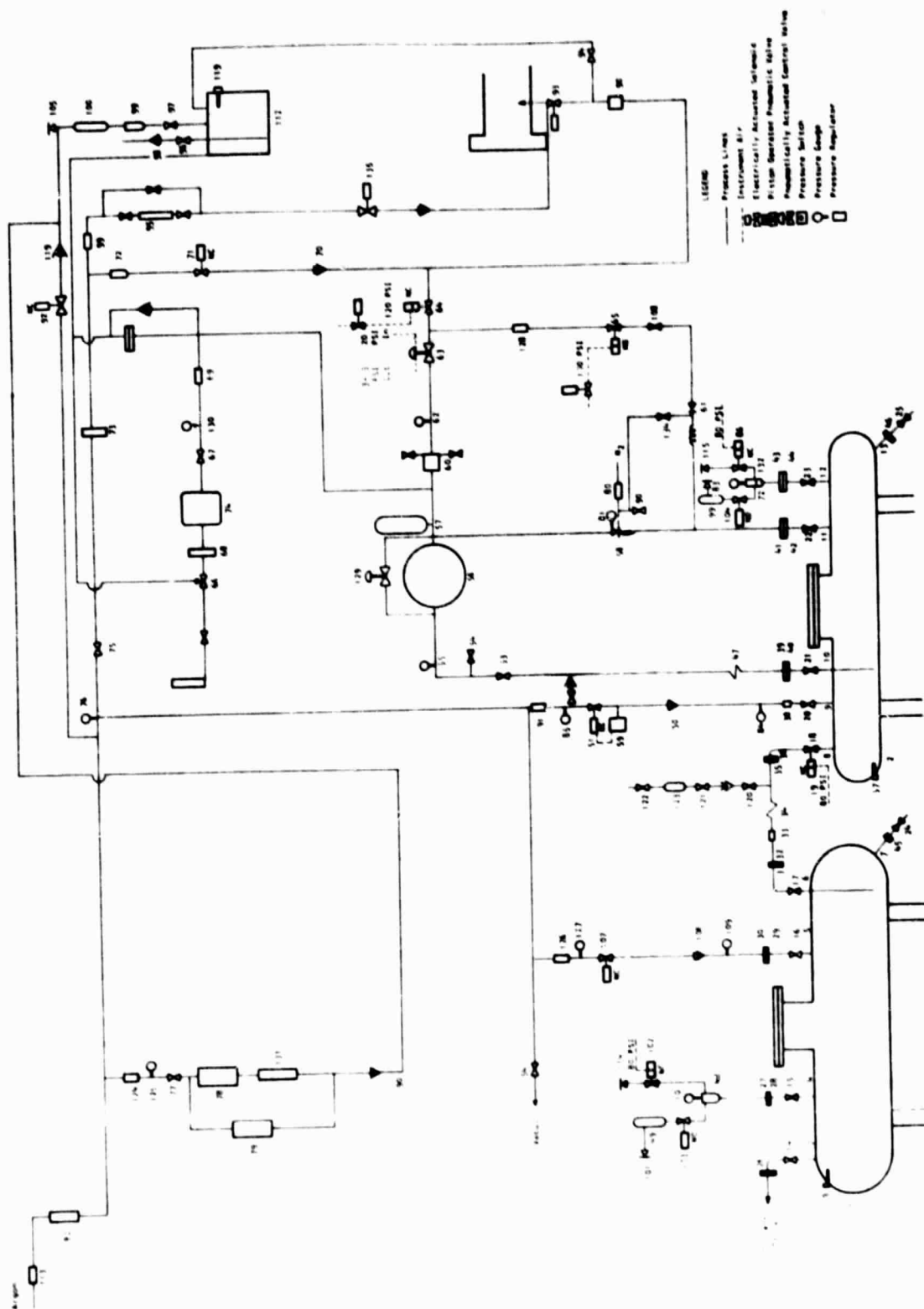
Figure STC-1 - Component Location Schematic for the SiCl$_4$ System

4-50

Table STC-1 - Component Identification For The SiCl₄ System

SiCl₄ Components

1. 4016 Gallon Storage Tank
2. 264 Gallon Storage Tank
3. 2" pipe - Connection to Tank Truck
4. 1" pipe - Argon Vent Line
5. 1" pipe - Argon Pressurization Line
6. 1" pipe - SiCl₄ Transfer Line
7. 3" pipe - Drain Line
8. 1" pipe - SiCl₄ Transfer Line
9. 1/2" pipe - Argon Purge Line
10. 1" pipe - Connection to SiCl₄ Injection System
11. 1" pipe - Pressure Relief Line
12. 1" pipe - Argon Vent Line
13. 2" pipe - Drain Line
14. 2" Worcester Ball Valve - Tank Truck Fill Line
15. 1" Worcester Ball Valve - Main Storage Vent
16. 1" Worcester Ball Valve - Main Storage Argon Pressure
17. 1" Worcester Ball Valve - SiCl₄ Transfer Line
18. 1" Worcester Ball Valve - SiCl₄ Transfer Line
19. Pneumatic Actuator - Worcester Series 30
20. 1/2" Worcester Ball Valve - Argon Pressure
21. 1" Worcester Ball Valve - SiCl₄ Feed
22. 1" Worcester Ball Valve - Bypass Line
23. 1" Worcester Ball Valve - Day Tank Fill
24. 3" Worcester Ball Valve - Main Storage Drain
25. 2" Worcester Ball Valve - Day Tank Drain
26. 2" Companion Flange
27. 1" 150# Carbon Steel Flange
28. 1" 150# Carbon Steel Flange
29. 1" 150# Carbon Steel Flange
30. 1" 150# Carbon Steel Flange
31. 1" 150# Carbon Steel Flange
32. 1" 150# Carbon Steel Flange
33. Orifice Plate Flow Meter
34. Stainless Steel Flexible Connector
35. 1" 150# Carbon Steel Flange
36. 1" 150# Carbon Steel Flange
37. SiCl₄ Liquid Level Probe
38. 1/2" Pipe Coupling
39. 1" 150 Carbon Steel Flange
40. 1" 150 Carbon Steel Flange
41. 1" 150 Carbon Steel Flange
42. 1" 150 Carbon Steel Flange
43. 1" 150 Carbon Steel Flange
44. 1" 150 Carbon Steel Flange

45. 3" 150# Carbon Steel Flange
46. 2" 150# Carbon Steel Flange
47. 3/4" Stainless Steel Flexible Connector
48. Vapor Trap - Main Tank
49. Moisture Trap
50. Check Valve
51. Solenoid Valve - Actuated by Pressure Switch # 59
52. 3/8" Nupro Stainless Steel Bellows Valve
53. 3/4" Worcester Ball Valve
54. 3/8" Stainless Steel Plug Valve for Vacuum
55. Pressure Gage - Pump Inlet Pressure - 30" to 15 psi
56. Milton Roy Diaphragm Pump
57. Accumulator
58. Grove System Over Pressure Relief Valve
59. Mercoid Pressure Switch
60. Main Flow Meter Orifice Plate Type
61. Bypass Back Pressure Regulator
62. Pressure Gauge - Pump Outlet Pressure - 0 - 100 psi
63. Proportioning Valve
64. Inject Valve
65. By Pass Valve
66. 3 Way Sampling Valve
67. Sample Inlet Valve
68. Sample Flowmeter
69. Sample Pressure Regulator
70. Check Valve
71. Blowdown Solenoid Valve
72. Vapor Trap - Day Tank Purge Line
73. Blowdown Flowmeter
74. 400 psig Rupture Disc
75. 3/8" Plug Valve Blowdown
76. Pressure Gauge - Main Argon Gas Pressure 0 - 180 psi
77. 3/8" Plug Valve - Argon Purity
78. Panametrik H₂O Analyzer
79. Westinghouse O₂ Monitor
80. Pressure Regulator - System + Bypass Over Pressure
81. Pressure Gauge - 0 - 1000 psi Over Pressure Relief
82. Flowmeter - Argon Main Flow
83. Pressure Relief Valve
84. Pressure Gauge - 0 - 15 psi
85. Pressure Gauge - 0 - 60 psi
86. 1" Worcester Ball Valve - Day Tank Vent
87. 50 psig Rupture Discs
88. 50 psig Rupture Discs

89. 600 psig Pressure Relief
90. Check Valve
91. Pressure Regulator
92. Argon Vent Purge Valve
93. SV-93 Blowdown
94. 3/8" Nupro Stainless Steel Bellows Valve - Blowdown Drain
95. Nozzle Cooling Argon Flowmeter
96. 3/8" Nupro Stainless Steel Bellows Valve
97. 3/8" Nupro Stainless Steel Bellows Valve
98. Check Valve
99. Argon Pressure Regulator
100. Vapor Trap
101. Check Valve
102. 1" Worcester Ball Valve - Main Storage Vent
103. Solenoid Valve
104. Solenoid Valve
105. Relief Valve
106. Check Valve
107. Main Tank Argon Valve
108. By Pass Throttling Valve
109. Pressure Gauge - 0 - 60 psi
110. Pressure Gauge - 0 - 60 psi
111. Pressure Gauge - 0 - 15 psi
112. SiCl₄ Blow Down Tank
113. Argon Pressure Regulator
114. Relief Valve
115. Relief Valve
116. Check Valve
117. Sample Bottle
118. Check Valve
119. Check Valve
120. 3/8" Nupro Stainless Steel Bellows Valve
121. 3/8" Nupro Stainless Steel Bellows Valve
122. 3/8" Nupro Stainless Steel Bellows Valve
123. Sampling Cylinder
124. Pressure Regulator
125. Pressure Gauge - 0 - 60 psi
126. Pressure Regulator
127. Pressure Gauge - 0 - 60 psi
128. Pressure Regulator
129. By Pass Valve
130. Pressure Gauge - 0 - 15 psi
131. Flowmeter - Panametrics
132. Flowmeter Vent
133. Flowmeter Vent
134. Bypass Back Pressure Loader
135. Argon Nozzle Cooling Gas Valve

cover gas loop so that the purity of the gas can be checked
during testing. The design of the SiCl$_4$ system included an
infrared process analyzer for real time analysis of the SiCl$_4$
purity. However, an analyzer was not built into the system
used for testing because a suitable supplier could not be
found, but a method for taking "grab samples" has been
provided. To pump SiCl$_4$ to the reactor a "Milton Roy Diaphram
Pump" is used with a capacity of 11.4 litre/min (3 gal/min).

The SiCl$_4$ is hydraulically injected into the reactor via
ten commercially available nozzles supplied by Spraying Systems
Co., Whelton, Ill. The nozzles are spaced equidistant around
the periphery of the reactor and are supplied from a common
manifold. The SiCl$_4$ enters the reactor chamber in the form
of a uniform, fine mist of liquid droplets.

A patent has been issued on the design of the Silicon
Tetrachloride Feed System. Photographs of the main storage
tank and the Injection Control Module are shown in Figures (STC-2)
and (STC-3), respectively.

Installation of the silicon tetrachloride storage and feed
system was completed in October, 1979 and the system functioned
satisfactorily during the December 8, 1979 reactant test.
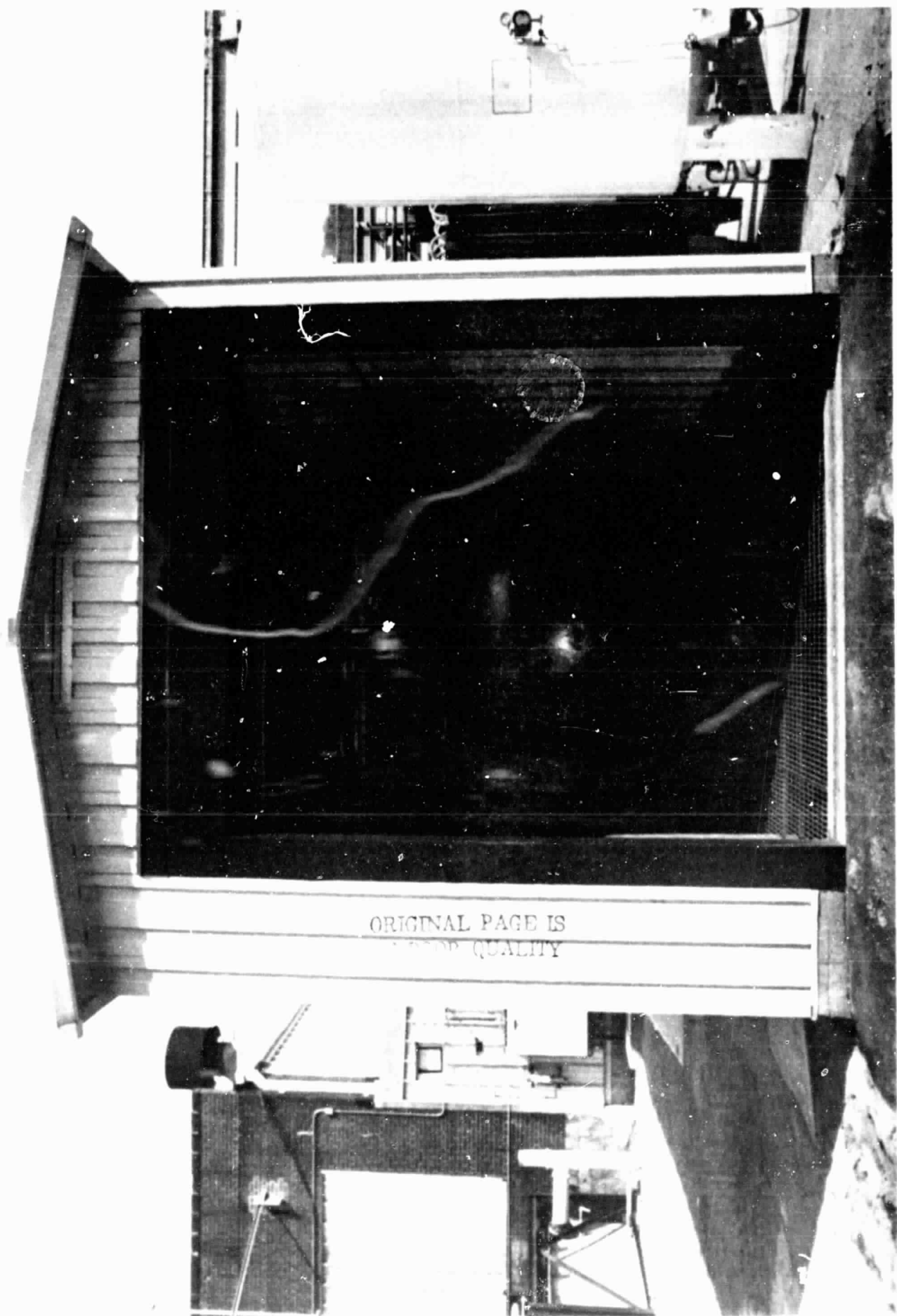
Figure STC-2 - Photograph Of The Main SiCl$_4$ Storage Tank Installation
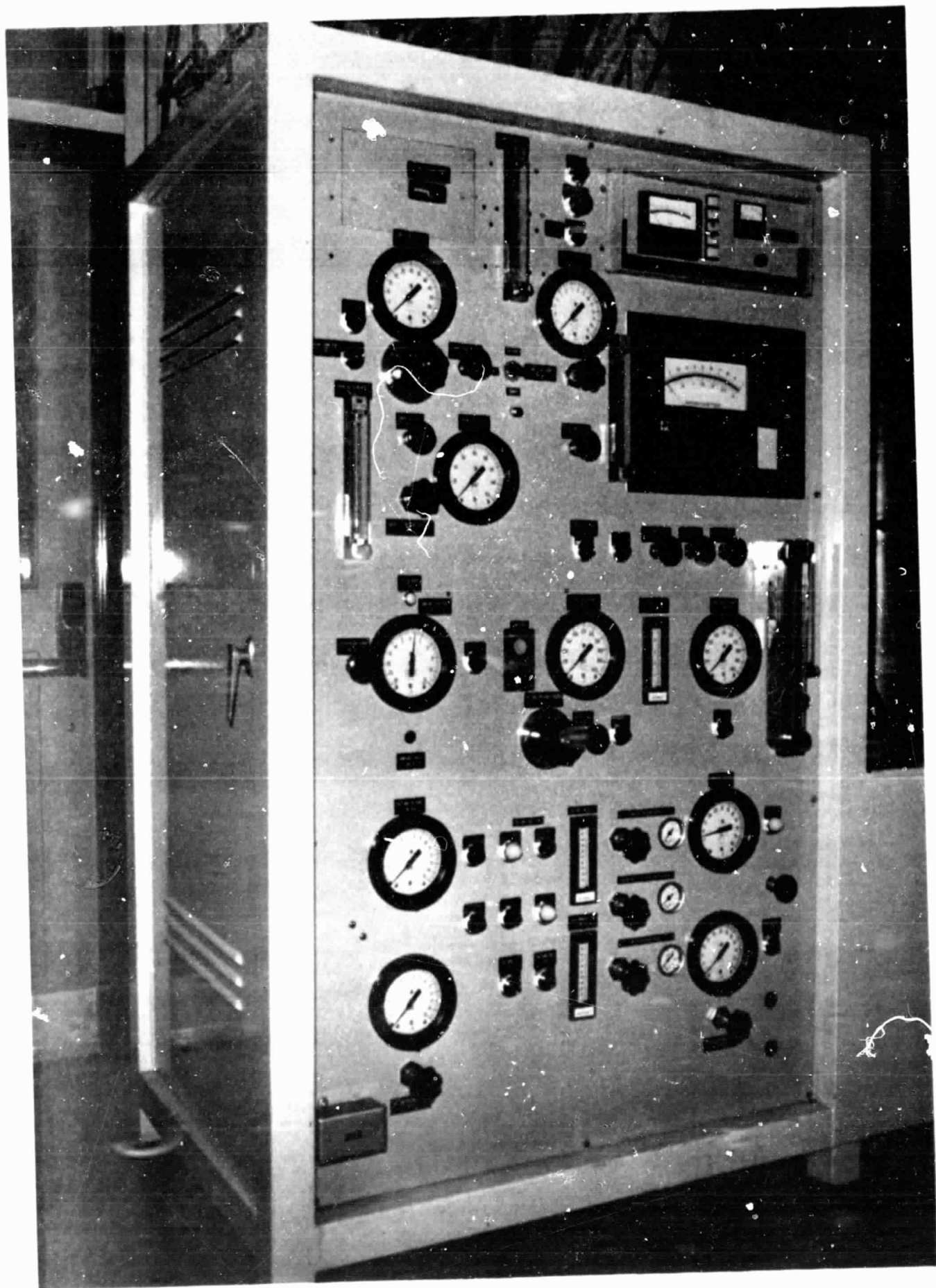
Figure STC-3 - Front Panel Of The $SiCl_4$ Injection Module

4.7 Sodium Storage and Feed System

The purpose of the sodium storage and feed system is to deliver sodium to the plasma reactor at the flow rate, purity and condition required by the process. The major design goals were to design the system to meet the above requirements with the minimum danger to personnel, and with the maximum reliability within reasonable cost and time restraints. Flexibility was also a design goal. Although initial silicon production tests were conceived as being relatively short term (1 to 2 hou.s) operations, the sodium system was designed for long term (several hours), continuous operation.

The reactive nature of sodium with normal atmosphere and the fact that sodium is in the solid state at normal ambient temperatures required special system design considerations. An inert gas system was designed to provide cover gas over the entire sodium system, thus eliminating contact with air. Electrical resistance heaters and thermal insulation were designed for installation over the entire sodium system to heat the system above the sodium melting point of 98°C.

The system was conceptually designed as illustrated in Figure (SS-1). Item "B" represents the 55 gallon (420 lbs.) sodium transport drums commercially supplied by a sodium manufacturing plant. Sodium is liquified and drained, one drum at a time, into the base tank, item "A". From the base tank, sodium is pumped by the electromagnetic pump (item "C"), through the flowmeter (item "J"), through one of the sintered metal filters (item "E"), and into the chemical reactor. During check-out and prestart operations, valve Na-14 can be closed and Na-13 opened allowing the sodium to recirculate through the base tank.

Cover gas pressure is controlled separately over the sodium

Drawing. 1693873

(A)	Sodium Base Tank
(B)	Sodium Drums
(C)	E M Pump
(D)	Pressure Indicator
(E)	Micro Metallic Filters
(F)	Vapor Trap
(G)	Flowmeter
(H)	Photohelic Pressure Control
(I)	Level Probes
(J)	Sodium Flowmeter
O	Pressure Relief Valve
⊠	Hand Operated Valve
⊠⊏	Remote Actuated Valve
——	Sodium Line
-----	Argon Line
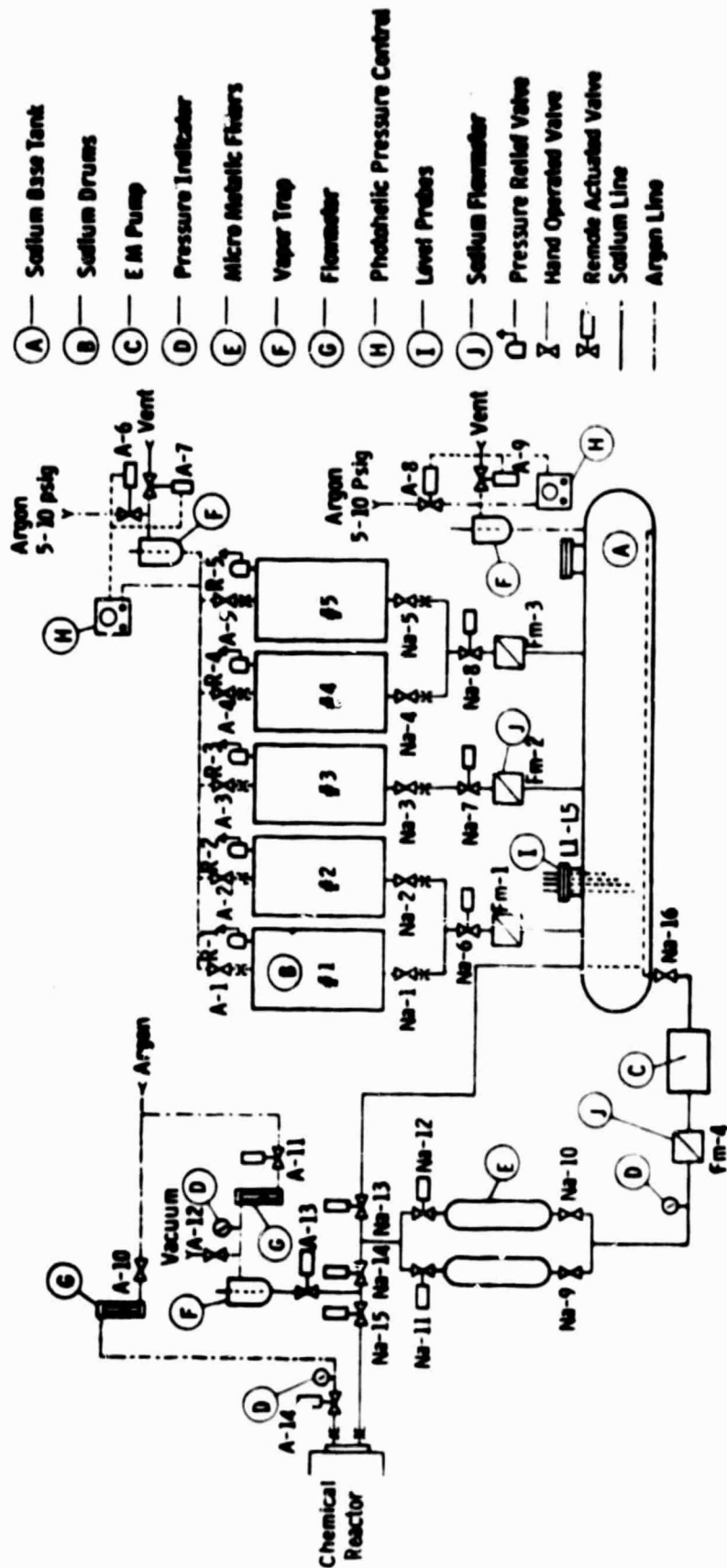
Figure SS-1 - Sodium Supply System

4-56

drums and the base tank. This allows sodium to drain freely into
the base tank by gravity. The sodium level in the base tank is
controlled automatically by sensing the level with the level
probes (item "I") and operating the sodium drain valves (Na-6,
7 & 8). Each sodium drum is also equipped with a pressure relief
valve (R-1 thru 5) to limit the internal drum pressure to less
than 5 psig in case of a malfunction of the drum cover gas pressure
control system.

The sodium system is designed and constructed basically from
300 Series stainless steel. The low solubility of iron
(< 5 wppm) and other elements in sodium at the projected operating
temperature between 150 and 200°C will prevent contamination of
the silicon product by the sodium feedstock. The sodium injection
nozzle, however, may erode because of the higher sodium velocity
through the nozzle and impingement of particles on nozzle surfaces.
Therefore, parts of the nozzle are being constructed from
Hastelloy which will not contaminate the silicon product (i.e.,
lower the photovoltaic efficiency) if erosion occurs.

A critical component of the sodium storage and injection
system is the sodium injection nozzle. The sodium must be
injected in a fine spray of particles so that complete vaporization
occurs within a reasonable axial length of the arc heated chemical
reactor chamber. Particles with medium volume diameters (MVD's) of
< 200 microns are required.

A nozzle design which overcomes many injection problems
is the Sonicore ® atomizing nozzle from the Sonic Development Corp.,
Upper Saddle River, New Jersey. This nozzle breaks up the liquid
with self-induced sonic energy pulses and produces very small
particle sizes at comparatively large liquid flows. This nozzle
was selected as the primary choice for the system.

A normal flanged arrangement has been designed for housing the sodium injection nozzle and installing it into the chemical reactor. This is shown schematically in Figure (SS-2). It features a jacked thermal control system for heating the nozzle during start-up and cooling the nozzle during full power operation. The sodium-potassium eutectic (NaK 78) was chosen as the heat transfer fluid because it is compatible with the system should a leak occur. It can operate effectively throughout the required temperature range and is liquid at normal room temperature. Figure (SS-3) is a schematic representation of the NaK system.

NaK is pumped by an electromagnetic pump through a 10 kW NaK heater, where the temperature is automatically controlled as required. The NaK then flows through the jacket of the sodium injection nozzle where it can either give up or absorb heat, depending upon the operating mode of the chemical reactor. From the nozzle, the NaK flows through a heat exchanger where the atomizing gas for the sodium nozzle is preheated. The NaK flow then continues through a 10 kW NaK/air heat exchanger, where the NaK temperature is cooled below the set point of the NaK heater, and finally the NaK flows back to the pump inlet.

Installation of the hardware portion of the sodium system was completed in March 1979. The application of trace heaters and insulation and electrical wiring were completed in October of 1979. A photograph of the completed system at the Arc Heater test facility in East Pittsburgh is shown in Figure (SS-4). Figure (SS-5) is a photograph of the Sodium System Control Panel.

Sonicore Nozzle

Reactor End Plate

NAK Out

Vacuum

NAK In
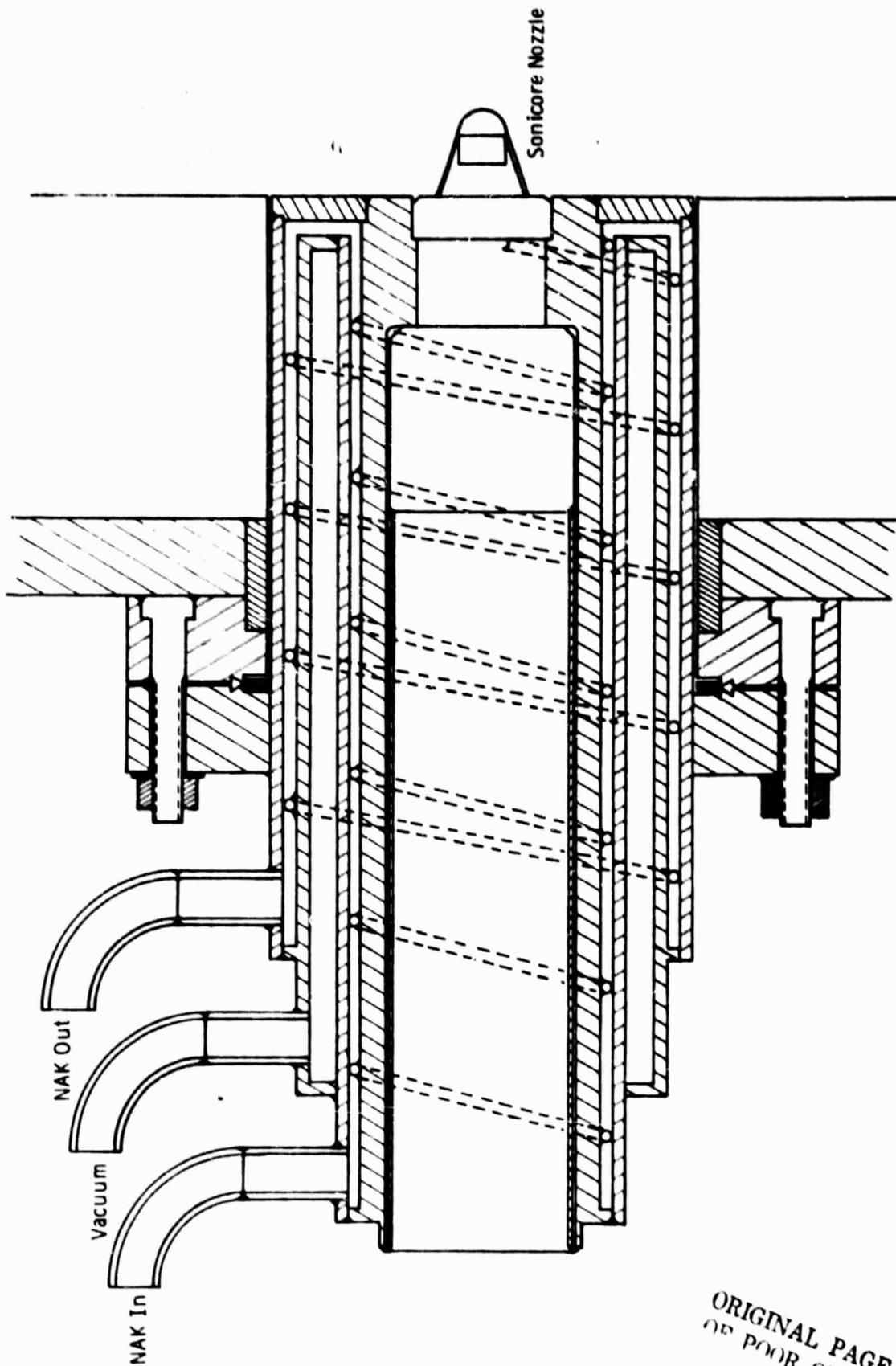
Figure SS-2 - Sonicore Nozzle Cooling System
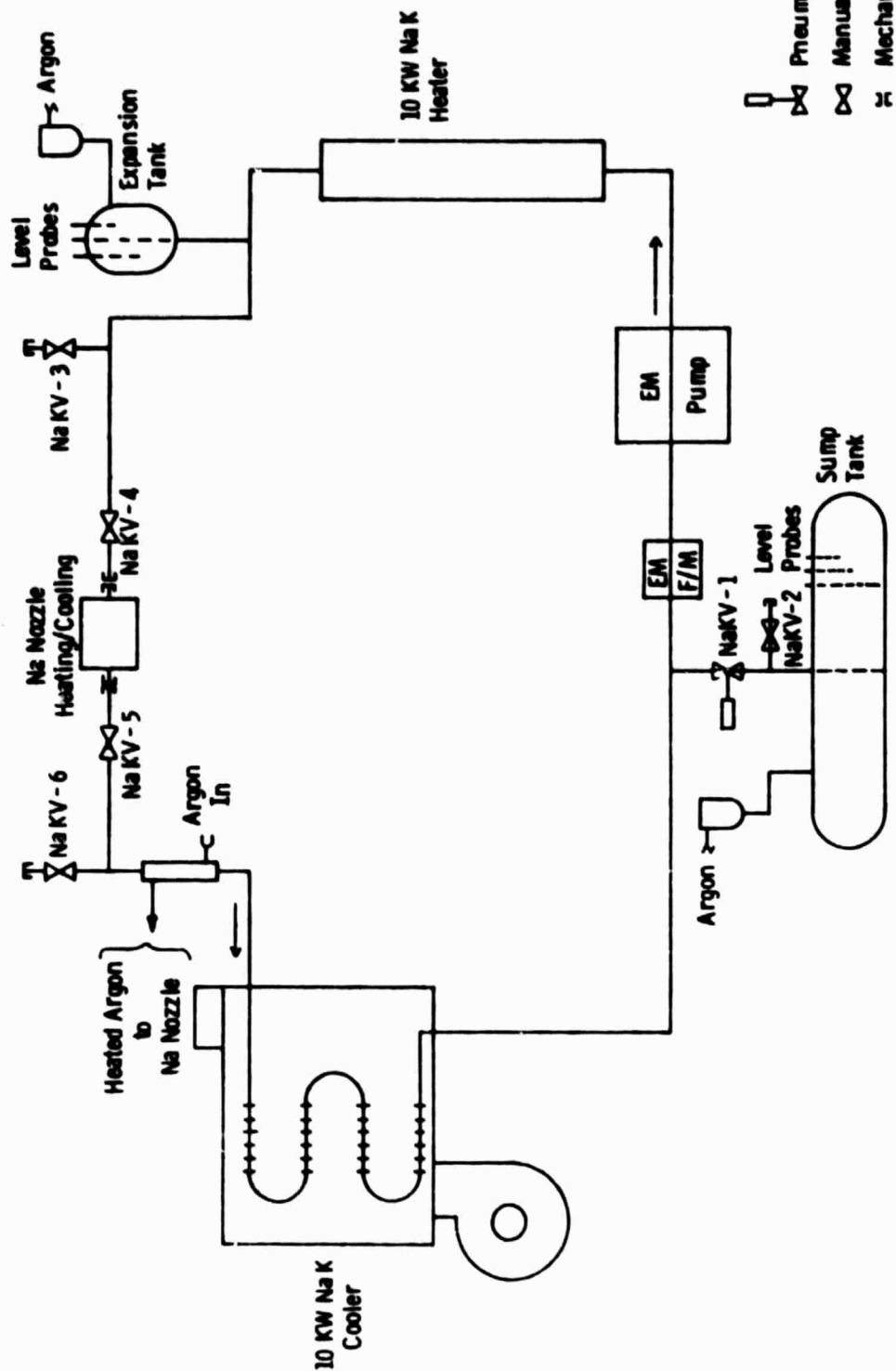
Figure SS-3 – NaK Loop For Na Nozzle Temperature Control
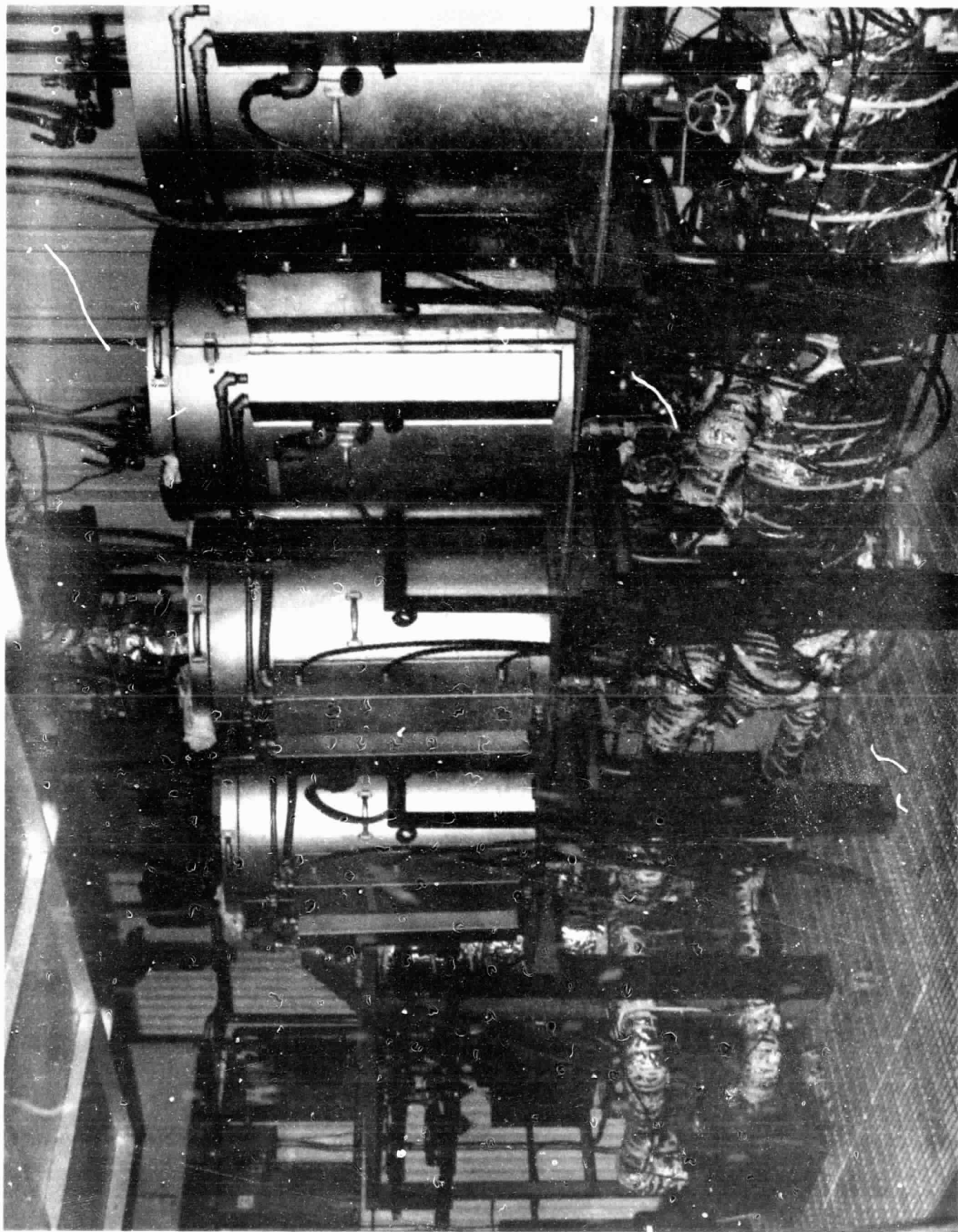
Figure SS-4 – Photograph of Sodium System Installation
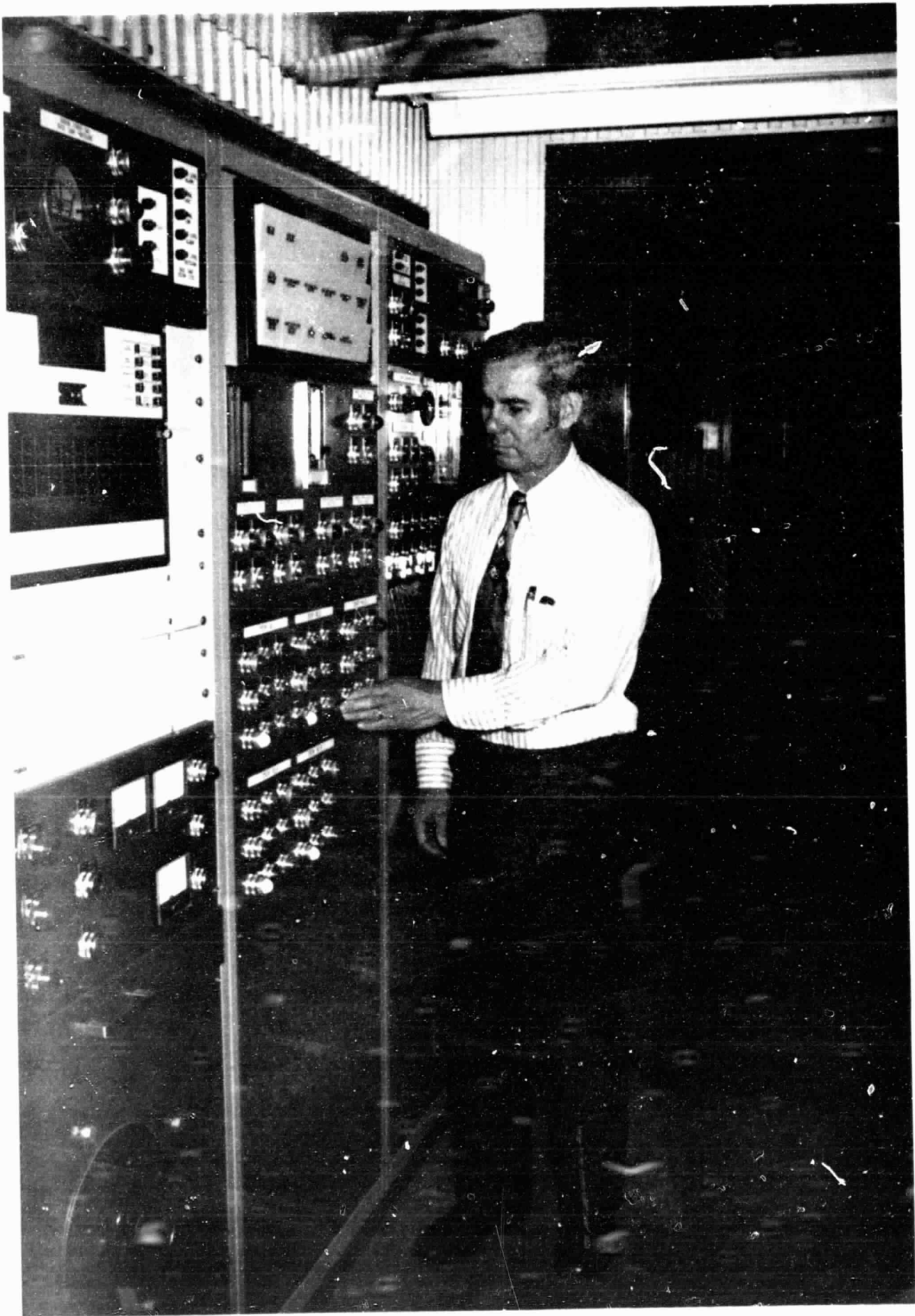
Figure SS-5 - Photograph Of The Sodium System Control Panel

4.8 Silicon Collection System

It is the function of the silicon collection system to
collect the liquid silicon product leaving the walls of the
cyclone separator and to preserve the purity of the product
without the introduction of additional contaminants. Since
the shakedown tests were planned to be short in duration, a
batch type collection system was selected over a continuous
casting method which would be much higher in cost. The batch
type collector was sized to hold the silicon produced from a
minimum of one hour continuous processing. The collector is
attached to the bottom of the silicon cyclone. The design
consists of a water cooled steel vessel lined with a layer
of refractory insulation creating a cavity to receive a graphite
crucible holder. The maximum dimension of the graphite is
30 inches O.D. in order to simplify raw material procurement.
A transition ring between the cyclone and the holder is the only
large graphite component necessary. This ring serves to direct
flow of the product leaving the cyclone. The ring is coated
with pyrolytic graphite to reduce product contamination since
all graphite grades in 30 inch O.D. and larger are quite
impure (i.e., >1000 ppm total impurities).

The graphite crucible holder is lined with an opaque, fused
quartz crucible. The quartz crucible liner is separated from
the graphite holder by a layer of alumina-ceramic fiber felt
and is held in place by the graphite transition ring. Figure (SC-1)
is a cross sectional drawing of the silicon collector. The
design of the silicon collection vessel was completed in
March 1978.

For the test conducted on December 8, 1979 it was decided
to replace the fused quartz crucible and graphite transition
ring with a less expensive expendable crucible. The expendable

4-63
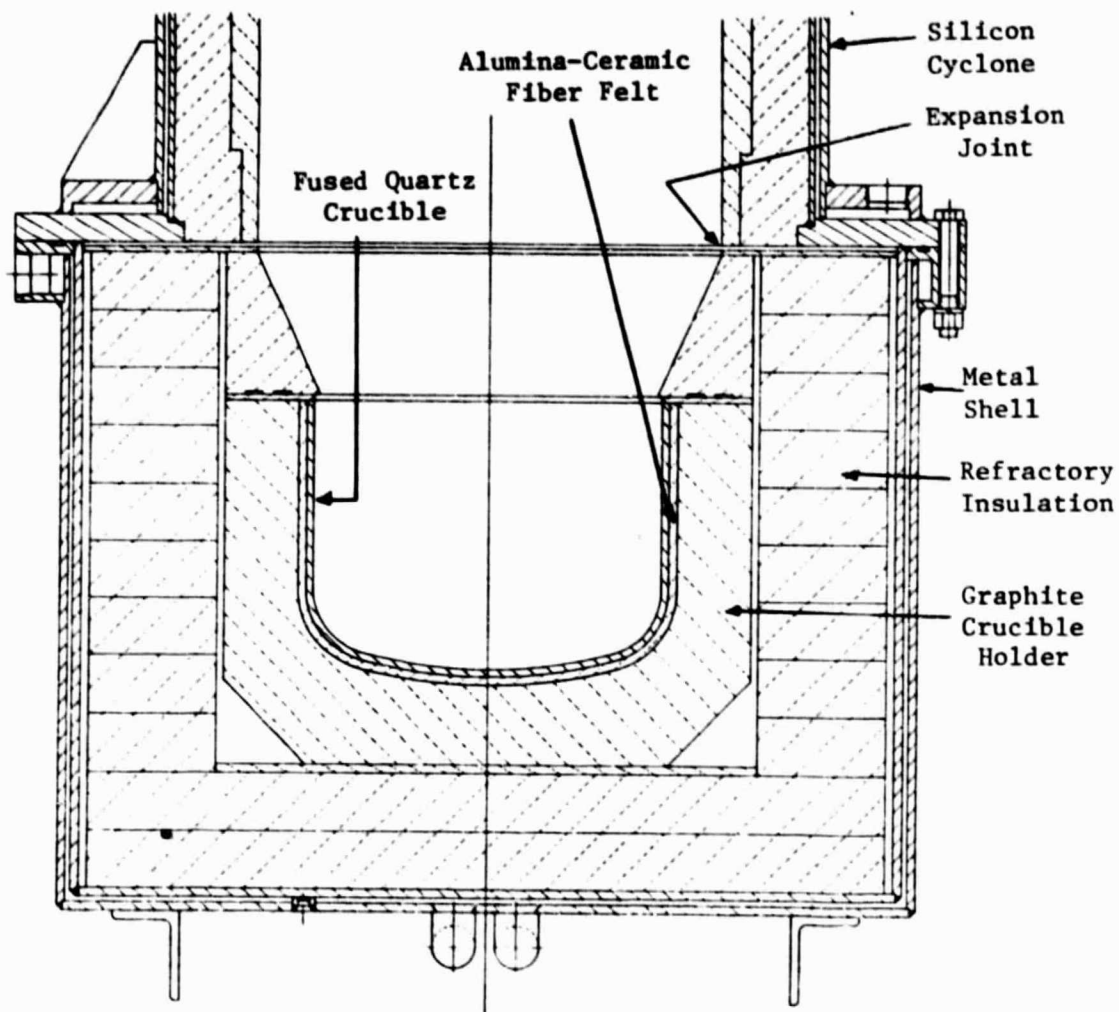
Figure SC-1 - Cross Sectional Drawing Of The Silicon Collector

crucible as shown in Figure (SC-2) consists of a stainless
steel can filled with a castable refractory similar to the
insulation brick. A cavity was molded into the casting to
provide for product collection. Assembly and installation
of the expendable collector was completed in February 1979.
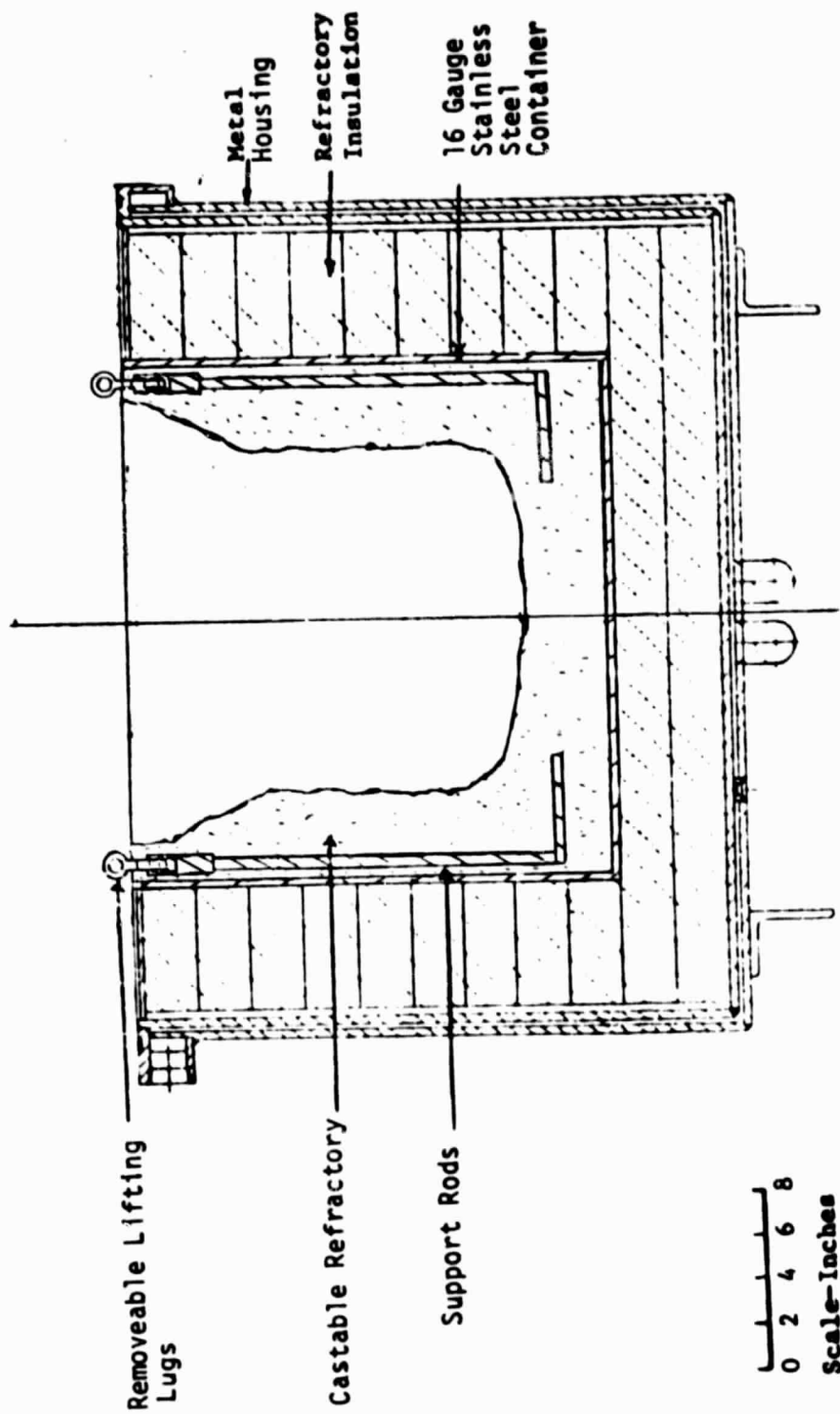
Figure SC-2 - Cross Sectional Drawing Of Expendable Silicon Collector For Shakedown Experiments

Metal Housing

Refractory Insulation

16 Gauge Stainless Steel Container

Removeable Lifting Lugs

Castable Refractory

Support Rods

0 2 4 6 8
Scale-Inches

4.9 Effluent Disposal System

The effluents (by-products) from the plasma reactor and silicon separator (cyclone) consist primarily of NaCl (vapor) and Ar-H$_2$ arc heated gases. However, small amounts of excess reactants Na or SiCl$_4$, uncondensed silicon, and limited amounts of Si subchlorides may be present in the effluent gas. Therefore, some method for cooling the arc heated gases and removing pollutants before burning off the hydrogen was necessary. The system designed consists of a venturi quencher-scrubber, a packed column scrubber demister, an effluent treatment along with automatic pH monitoring and control equipment and all interconnecting piping between each piece of equipment. The venturi quencher-scrubber is located downstream of the silicon cyclone and is connected to the cyclone with an insulated U-bend section of piping. Figure (ED-1) is a photograph of the venturi quencher-scrubber and the packed column scrubber-demister. Figure (ED-2) is a photograph of the effluent treatment tank installed beneath the gas burnoff stack (reported in the following sections).

The gases (argon and hydrogen) and the sodium chloride vapor exit the cyclone and enter the venturi at a temperature of approximately 2300°K. A spray of water (25 gpm) cools the gases to approximately 300°K and the sodium chloride vapor condenses to crystals. As the gases and solids pass through the throat of the venturi, most of the sodium chloride crystals are scrubbed out of the gases. Any salt that passes onto the packed column with the gases is scrubbed out with water (150-200 gpm) as are other chlorides such as HCl that might have been formed in the reactor. The gas scrubbing equipment is reported to be 95% efficient for all particles 0.1 micron in diameter or larger and 99% efficient for all particles 0.3 micron in diameter or larger.
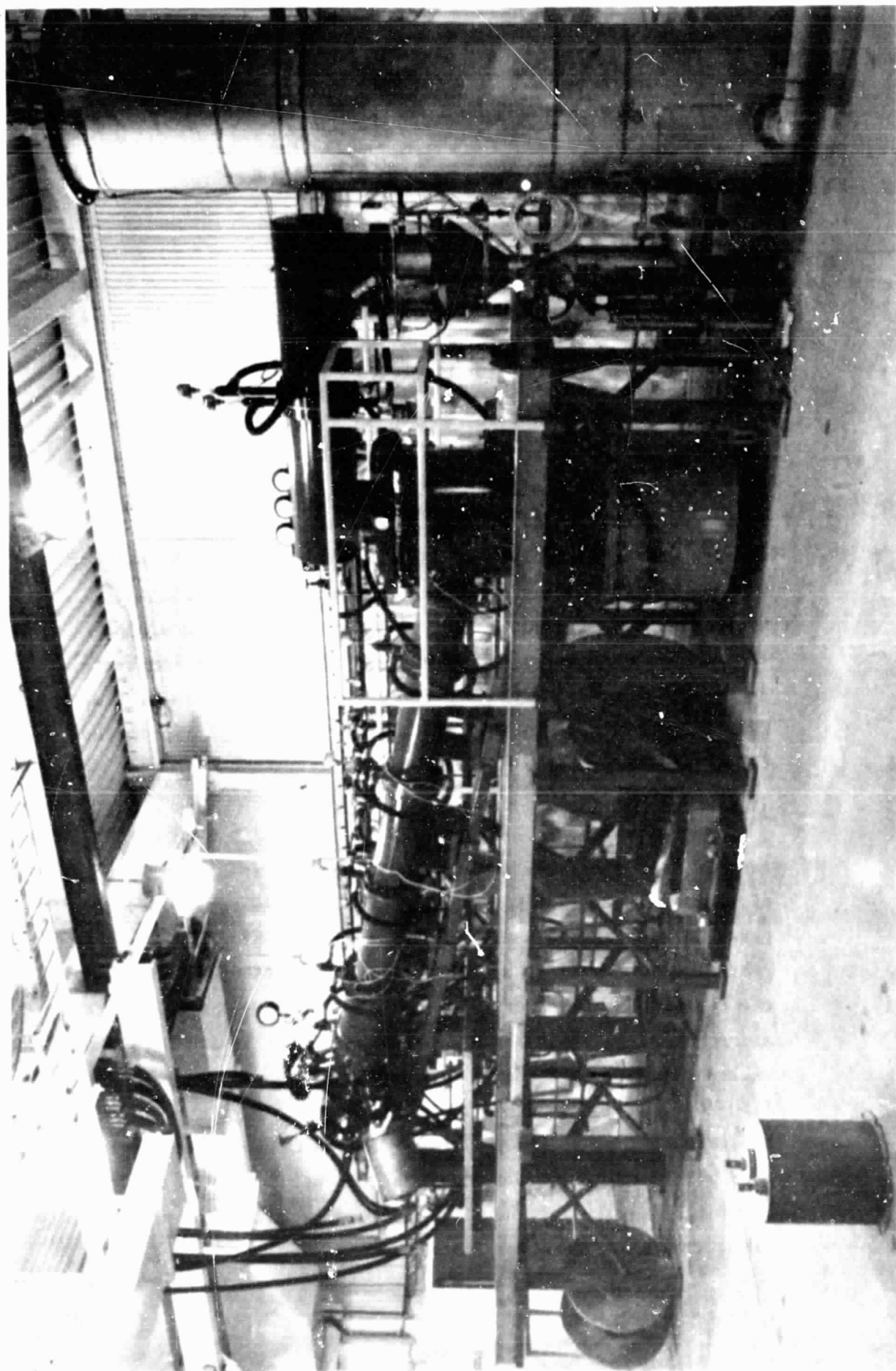
Figure ED-1 - Photograph Of The Venturi Quencher-Scrubber And The Packed Column Demister
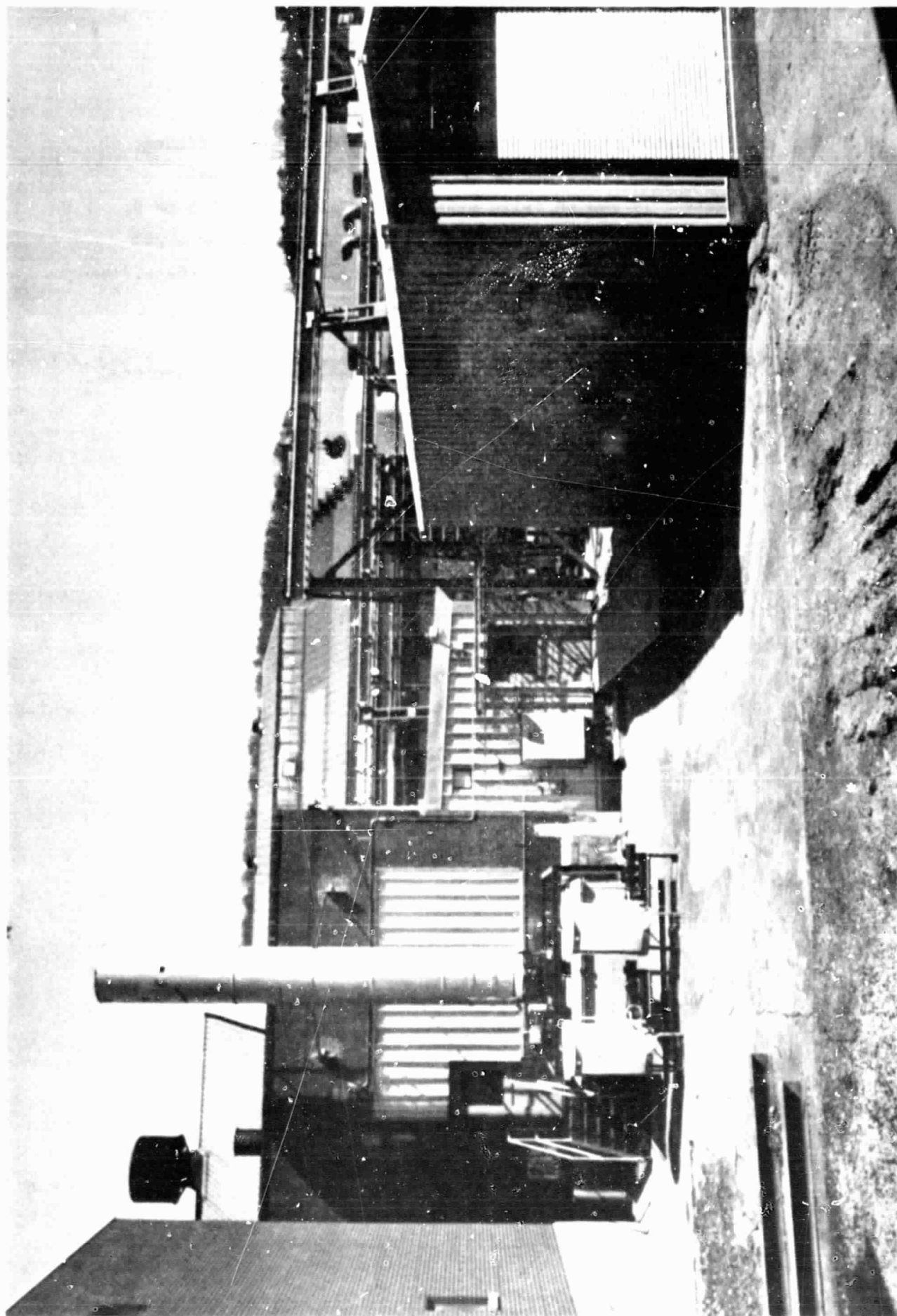
Figure FD-2 - Photograph Of The Gas Burnoff Stack And Effluent Treatment Tank (Installed Beneath Stack)

The water from the scrubbing system enters the effluent treatment tank where the pH of the water is continuously monitored. If the pH falls outside of a range from 5.5 to 9, then the pH is adjusted automatically by adding either a 20% solution of NaOH or a 32% solution of HCl. The pH of the effluent is monitored again just before it enters the drain.

Installation of the Effluent Disposal System was completed in October, 1979.

4.10 Gas Burnoff Stack

The Westinghouse Arc Heater process for producing silicon
utilizes hydrogen gas as a heat transfer medium. After passing
through the reactor and scrubber the hydrogen exits the process
and must be disposed of. The purpose of the burnoff stack is
to burn the hydrogen gas as it leaves the system. The stack
as designed is a jacketed water cooled pipe approximately
3 feet in diameter and 25 feet high. The bottom and top
ends of this stack are open to the atmosphere. The exhaust
mixture of hydrogen and argon enters the base of the stack at
a central location and is ignited by an attached igniter
torch. Air for combustion is supplied by aspiration and natural
draft at the base of the stack. Figure (ED-2) in the Effluent
Disposal Section of this report includes a photograph of the
gas burnoff stack.

Installation of the gas burnoff stack including igniter
was completed in February of 1979. Operation of the stack
during the December 8, 1979 reactant test proved to be both
safe and reliable.

4.11 Decontamination and Safety

The objective of this task is the elimination of personal injuries, occupational diseases, or property damage resulting from accidents, work exposures, or the products produced. To achieve this objective the following was proposed:

- Provide safe and healthful working conditions to the maximum extent practicable for all employees.

- Make available safety devices and personal protective equipment whenever their use was warranted.

The equipment that was purchased and installed can be divided into two categories. First, there is equipment for system safety or general safety of personnel, equipment, and facilities, and second is the equipment or devices for specific personal safety. In the category of system safety is emergency ventilation equipment in the silicon tetrachloride pump room, the sodium room, the silicon test cell and the blowout panels in the silicon test cell. Also in this category are the hydrogen gas and oxygen concentration detection and alarm units located in the $SiCl_4$ storage and pump areas, the sodium pump room and the silicon test cell. The ventilation equipment is required because of the highly reactive nature of sodium and silicon tetrachloride should these materials come in contact with the environment. The blowout panels and the hydrogen gas detector are required because of the explosive potential of small concentrations of hydrogen in air. The oxygen level detector is required to insure there is a sufficient quantity of oxygen in the air to support life. Argon is heavier than air, does not support life, and could collect in low or stagnant parts of the buildings should a leak occur. The fire fighting

equipment located in each room of the Arc Heater Laboratory includes fire extinguishers for fighting general fires, electrical fires and liquid metal fires. This equipment is also considered part of system safety. The last item in the system safety category is the "Emergency Shutdown Circuit" that interlocks all the subsystems together in such a manner that by activating any one of the four emergency stop buttons all systems are placed in a fail safe mode and shut down automatically. The emergency stop buttons are located on each of the four control panels (electrical, sodium, silicon tetrachloride, and main process).

In the category of personal safety, each operator was issued appropriate safety equipment including hard hat with face shield, safety goggles, safety glasses, and a chemical type respirator. In addition, each operator was issued a complete set of protective clothing appropriate for the particular material being handled, i.e., leather suits for working around liquid sodium, and vinyl suits for working around $SiCl_4$. Also given to each operator was a copy of the Safety Manual written for the JPL Project. There are also available two self-contained respirators with air tanks. One is located in the sodium control room the other is in the main control room.

To insure continuity of the two safety categories, two operator safety training sessions were conducted. The first was conducted on October 10, 1979 at the (W) R&D Center and the second was conducted on October 11, 1979 at the (W) Arc Heater Laboratory. A copy of the agendas for these training sessions is shown in Figures (DS-1) and (DS-2). In addition, the Westinghouse East Pittsburgh in plant fire fighting personnel were also given training in fighting liquid sodium fires and shown the location of all fire fighting equipment within the Arc Heater Laboratory.

OPERATOR TRAINING SESSION I

8:30 A.M. - October 10, 1979
Building 303 - R&D Center

Safe Handling Of Sodium & NaK ----------------------------- A. R. Keeton

    Properties
    Health Hazards
    Fire Hazards --- Demonstration
    Protective Clothing
    First Aid
    Handling Of Small & Large Spills
    Emergency Procedures

Safe Handling Of Silicon Tetrachloride --------- G. C. Burrow, P. A. Ciarelli

    Properties
    Health Hazards
    Handling
    Protective Clothing
    First Aid
    Handling Of $SiCl_4$ Spills
    Opening $SiCl_4$ Closed Systems
    Emergency Procedures

Figure DS-1

OPERATOR TRAINING SESSION II

8:30 A.M. - October 11, 1979
MX-10 Lab, East Pittsburgh

Arc Heater & Reactor System ----------------------------------- T. N. Meyer

    Precautions During Assembly & Disassembly

Effluent Disposal --------------------- ----------------------- J. W. George

    Scrubber, Demister & Piping
        Precautions During Disassembly
    Handling HCl & NaOH
    Health Hazards
    Protective Clothing
    First Aid
    Igniter-Pilot
        Operation
        Fire Hazard-Propane

Electrical System --- P. E. Martin

    General Precautions
    Specific Hazards
    Location Of Main Breakers

Gas System -- J. W. George

    Argon & Hydrogen
        Properties
        Health Hazards
        First Aid
        O_2 & H_2 Sensors
        Fire Hazards
        Precautions-Operations
        Location Of Main Hand Valves

Cooling Water System -- J. W. George

    General Precautions
    Maintenance
    Location Of Shutoff Valves
    Backup System Function

General Emergency Procedures -------------------------- J. W. George, T. N. Meyer

    Before, During & After Operation
    Effect & Consequences

Figure DS-2

Installation of all safety equipment and apparatus was completed in October 1979.

5. <u>TESTING</u>

5.1 <u>Procedure Manuals</u>

Three procedure manuals were prepared for this project to
insure a safe and reliable testing program. The specific manuals
are 1) a safety manual, 2) a system operational manual, and 3) an
analytical procedures manual. The safety manual encompasses all
phases of system and personnel safety in terms of sodium handling,
$SiCl_4$ handling, high temperature systems, electrical systems,
gas systems, mechanical systems, personnel protection, fire
safety, decontamination, emergency situation procedures, etc.
This manual served as the document for training the system
operators.

The operation manual details procedures for checkout,
start-up, test operation, shutdown and post test operation of the
subsystems and overall experimental verification system. This
manual was also used for operator training.

Finally the analytical manual describes the methods,
procedures and requirements for evaluating the silicon system.

5.2 Shakedown Tests

Initial shakedown tests of the subsystems began in early 1979. Tests were conducted on the gas, cooling water, electrical, and associated control and instrumentation systems. The reactor and burnoff stack were operated together for the first time in late spring of 1979 on a mixture of hydrogen and argon but no arc power. No leaks were detected in the reactor and the burnoff stack performed satisfactorily. Shakedown testing of the arc heaters/ reactor proceeded with an electrical power input level of 100 kW to 125 kW. Initially the arc heaters were run on pure argon only. A second run made with power to the arc heater used a mixture of hydrogen and argon gases (i.e., in the 0.5 H_2:1 Ar to 1 H_2:1 Ar range) and a power level of 300 kW to 750 kW. The variable power levels were obtained by varying the output voltage of the generator and changing the gas composition and flow rate. The arc heater/reactor was operated successfully for a period of 2 hours during this second run.

During August 1979 another set of gas only tests was conducted to continue shakedown of the arc heater/reactor, the gas, water and the control and instrumentation systems. The tests were used to determine operation characteristics of the arc heaters and to establish optimum flow rates and gas ratios. Following this series of tests it was determined that the capability of the liquid argon evaporators had to be increased in size and the regulators for the argon supply had to be changed to increase capacity. In addition one of the two hydrogen regulators at the tube trailer had to be replaced due to leaking. Also noted during testing was a malfunctioning of the igniter in the gas burnoff stack. The original igniter had a flame monitoring and relighting circuit that would attempt to relight the igniter flame if it should go out. This circuit began malfunctioning and after several repair attempts, it was replaced with a thermocouple device that monitors

the flame and shuts off the propane supply to the igniter and
energizes partial system shutdown if the temperature drops below a
preset point. The igniter must be manually lighted or relighted.

In September 1979 an arc heater/reactor test was conducted
with the arc heater running for a period in excess of 3 hours.
Examining data from this test, it was determined that the thermal
efficiency of the arc heaters was marginal. Two additional
gas only arc heater tests were conducted in October 1979 to verify
this finding. The power per arc heater was varied from 380 kW
to 530 kW with gas flows ranging from 56 scfm (1.6 m^3/min) to
112 scfm (3.2 m^3/min) and 4 H$_2$:1 Ar gas mixture. The results
verified the findings made in September and the arc heaters were
modified by placing a graphite liner in the bore of the electrodes
to reduce heat loss to the cooling water and to improve heat
transfer from the arc to the gas. In November 1979 a single
modified arc heater was successfully tested in the reactor. The
ports in the reactor for the other arc heaters were blanked off.
During the test the flow of hydrogen and argon gas was varied
from 60 scfm (1.7 m^3/min) to 80 scfm (2.3 m^3/min). An arc power
level of 575 kW was attained and a thermal efficiency exceeding
70% was achieved. The maximum gas temperature was determined to
be about 4000°K.

Based on the success of the November test a full system test
was scheduled and conducted on December 8, 1979. It was planned
to run the arc heaters at a combined power level of 1500 kW, a
gas flow rate of 255 scfm (7.2 m^3/min), a gas ratio of 4 H$_2$:1 Ar,
and a reactant feed rate equivalent to a production rate of
100 pounds (45.4 kg) of silicon per hour. In order to preheat
the reactor prior to injecting reactants, the arc heaters were
run for approximately 1 1/2 hours at a power level of 1500 kW,
a gas flow rate of 254 scfm (7.2 m^3/min) and a gas ratio of

4 H_2:1 Ar. During this time period, the reactor inside wall temperature did not go above approximately 900°K, but it was decided to go ahead with the injecting of the reactants. However, after having run the motor/generator set to provide 1500 kW of power to the arc heaters during the preheat period, the temperature of the motor was precariously close to the thermal trip point and the trip energized. Therefore, the power to the arc heaters was reduced slightly to approximately 1400 kW before introducing the reactants.

While the reactor was being preheated, the sodium and $SiCl_4$ flows were placed in the recirculating mode and the rates adjusted to 50% of the desired production rate of 100 pounds (45.4 kg) per hour of silicon.

Injection of $SiCl_4$ into the reactor was initiated first. The flow rate stabilized within two minutes and then the sodium was introduced. The flow rate of sodium also stabilized very quickly and both reactant flow rates were increased to 100%. Reactants were injected at the 100% rate for approximately 33 minutes when the automatic shutdown circuit was energized and the power to the arc heaters was turned off. Also the two reactarts were directed from the reactor into a recirculating mode. After a review of the alarm circuit and the apparatus, it was concluded that the gas exhausting from the demister was carrying over water into the exhaust pipe. The gas flowing thru this pipe produced a slugging that splashed water onto the thermocouple detecting the flame in the burnoff stack. The cooled thermocouple normally indicative of a "flameout" caused the shutdown. The arc heaters were restarted with no difficulty and run for a period of approximately one half hour without reactants to drive off any unreacted materials in preparation for disassembly of the reactor. Following this period, power to the arc heaters was stopped and the reactor was allowed to cool. The reactor was

cooled by purging with argon gas and allowing the cooling water
to run for about two hours. No disassembly was attempted until
the reactor and collector had cooled completely.

The Sodium Storage and Feed System operated in accordance
with the design specifications during the test. Sodium was
injected for approximately 33 minutes at a flow rate of 310 lb./hr.
to 335 lb./hr. (140 kg/hr. to 152 kg/hr.). The slight variation
in flow rate during injection of the sodium is believed to have
been caused by fluctuations in pressure within the reactor. To
produce atomization of the sodium, argon was supplied to the sodium
nozzle at a rate of 40 scfm (1.1 m^3/min). The injection temperature
of the sodium ranged from 190°C to 235°C. Prior to the start of
injecting sodium into the reactor, the programmable controller
that was programmed to control the temperature of the sodium system
malfunctioned and it was necessary to switch to manual control.
However, this inconvenience did not cause any problems during
the test. Switching the flow of sodium from the recycle mode to
the inject mode and back to recycle was done with no problem, but
it must be done with the flow controller in the manual mode.

The $SiCl_4$ Storage and Feed System functioned as planned.
Silicon tetrachloride was introduced into the reactor first,
followed by sodium approximately two minutes later. The $SiCl_4$
was injected for slightly less than 36 minutes at a rate of
605 lb./hr. (274.4 kg/hr.). Although the flow rate in the recycle
mode showed some instability, once the $SiCl_4$ was placed in the
injection mode the flow rate became very stable and easy to control.
Switching the flow from the recycle mode to the inject mode and
back to recycle was accomplished without problems and only minimal
variation in the flow rate.

In general, the system as a whole operated extremely well

during the test and those operational problems noted can be readily corrected.

5.3 Data Acquisition and Analysis

Data acquisition was accomplished with an Acurex Autodata-Nine data logger capable of collecting data on one hundred channels. The data collected in raw form was printed as either volts or millivolts on paper tape and stored simultaneously on magnetic tape. The magnetic tape was subsequently processed via a computer program to expedite data reduction and subsequent analysis.

During the reactant test, the data logger was run continuously and a complete scan of all points was made every 43 seconds. Data analysis was done using a typical single data scan. Figure DA-1 is a printout of a single data scan without reactants and Figure DA-2 is a scan with reactants. Each scan looks at one hundred channels numbered zero (000) thru 99 (099). The data that is recorded on the magnetic tape is recorded as volts or millivolts. A computer program written at the Westinghouse R&D Center converts the data to engineering units, identifies the sensor number and describes its function.

In addition to the data logger, Penn Environmental Consultants, Inc. were contracted to collect samples from the effluent treatment system and to monitor and sample the gas entering the burnoff stack during the reactant test. They were to then analyze these samples and report the pH, chloride content, sodium content and silicon content.

Table DA-1 is a summary of the data gathered from the gas only portion of the test run of December 8, 1979. The list headed "Calculated" is the set of conditions required to achieve the desired end results. The list headed "Actual" is, of course, the set of conditions that was actually achieved.

CHANNEL NUMBER	MAG TAPE	ENGINEERING UNITS	SOURCE	DESCRIPTION OF SOURCE
001	40.71 MV	95.71 GPM	CB-F1	M.P. HEAT EXCHG. FLOW RATE
002	35.76 MV	89.70 GPM	CB-F2	N.P. REACT EXCHG. FLOW RATE
003	33.08 MV	118.07 GPM	CB-F3	REACTOR OUTLET FLOW
004	78.95 MV	221.53 GPM	CB-F4	ARC HEATER OUTLET FLOW
005	65.78 MV	41.78 GPM	CB-F5	STACK COOLING WATER (INLET)
006	95.00 MV	40.00 DEG. C	NAK-T2	NAK TEMP INLET (NAK HEATER)
007	53.00 MV	53.00 DEG. C	NAK-T1	NAK TEMP OUTLET (NAK COOLER)
008				
009				
010	1.388 V	11.828 DEG. C	CB-T1	CITY WATER 6 AMSD MAIN
011	1.330 V	33.400 DEG. C	CB-T3	HEAT EXCHANGER OUTLET
012	1.336 V	38.100 DEG. C	CB-T4	REACTOR INLET TEMPERATURE
013	1.041 V	39.020 DEG. C	CB-T5	ARC HEATER INLET TEMPERATURE
014	2.708 V	47.700 DEG. C	CB-T6	ARC HEATER OUTLET TEMPERATURE
015	1.765 V	18.035 DEG. C	CB-T8	STACK OUTLET TEMPERATURE
016	1.055 V	61.475 DEG. C	CB-T9	SILICON COLLECTOR OUTLET TEMP
017	1.337 V	40.278 DEG. C	CB-T10	CYCLONE OUTLET TEMPERATURE
018	3.119 V	42.975 DEG. C	CA-T11	TRANSITION OUTLET TEMP
019	3.730 V	44.475 DEG. C	CA-T11	REACTOR OUTLET TEMP
020	3.080 V	45.650 DEG. C	CA-T12	REACTOR OUTLET TEMP
021	2.980 V	49.500 DEG. C	CA-T13	REDUCER OUTLET TEMP
022	1.145 V	53.475 DEG. C	CA-T14	PLENUM OUTLET TEMP
023	3.521 V	63.025 DEG. C	CA-T15	SODIUM INJECTOR OUTLET TEMP
024	3.682 V	67.050 DEG. C	CA-T16	U-TUBE (CYCLONE) OUTLET TEMP
025	3.041 V	40.850 DEG. C	CA-T17	U-TUBE (SCRUBBER) OUTLET TEMP
026	2.539 V	41.025 DEG. C	CA-T18	SILTLY INJECTOR OUTLET TEMP
027	2.075 V	38.350 DEG. C	CA-T19	VENTURI OUTLET TEMP
028	2.660 V	40.725 DEG. C	CA-T20	CYCLONE OUTLET TEMP
029	1.095 V	41.500 DEG. C	CA-T21	CYCLONE ADAPTOR
030	1.266 V	2.307 DEG. C	GS-T2	ARGON TEMP GAS BLEND PANEL
031		6.375 DEG. C	GS-T1	HYDROGEN TEMP GAS BLEND TEMP
032				
033				
034				
035				
036				
037				
038				
039				
040	1.452 V	14.520 PSIA	RP-P1	PRESSURE IN REACTOR (PLENUM)
041	1.005 V	18.050 PSIA	RP-P2	PRESSURE IN VENTURI THROAT
042	2.972 V	14.A60 PSIA	RP-P3	PRESSURE IN SCRUBBER
043	1.232 V	58.000 DEG. C	RS-T1	SODIUM INJECTION SECTION #1
044	1.046 V	12.025 DEG. C	RS-T2	
045	3.044 V	736.000 DEG. C	RS-T3	PLENUM #1
046	3.657 V	664.750 DEG. C	RS-T4	
047	2.252 V	313.000 DEG. C	RS-T5	REDUCER SECTION #1
048	1.820 V	205.000 DEG. C	RS-T6	
049	2.163 V	290.750 DEG. C	RS-T7	REACTOR CHAMBER #1
050	2.030 V	298.750 DEG. C	RS-T8	
051	1.188 V	90.425 DEG. C	RS-T9	#2
052	1.668 V	142.000 DEG. C	RS-T10	#3
053	1.088 V	214.500 DEG. C	RS-T11	#4
054	1.708 V	177.000 DEG. C	RS-T13	TRANSITION SECTION #1
055	1.750 V	187.500 DEG. C	RS-T14	#2
056	1.700 V	176.000 DEG. C	RS-T15	CYCLONE #1
057	1.688 V	172.000 DEG. C	RS-T16	#2
058	1.326 V	221.000 DEG. C	RS-T17	COLLECTOR #1
059	1.326 V	50.500 DEG. C	RS-T18	#2
060	1.231 V	57.750 DEG. C	RS-T19	TOP OF CYCLONE #1
061	1.314 V	79.750 DEG. C	RS-T20	TOP OF CYCLONE ELBOW #2
062	1.290 V	72.500 DEG. C	RS-T21	TOP OF SCRUBBER ELBOW #1
063	1.188 V	46.950 DEG. C		
064				
065				
066				
067				
068	0.772 V	135.440 PSIG	GS-PEB	ARGON ORIFICE PRESSURE
069	0.128 V	122.560 PSIG	GS-PEA	HYDROGEN ORIFICE PRESSURE
070				
071				
072				
073				
074				
075				
076				
077				
078				
079				
080	20.73 MV	621.90 VAC	API-24	ARC HEATER VOLTAGE 01A
081	22.35 MV	670.50 VAC	API-25	02B
082	25.38 MV	640.80 VAC	API-26	03C
083	25.20 MV	961.00 AMP	API-21	ARC HEATER CURRENT 01A
084	140.40 MV	924.00 AMP	API-22	02B
085	122.60 MV	980.00 AMP	API-23	03C
086	.29 MV	23.20 AMP	API-101	ARC HEATER 30 FIELD CURRENT
087	31.89 MV	1530.72 KW	API-27	ARC HEATER DC POWER
088	99.29 MV	79.14 MV	INTERVAL	CALIBRATION CHAN. DATA LOGGER
089				
090				
091	31.91 MV	.38 GPM	S-PEA	SILTLY FLOW RATE
092	22.46 MV	.36 GPM	NA-PEA	SODIUM FLOW RATE
093	30.92 MV	24.34 SCFM	A-PEA	ARGON FLOW RATE (INJECTION)
094	.05 MV	.05 PSIA	NA-PEB	EXP. PUMP DISCHARGE PRESSURE
095	93.93 MV	333.33 DEG. C	NA-T17	NA BASE TANK TEMPERATURE
096	66.77 MV	333.33 DEG. C	NA-T22	NA FEED INLET TEMPERATURE
097				
098				
099				

Figure DA-1 - Gas Only (No Reactants)

CHANNEL NUMBER	MAG TAPE	ENGINEERING UNITS	SOURCE	DESCRIPTION OF SOURCE
000				
001	41.71 MV	96.87 GPM	CB-F1	H.P. HEAT EXCHG. FLOW RATE
002	36.20 MV	90.25 GPM	CB-F2	L.P. HEAT EXCHG. FLOW RATE
003	31.74 MV	112.48 GPM	CB-F3	REACTOR OUTLET FLOW
004	78.22 MV	221.11 GPM	CB-F4	ARC HEATER OUTLET FLOW
005	68.38 MV	62.02 GPM	CB-F5	STACK COOLING WATER(INLET)
006	33.39 MV	33.39 DEG. C	NAK-T2	NAK TEMP INLET(NAK HEATER)
007	37.01 MV	37.01 DEG. C	NAK-T1	NAK TEMP OUTLET(NAK COOLER)
008				
009				
010	1.451 V	11.275 DEG. C	CB-T1	CITY WATER 6 INCH MAIN
011	2.644 V	38.400 DEG. C	CB-T2	HEAT EXCHANGER OUTLET
012	2.379 V	34.475 DEG. C	CB-T3	HEAT EXCHANGER OUTLET
013	2.603 V	40.375 DEG. C	CB-T4	REACTOR INLET TEMPERATURE
014	2.643 V	41.075 DEG. C	CB-T5	ARC HEATER INLET TEMPERATURE
015	2.973 V	49.325 DEG. C	CB-T6	ARC HEATER OUTLET TEMPERATURE
016	1.749 V	18.725 DEG. C	CB-T7	STACK OUTLET TEMPERATURE
017	3.138 V	53.450 DEG. C	CB-T8	SILICON COLLECTOR OUTLET TEMP
018	2.818 V	45.450 DEG. C	CB-T9	CYCLONE OUTLET TEMPERATURE
019	2.959 V	46.975 DEG. C	CB-T10	TRANSITION OUTLET TEMP
020	2.995 V	49.875 DEG. C	CB-T11	REACTOR OUTLET TEMP
021	3.092 V	52.300 DEG. C	CB-T12	REACTOR OUTLET TEMP
022	3.283 V	57.075 DEG. C	CB-T13	REACTOR OUTLET TEMP
023	3.433 V	60.625 DEG. C	CB-T14	REDUCER OUTLET TEMP
024	3.772 V	69.300 DEG. C	CB-T15	PLENUM OUTLET TEMP
025	3.912 V	72.800 DEG. C	CB-T16	SODIUM INJECTOR OUTLET TEMP
026	2.840 V	46.000 DEG. C	CB-T17	U-TUBE(CYCLONE) OUTLET TEMP
027	2.873 V	46.825 DEG. C	CB-T18	U-TUBE(SCRUBBER) OUTLET TEMP
028	2.612 V	40.300 DEG. C	CB-T19	SILTET INJECTOR OUTLET TEMP
029	3.193 V	54.825 DEG. C	CB-T20	VENTURI OUTLET TEMP
030	2.881 V	47.025 DEG. C	CB-T21	CYCLONE OUTLET TEMP
031	2.836 V	45.900 DEG. C	CB-T22	CYCLONE ADAPTOR
032	1.312 V	7.600 DEG. C	GS-T2	ARGON TEMP GAS BLEND PANEL
033	1.299 V	7.475 DEG. C	GS-T1	HYDROGEN TEMP GAS BLEND TEMP
034				
035				
036				
037				
038				
039				
040	1.487 V	14.870 PSIA	RP-P1	PRESSURE IN REACTOR(PLENUM)
041	2.810 V	28.100 PSIA	RP-P2	PRESSURE IN VENTURI THROAT
042	3.013 V	15.065 PSIA	RP-P3	PRESSURE IN SCRUBBER
043				
044	1.260 V	65.000 DEG. C	RS-T1	SODIUM INJECTION SECTION #1
045	1.049 V	12.225 DEG. C	RS-T2	#2
046	3.679 V	669.750 DEG. C	RS-T3	PLENUM #1
047	3.430 V	607.500 DEG. C	RS-T4	#2
048	2.328 V	332.000 DEG. C	RS-T5	REDUCER SECTION #1
049	2.027 V	256.750 DEG. C	RS-T6	#2
050	2.307 V	326.750 DEG. C	RS-T7	REACTOR CHAMBER #1
051	2.153 V	288.250 DEG. C	RS-T8	#2
052	1.233 V	58.250 DEG. C	RS-T9	#3
053	1.657 V	164.250 DEG. C	RS-T10	#4
054	2.109 V	277.250 DEG. C	RS-T11	#5
055	1.859 V	214.750 DEG. C	RS-T12	#6
056	1.950 V	237.500 DEG. C	RS-T13	TRANSITION SECTION #1
057	1.935 V	233.750 DEG. C	RS-T14	#2
058	2.766 V	467.000 DEG. C	RS-T15	CYCLONE #1
059	2.291 V	310.250 DEG. C	RS-T16	#2
060	1.483 V	120.750 DEG. C	RS-T17	COLLECTOR #2
061	1.343 V	85.750 DEG. C	RS-T18	TOP OF CYCLONE #1
062	1.594 V	148.500 DEG. C	RS-T19	TOP OF CYCLONE ELBOW #1
063	1.502 V	125.500 DEG. C	RS-T20	TOP OF CYCLONE ELBOW #2
064	1.378 V	94.500 DEG. C	RS-T21	TOP OF SCRUBBER ELBOW #1
065				
066				
067				
068	4.549 V	130.880 PSIG	GS-PEB	ARGON ORIFICE PRESSURE
069	4.291 V	125.820 PSIG	GS-PEA	HYDROGEN ORIFICE PRESSURE
070				
071				
072				
073				
074				
075				
076				
077				
078				
079				
080	20.46 MV	613.60 VAC	API-24	ARC HEATER VOLTAGE 01A
081	20.81 MV	-24.35 VAC	API-25	02B
082	19.71 MV	591.30 VAC	API-26	03C
083	117.10 MV	736.80 AMP	API-21	ARC HEATER CURRENT 01A
084	116.16 MV	9-5.28 AMP	API-22	02B
085	125.06 MV	9.0.25 AMP	API-23	03C
086	.32 MV	25.00 AMP	API-01	ARC HEATER DC FIELD CURRENT
087	28.77 MV	1380.98 KA	API-27	ARC HEATER DC POWER
088	99.84 MV	99.84 MV	INTERVAL	CALIBRATION CHAN, DATA LOGGER
089				
090				
091				
092	69.28 MV	.83 GPM	S-PEA	SIL-TET FLOW RATE
093	4.57 MV	.69 GPM	NA-PEA	SODIUM FLOW RATE
094	43.95 MV	35.16 SCFM	A-PEA	ARGON FLOW RATE(INJECTION)
095	14.36 MV	14.36 PSIG	NA-PEB	E.M. PUMP DISCHARGE PRESSURE
096	37.59 MV	187.95 DEG. C	NA-T17	NA BASE TANK TEMPERATURE
097	46.54 MV	232.73 DEG. C	NA-T22	NA FEED INLET TEMPERATURE
098				
099				

Figure DA-2 - Reactants Flowing

C-2

Table DA-1

Summary Of Data For Gas Only Tests

	Calculated	Actual
Power Input	1500 kW	1531 kW
Efficiency	70%–75%	70.8%
Gas Flow Rate		
Argon	51 CFM (1.44 m^3/min)	58 CFM (1.64 m^3/min)
Hydrogen	204 CFM (5.78 m^3/min)	198 CFM (5.61 m^3/min)
Total	255 CFM (7.22 m^3/min)	256 CFM (7.25 m^3/min)
Ratio	$4H_2$:1AR	$3.4H_2$:1Ar
Gas Temperature At Arc Heater Exit	3450°K–3500°K	3450°K

The efficiency reported is the thermal efficiency or amount of energy transmitted to the gas from the arc heaters and not lost to the walls of the arc heater compared to the electrical energy supplied to the arc. The flow rate of gas is the total flow of each gas to the three arc heaters over time and corrected to 70 degrees Fahrenheit and 1 atmosphere pressure. The ratio of gases is a mole ratio. The gas temperature is a calculated temperature and is inversely proportional to the heat loss from the gas to the cooling water and the mass of gas entering the arc heaters. Table DA-2 is similar to Table DA-1 except the reactant flow rates have been added. The rates listed under "Actual" are the rates that existed the instant the data was taken and will be slightly different over the entire test period. The reactant ratio like the gas ratio is expressed in moles.

Table DA-3 reports the products recovered at the skull wall and in the collector and the products determined to be in the effluent tank and in the gas stream to the burnoff stack. The quantity of product in the collector was determined by removing it from the crucible and weighing it. The mass of product collected as the skull wall was determined by removing samples of the wall from each section, determining their density, estimating the volume of material in each section and then calculating the mass from these two determinations. The amount of material in the effluent tank and stack gas was determined from the results of the analyses submitted by Penn Environmental Consultants, Inc. on the samples taken from these two areas.

Table DA-4 displays the mass balance both theoretical and actual. Also shown is the actual input of reactants and the theoretical total product yield from that input. Although insufficient

5-11

Table DA-2

Summary Of Data With Reactants

	Calculated	Actual
Power Input	1500 kW	1381 kW
Efficiency	70%-75%	70.5%
Gas Flow Rates		
Argon	51 CFM* (1.44 m³/min)	54 CFM (1.53 m³/min)
Hydrogen	204 CFM (5.78 m³/min)	205 CFM (5.81 m³/min)
Total	255 CFM (7.22 m³/min)	259 CFM (7.34 m³/min)
Ratio	4H₂:1Ar	3.8H₂:1Ar
Gas Temperature At Arc Heater Exit	3450°K-3500°K	3375°K
Reactants Flow Rates		
Na	328#/hr (148.8 kg/hr)	312#/hr (141.5 kg/hr)
SiCl₄	605#/hr (274.4 kg/hr)	612#/hr (277.6 kg/hr)
Ratio	4Na:1SiCl₄	3.8Na:1SiCl₄**

*Based on 1 atm pressure and 70°F (21.1°C)
**Based on single scan of data taken at time 13:21:57 12/8/79

Table DA-3

Products Recovered

Silicon Collector	110 lbs	(49.9 kg)
Skull Wall	159 lbs	(72.1 kg)
Total	269 lbs	(122 kg)

Product In Effluent

Effluent Tank	154 lbs	(69.9 kg)
Burnoff Stack	59 lbs	(26.8 kg)
Total	213 lbs	(96.6 kg)
Cumulative Total	482 lbs	(218.6 kg)

Percentage Of Theoretical Yield

Percentage Recovered	53%
Percentage In Effluent	42%
Total	95%

Table DA-4

Summary Of Data With Reactants

Mass Balance

Theoretical

$$4 \ Na + 1 \ SiCl_4 \longrightarrow 1 \ Si + 4 \ NaCl$$

Actual

$$*3.42 \ Na + 1 \ SiCl_4 \longrightarrow .86 \ Si + 3.42 \ NaCl + .14 \ SiCl_4$$
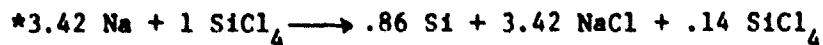
Actual Reactant Input			Theoretical Total Product Yield		
Na	160.5 lbs	(72.8 kg)	Si	49.2 lbs	(22.3 kg)
$SiCl_4$	346 lbs	(156.9 kg)	NaCl	408 lbs	(185 kg)
			$SiCl_4$	49.3 lbs	(22.4 kg)
Total	506.5 lbs	(229.7 kg)		506.5 lbs	(229.7 kg)

	Total Element Recovered (All Forms)**		% of Input
Si	52.3 lbs	(23.7 kg)	91.5%
Na	127.2 lbs	(57.7 kg)	79.3%
Cl	259.2 lbs	(117.6 kg)	89.8%

*Based on total material injected during the test on 12/8/79.
**Based on analyses by Penn Environmental Consultants, Inc.

sodium was supplied to react all the $SiCl_4$, additional silicon
will have been produced by reaction of the $SiCl_4$ with hydrogen.

$$SiCl_4 + 2H_2 \longrightarrow Si + 4HCl$$
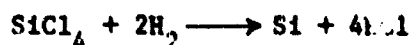
The "Total Element Recovered" reported on in Table DA-4 was
also derived from the analyses performed by Penn Environmental
Consultants, Inc. To determine the chloride content they use
a titrimetric procedure Standard Method 304. They report the
standard deviation for this method is ±3.3% and the error is
±2.9%. Sodium is quantified by atomic adsorption with a
reported error of ±10%. To quantify silicon, atomic absorption
was used on the soluble forms and gravimetric analysis used on
the insoluble forms with an error of ±5%. The cumulative error
of these test methods helps explain the difference between the
quantity of product recovered and found in the effluent and
that reported as Si, Na, and chlorides. Following is a summary
of the reports on samples taken during testing and submitted
by Penn Environmental Consultants, Inc.

The name such as "City Water" identifies where the sample
was taken and the time and date indicates when it was taken.
The nonfilterable residue is the dissolved solids and the
filterable residue is the solids that are gathered on the filter
paper.

City Water   Time – 8:30 A.M.   Date – 12/8/79

    pH 8.5
    Cl (mg/l) . . .   14
    Na (mg/l) . . .   31
    Si (mg/l) . . .   2.0

        Residue

        Nonfilterable (mg/l)   4
        Filterable (mg/l). 19.9

Effluent   Time - 1:05 P.M.   Date - 12/8/79

    pH 9.0
    Cl (mg/l) . . . 275
    Na (mg/l) . . . 173
    Si (mg/l) . . . 30.3

        Residue

            Nonfilterable (mg/l) 54
            Filterable (mg/l). 606

Effluent   Time - 1:20 P.M.   Date - 12/8/79

    pH 9.7
    Cl (mg/l) . . . 1350
    Na (mg/l) . . . 870
    Si (mg/l) . . : 148

        Residue

            Nonfilterable (mg/l) 308
            Filterable (mg/l). 2652

        In addition to the samples taken during testing, samples
from both the skull wall and the collector were submitted to
Penn Environmental Consultants, Inc. for determination of
Cl, Na and Si. Following is a summary of these analyses. Each
of the elements is reported as a weight percentage. As
explained previously, because of experimental error the percentages
will not necessarily total to 100%. To determine pH, 20 grams
of solid sample were added to 200 ml of distilled water.

        Reactor Section Inlet "E"   Date - 12/12/79

    pH 8.4
    Cl 33.2%
    Na 13.0%
    Si 46.7%
    C 1.2%

Reactor Section Inlet "H"   Date - 12/12/79

    pH 6.0
    Cl 68.6%
    Na 24.7%
    Si 10.5%

Silicon Collector

    pH 8.6
    Cl 65.8%
    Na 26.5%
    Si 8.2%

The sampling of the gases going to the burnoff stack was done by WFI Sciences Co. in conjunction with Penn Environmental Consultants, Inc. A port was provided in the exhaust pipe leading from the scrubber to the burnoff stack and a sampling probe was inserted into this port. The gas was sampled continuously throughout the test. The sample gas was passed through a series of cold traps where the condensables were taken out of the gas. The chemical analysis was performed by Penn Environmental Consultants, Inc. on the condensables and is reported in Table DA-5.

As reported in the section on the Plasma Reactor, one of the objectives of the reactor wall design was to create balanced cooling to maintain the thickness of the silicon skull wall reasonably close to the desired value of 2 cm. The expected heat transfer rates were determined in the condensation calculations and are plotted as a function of reactor axial position in Figure DA-3. For comparison the actual heat transfer rates, with reactants flowing at the conditions given in Table DA-2, are also plotted on this figure. Since (1) the equilibrium thickness of the skull wall had not been established (i.e., a inside diameter of 15cm) and (2) the power level of 1400 kW was well below the anticipated level of approximately 1800 kW, the calculations were not done for the conditions of data reported. Thus, the comparison can be expected to provide only qualitative information. The third line plotted on Figure DA-3 is the heat flux with arc heater power

Table DA-5

CHEMICAL ANALYSIS

ARC HEATER - SILICON PRODUCTION REACTOR
AIR QUALITY TESTS
WESTINGHOUSE ELECTRIC CORPORATION
DECEMBER 8, 1979

UNITS	Gr/SDCF*	Gr/ACF**	Lb/Hr	%
TOTAL PARTICULATE	16.46	14.89	98.3	---
Silicon	5.16	4.67	30.8	31.34
Sodium	3.64	3.29	21.7	22.12
Chloride	1.02	0.92	6.1	6.21
Carbon	0.02	0.02	0.1	0.11
TOTAL	9.84	8.90	58.7	59.78
INSOLUBLE PARTICULATE	5.89	5.33	35.2	---
Silicon	4.79	4.34	28.7	81.4
Sodium	0.22	0.20	1.3	3.7
Chloride	0.03	0.03	0.2	0.52
Carbon	0.02	0.02	0.1	0.31
TOTAL	5.06	4.59	30.3	85.93
SOLUBLE PARTICULATE	10.57	9.56	63.1	---
Silicon	0.36	0.33	2.2	3.44
Sodium	3.42	3.10	20.4	32.4
Chloride	0.99	0.90	5.9	9.38
TOTAL	4.77	4.33	28.5	45.22

*Gr/SDCF: Grains per standard cubic foot
**Gr/ACF : Grains per actual cubic foot

Figure DA-3 - Heat Flow vs. Reactor Length
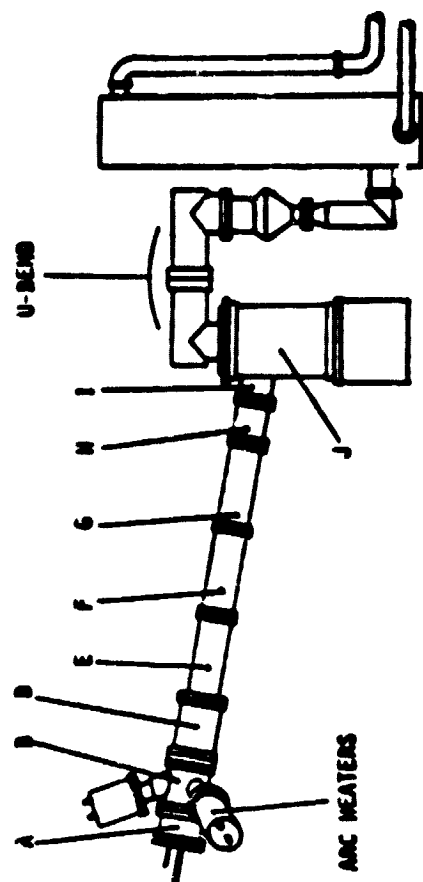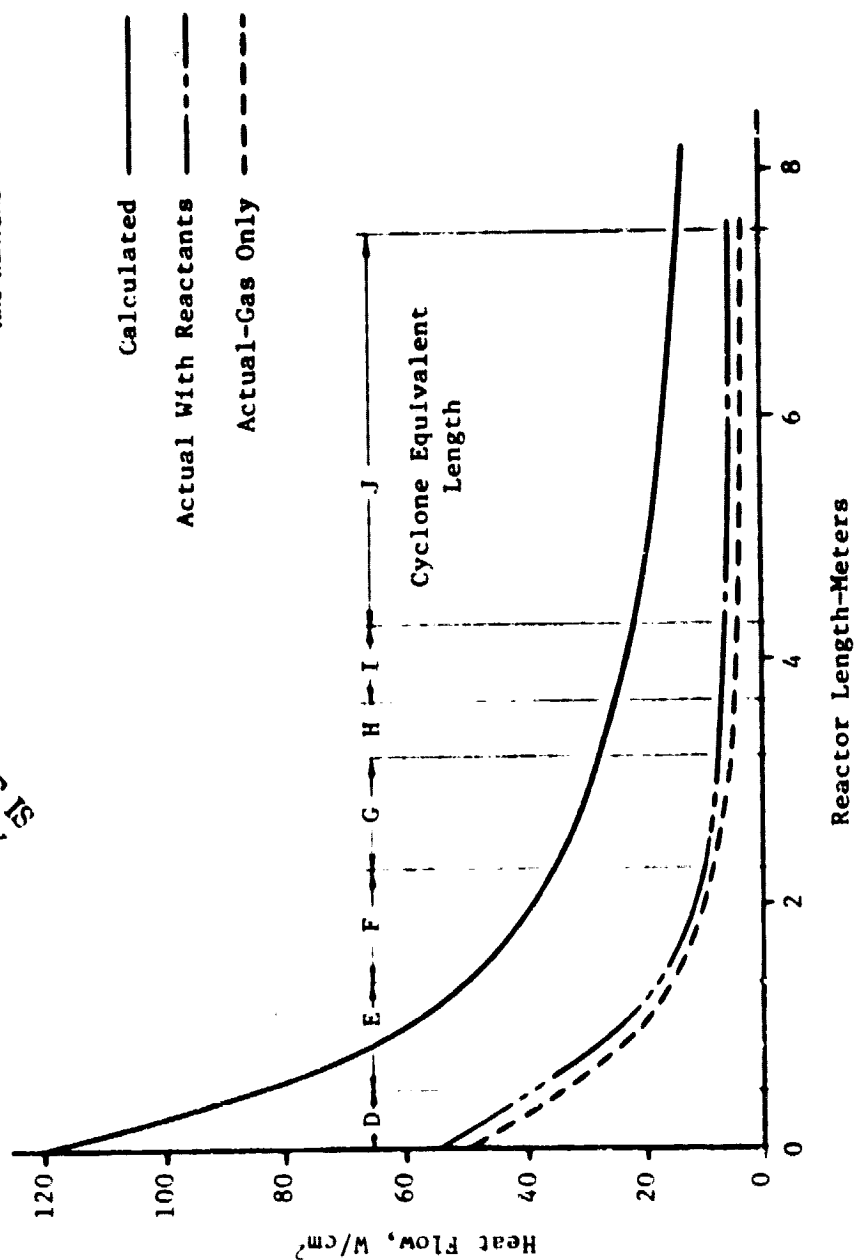
but no reactants flowing (gas only) and with conditions as given in Table DA-1. The expected heat flux was based on an assumed product stream temperature of 3500°K and a wall temperature of 1685°K (1412°C). Figure DA-4 and DA-5 show the calculated wall temperature (T_W), the liner outside wall temperature T_0, the heat loss to the cooling water (Q), and the heat flux at the wall (q), without reactants flowing and with reactants flowing at each reactor section and conditions given in Tables DA-1 and DA-2. The wall temperature was calculated using the following formula:

$$T_w = T_o + \frac{Q \ln R_2/R_1}{2\pi KL}$$

where T_w = Inside wall temperature of reactor liner (°C)

T_o = Outside wall temperature of reactor liner (°C)

Q = Heat loss to cooling water (kW)

R_1 = Inside radius of reactor liner (cm)

R_2 = Outside radius of reactor liner (cm)

L = Length of reactor section (cm)

K = Thermal conductivity (w/cm °C)

   = 1.4 w/cm°C for Sections A, B, and J

   = 0.5 w/cm°C for Sections D, E, F, G, and H

The average outside wall temperature (T_o) is determined from the measurements made by thermocouples numbered RS-T1 thru RS-T21. The heat loss to the cooling water, Q, is calculated from the temperature rise of the cooling water for a particular section as determined from the cooling water temperature measurements CW-T1 thru CW-T22 and the amount of water flowing per unit time in the reactor (CW-F3). Table DA-6 shows the heat lost to the cooling water in each of the reactor sections.
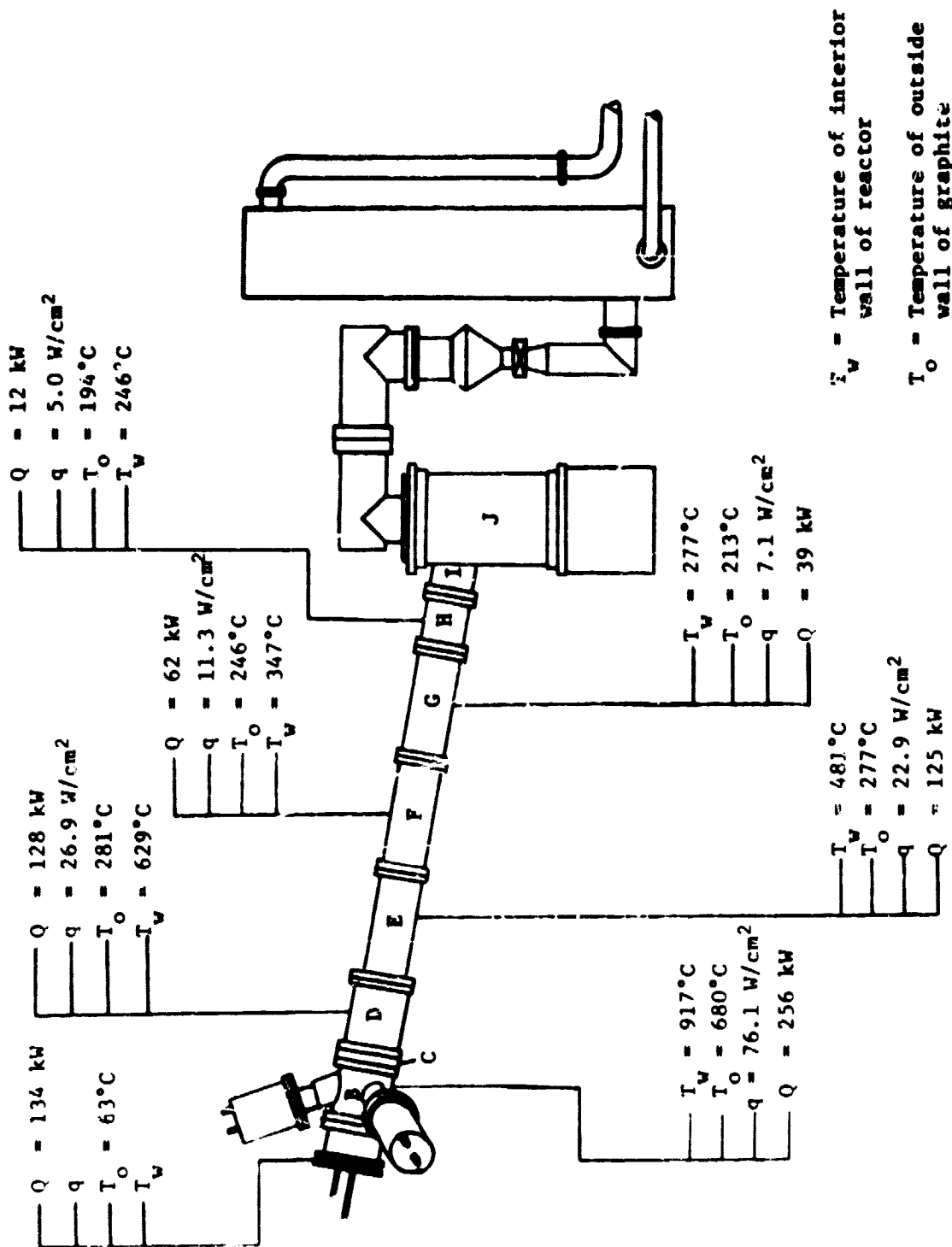
Figure DA-4 — Calculated Thermal Data Gas Only (without Reactants)

Q = 12 kW
q = 5.0 W/cm^2
T_o = 194°C
T_w = 246°C

Q = 62 kW
q = 11.3 W/cm^2
T_o = 246°C
T_w = 347°C

Q = 128 kW
q = 26.9 W/cm^2
T_o = 281°C
T_w = 629°C

Q = 134 kW
q
T_o = 63°C
T_w

T_w = 277°C
T_o = 213°C
q = 7.1 W/cm^2
Q = 39 kW

T_w = 481°C
T_o = 277°C
q = 22.9 W/cm^2
Q = 125 kW

T_w = 917°C
T_o = 680°C
q = 76.1 W/cm^2
Q = 256 kW

T_w = Temperature of interior wall of reactor

T_o = Temperature of outside wall of graphite

Q = 18 kW
q = 7.6 W/cm^2
T_o = 236°C
T_w = 313°C

Q = 65 kW
q = 11.9 W/cm^2
T_o = 282°C
T_w = 388°C

Q = 104 kW
q = 21.9 W/cm^2
T_o = 294°C
T_w = 577°C

Q = 80 kW
q =
T_o = 65°C
T_w =

T_w = 348°C
T_o = 277°C
q = 8.6 W/cm^2
Q = 47 kW

T_w = 543°C
T_o = 307°C
q = 26.5 W/cm^2
Q = 245 kW

T_w = 862°C
T_o = 639°C
q = 71.3 W/cm^2
Q = 240 kW

T_w = Temperature of interior wall of reactor

T_o = Temperature of outside wall of graphite

Figure DA-5 – Calculated Thermal Data with Reactants

Table DA-6

Heat Loss With Reactants
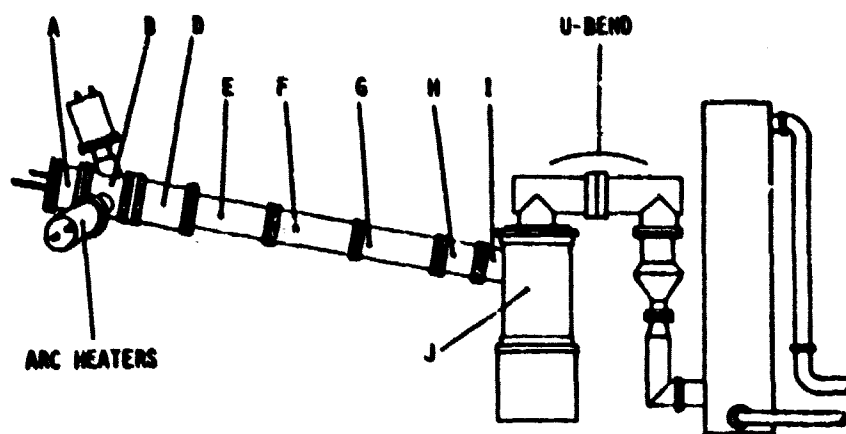
	kW
INPUT	1361
LOSS IN ARC HEATERS	408
Section A	80
Section B	240
Section D	104
Section E	145
Section F	65
Section G	47
Section H	18
Section I & J	144
U-Bend	21
Total Loss In Reactor	1272

5.4 Product Characterization

The test conducted on December 8, 1979 was directed to the operation of the entire experimental verification unit with reactant flow ($SiCl_4$ and Na) to produce the initial silicon product. As mentioned previously, the subsystems functioned properly in accordance with the design specifications. A reactant flow was achieved equivalent to the production of 100 lb_m/hr of silicon, thus equalling the designed rate. System control and operation were excellent including the control of both the sodium and $SiCl_4$ input flows. Based upon observations of the reactor system internals following the test, a skull of product material was formed of increasing thickness which verified the reactor design analysis and kinetics work.

Samples of the product produced during the test were taken at various locations along the reactor length (see Section 5.5). These skull wall samples were removed with ease from the graphite reactor liners. All internal reactor parts (graphite liners) were observed to be in excellent condition following the test, i.e., no erosion or chemical attack was noted. These liners would be reusable if any future tests are to be conducted.

Since this initial shakedown test of the system was to verify subsystem operation and produce a product from the Na + $SiCl_4$ reaction, the purity of the silicon product was not critical for this first test. Therefore, the reactor liners were not washed following the gas only shakedown test and a castable refractory was used in place of a quartz crucible in the silicon collector. As a result, the silicon collected exhibited a higher level of impurities than would normally be expected. Also, as can be seen in Section 5.3 on Data Acquisition and Analysis, the inside wall temperature of the

reactor liners did not achieve the required temperature of
1412°C to effect separation of the silicon produced from the
sodium chloride coproduct. Therefore, the majority of the
silicon produced was in the form of a brownish amorphous silicon
that was condensed from the gas stream along with the sodium
chloride and collected on the walls of the reactor, cyclone,
and collector. Three samples removed from the reactor and
collector for analysis indicate (1) 47% silicon by weight for
the skull sample near the $SiCl_4$ injection ring, (2) 10.5%
silicon for the skull sample just upstream of the cyclone and
(3) 8.2% silicon for the material removed from the top surface
of the collector crucible. Two small, silver-gray samples of
material found in the crucible were analyzed and found to be
97% silicon. A complete analysis was done on this material and
the results are shown in Figure PC-1. The extremely high content
of copper can be explained by the fact that many hours of shakedown
testing were done to determine the operating parameters for the
arc heaters. During these tests, various H_2-Ar gas ratios were
used in addition to various arc heater field coil current settings.
As a result, some operating conditions caused erosion of the
copper electrodes to a greater extent than other settings. It is
believed that copper was deposited on the walls of the reactor and
since the reactor was not thoroughly cleaned prior to the reactants
test, the copper was contained in the silicon product. Cleaning
the reactor walls will mitigate this problem.

As previously stated in Section 5.2 on Shakedown Testing,
during testing of the arc heaters it was determined that to
improve the arc heater performance (i.e., higher arc voltage) the
inside diameter of the electrodes must be reduced. The most
expedient way to reduce this diameter was to place a graphite liner
in the electrodes. This was done and as a side effect the carbon
content of the silicon was raised to a level higher than

Element	Al	Ag	B	Ba	Be	Bi	Ca	Cd	Co	Cr	Cu	Fe	Ga	Ge
"A" piece	.003	<.001	<.001	<.01	<.001	<.001	<.01	<.003	.002	<.003	>1	.02	<.003	<.003
"B" piece	.002	<.001	<.001	<.01	<.001	<.001	<.01	<.003	.003	.01	>1	.003	<.003	<.003

Element	K	Li	Mg	Mn	Mo	Na	Nb	Ni	P	Pb	Sb	Si	Sn
"A" piece	<.003	<.001	.01	.003	<.001	.03	<.003	.001	<.03	<.01	<.03	Major	<.003
"B" piece	<.003	<.001	.001	.003	<.001	.06	<.003	.002	<.03	<.01	<.03	Major	<.003

Element	Sr	Ti	V	W	Zn	Zr	C
"A" piece	<.003	.001	<.001	—	<.003	.002	1.53 / 1.51
"B" piece	<.003	.001	<.001	—	<.003	.001	4.7 / 4.7

REMARKS: Values are wt. %

ANALYSIS REQUEST WESTINGHOUSE FORM 42909A

Book No. 2CE...
Page 125
Engr. H.L....

Figure PC-1 – Analysis Of Silicon Collector Product, 2 Samples

normally expected. This problem would be eliminated by using reduced-sized copper electrodes.

Other impurities are attributed to (1) the use of a castable refractory material as a crucible in the silicon collector and (2) inadequate separation between the Si and NaCl because of the lower temperatures in the reactor, cyclone, and collector. As discussed in the Process Evaluation section, the temperature can be increased by increasing the insulation between the graphite liner and the cooling water shell. Of course, the quartz crucible would be used for product collection in any future testing to preserve product purity.

Thus, b making some minor design changes, it is indicated that high purity silicon can be produced with the Westinghouse Arc Heater process.

5.5 Disassembly and Decontamination

The effort required to disassemble, decontaminate and inspect the reactor interior following operation was far less than had been expected. The individual sections including the collector were carefully removed with ease. Figure (DD-1) is a photograph of the reactor section "H" looking downstream. As can be seen in Figure (DD-1), sections of the skull were readily separated from the graphite liner interior. Decontamination was not necessary because unreacted materials were not found in any of the disassembled sections. The skull formed on the inner wall over the entire region between the $SiCl_4$ injection nozzles and the silicon collector. The skull thickness increased from about 1.6 mm thick at the first section downstream from the $SiCl_4$ injection to 9.5 mm thick for the section just upstream of the cyclone separator. With the exception of the sodium nozzle reflector cup being lost in the high temperature environment, the reactor internal parts are in excellent condition.

As determined from the injection studies, the nozzle produces an excellent spray pattern without the cup. The graphite near the sodium injection was not noticeably damaged due to any graphite/sodium interaction. This was a serious concern of JPL. The ease of disassembly will greatly facilitate and reduce the cost of testing if potential follow on tests are conducted and a lower maintenance cost is projected during full scale operation of a system.

To date, the entire skull wall has not been removed from the reactor, cyclone, and U-bend sections. However, the crucible and insulating brick have been removed from the collector shell and the product material has been removed from the disposable crucible. A total of 49.7 kg (110 pounds) was removed from the crucible and placed in polyethylene bags. From this total, two-1 kg
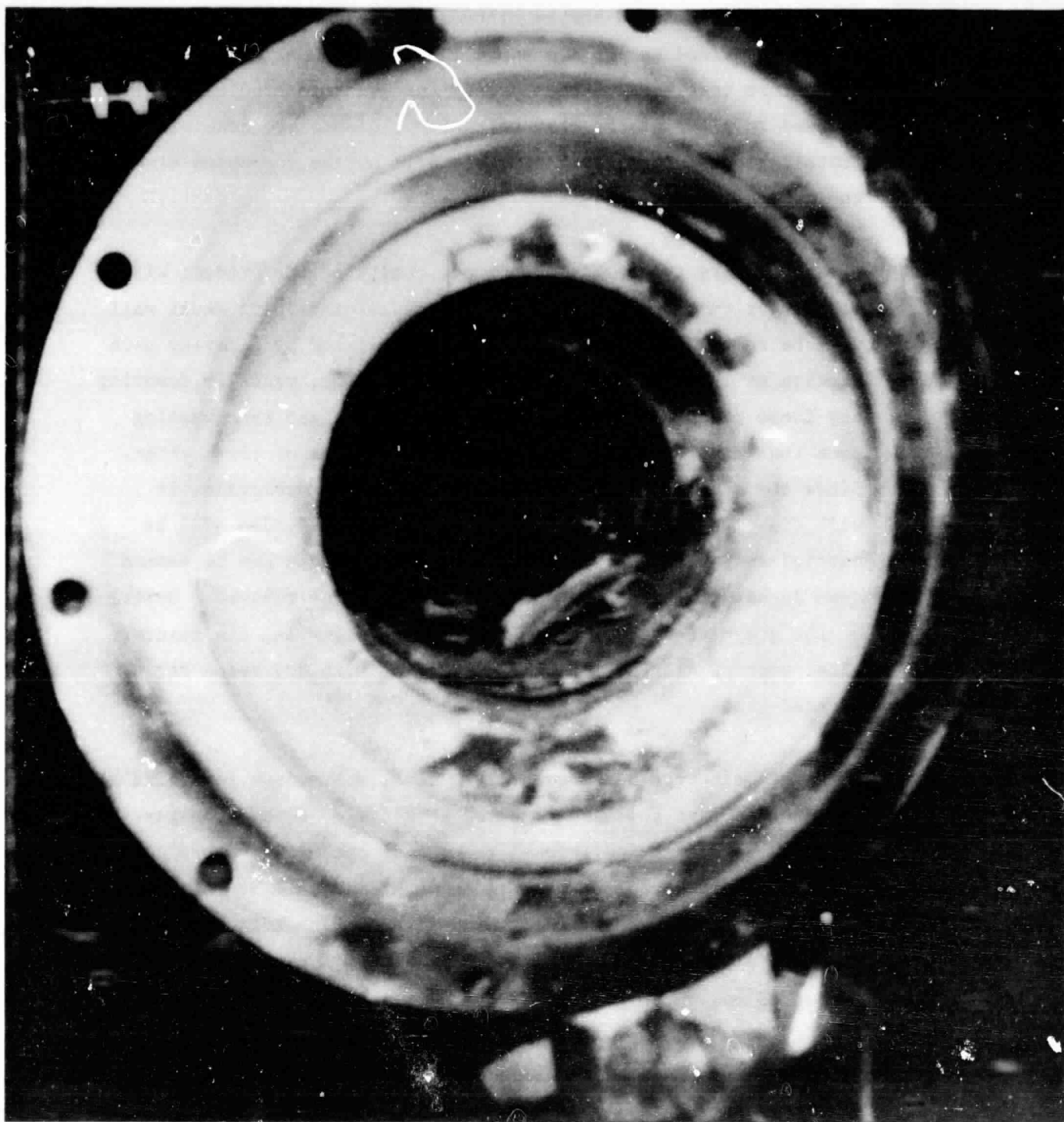
5-28

Figure DD-1 - Photograph Of Reactor Section H, Inside Diameter,
Looking Downstream Toward Cyclone

samples were selected and submitted to JPL. Photographs of the
samples provided to JPL are shown in Figures (DD-2 & 3). For
any future test work, a high purity fused quartz crucible would
be used in place of the cast refractory, disposable crucible.
Installation of the quartz crucible will not be a problem since
the design is complete.

If future testing is performed, purity of the product will
be a major concern. Therefore, the present remaining skull wall
must be removed. This can best be accomplished by removing each
section of the reactor from the mounting frame, manually removing
any loose pieces of material from the section and then washing
down the interior of the graphite with a stream of clean water.
Since the skull is composed primarily of sodium chloride, it
will dissolve readily in the water and the insolubles will be
carried away with the running water. The cyclone can be washed
down in-situ with the product collector and top removed. Drying
of the graphite can be accomplished by reassembling the reactor
after washing all sections and purging it with dry argon for
several hours.

Following the December 8, 1979 test, the sodium feed line
was drained into the base tank and back filled with argon gas.
However, before any additional testing is conducted, where purity
will be of prime concern, the sodium system should be completely
drained including the base tank and flushed with high purity
sodium. Also the sodium injection nozzle will have to be removed,
inspected and decontaminated before reinstalling.

The $SiCl_4$ feed system also was drained of $SiCl_4$ and purged
with argon gas following the December 8, 1979 test. Also one
of the ten injection nozzles was removed and inspected for damage
and/or contamination. No apparent damage was found and the filter
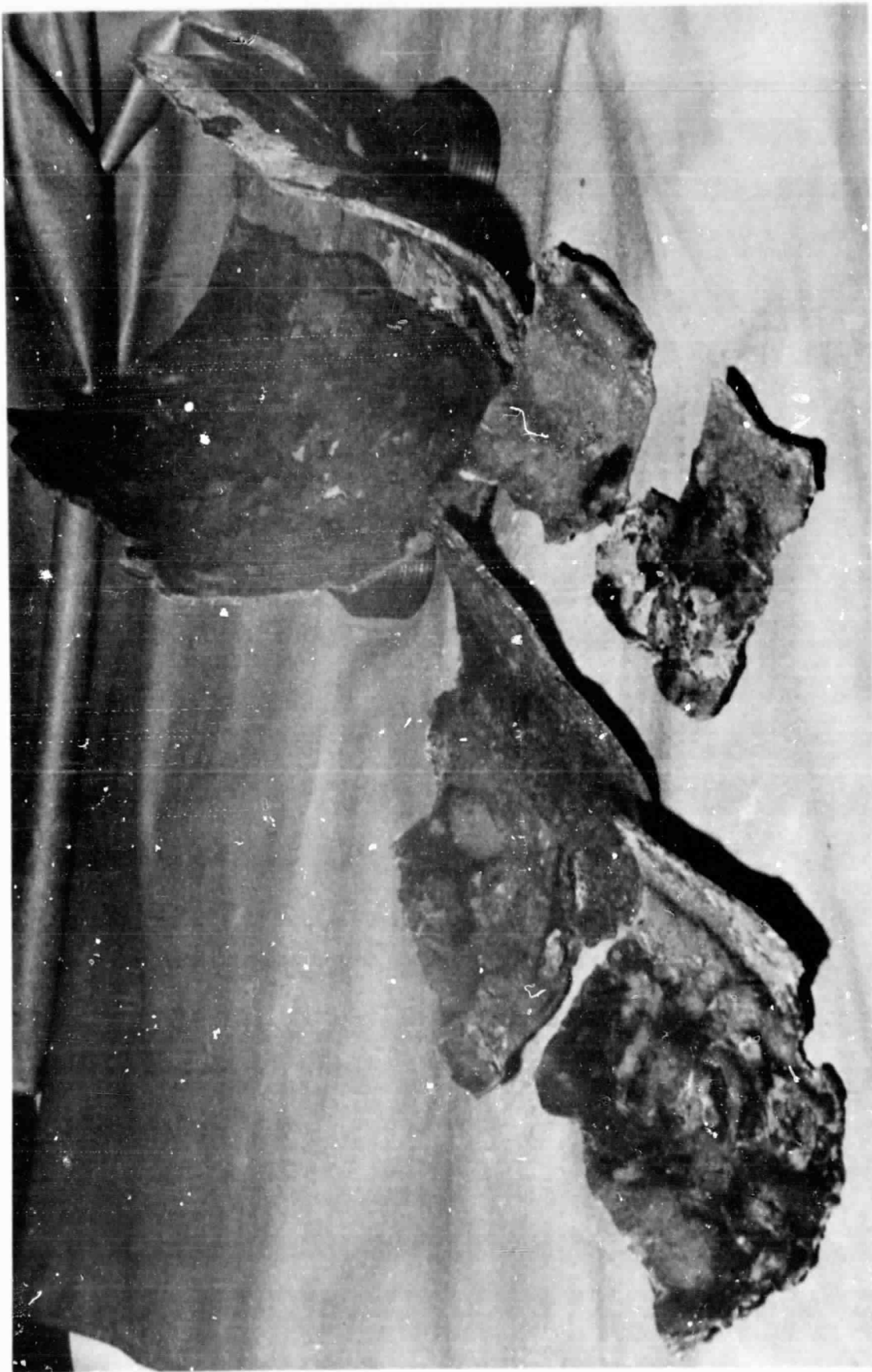
Figure DD-2 - Photograph of Silicon Product Sample
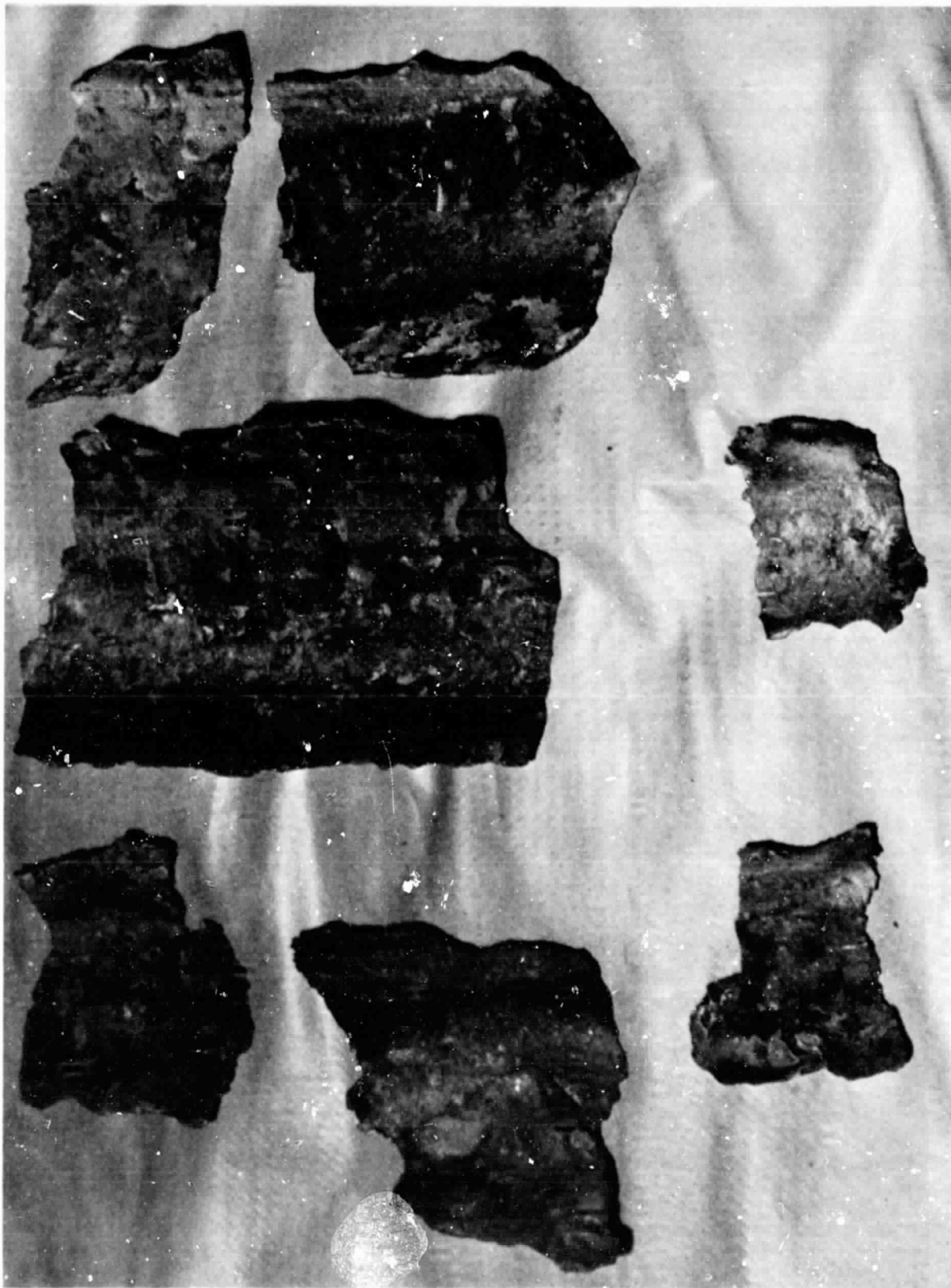
Figure DD-3 — Photograph of Silicon Product Sample

screen internal to the nozzle was clean indicating no moisture or other contaminants had entered the $SiCl_4$ system. The $SiCl_4$ Storage and Feed System has been pressurized with an argon cover gas since the December 8, 1979 test and requires no further decontamination. There are no foreseeable major problems to bring the two reactant feed systems back on stream for continuing the test program.

5.6 Component Evaluation

1. Electrical System

The electrical system performed satisfactorily during the shakedown test and no major problems were encountered. 1500 kW of power was supplied to the arc heaters during the 1 1/2 hour preheat period. However, the temperature of the motor to the motor-generator set at Station #1 of the Westinghouse High Power Laboratory began approaching the high temperature trip point at that power output level. Subsequently, the output was cut back to 1400 kW. This did not cause any problem since the resultant gas temperature was very near to that theoretically required. Before any future testing, the possibility of raising the high temperature trip point should be investigated.

2. Control and Instrumentation

The Control and Instrumentation System met the design objectives and functioned well during the shakedown test. Reactant flow was controlled at a sodium to $SiCl_4$ ratio of 3.8:1 with 4:1 being stoichiometric. Gas flow was also controlled very close to the required mole ratio of 4:1 for hydrogen to argon. The pH control equipment associated with the water treatment was used to monitor the pH and not to control it during the reactant test. For future longer term testing the pH control equipment (chemical additive pumps) will need to he calibrated for control purposes. However, it appears that the pH will stay within the 5.5 to 9.0 limits established by the local environmental authority without chemical additives. This was verified by pH readout instruments and subsequent analyses of the effluent.

The programmable controller that was to automatically control the heating of the sodium system malfunctioned just

prior to the start-up of the reactant test, however, it has
since been repaired and is ready for future testing. If the
system has reached operational temperature, manual operation
is not difficult.

3. Cooling Water

The Cooling Water System performed without fault during
the reactant test. However, it was discovered during the
cool down phase following testing that the large solenoid
valves in the emergency cooling loop were sticking. This
has been an intermittent problem with the valves. They
have been taken apart, cleaned and reassembled several times.
It is strongly suggested that the valves be replaced with
pneumatically operated ball valves. Failure of valves to
operate properly could cause serious damage to the reactor.

4. Gas System

The Gas System performed extremely well during the
reactant test. It would be desirable to increase flow
capability.

5. Plasma Reactor

The Plasma Reactor functioned well during the reactant
test. The wall temperature of the graphite liner did not
approach the $1685°K$ required to achieve separation of the Si
and NaCl. As a consequence, the two products condensed out
of the product stream together. This problem can be corrected
by machining down the outside diameter of the graphite liner
and adding a layer of insulating material between the graphite
and the reactor shell wall. On the positive side, the
disassembly of the reactor was performed with ease and with
no damage to the liners. Decontamination was not necessary

because the reaction had sufficient time to go to completion
and a skull wall was formed as predicted. The interior of
the reactor is in extremely good condition and can be
reassembled for a future test after easily removing the
existing skull wall.

6. $SiCl_4$ Storage and Feed System

The $SiCl_4$ Storage and Feed System functioned well during
the reactant test and no major problems were encountered.
Control of the flow rate is somewhat erratic in the recycle
mode, but it smooths out in the inject mode. Correction of
the erratic flow is a matter of back pressure regulation
and can be done with the existing equipment. No major
modifications of the system are anticipated.

7. Sodium Storage and Feed System

With the exception of the malfunctioning programmable
controller, the Sodium Storage and Feed System functioned
as specified by design. The controller which was designed
to control the temperature and heating cycle of the drums
of sodium stopped functioning and control was switched to the
manual mode for the reactant test. No problems were
experienced with the manual mode. The programmable controller
has since been repaired and is ready for use. The sodium
injection nozzle reflector cup was lost in the high temperature
environment during the reactant test but as determined from
the injection studies, the nozzle produces an excellent
spray pattern without the cup. After decontaminating the
sodium nozzle the system will be ready for additional
testing.

8. Silicon Collection

The Silicon Collector functioned as designed with no problems being encountered during testing. For future testing a fuzed quartz crucible will be used in place of the refractory crucible.

9. Effluent Disposal System

Generally the Effluent Disposal System functioned well during the reactant test. The gas stream was adequately cooled upon passing thru the venturi scrubber (94°F) and no large quantities of particulate were observed leaving the stack. However, the gas stream passing through the packed column portion of the scrubber carried water into the exhaust piping leading from the column to the stack. As the piping filled with water a slugging action took place which eventually caused water to be splashed onto the igniter thermocouple. The cooled thermocouple normally indicative of a "flameout" condition caused a shutdown. A simple drain added to the bottom of the exhaust piping will readily eliminate this problem in the future.

The water treatment tank operated without incident, but as mentioned under Instrumentation and Control, the pH control equipment was used only to monitor the pH and not for control. In the future the equipment (chemical additive pumps) will need to be calibrated for pH control purposes. However, it appears that the pH is maintained within the 5.5 to 9.0 limits established by the local environmental authority without chemical additives.

10. Gas Burnoff Stack

The Gas Burnoff Stack functioned well during the reactant

test. The only problem encountered involved the igniter
thermocouple described under the Effluent Disposal System
section. As a precaution against water splashing on the
thermocouple in the future, the thermocouple will be
relocated and shielded against the possibility of being
splashed.

11. Decontamination and Safety

Decontamination of the reactor was not necessary because
the reaction between $SiCl_4$ and Na essentially went to
completion. The sodium system will need to be flushed
with high purity sodium before future high purity testing
is undertaken.

No incidents involving safety were experienced during
the reactant testing.

6. REFERENCES

1. M. G. Fey, et al, Quarterly Report, DOE/JPL 954589-77/4, Silicon
    Materials Task, October-December, 1977.

2. M. G. Fey, et al, Quarterly Report, DOE/JPL 954589-78/5, Silicon
    Materials Task, January-March, 1978.

3. M. G. Fey, et al, Quarterly Report, DOE/JPL 954589-78/6, Silicon
    Materials Task, April-June, 1978.

4. M. G. Fey, et al, Quarterly Report, DOE/JPL 954589-78/7, Silicon
    Materials Task, July-September, 1978.

5. C. Y. Ho and R. W. Powell, The State Of Knowledge Regarding The
    Thermal Conductivity Of The Nonmetallic Elements, Proceedings of
    the Seventh Conference, 1967; National Bureau of Standards
    Special Publication 302, 1968.

6. W. R. Runyan, Silicon Semiconductor Technology, McGraw-Hill Book Co.,
    1965, pg. 219.

7. Materials Properties Data Book, NERVA Program, Aerojet-General Corp.,
    1966, pg. VII-B-10, 11A.

The following Appendices have been attached to document the final results of project subtasks not directly addressed in the main body of the final report. These project subtasks include such areas as product separation analysis, injection techniques, economics, kinetics experiments, etc.

APPENDIX A

PRODUCT SEPARATION ANALYSIS

PRODUCT SEPARATION ANALYSIS

1. Task Description

The objective of this task was to determine a reactor design which provides effective silicon product separation. The product separation and reactor design were analyzed for two modes of operation. The first mode (homogeneous reaction) examines silicon product separation via condensation following a high temperature reaction producing superheated silicon vapor. The second approach depends upon a heterogeneous reaction mode which permits a two-phase product separation.[1] The results of the condensation mode were considered to be the more attractive design/operation mode and served as the basis for the system design.[2]

2. Summary

The analysis of the condensation mode provided heat transfer and silicon transport to the reactor walls as functions of the axial length. Rates of heat and mass transfer to the reactor wall were based upon developing turbulent boundary layer transport relations for tube flow. Since the condensation occurs before the silicon reaches the wall, a boundary layer analysis was developed to estimate this effect upon the heat and mass transfer. The results of the condensation model indicated that over 80% of the silicon can be removed from the reactor described in this report.[2]

The second approach depends upon a heterogeneous reaction mode which permits effective product separation. The analysis examined a partial low temperature reaction followed by a high temperature thermal treatment process step.[1] The first step is a partial reaction of reactants forming particles (molten and/or solid) of Na, NaCl, and Si. The second step immerses these particles in an arc heated gas stream to vaporize the Na and NaCl from the silicon and react the remaining Na and $SiCl_4$. The final step involves the collection of small product particles formed in the final reaction by those formed in the initial step. If necessary, it is possible to introduce seed particles to expedite the collection. This mode is weakened by the uncertainty in the effectiveness of the particle formation and collection mechanisms.

3. Homogeneous/Condensation Mode

An analysis is developed to determine silicon mass and heat transport to the reactor wall. The product flow is turbulent and initially all vapor. Plug flow is utilized for the mass and energy balance in the stream where composition and properties are governed by thermodynamic equilibrium. It can be shown that the momentum losses are negligible for the conditions considered. The analog between mass and heat transfer is invoked. Published

-1-

values for the transport coefficients of developing turbulent flow in a tube are utilized.[1,2] These values are modified to account for the effect of silicon vapor condensation within the boundary layer. This modification is developed by an analysis utilizing a constant property universal velocity profile. Thus, the mass transfer is written as:

$$\frac{d\dot{m}}{dZ} = - Nu' D_{Si-M} \pi C \left(X_{Si} - X_{Si_w} \right) R_m$$

The mass transfer correction, R_m, resulting from condensation within the boundary layer is represented[2] as:

$$R_m = \frac{T_s - T_w + \frac{\lambda}{C_p} W_s}{\left[\left(\frac{dT}{dW} \right)_* + \frac{\lambda}{C_p} \right] \left(W_s - W_w \right)}$$

Similarly, the energy balance is written in terms of the temperature gradient[2] as:

$$\frac{dT_s}{dZ} = \frac{1}{\dot{m}C_p} \left[- Nu \, K\pi \, (T_s - T_w) \, R_Q - \frac{d\dot{m}}{dZ} \left(h_{Si(v)_{T_s}} - h_{Si(\ell)_{T_w}} \right) \right]$$

The heat transfer correction, R_Q, resulting from condensation within the boundary layer[2] is represented as:

$$R_Q = \frac{T_s - T_w + \frac{\lambda}{C_p} W_s}{T_s - T_w}$$

To numerically solve these equations, the transport properties and stream composition must be known. After the initial elemental composition is given (e.g., 2.0 Na, 2.0 Cl, 0.5 Si, 3.31 H_2, 0.83 Ar), the properties are functions of temperature, pressure and fraction of silicon (β) remaining in the stream. The pressure is assumed constant at one atmosphere and this is later verified

to be a valid assumption. The transport properties are calculated for a specific number of "β" values and the results inputed to the computer. The computer uses an interpolation routine to determine properties for any temperature or "β" required in the numerical solution.

The results of the numerical solution are shown in Figures 1 & 2 for a 10 cm and 15 cm diameter tube, respectively. The heat flux to the wall, the fraction of the silicon remaining in the stream, and the nondimensional position of silicon condensation are represented as functions of axial position, X. Both figures indicate over 80% of the silicon is removed after an axial flow length of approximately 5 meters. As a result of this calculation showing satisfactory silicon removal, the heat flux was utilized for the 15 cm diameter reactor to establish the proper wall thermal impedance (e.g., see text on reactor design).

For a detailed development of the modification coefficients, the transport relations used and the general analysis, the reader is referred to References 1 & 2.
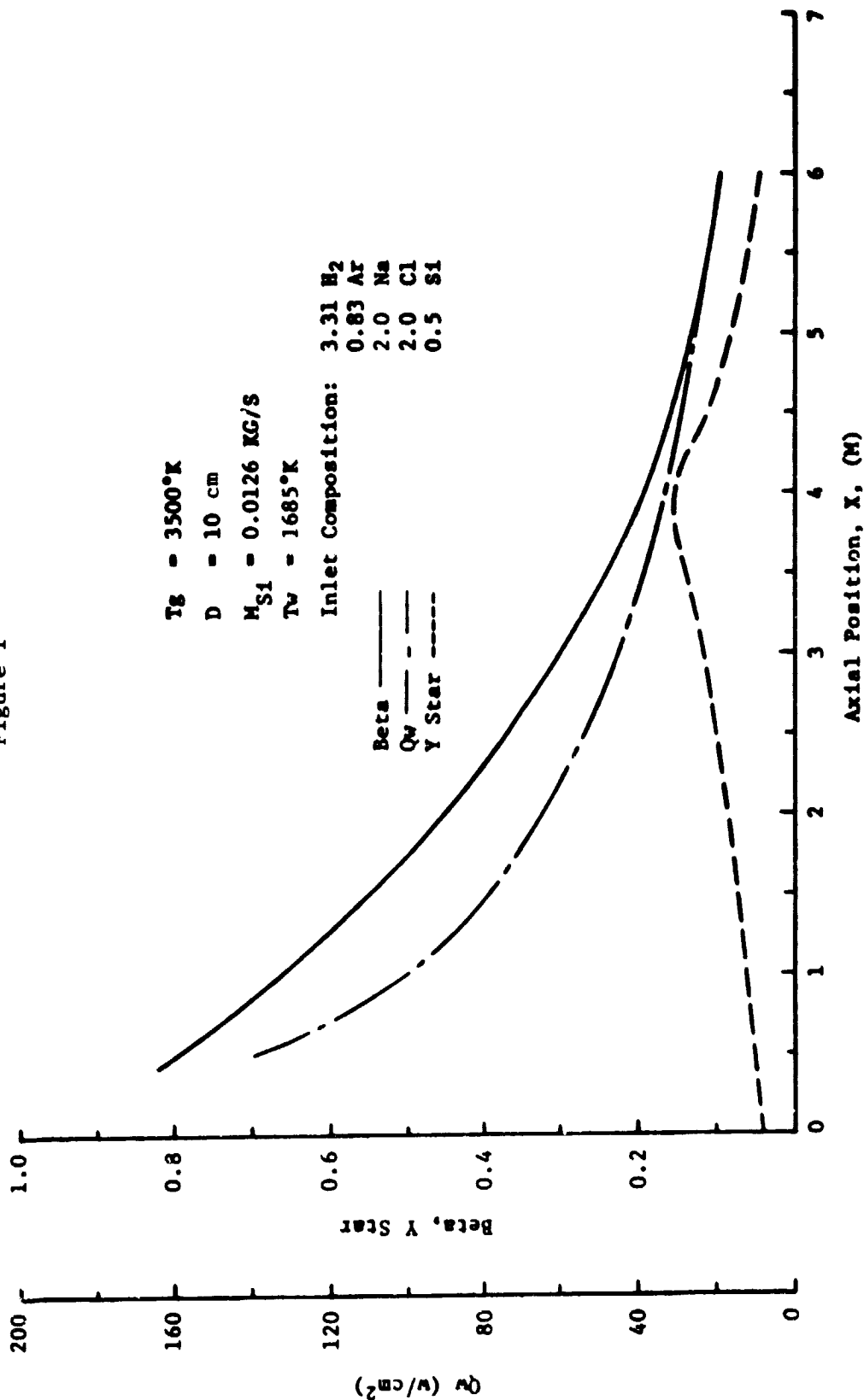
4. Heterogeneous Reaction

The basic chemical reaction in the arc heater reduction of silicon tetrachloride by sodium can occur in a heterogeneous manner. Two heterogeneous paths are possible in which product separation appears experimentally feasible. First, gaseous $SiCl_4$ and sodium vapor, which have been produced by injecting liquid sodium droplets into an arc heated gas stream, react on the surface of seed particles to produce liquid silicon and gaseous sodium chloride. The relatively large molten droplets of silicon are then separated by inertial means. Second, gaseous $SiCl_4$ reacts at low temperatures on the surface of liquid sodium droplets to produce solid silicon and sodium chloride. The product particles are then entrained into an arc heated gas stream where (1) any unreacted sodium is vaporized; (2) sodium chloride is melted and vaporized; and (3) silicon is melted. The result of this thermal treatment results in relatively large droplets of silicon which can be collected inertially.

4.1 Partial Low Temperature Reaction

The low temperature partial reaction is modelled for sodium droplets entering a tubular reactor in the presence of hydrogen, argon and $SiCl_4(v)$. The droplets are assumed to be distributed uniformly throughout the gas and moving axially along the cylindrical reactor tube at the same velocity as the gas. Similar calculations involving the motion of droplets in a stream indicate that momentum equations defining differences in velocity between these small particles and the gas can be

Figure 1

$Tg = 3500°K$
$D = 10$ cm
$M_{Si} = 0.0126$ KG/S
$Tw = 1685°K$

Inlet Composition:
3.31 H_2
0.83 Ar
2.0 Na
2.0 Cl
0.5 Si

Beta ———
Qw —·—
Y Star ----

Axial Position, X, (M)

Beta, Y Star

Qw (w/cm²)

Beta: Is the ratio of total silicon mass flow to the initial value (X = 0)
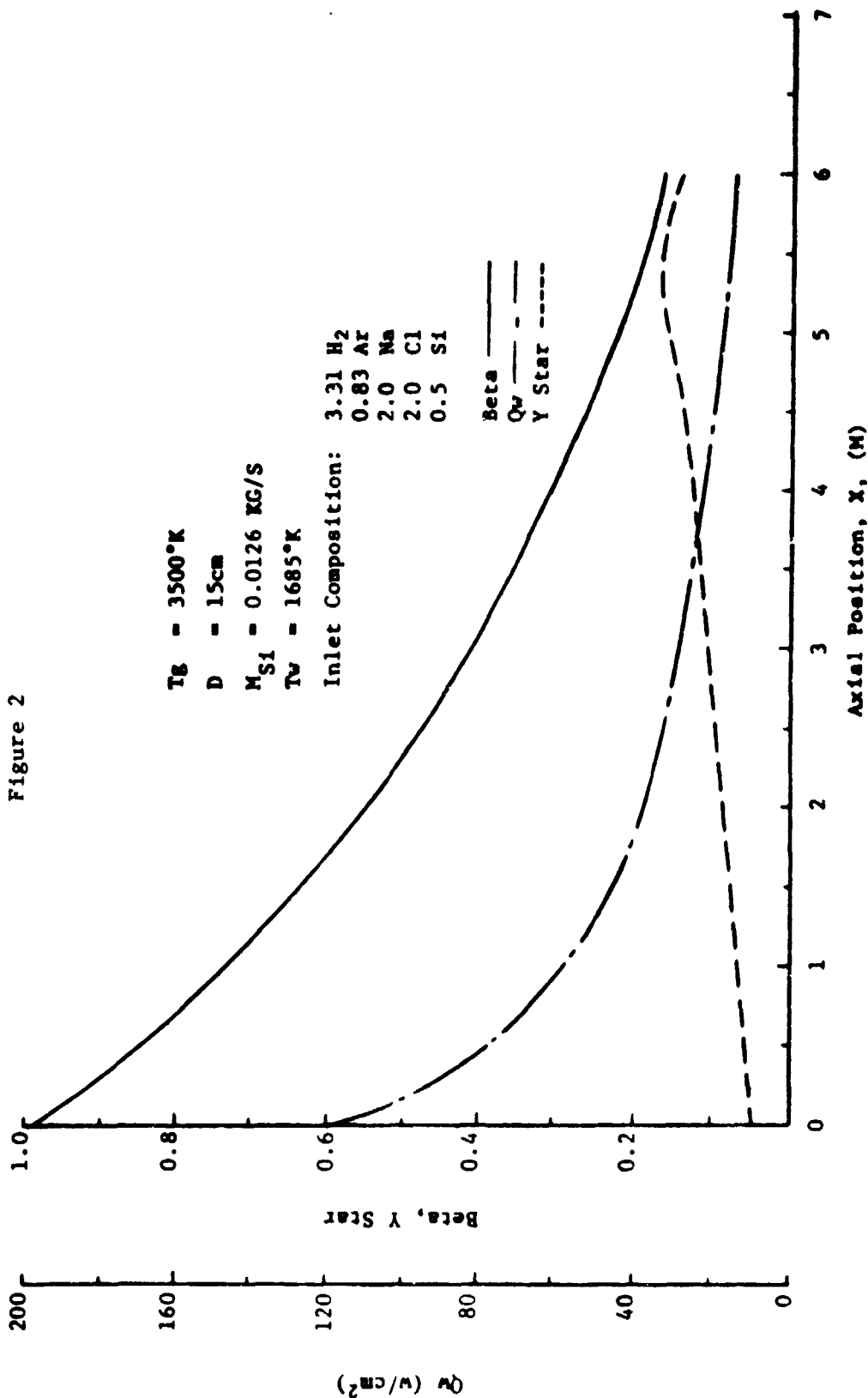**Y Star:** Is the ratio of radial distance from the wall where transition from saturation to superheat occurs to the reactor radius.
Qw: Is the reactor wall heat flux (w/cm²)

Dependence Of Product Separation (Beta), Condensation Location (Y Star) And Heat Flux (Qw)

Upon Axial Position (Equilibrium)

Figure 2

Figure 2

T_g = 3500°K

D = 15cm

M_{Si} = 0.0126 KG/S

T_w = 1685°K

Inlet Composition: 3.31 H_2
0.83 Ar
2.0 Na
2.0 Cl
0.5 Si

Beta ———
Qw —·—·—
Y Star ------

Beta: Is the ratio of total silicon mass flow to the initial value (X = 0)
Y Star: Is the ratio of radial distance from the wall where transition from saturation to superheat
occurs to the reactor radius.

Qw: Is the reactor wall heat flux (w/cm²)

Dependence Of Product Separation (Beta), Condensation Location (Y Star) And Heat Flux (Qw)
Upon Axial Position (Equilibrium)

Axial Position, X, (M)

Beta, Y Star

Qw (w/cm²)

-5-

neglected. The $SiCl_4(v)$ diffuses to the droplet surface and reacts to form NaCl and Si which remain part of the droplet. For this exothermic reaction, heat is liberated and results in heating of the droplet and some heat transferred to the surrounding gas and wall. For a given initial fraction, f, of $SiCl_4$ required for stoichiometry, the extent of the reaction is determined as a function of axial movement. The reaction rate is assumed to be limited only by the gaseous diffusion to the droplet. The extent of the reaction is shown in Figure 3 as a function of the axial distance. For fractions of $SiCl_4$ greater than 0.1, the droplet heats to a level where sodium vaporization takes place. It is seen from Figure 3, that $SiCl_4(v)$ has completely reacted in an axial distance of 5 cm for a $SiCl_4$ fraction of 0.1. In the mass transfer relations, the high mass transfer corrections for diffusion[1, 2] are taken into account. To examine the detailed relations incorporated into the model the reader is referred to References 1 & 2.

4.2 Thermal Treatment

After this initial reaction is completed, 10% of the sodium has been reacted and the particles contain the remaining 90% of the sodium and the products NaCl plus Si. This stream of droplets is then entrained into a highly arc heated gas stream of H_2 and Ar at 3500°K. The heated stream affects the vaporization of Na, the melting of NaCl, the vaporization of NaCl, and finally the melting of the remaining silicon. These stepwise processes are illustrated by the results shown in Figure 4. The heat and mass transfer between the droplet and the gas are governed by coefficients corrected for the high mass transfer rates. It is seen from Figure 4 that pure molten silicon droplets are obtained in a distance of less than 50 cm from the injection of the initial sodium droplets. It is assumed that these initial droplets are sufficient in size and number to collect the submicron particles formed between the $SiCl_4(v)$ and the Na(v). In both analyses, the rules governing mass and energy conservation are upheld for the gas. Similarly, the basis governing mass, energy and momentum are upheld for the droplet. As in the case of the condensation model, the results of the analysis indicate the pressure is essentially one atmosphere everywhere and the momentum equation for the gas need not be involved. Again the reader is referred to References 1 & 2 for a more detailed account of these analyses.

Diameter = 30.48cm

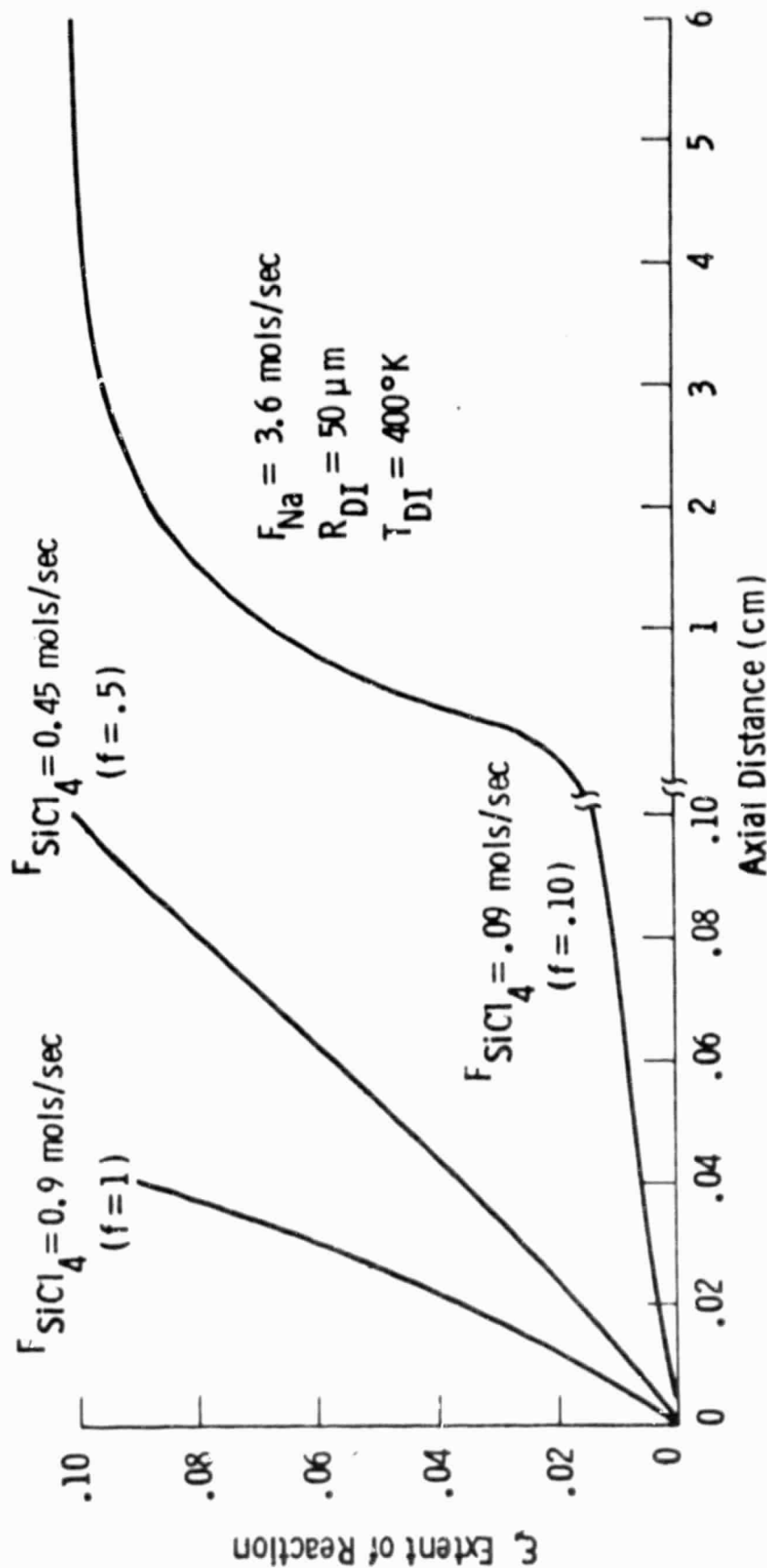$4H_2:1Ar = 0.7$ moles/sec

Curve 693968-A

$F_{Na} = 3.6$ mols/sec
$R_{DI} = 50 \mu m$
$T_{DI} = 400°K$

$F_{SiCl_4} = 0.45$ mols/sec
(f = .5)

$F_{SiCl_4} = 0.9$ mols/sec
(f = 1)

$F_{SiCl_4} = .09$ mols/sec
(f = .10)

Axial Distance (cm)

ξ Extent of Reaction

Figure 3 - Extent Of Reaction, ξ, As A Function Of The Axial Distance For The Reaction Model
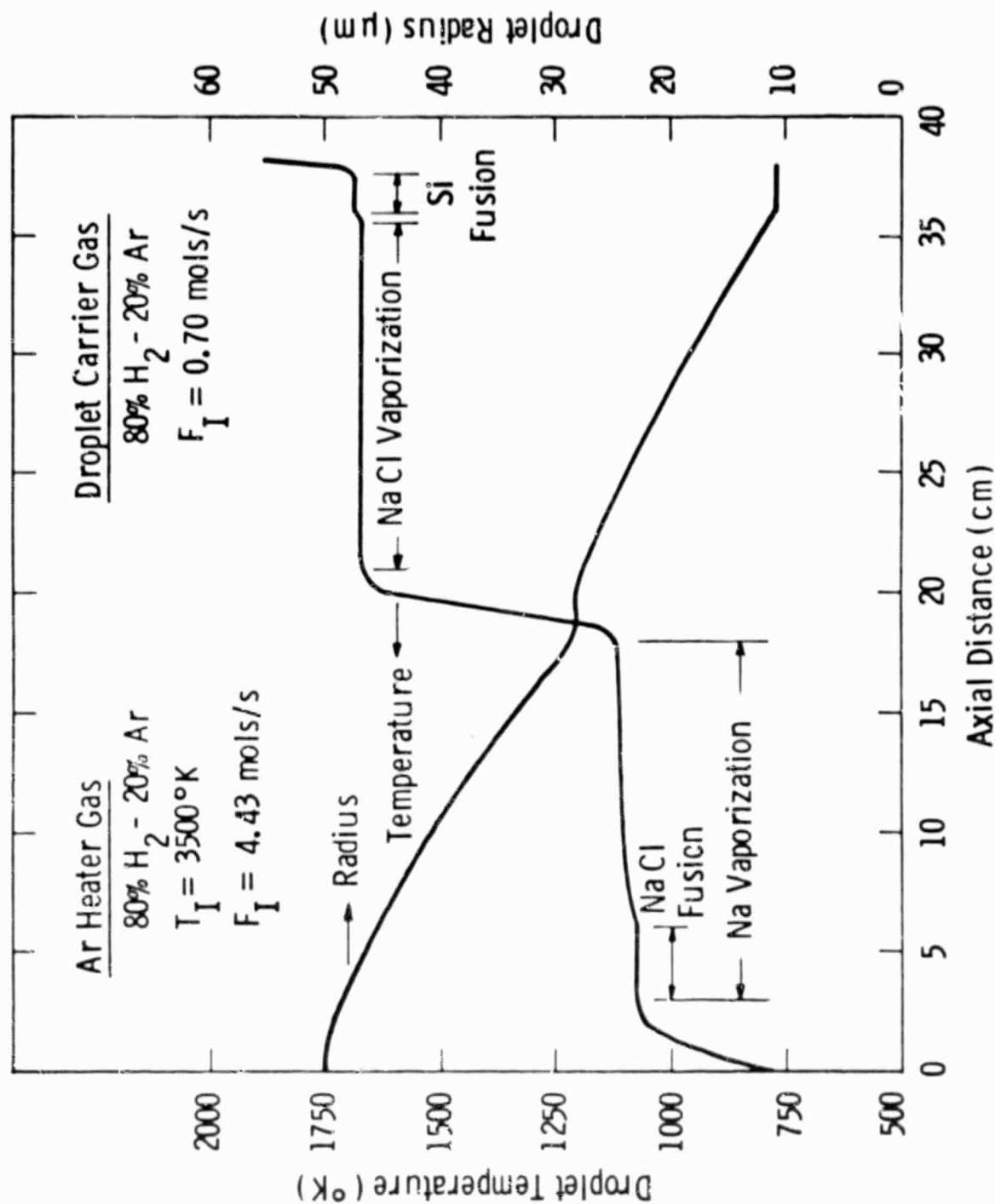
Figure 4 - Temperature and radius results for droplets with an initial sodium flowrate of 3.6 mols/s, an initial silicon tetrachloride flowrate of 0.9 mols/s and 10% conversion

References

1. M. G. Fey, et al, Quarterly Report DOE/JPL 954589-77/4, Silicon Materials Task, JPL Contract No. 954589, October-December, 1977.

2. M. G. Fey, et al, Quarterly Report DOE/JPL 954589-78/5, Silicon Materials Task, JPL Contract No. 954589, January-March, 1978.

APPENDIX B

LABORATORY SCALE EXPERIMENT FOR STUDYING THE REDUCTION OF $SiCl_4$ BY Na AT PLASMA TEMPERATURES

J. V. R. Heberlein, J. F. Lowry, D. F. Ciliberti, D. W. Feldman

Westinghouse R&D Center
Pittsburgh, PA   15235

December 18, 1979

THE REDUCTION OF TETRACHLOROSILANE BY SODIUM AT HIGH TEMPERATURES IN A

LABORATORY SCALE EXPERIMENT*

J. V. R. Heberlein, J. F. Lowry, T. N. Meyer and D. F. Ciliberti
Westinghouse R&D Center, Churchill Site
1310 Beulah Road, Pittsburgh, PA 15235, U.S.A.

ABSTRACT

In support of a project to develop a low cost solar grade
silicon production process, tetrachlorosilane was reduced by sodium at
plasma temperatures (3000°K) in a laboratory scale experiment. The
reaction product silicon was separated and collected on the reaction tube
wall through condensation. The experimental results show a basic agree-
ment with results obtained from a heat and mass transfer model, and the
observed differences can be qualitatively attributed to the model
characterization of the experiment.

---

1. INTRODUCTION

The economic production of electric power using solar photo-
voltaic arrays depends upon the availability of sufficiently pure,
inexpensive silicon. The Jet Propulsion Laboratory has undertaken the
development of low cost silicon photovoltaic arrays as part of the
National Photovoltaic Program.[1] In order to achieve the overall cost
objectives, it is necessary to reduce the cost of polycrystalline silicon
by nearly an order of magnitude. In a large scale process currently
under development,[2] silicon will be produced by means of the high tem-
perature reduction of tetrachlorosilane ($SiCl_4$) by metallic sodium (Na)
in an arc heated hydrogen-argon gas mixture. As part of this development
program, a more flexible, laboratory scale system was designed and
operated to study reaction rates, product yield and product separation
techniques. Results of this experiment and model are presented.

2

2. DESCRIPTION OF EXPERIMENT

The experimental system (see Figure 1) consisted of a commercial DC plasma torch to provide the arc heated stream of hydrogen and argon, a special nozzle for injecting the sodium and tetrachlorosilane into the gas stream, a test chamber with viewing ports for optical diagnostics and having a means for product collection by condensation or by filtration, a scrubber for removal of HCl and NaCl from the gas stream, and a hydrogen burn-off stack.

The liquid sodium was forced by argon pressure from a heated tank through heated lines to the injection nozzle. A manual valve controlled the   flow which was monitored by an electromagnetic flowmeter. The tetrachlorosilane supply system consisted of a reservoir and an evaporator. Argon gas pressure forced tetrachlorosilane out of the reservoir into the evaporator. Flow was controlled by three valves and measured with a glass tube rotameter. Both sodium and tetrachlorosilane reactants were delivered through separate heated manifolds to the heated injection nozzle, the temperature of which was maintained above the melting point of sodium (above 100°C) by a high pressure, hot water cooling system. The plasma flow channel through the injection nozzle was lined with a graphite sleeve, and the sodium was injected through radial holes in this sleeve, whereas the tetrachlorosilane injection holes were oriented towards the downstream direction.
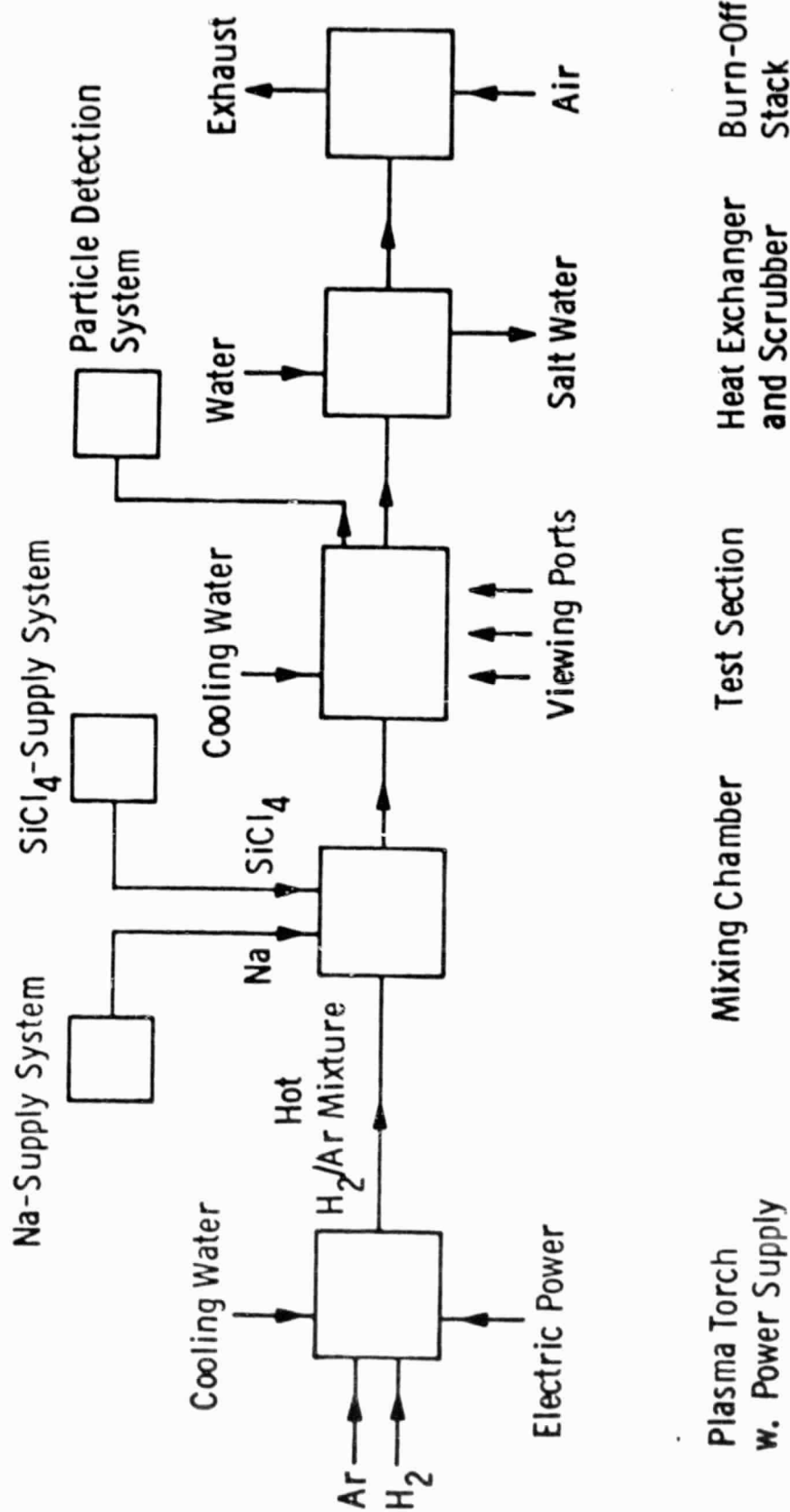
3

Dwg. 6425A81

Fig. 1 — System lay-out schematic of kinetics experiment

The mixture of hydrogen-argon gas, reactants and products entered a flow channel consisting of several sections of a 25 mm diameter silicon carbide tube (see Figure 2). The tube sections were contained in four water-cooled stainless steel reaction chamber sections. Thus the heat transferred to each section was obtained by normal calorimetric measurements. Following the last section, the gas entered a duct to the conventional water-spray scrubber.

The nominal gas and reactant input composition[3] (6.62 H_2: 1.66 Ar: 1.0 $SiCl_4$: 4.0 Na) was determined by the process energy requirements, the arc heater operating characteristics and the silicon product purity requirements. The total mass flow rate was scaled according to the power capability of the torch to provide the desired operating temperatures.
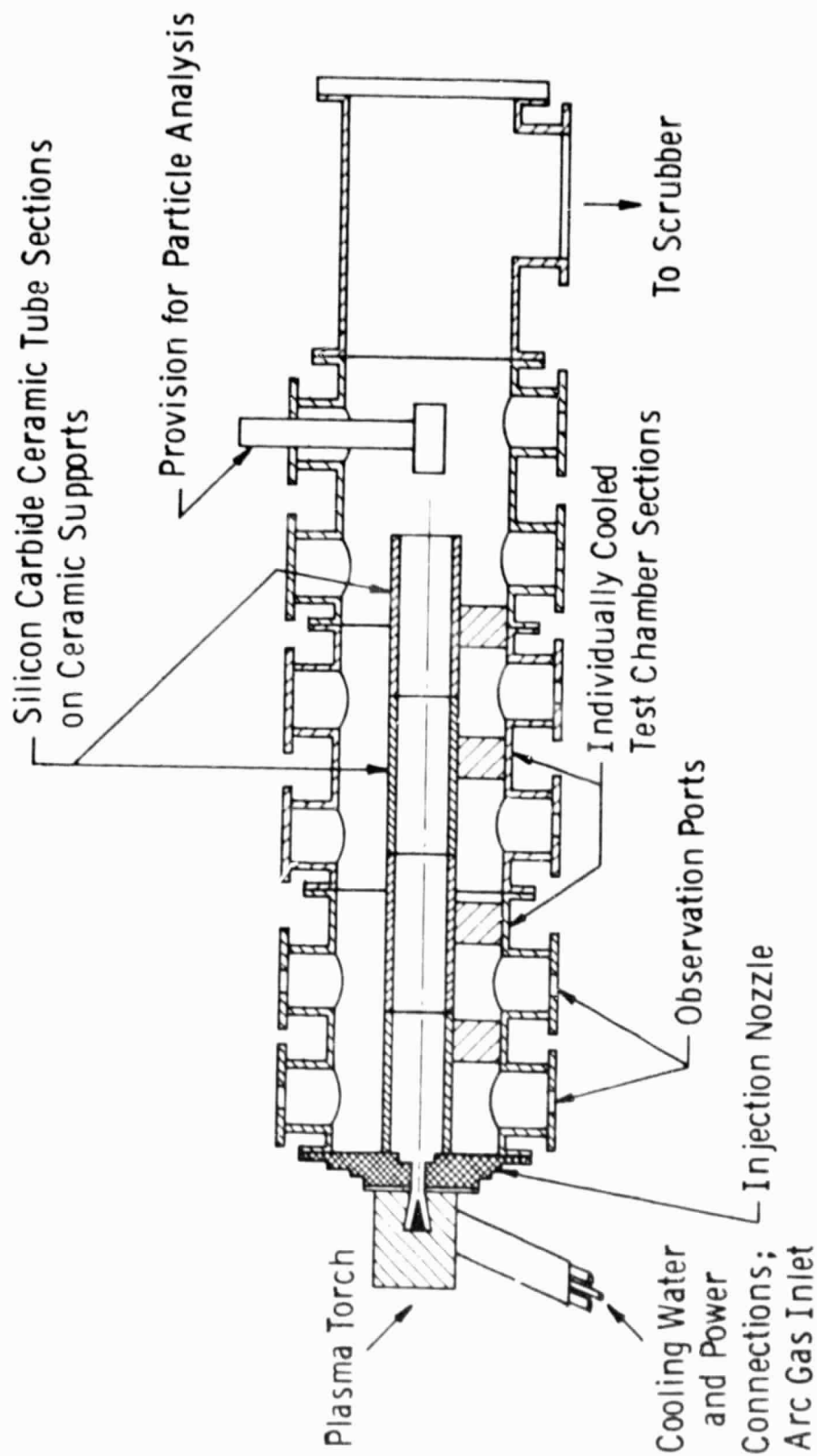
5

Dwg. 7691A62

Silicon Carbide Ceramic Tube Sections
on Ceramic Supports

Provision for Particle Analysis

To Scrubber

Individually Cooled
Test Chamber Sections

Observation Ports

Injection Nozzle

Plasma Torch

Cooling Water
and Power
Connections;
Arc Gas Inlet

Fig. 2 — Assembly drawing of test apparatus

3. THEORY OF PRODUCT SEPARATION

Early in the process development it became evident[4] that the reaction rates are mixing limited. Thus, the major analytical consideration was given to the means of silicon product separation. A model was developed[3] to predict the transfer of silicon from the product gas stream to the reactor wall in a molten state by condensation. The model was developed for a turbulent stream (Re ~50,000) representative of the large scale reactor.[3] In addition, the model included the effects of condensation in the boundary layer upon the transfer process. Due to size and power limitations, the laboratory scale experiment operated in the laminar mode (Re ~2000). The model was applied to these laminar flow conditions by substituting those relations defining the heat and mass transport, and by involving the analogy between heat and mass transfer.[5] The effect of condensation in the boundary layer was neglected. Since the axial pressure drop is negligible (< 0.1 atm), the pressure was taken to be 1 atm throughout the tube. The conservation equations representing the stream temperature and silicon content were integrated numerically along the axis, using the calculated equilibrium composition and associated transport properties at the specific temperature. Two cases were calculated, one using Nusselt numbers for thermally and hydrodynamically developing flow,[5] the other with a constant Nusselt number representing developed flow. A constant wall temperature above the melting point of silicon (1683°K) was assumed. At this wall temperature, only

7

silicon is condensing and collected at the wall, with all other species remaining gaseous.

Figure 3 shows the fraction of silicon remaining in the gas stream as a function of axial location and the axial temperature distribution for the two cases (developed and developing flow, respectively). The results for the developing flow indicate a rapid removal of silicon at the entrance, coinciding with a comparable change in the stream temperature. The experimental arrangement of a high velocity jet from a small diameter nozzle entering a tube of significantly larger diameter, is expected to produce results between these limiting cases.
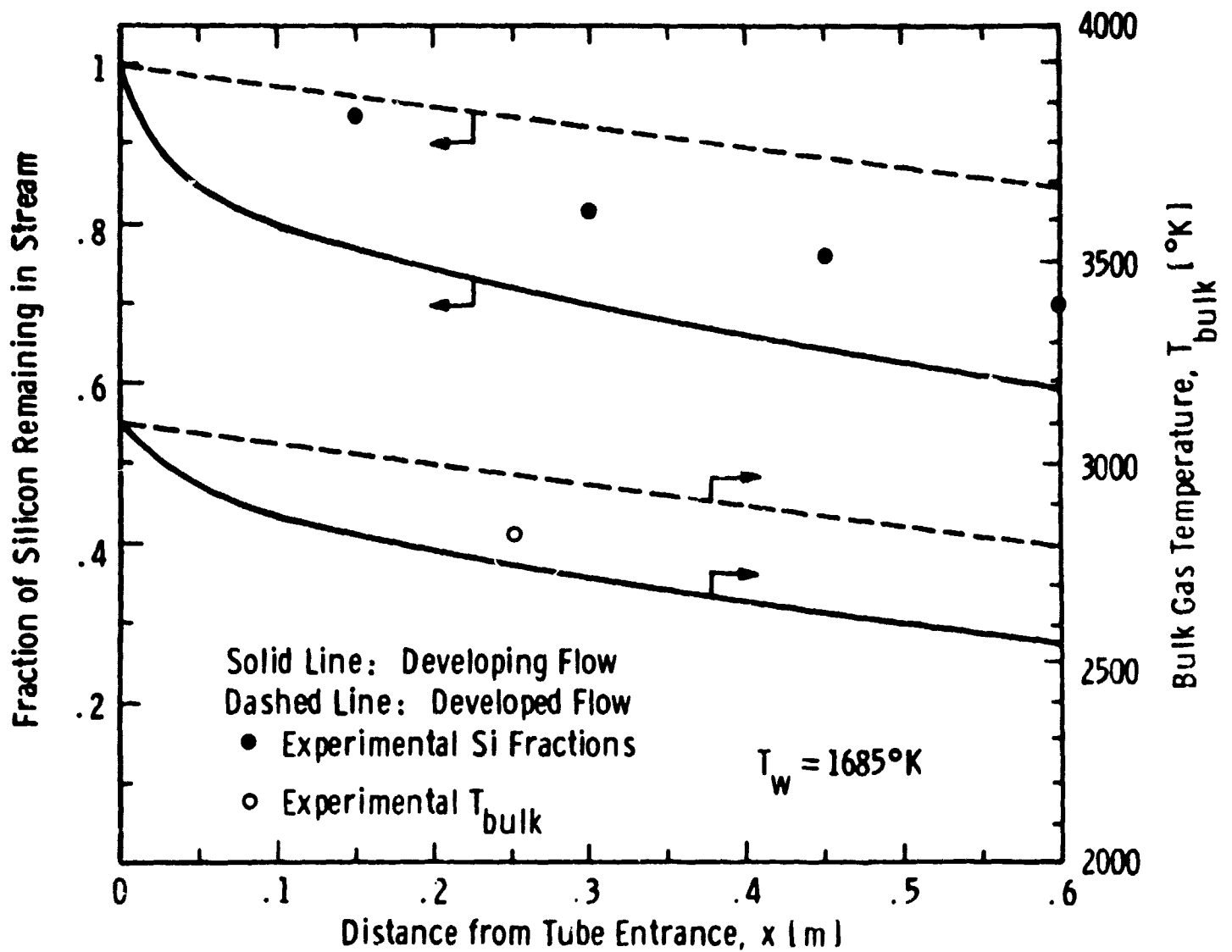
Fig. 3 — Theoretical and experimental axial distribution of the fraction of silicon remaining in the gas stream, and axial bulk temperature distribution

4. RESULTS

Based upon the values for the power input and the calorimetric measurements of the heat losses, the bulk gas temperatures at the torch and injection nozzle exits and at the end of the first test section were determined from thermodynamic equilibrium properties. Table 1 lists bulk temperature values. Pyrometrically measured tube wall temperatures are also shown in this table. Weighing of the different silicon carbide tube sections before and after each run indicated the amount of material deposited. This product was then separated into water soluble and insoluble substances, and analyzed by Electron Dispersive Analysis of X-rays (EDAX), which gives the elemental composition, and by x-ray diffraction, to find the crystalline components.

The products were collected in the following forms:

(a) In the regions where the silicon carbide tube wall temperature was above the melting point of silicon and the dew point of sodium chloride, the wall was covered with silicon. During cooling after the experiment, this silicon formed mounds around the circumference and frozen pools at the bottom of the silicon carbide tube.

(b) In the regions where the tube wall temperature was slightly below the melting point of silicon, the inside wall was covered with a gray scale which could be easily scraped off in the form of large flakes. These flakes consisted of crystalline silicon and varying amounts of sodium

10

TABLE 1

TUBE WALL TEMPERATURES AND BULK GAS TEMPERATURES AT A TORCH POWER OF 26 kW

Axial Location (see Figure 2)	Distance From Injection Nozzle	T_{bulk} °K	T_{wall} °K
Torch exit		3670	
Injection Nozzle Exit	0	3100	
1st Window	5 cm		1900
2nd Window	16 cm		1650
End of Test Section I	25 cm	2820	

chloride ranging from trace values (1 to 2% of sodium chloride) in the flakes from tube sections with a wall temperature only slightly below the dew point of NaCl to more than 50% farther downstream.

(c) The end sections of the silicon carbide tube were covered with a glassy layer of sodium chloride, containing some silicon.

(d) The rest of the product in the gas stream formed brown particles upon mixing with cold gas. These particles ranged in size from 3 μm to 70 μm and consisted of a mixture of amorphous silicon and NaCl.

Figure 3 contains also the experimental silicon condensation results obtained by weighing the tube sections after one representative experiment. The shape of the experimental distribution is similar to the theoretical distribution for developing flow, but displaced in the downstream direction. There are two explanations for this downstream shift: (a) the flow condition of a small diameter jet entering a tube of larger diameter would mean that the vapor stream would not contact the tube wall until it had travelled a certain distance; (b) evaporation of the sodium droplets and the subsequent gas phase reaction process may not have been completed and equilibrium may not have been reached until the stream was well into the first tube section. The evidence of reduced flow-rates leading to an increased initial condensation rate supports either explanation.

The calorimetrically determined bulk gas temperature value at the end of the first test section seems to indicate the applicability of the developing flow analysis for the heat transfer.

12

5. DISCUSSION

Since this experiment was conducted as part of a larger development program, we would like to consider the implications of the results on this development:

(a) We would like to point out that the model was developed for the flow geometry of the large scale reactor in which the effects to which we attribute the differences between theoretical prediction and experimental results would not be present. Therefore, the basic agreement between model predictions and experiment support the model used to predict the silicon collection rate.

(b) The much higher Reynolds number characterizing the flow in the large scale reactor will lead to increased heat and mass transfer to the reactor wall, and, therefore, to larger collection rates.

(c) The low power levels used in the laboratory scale experiment had the consequence that the collector tube wall temperature dropped below the dew point of sodium chloride after relatively short distance, leading to collection of sodium chloride together with the silicon. The design and operating power levels of the large scale reactor avoid this problem.

6. CONCLUSIONS

We can draw the following conclusions from our results:

- The controlled reduction of tetrachlorosilane by sodium at plasma temperatures proceeds as predicted from thermodynamic considerations.

- The reaction product silicon can be separated and collected on a wall at a temperature above the dew point of sodium chloride.

- The experimentally determined condensation rate essentially follows the predictions from model calculations, and the observed differences can be explained by the simplifying assumptions made in the model characterizing the experiment.

* * *

This paper was typed by Leslie A. Arthrell.

ACKNOWLEDGEMENTS

REFERENCES

1. "Proceedings of the U. S. DOE Photovoltaics Technology Development and Applications Program Review", CONF-78-1192, United States Department of Energy, Arlington, VA, Nov. 7-9, 1978.

2. Reed, W. H., T. N. Meyer, M. G. Fey, F. J. Harvey, F. G. Arcella, "Development of a Process for High Capacity Arc Heater Production of Silicon", 13th IEEE Photovoltaic Specialists Conference, Washington, DC, June 5-8, 1978.

3. "Development of a Process for High Capacity Arc Heater Production of Silicon for Solar Arrays", Quarterly Progress Report, ERDA/JPL 954589-78/1, Silicon Materials Task, JPL Contract No. 954589, March 1978.

4. Kamenar, B., D. Grdenić, "Z. anorganische und allgemeine Chemie", 321, 113, 1963.

5. Bird, R. B., W. E. Stewart, E. N. Lightfoot, "Transport Phenomena", (John Wiley and Sons, Incorporated, New York, 1960).

6. Kays, W. M., "Convection Heat and Mass Transfer", (McGraw-Hill, New York, 1966).

APPENDIX C

SPRAY ATOMIZATION OF LIQUID SODIUM
AND SILICON TETRACHLORIDE (INJECTION TECHNIQUES)

SPRAY ATOMIZATION OF LIQUID SODIUM AND
SILICON TETRACHLORIDE

by

M. G. Down, A. R. Keeton, and J. E. Bauerle
Physical and Inorganic Chemistry

Westinghouse R&D Center
Pittsburgh, Pennsylvania 15235

ABSTRACT

A Department of Energy funded project at the Westinghouse
Power Circuit Breaker Division for the development of an arc heater process
for the reduction of silicon tetrachloride by sodium to produce
photovoltaic grade silicon required the introduction of both reactants
in liquid aerosol form. This report describes experiments in which
spray nozzles were tested and characterized for this purpose under
prototypic conditions. Particular attention was paid to the limiting
operational parameters of the nozzles, and to the size distribution
o. he aerosol produced. For liquid sodium injection, a novel sonic
gas atomizing nozzle has been chosen and fully characterized.

1.0 INTRODUCTION

The realization of low cost electric power from large-area
silicon photovoltaic arrays will depend on the development of new methods
for the production of solar grade silicon. An important goal of the
U.S. Department of Energy (DOE) National Photovoltaic Program is a reduction
in the cost of silicon ingot from the present $66 per kg. to a figure
of less than $10 per kg. by 1986. Among several process development
programs currently underway to achieve this end is the one at the Westinghouse
Power Circuit Breaker (PCB) Division being supported by NASA Contract
No. 954589 out of the Jet Propulsion Laboratory for DOE. This process
is based upon the high temperature, sodium reduction of silicon tetra-
chloride, $SiCl_4$, utilizing electric arc heaters to facilitate product
separation and to increase temperatures for higher reaction efficiency.
The silicon produced from this reaction will be collected in the liquid
state, while the co-product, sodium chloride, exits the reactor as a
vapor.

The reactor, presently under construction at the Westinghouse
East Pittsburgh site by the Arc Heater Project Team, is shown schematically
in Fig. 1. Liquid sodium is sprayed axially into the reactor plenum from
the left, in the form of small droplets (< 200 µm). The flowing sodium
is entrained within an arc heated stream of 4:1 hydrogen/argon gas
mixture. The heated gas causes rapid vaporization of the sodium droplets,
after which silicon tetrachloride is injected into the stream. A rapid,
exothermic reaction occurs, and the silicon product is separated from the
gas stream by condensation as free flight droplets which are then collected
in the molten state by a cyclone separator and a quartz-lined crucible.
The co-product vapors ($NaCl$, H_2, Ar, HCl, etc.) are exhausted from the

2

cyclone separator. Nominal flow conditions are 0.047 ls^{-1} (45 GPH) for each reactant, sodium and silicon tetrachloride, to produce $\sim$ 45 kg/hr (99 lb/hr) of silicon.

One of the major areas of concern in the development of this process is the injection of the two reactants into the reactor. Neither silicon tetrachloride nor the reductant, liquid sodium, has previously been tested for this purpose. Ideally, these fluids would be injected into the chemical reactor as pure vapors, since the reaction takes place in the vapor phase. Sodium vapor injection at the required pressures, however, is at the fringe-of-the-art and is unattractive from an energy conservation viewpoint. This research program was therefore instigated in order to study liquid sodium and silicon tetrachloride injection using spray atomizing nozzles. In order for the sodium, and to a lesser extent the $SiCl_4$, to be in the vapor phase at the point of reaction, it is an essential prerequisite for such nozzles that the spray particle size be relatively small (< 200 μm), thereby ensuring efficient vaporization in the arc heated carrier gas stream.

The major objectives of the nozzle optimization program, therefore, were to evaluate techniques for injecting the reactants into the chemical reactor and to integrate the results into the design of the pilot scale system. Particular attention was paid to the operating parameters (pressures, flow rates etc.) of the nozzles and the particle size distribution produced.

2.0 CONCLUSIONS

1. Liquid sodium at 150°C can be successfully sprayed at flow rates of 0.05 ℓs^{-1} (45 GPH) and liquid pressures $\sim$ 20 psig using a Sonicore gas atomizing nozzle.

2. The pressure ($\sim$ 40 psig) and flow rate ($\sim$ 50 SCFM) of inert atomizing gas required for such spraying will not seriously upset the heat balance in the silicon production reactor.

3. The particle size distribution of the liquid sodium spray indicates tnat the major proportion of the sodium mass will be in the form of small, easily vaporized droplets suitable for the chemical reactor process, i.e., in the range 20-140 μm diameter.

4. The forward velocity of the liquid sodium spray is low enough to ensure efficient vaporization in the arc heater gas stream.

5. Silicon tetrachloride can be successfully sprayed at the required flow rates and particle sizes using hydraulic atomizing nozzles.

4

3.0 RECOMMENDATIONS

1. It is recommended that the Sonicore 312T gas
    atomizing nozzle be used to inject liquid sodium
    into the developmental silicon production reactor.

2. The nozzle should be operated at an atomizing gas
    to liquid mass flow ratio of at least 0.8:1.

3. The liquid sodium flow through the nozzle should
    only be initiated subsequent to the gas flow,
    and should be terminated prior to cessation of
    the gas flow.

4. The Sonicore nozzle should be positioned in the
    reactor as close as possible to the arc heater
    gas stream, since the included spray angle is
    large.

5. It is also recommended that the Spraying Systems
    Co. 1/4 LN6 hydraulic atomizing nozzle be used
    for silicon tetrachloride injection into the
    chemical reactor.

6. The required silicon tetrachloride pressure at
    the nozzle should be as outlined in the results
    section of this report.

4.0 TECHNICAL BACKGROUND

4.1 Liquid Atomization

Spraying and atomizing are terms describing the process whereby liquids are transformed into droplets dispersed in air or other gases. Spraying refers to the formation of more or less coarse droplets, while atomizing means the production of fine droplets or a mist. In industrial operations, a large variety of liquids, solutions, slurries,etc.,are atomized, and each has its own particular physical properties. These properties and the requirements of the application make the choice of the correct nozzle an exact and important one. Liquid disintegration, or breakup, comes about quite differently for different conditions and may take place in successive stages involving one or more mechanisms. Of the numerous factors upon which breakup depends, the most important are the properties of the liquid, the design and construction of the atomizing device, the conditions of pressure and flow rate under which the atomizer is operated, and the conditions and properties of the gas into which the liquid is injected. The detailed theory of liquid stream disintegration is beyond the scope of this report, but has been thoroughly dealt with elsewhere.[1]

4.2 Particle Size Distribution

The ultimate spray from any nozzle or atomizer consists of a large number of essentially spherical droplets of various diameters, d. From the number of droplets ΔN within each size interval Δd one can define the size distribution function $f_N(d)$:

$$f_N(d) = \frac{\Delta N}{\Delta d} \tag{4.1}$$

6

Plots of $f_N(d)$ vs. d provide a convenient means for presenting and comparing experimental data on droplet sizes.[*] A second useful concept is the <u>cumulative size distribution function</u> N(<d), defined as the total number of droplets smaller than the specified diameter d. These two functions are closely related since one is just the integral of the other:

$$N(<d) \equiv \int_0^d \Delta N = \int_0^d f_N(d) \, \Delta d \qquad (4.2)$$

Typical behavior of these functions is shown in Figs. 2 and 3.

For chemical engineering purposes, it is generally much more useful to employ distribution functions based on the <u>mass</u> of droplets (rather than <u>number</u>) within each size interval. Therefore, by analogy with (4.1) and (4.2) one has

$$f_M(d) = \frac{\Delta M}{\Delta d} \qquad (4.3)$$

for the size distribution function (mass-basis), and

$$M(<d) \equiv \int_0^d \Delta M = \int_0^d f_M(d) \, \Delta d \qquad (4.4)$$

for the cumulative distribution function (mass-basis). It should be noted that the number-based and mass-based distribution functions are distinctly different, yielding different size averages and size dispersions. In the discussion here, mass-basis concepts will be adhered to.

For many applications it is sufficient to know just the average particle size and the spread of particle sizes. The most familiar parameters for this purpose are the arithmetic mean droplet

---

[*] Plots of ΔN vs. d are equivalent to the above plots if a constant size interval Δd is employed.

size, d_a, and the arithmetic standard deviation, σ_a. These may be
calculated either from the raw experimental data (ΔM for each Δd) or
from the size distribution function ($f_M(d)$) as follows:

$$d_a = \frac{\sum d\Delta M}{\sum \Delta M} = \frac{\sum d f_M(d) \Delta d}{\sum f_M(d) \Delta d} \qquad (4.5)$$

$$\sigma_a = \left[\frac{\sum (d-d_a)^2 \Delta M}{\sum \Delta M}\right]^{1/2} = \left[\frac{\sum (d-d_a)^2 f_M(d) \Delta d}{\sum f_M(d) \Delta d}\right]^{1/2} \qquad (4.6)$$

The arithmetic parameters d_a and σ_a have the following
convenient property: If the particle distribution is of the normal
probability type, then one can use d_a and σ_a to write the distribution
function explicitly as

$$f_M(d) = \frac{\sum \Delta M}{\sqrt{2\pi}\,\sigma_a}\, \exp\left[-\frac{1}{2}\left(\frac{d-d_a}{\sigma_a}\right)^2\right] \qquad (4.7)$$

This form is useful if further mathematical analysis of particle properties
is required. In addition, normal probability paper is available for
graphically determining d_a and σ_a from experimental data.

Experimentally it has been found that most atomizer droplet
distributions extend over several decades of droplet diameter. As
a result, these distributions cannot be adequately described by the
simple normal probability function (Eq. 4.7) which is better adapted
to relatively narrow distributions. An effective remedy for this
problem is to replace d in the distribution function with logarithm
of d; the result is called the log-normal distribution, given by

$$f_M(\log d) = \frac{\sum M}{\sqrt{2\pi}\,\log \sigma_g}\, \exp\left[-\frac{1}{2}\left(\frac{\log d - \log d_g}{\log \sigma_g}\right)^2\right] \qquad (4.8)$$

8

The parameters describing this distribution are the **geometric** mean droplet size, d_g, and the **geometric** standard deviation, σ_g. The basic definitions for these geometric parameters are very similar to those for the arithmetic parameters, d_a and σ_a with d replaced by log d; thus

$$\log d_g = \frac{\sum (\log d)\Delta M}{\sum \Delta M} \tag{4.9}$$

$$\log \sigma_g = \left[\frac{\sum (\log d - \log d_g)^2 \Delta M}{\sum \Delta M} \right]^{1/2} \tag{4.10}$$

Note that σ_g is essentially a ratio of two d's and therefore is dimensionless.* Calculating the two parameters d_g and σ_g is tedious, but can be avoided by the use of log-normal probability graph paper. A plot of cumulative mass (%) vs. droplet diameter on this paper yields a straight line if the data obey a log-normal distribution. An example of this is shown in Fig. 4, which also demonstrates the difference between number (count) and mass distributions. The diameter corresponding to 50% cumulative mass is d_g. The ratio of diameter for 84.1% cumulative mass to diameter for 50% cumulative mass is σ_g. If the data do not follow a log-normal distribution, a curved line will result. Regardless of the exact distribution, a cumulative plot of this type is a useful form for presenting the data since one can readily obtain a mean droplet diameter (50% value of d), a measure of the spread in droplet diameters (10% to 90% values of d, for example), or simply the percentage of droplet mass within any given size range d_1, d_2, this being equal to $M(<d_1) - M(<d_2)$.

---

*A better understanding of σ_g can be obtained by the following examples:

For an ordinary normal distribution, 68.3% of the total is included in the size range, $d_a - \sigma_a$ to $d_a + \sigma_a$.

For a log-normal distribution 68.3% of the total is included in the size range d_g/σ_g to $d_g \cdot \sigma_g$.

4.3 Nozzle Types

Although there are many different types of devices for
producing liquid sprays, the most widely used ones can be classed as
either pressure (hydraulic) nozzles or two-fluid atomizers (pneumatic).
The former is the simplest method of causing the disintegration of a
liquid stream; pressure energy is converted into kinetic energy as the
liquid is forced through nozzle ports, and liquid jet instability
results. Among the variations on this general principle are the
fan, swirl, and impact nozzles.

Two-fluid atomizers rely on a high-velocity gas stream to
disintegrate the liquid stream. Unlike pressure atomizers, in which
all the required energy is contained in the liquid itself, the two-
fluid device draws on the energy of the gas as well. Since the gas-
contained energy is independent of the quantity of the liquid, smaller
droplet sizes and wider spray angles can be achieved at low liquid flow
rates. In general, two-fluid atomizers are far more efficient at producing
very fine sprays ($\leq$ 20 μm mean diameter) even at relatively high
liquid flow rates.

The distribution of droplet sizes within gas atomized sprays
generally follows a log-normal relationship, although deviations at
the larger sizes are not uncommon. The median drop diameter is largely
determined by the mass ratio of gas to liquid, and by the relative
velocities of the gas and liquid streams. Nukiyama and Tanasawa[2]
produced an often quoted empirical expression relating the mass mean
diameter, d_{gm}, to the physical properties and velocities of the
fluids:

$$d_{gm} = \frac{585}{V} \frac{\gamma}{\rho} + 597 \left(\frac{\mu}{\gamma}\right)^{0.45} \left(\frac{1000 \, Q_\ell}{Q_a}\right)^{1.5} \qquad (4.11)$$

where V = relative velocity of gas and liquid streams

γ = surface tension of liquid

10

ρ = density of liquid

μ = viscosity of liquid

Q_ℓ, Q_a = volume flow rates of liquid and gas respectively

This expression, however, is only claimed to apply to small, converging nozzles at certain capacities and for a small range of liquid properties. It has not been found to hold for nozzles of markedly different design from those in the original study.

A more generally applicable correlation has recently been derived by Lubanska.[3] Of relevance to the present study is the fact that his expression was specifically aimed at the inclusion of data on the atomization of liquid metals. Agreement between different workers' data was achieved by the use of a constant factor, K, dependent on the exact design of the nozzle used. Over an extensive range of size and liquid properties, the expression is

$$d_{gm} = K \frac{\nu_m}{\nu_g W} \left(1 + \frac{M}{A}\right)^{1/2} \tag{4.12}$$

where   D = diameter of liquid stream

ν_m, ν_g = kinematic viscosity of liquid and gas respectively

$W = \dfrac{\rho V^2 D}{\gamma}$ = Weber number

M = mass flow rate of liquid

A = mass flow rate of gas

Recently a new style of gas atomizing nozzle has become available which relies on an intense sonic energy field to break up the liquid. These sonic, or ultrasonic, spray nozzles feature a high velocity gas stream which impinges on a resonator cavity thereby producing the energy field. The liquid stream is then introduced into this field and a highly efficient atomization is achieved. It is claimed that these nozzles can produce a uniform particle distribution

11

with very low median diameters and at lower gas to liquid mass ratios than can conventional two fluid atomizers. The fact that larger liquid orifice diameters can be used means that high liquid flow rates can be achieved at reasonable pressures. Also, relatively viscous or particle-contaminated fluids can be sprayed.

4.4 Particle Size Determination

There are a number of different techniques that have been applied to the measurement of drop sizes. They can be conveniently grouped into six general methods.

4.4.1 Microscopy

In this technique droplets are simply collected on a slide and examined microscopically. Modern instruments utilize a T.V. camera and a processor which analyses the pulses in the T.V. scans and automatically determines the size distribution. For the testing of a sodium spray, this method would have the advantages of a wide size range ($\sim$ 1-1000 μm), and a small amount of test material required ($\sim$ 0.5g). The major disadvantage would be the difficulty in dispersing particles on the slide without aggregation, and the reactivity of sodium with air and moisture. In addition, if the slide is simply suspended in the spray, distortion of droplet shape can occur and the smallest particles can be missed due to the gas stream flowing around the slide.

4.4.2 X-Ray Sedimentation

In this technique solidified spray particles are dispersed in a liquid of appropriate density and viscosity and placed in a flat vertical cell. A beam of soft x-rays traversing the cell is used to monitor the mass of particles in the cell at a given position as a function of time. The rate of settling of the particles is used to determine the particle size distribution, which is then automatically calculated by the instrument and recorded graphically. Among the disadvantages of this technique are the possibility of particle agglomeration and the need for a relatively large quantity of material

12

(5-10g). Also, a peristaltic pump is used which might deform clusters of soft metal particles. The upper size limit of the instrument is low (50-100 μm).

4.4.3 Inertial Separation

A cascade impactor is essentially a series, or cascade, of flat surfaces mounted directly in front of ports, or jets, through which a spray may be drawn. The jets decrease in size as the spray progresses through the device. This causes the gas velocity to increase and traversing droplets find increasing difficulty in passing obstacles. The final position of capture of these droplets is related to their size, and the particle size distribution is obtained by weighing the individual collection plates. The impactor is essentially a direct sampling, on-line device, but has the disadvantage, for the present application, of being restricted to low size ranges ($\leq$ 30 μm).

4.4.4 Photographic Analysis

Droplet sizes determined by photographing a spray should in theory be the most direct and least affected by coalescence. It is, however, extremely difficult to photograph fast moving, small ($\sim$ 20 μm) droplets, and to decide which are in focus and which are not. Moreover, the results of a photographic size analysis are a spatial rather than a temporal distribution. For our tests, it was considered that the very high spray flow rates and consequent high particle densities would preclude the successful use of photography for particle sizing.

4.4.5 Optical Methods

Optical methods involving the measurement of the intensity, color, and polarization of light scattered by a spray as well as light transmission and diffraction, have only found specialized application in the past. With the development of inexpensive but sophisticated laser technology, however, these methods are finding a wide appeal. Details of this general technique are included in Section 5.3.1.

13

4.4.6 Sieving

Sieving is, of course, a well-known technique which employs
a series of wire screen separators of decreasing screen size plus some
type of mechanical agitation to effect the particle separation. The size
distribution is then obtained by weighing the separated fractions. The
advantages of this method are the great flexibility in choice of size
ranges; the fact that a mass distribution is obtained directly; and the
small amount ($\sim$1g) of material required. In addition, a liquid sodium
spray readily lends itself to rapid freezing. This particle solidification
process is often achieved using liquid nitrogen because of its low
temperature, but also because its low surface tension permits easy
penetration by the droplets.

A comparative chart of the particle size ranges of the
methods considered for sodium particle sizing is shown in Fig. 5. Of all
these techniques, sieving was chosen as the primary method by virtue
of its flexibility, reliability and its lack of experimental complications.

5.0 DESCRIPTION OF EXPERIMENTS

5.1 Spray Test Equipment

5.1.1 Test Chamber

Candidate nozzles were tested in a cylindrical, stainless steel (AISI type 304) chamber shown schematically in Fig. 6. The chamber was 34 cm in diameter and 81 cm in height and was supported on a stand 60 cm above the ground. The chamber was flanged at both ends and was equipped with two viewing ports, 180° apart and at a 45° angle to the horizontal. The windows of these ports were fitted with an inert gas sweep system to reduce the possibility of sodium aerosol deposition. Test nozzles were mounted in a nozzle holder at the top of the chamber to which were attached sodium and gas inlet lines; these lines and the nozzles were equipped with tubular heaters. To the base flange was attached a collection funnel and valved glass bulbs to facilitate the removal of solid sodium spray particles without contamination of the chamber atmosphere.

Excessive pressure build-up in the chamber could be relieved via an adjustable pressure relief valve set at ∿ 15 psi. This relief valve was vented through a high capacity (300 SCFM) filter to remove any finely divided sodium particles. The chamber was also equipped with an internal stainless steel filter, Fig. 7, through which normal (< 15 psi) gas pressures were vented during spray testing.

5.1.2 Argon Supply System

Inert gas for use in testing the two-fluid gas atomizing nozzles was supplied from a rack of three argon cylinders linked through a manifold. Before entering the nozzle, the gas was passed through a high capacity flow meter (100 SCFM max.), pressure gauges and a

15

copper gas heater. This heater precluded the possibility of premature freezing of sodium in the nozzles due to a cold gas flow. The gas flow was controlled by solenoid operated valves.

5.1.3 Sodium Supply System

The sodium supply tank consisted of a three gallon cylindrical stainless steel reservoir (61 cm x 15 cm) with hemispherical end caps, Fig. 8. This tank was equipped with two level probes and clamshell type heaters, and was linked to the nozzle holder via a fast-operating, electrically controlled pneumatic valve. Liquid sodium flow from the tank to the nozzle was controlled by pressurizing the sodium surface with argon.

The flow rate was monitored by an electromagnetic flow meter (MSA, Style FM2) the output of which could be recorded on a high speed Visicorder chart recorder (max. chart speed: 406 cm s^{-1}). The sodium reservoir was filled with high purity sodium by transferring the liquid metal from a storage drum via a stainless steel line which incorporated a 15 μm sintered metal filter.

The entire sodium injection test system, comprising chamber, sodium tank and gas heater, is shown in Fig. 9.

5.1.4 Silicon Tetrachloride Supply System

The pumped supply system used for testing the silicon tetra-chloride injection nozzle is shown schematically in Fig. 10. The liquid was pumped from a 5 liter steel storage cylinder using a positive dis-placement pump (Tuthill Pump Co., Chicago, Pump No. OLE) with a maximum capacity of 0.1 ℓ s^{-1} (90 GPH) at 690 kPa (100 psi). A flow meter and pressure gauge were incorporated in the line which delivered the silicon tetrachloride into the test chamber nozzle holder. The entire apparatus was pressure checked with argon at 690 kPa (100 psi) before filling. Silicon tetrachloride (Van de Mark Chemicals, > 99.9%) was introduced into the 5 liter reservoir by vacuum distillation at room temperature from a storage drum (10 gallon).

5.2 Test Nozzles

A review of the performance characteristics of the different
nozzle types outlined in Section 4.3 led to the conclusion that a gas
atomizing nozzle was preferable for the task of sodium injection into
the prototype reactor. Because of its lower gas flow requirements, a
sonic nozzle (Sonicore 312T, Sonic Development Corporation, New Jersey)
was chosen as the prime candidate for testing. A schematic of the
nozzle, Fig. 11, shows how a high velocity gas stream is directed through
the body of the nozzle and impinges on an externally mounted resonator cup.
An intense sonic energy field is thereby produced in the cavity between
the nozzle and the cup, the details of which have been treated
theoretically and experimentally by the inventors.[4] Liquid is injected
into this energy field and an efficient atomization results. The
nozzle body, Fig. 12, is constructed of type 316 stainless steel and the
resonator cup of Hastelloy B, a high nickel alloy. The flow rates
and pressures recommended for the atomization of water with compressed
air using this nozzle are shown in Fig. 13. These data were used
as a guide for testing the nozzle with liquid sodium.

In addition to the Sonicore nozzle, a more conventional
gas atomizing nozzle (Sprayco, Nashua, New Hampshire, nozzle No.
49267650) was procured as a backup in case the sonic nozzle was deficient
in some aspect of its operation.

For the injection of silicon tetrachloride, a lower liquid
flow rate was required, 0.01 ℓ s^{-1} (9 GPH), since it was planned to
use five nozzles in the arc heater silicon process pilot facility. For
this reason, and since ultra-fine particle size was not essential,*
a hydraulic nozzle (Spraying Systems Co., 1/4 LN6) was chosen for
testing.

---

* It should also be noted that since SiCl4 boils at 57°C at one atmosphere
pressure, its rapid vaporization in the hot arc heater gas stream was
less dependent on achieving a fine particle size.

17

5.3 Test Procedures

The test plan for the characterization of the sodium injection nozzle was divided into three phases. Firstly, a general, semi-quantitative investigation of the mode of operation of the nozzle using water as the test fluid was pursued. These tests involved measuring spray angles, liquid and gas pressures and flow rates, and assessing the mean spray velocity with the aid of high speed photography and video recording equipment (Instar). Secondly, a quantitative determination of the particle size produced by the sodium nozzles was performed using laser imaging techniques (described below), again with water as the test fluid. Finally, the particle size and operating characteristics of the nozzle were confirmed with liquid sodium as the test fluid and sieving as the size analysis technique. A theoretical comparison of nozzle performance between water and sodium was also made.

5.3.1 Particle Size Analysis - Laser Technique

Both the Sonicore and Sprayco candidate sodium nozzles were tested at a specialized aerosol particle sizing laboratory (Particle Measuring Systems Inc. (PMS) Boulder, Colorado). The nozzles were mounted in a wind tunnel facility, Fig. 14, which enabled the atomized spray to be swept through an instrument station equipped with laser spectrometers for determining the precise particle size distribution.

The basic principal of operation of these spectrometers can be described with the aid of Fig. 15. A collimated laser beam illuminates a particle in the vicinity of the object plane of an imaging system. The shadow of the particle is projected at a known magnification and moves across a linear photodiode array. The shadow of a particle is related to the particle size by the magnification.

Two types of processing electronics are used in conjunction with these arrays. The Optical Array Spectrometer simply determines the number of elements shadowed by the particle and thus provides a particle diameter measurement (1-D Spectrometer). The second type obtains

18

full two-dimensional shadow images of particles (2-D Spectrometer) by simultaneously sampling the output of each photodiode element in the array at a very fast rate to provide sequential image slices as the shadow transits the array.[5]

In our testing both the 1D and 2D Spectrometers were used, covering the particle size ranges 20-300μ and 25-600μ respectively.

To a first approximation, the sample cross section in these Optical Array Spectrometers is the product of the array width and the particle depth-of-field. In the case of the 1-D Spectrometer, end elements of the array are used to reject partial shadow conditions which would result in undersizing. In the case of the 2-D spectrometer, partial shadows are handled through software in the analysis of the image data. To complete the sample cross section definition, one needs only to define the depth-of-field. If the illuminated regions are well collimated, the depth-of-field is limited only by diffraction-induced divergence of the shadow region behind the particle,which causes gradual filling and fading of the shadow boundaries.[6] For present discussions, we need only to recognize that this divergence leads to inaccurate measurements at large depths-of-field and that the available depth-of-field where accurate measurements can be made varies as the square of the particle radius. A particle 20 μm in diameter has a 1 mm depth-of-field while a particle several hundred microns in diameter may have up to a meter depth-of-field. In an instrument sizing these larger particles, the depth-of-field is invariably truncated by the mechanical limits of the sampling aperture. However, with sizing small particles, the depth-of-field must be truncated by other than mechanical means if a large percentage of the particles are to be sampled in situ. The method most commonly used to provide optical depth-of-field truncation is through the use of multiple thresholding in the processing of the shadow signals from each photodetector element. One threshold is obviously required for sizing and a second for depth-of-field limiting. For accurate particle sizing, the appropriate shadow threshold is approximately 50%. In order to truncate the depth-of-field it is desirable that a secondary

19

threshold be set at a darker level. This lower threshold must be reached by at least one of the shadowed elements during particle transit. This seccndary threshold need only be slightly lower than 50% (roughly the amount equivalent to the noise band). If maximum depth-of-field is desired, a setting of about 60% is used. If a shorter depth-of field is desired, settings of up to 80% are used.

In the 1-D Spectrometers depth-of-field calibration is performed over the size range through actual measurements. It can be calibrated to better than 10% for spherical particles.

When the 2-D Spectrometer is applied to measurements of small particle size, the method just described can be used or multiple shadow density levels can be simultaneously measured and displayed in the imagery to provide a grey-scale which contains the needed depth-of-field information. This again can be processed by software. The depth-of-field can be more accurately specified since particle morphology information is also available.

The detailed results obtained during our tests at PMS are presented in full in Section 6.2.1.

5.3.2 Sodium Injection Procedure

In order to collect the droplets generated in the sodium injection test for size analysis, they had to be frozen before they contacted any test chamber surface. They then settled to the bottom of the chamber where the collection system, Fig. 6, was located.

A minimum condition for freezing the sodium droplets is that a suitable overall heat balance be achieved. Assuming injection conditions of 0.75 GPM of sodium at 150°C and 50 SCFM of argon at 150°C combining to produce sodium aerosol which is then cooled to 50°C, calculation shows that 13.3 kW of cooling power would be required.

Continuous operation of the injector under these conditions could have been achieved by continuously flowing precooled gas through the

injection chamber to supply the necessary cooling; however, this would require 216 SCFM of argon at -100°C or 132 SCFM of argon at -196°C. Cooling on a continuous basis thus appeared impractical, not only because of the large volumes of precooled argon required, but also because essentially all of the sodium aerosol generated would be swept from the injection chamber by the high velocity cooling gas.

Intermittent operation of the injector was therefore necessary, with the test chamber filled with precooled argon gas just prior to the injection. There is then sufficient cooling capacity stored in the chamber to handle the heat load, provided the injection period is short. With the chamber gas cooled to -100°C the maximum injection period is 1.3 seconds, for gas at -196°C the allowable period becomes 4.6 seconds. A final aerosol temperature of 50°C is assumed here, as in the earlier estimates.

Verification of the nozzle operation with liquid sodium was achieved, therefore, by making a series of short duration (1-3 seconds) test injections into a pre-cooled chamber. The frozen sodium particles were then collected at the base of the chamber and removed to an inert atmosphere glove box for sieving and weighing. Six stainless steel U.S. standard sieves were used in the size range 38-425 µm. Each injection was controlled automatically by a programmable controller (Texas Instruments, 5TI) to which the solenoid valves (gas line), pneumatic valve (sodium line), gas heater, and visicorder were electrically connected. The controller was programmed to operate each injection in the following sequence:

1. Gas heater on

2. Argon flow on

3. Visicorder on

4. Sodium flow on

5. Sodium flow off

6. Visicorder off

21

7. Gas heater off

8. Argon flow off

The time interval between each of these steps was variable down to
0.1 seconds. Each injection was visually observed through the viewing
ports, but attempts to take high speed photographs of the spray were
hampered by the difficulty in transmitting sufficient light through
the dense aerosol.

The sodium flow profile for these short duration injections
was recorded by passing the electromagnetic flow meter signal
into the visicorder. A typical flow profile is shown in Fig. 16
which is a plot of the signal (in millivolts) against time for a
two second injection. The profile exhibits a sharp increase when
the pneumatic sodium valve is first opened and a small initial peak after
$\sim$ 1/10 second. This is followed by a gradual decrease for the main
duration of the injection, followed by a fairly sharp cut-off. This type
of profile enabled an accurate calculation of the sodium flow rate using
standard calibration tables.

6.0 RESULTS

6.1 General Nozzle Characteristics

6.1.1 Spray Angle

The Sonicore nozzle was initially studied by taking still photographs, Fig. 17, and high speed video tapes with water as the spraying liquid. These photographic records showed that the nozzle spray was not quite homogeneous, but was split into 3 segments of greater spray density, presumably caused by the 3 struts supporting the nozzle resonator cup. The average included spray angle, however, was of the order of 60-70°. There was very little evidence of dripping from the nozzle during continuous operation.

Subsequently, the nozzle was mounted in an adjustable cylindrical shroud, Fig. 18. The distance, L, was variable, enabling either spraying directly into the atmosphere or, alternatively, from within an enclosed cylinder. It was felt that this latter mode would simulate, to some extent, the situation expected in the silicon production reactor. At various values of L between 0 and 12", the sprayed water impinging on the cylinder walls in a given time was collected and measured. The results are presented in Fig. 19 as percentage water recovered versus L. With the nozzle 10" from the edge of the shroud, only ∿20% of the injected water emerged from the cylinder. This result is significant since, at L = 10", the angle between the nozzle and the edge of the shroud is 60°, indicating that the spray angle for the shroud-enclosed nozzle was greater than for the non-enclosed case. This same effect is seen at all distances within the cylinder. The most probable explanation for this phenomenon is that the high velocity, conical spray draws air from the dead space behind it; this air cannot readily be replaced, thereby producing a tendency for the spray cone angle to increase.

23

This result may be of importance in the chemical reactor, since a very large spray angle could result in the atomized liquid particles impinging directly on the cylindrical reactor walls before they can be entrained in the arc heater gas stream. A possible solution would be the introduction of a secondary inert gas flow around the nozzle, thereby cancelling out the aspirator effect. Such a course of action would upset the heat balance of the reactor, however, and a better approach would be to simply position the nozzle as close as possible to the arc heater gas stream.

6.1.2 Spray Velocity

A rough theoretical estimate of the <u>maximum</u> aerosol velocity shortly after it emerges from a nozzle can be obtained from consideration of momentum conservation:

$$\text{Initial Momentum Rate of Gas + Initial Momentum Rate of Liquid =}$$
$$\text{Final Momentum Rate of Aerosol} \qquad (6.1)$$

For a nitrogen flow of 35 SCFM, a water flow of 1.5 GPM, and a nozzle diameter of 1 cm, one has

$$(20.6 \text{ g /sec}) \times (210 \text{ m/sec}) + (94.6 \text{ g /sec}) \times (0) = (115.2 \text{ g /sec})$$
$$\times \text{ mean aerosol velocity} \qquad (6.2)$$

from which one obtains a mean aerosol velocity of about 38 ms^{-1}. A second momentum exchange process becomes appreciable after the aerosol has traveled only 4 to 5 nozzle diameters from the nozzle:[7] a jet flow develops which entrains adjacent gas into the jet, further decelerating it. After a distance of about 10 nozzle diameters, a fully developed turbulent free jet is established which entrains gas equivalent to the nozzle fluid mass flow for about every 3 nozzle diameters along the jet axis; consequently the jet deceleration may become quite pronounced.

24

In the case of the Sonicore nozzle, however, considerably lower velocities might be expected after the stream impinges on the resonator cup. This was confirmed by a photographic analysis of the spray produced by the nozzle in both its normal mode and with the resonator cup removed. Without the cup, the nozzle still operates like a two-fluid atomizer, although it produces coarser particles, and in this manner might be expected to approximate more to the theoretical prediction given above.

High speed strobe photographs of the spray showed that without the sonic cup in position, the particles at a distance of 3 feet from the nozzle were effectively frozen using a flash speed of $\frac{1}{25600}$ seconds. At a reduced flash speed of $\frac{1}{6400}$ seconds, however, each particle in the field of view clearly left a trail on the print indicating a finite degree of movement during the duration of the exposure. Measurement of these distances directly from the prints enabled approximate velocities to be calculated. It was clear that there was a considerable spread in velocities, the majority lying in the range 8-20 ms^{-1}. In contrast, with the resonator cup in position, the particle velocities were so much slower that even at the lowest flash speeds no movement could be detected.

The particle velocities were estimated, however, from high speed video films taken at 120 frames per second. Analysis of those films indicated particle velocities in the range 1-2 ms^{-1}.

6.2 Sodium Nozzle Size Distribution

6.2.1 Laser Imaging Results

The operating parameters for the nozzle tests performed at Particle Measuring Systems (P.M.S.) are shown in Table 1. A total of seventeen tests was run on the Sonicore and Sprayco nozzles at varying water flow rates and gas-to-liquid mass ratios. The Sprayco nozzle has an adjustable outlet which controls its spray pattern and particle size, and the distances in parentheses are a measure of this adjustment.

The results are printed out by the computer in a number of different forms, viz, plots of mass distribution, number distribution, cumulative mass distribution, and a table of the precise data from which the plots are compiled.

Figure 20 is an example of a simple mass distribution plot which shows the percentage of the total mass which is present as particles ^ articular size. The size axis is divided into 15 channels (30 . .he 2D spectrometer), each with a 20 μm span and covering the total range 20-300 μm for the 1D spectrometer and 20-600 μm for the 2D.

A second way of presenting this same information is shown in Fig. 21, a cumulative mass distribution, which shows the percentage of the total mass present as particles less than a given size.

Each of the seventeen tests was run for at least 3 minutes of continual nozzle operation and plots such as Figs. 20 and 21 were obtained at ten second intervals. Rather than reproduce all of this data, the results are presented in Figs. 22-25 as log-normal distributions (see Eq. 4.8) for the Sonicore and Sprayco nozzles as determined by the 1D and 2D spectrometers. The results for a given nozzle and spectrometer are presented as a band within which all of the individual plots (every 10 seconds) fall. Although the relationships obtained were not all perfectly linear, it was felt that the log-normal distribution was the best method for presenting and comparing the different nozzles.

One striking feature of the results was the very large number of particles observed in the smallest size channel, i.e., 20 μm. The distributions depicted, however, are converted into mass, which shifts the mean diameter to a higher value.

Comparisons of Fig. 22 with Fig. 23, and of Fig. 24 with Fig. 25, reveal a significant difference between the 1D and 2D results for the same nozzle. The mean diameter obtained from the 1D is 5-10 times larger than that from the 2D. This apparent anomaly has been shown to be due to a high degree of coincidence error inherent in the less sophisti'ated

1D instrument. This effect is due to the very high concentration of small particles noted earlier, which can cause particle events which are actually two or more small particles passing through the sample area simultaneously, Fig. 26. The computer analysis of the data from the 2D spectrometer includes certain rejection criteria to eliminate such coincidence errors that can occur in the 1D. These are:

(i) Bulk Area – A rectangle is drawn around the image such that the sides of the rectangle touch the extremities of the image (see Fig. 27). If the ratio of the particle area (number of shadowed elements in the image) to the area of the rectangle is < .5, the particle is rejected.

(ii) Light Slice – Figure 26 shows the relationship of the optical array to two particles. The particles would be seen by the OAP-1D as one particle event and sized as 22 elements. The Light Slice computer algorithm rejects this event because there is a light slice normal to the optical array.

(iii) Aspect Ratio – Particles with dimensions normal to the optical array of > 3 times the dimension parallel to the array are rejected. This helps eliminate streakers which may result from impact with part of the probe such as the tips.

Further computer analysis of the 2D data was performed with these rejection criteria deliberately omitted from the program. This resulted in an increase in the apparent particle sizes to values similar to those reported by the 1D instrument. This check thereby confirmed that the large 1D values were caused by the inability of the instrument to include the more rigorous rejection criteria of the 2D. Since the 1D data cannot be modified to accept these computer algorithms, they cannot be included in our assessment of the nozzle performance. The 2D data, however, is considered to be fully representative of the nozzle spray produced.

27

A detailed study of this 2D data for the Sonicore nozzle, Fig. 23, shows several features of interest. Firstly, when the nozzle was operating in its normal mode, the mass median drop size varied between 18 and 68 μm. As expected, however, when the resonator cup was removed from the nozzle, causing it to operate like a more conventional gas atomizer, the median diameter increased to ∿ 240 μm. Equations 4.11 and 4.12 indicate that the mean diameter might be expected to decrease with increasing gas to liquid mass ratios. Within the band of results in Fig. 23, this was generally found to be true, although the relationship was not sufficiently reproducible to enable an empirical dependence such as Eq. 4.12 to be formulated. From this, we can conclude that since the highest gas to liquid ratio in these tests was 0.28, the higher values permitted in the silicon reactor (up to 1.0) should easily produce a mass median drop size < 25 μm.

Figure 25 shows that the results for the Sprayco nozzle were similar in range and spread to those for the Sonicore. Again, there was an overall tendency towards smaller median diameters as the gas to liquid mass ratio increased. In fact, the drop sizes for the Sprayco were generally slightly smaller than those for the Sonicore nozzle.

6.2.2 Sieving Results

The results of the sodium particle sieving experiment for the Sonicore nozzle, described in Section 5.3.2, are presented in Table 2. These data are shown to obey a log-normal distribution in Fig. 23 which also includes the 2D data for the same nozzle. The mass median diameter is 140 μm and the σ_g value is 1.85. Both of these figures reflect a noticeable difference between these results and those obtained by the laser technique, 6.2.1. The larger median diameter indicated by the sieving data is not inconsistent with the inherent limitations of the two techniques. In the sieving experiment, the very smallest particles tended to be swept upwards in the injection chamber and were later found to have been trapped on the filter. These particles,

of course, were extremely small and probably have little effect on the overall mass distribution. A more serious source of error which might lead to high results, however, is the possibility of larger particles, or even drips, being produced when the spray is first started up or switched off. These larger particles would certainly fall to the bottom of the chamber and be collected. In the laser experiment, however, the spray was only sampled while the nozzle was continually operating in a steady state. Any larger, non-typical particles formed during start up would not show up in this analysis. Another reason why the laser experiments might miss some larger particles is that the water was sprayed horizontally as opposed to vertically downwards in the sodium freezing and sieving tests. Some heavier particles could therefore have been gravitationally separated from the spray before reaching the spectrometer probes.

The atomization of water and sodium may be theoretically compared by substitution in Lubanska's empirically derived equation (Eq. 4.12) described in Section 4.3. The marked similarity in the density, viscosity and surface tension of water at 25°C and sodium at 150°C, dictate that the mean particle diameter of atomized sodium should be very similar to that of water in the same nozzle and under identical flow conditions.

6.3 Silicon Tetrachloride Nozzle Test

The nozzle chosen for the task of silicon tetrachloride injection (Spraying Systems Co., Nozzle No. 1/4 LN6) has been fully characterized by the manufacturers. For this reason, the laboratory tests were conducted simply to demonstrate the feasibility of producing a fine silicon tetrachloride spray under the proposed reactor conditions. The particle size distribution for the nozzle at the projected flow conditions (9 GPH, 100 psi) is shown in Fig. 28. The mass median diameter is close to 120 μm with a σ_g of 1.44.

29

A series of test injections with silicon tetrachloride was run at 9 GPH and 100 psi for up to a minute. The resultant spray was recorded using high speed (1000 frames per second) cine-photography. Films were shot to show the nozzle during both start up and steady state continual operation.

7.0 DISCUSSION

The main purpose of the project was to select and characterize a nozzle suitable for the spray atomization of liquid sodium into small (< 200 μm) particles at relatively high flow rates (45 GPH). The results, presented in Section 6.0, show the Sonicore 312T sonic gas atomizing nozzle to be suitable for this task. The Sprayco gas atomizing nozzle also gave every indication that it could produce particles of a sufficiently small size to be used in the reactor. The efficient operation of the latter nozzle was, however, very sensitive to the adjustment of the spray orifices. This added complexity led to the decision to concentrate testing on the Sonicore nozzle, but it is felt that the Sprayco could also perform satisfactorily if more development time were to be expended on it. In addition to the collection of particle size data, it was necessary to acquire operating experience with the nozzle and to pay particular attention to the manner in which the nozzle would be integrated into the sodium supply system of the silicon product reactor.

It has been mentioned in Section 6.1.1 how the spray angle produced by the nozzle dictates that it be positioned as close as possible to the arc heater gas stream. The discovery that the spray velocity is relatively low compared with other types of nozzles, is also of relevence to the reactor since longer residence times in the hot gas stream near the arc heaters will facilitate vaporization of the sodium.
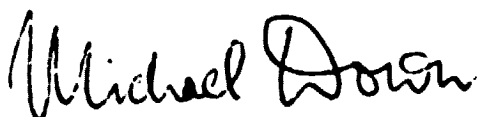
The theoretical and experimental study of the dependence of particle size on gas-to-liquid mass ratio is also directly related to the silicon process pilot unit. For the initial tests, to be run at 45 GPH sodium, an argon atomizing gas flow of 50 SCFM has been

31

recommended. This should enable the nozzle to operate smoothly for long periods of time with the minimum amount of dripping, and to provide sufficiently small particle sizes. By consideration of both the laser imaging and the sieving results, the mass median particle size is expected to be in the range 20-140 μm. This is certainly within the limits required for efficient vaporization.

The testing of the silicon tetrachloride nozzle was also successful. The chosen hydraulic nozzle was shown to operate efficiently at the required conditions of 9 GPH and 100 psi.

8. ACKNOWLEDGEMENTS

Acknowledgements are due to A. F. Berringer of the Materials Chemistry Section, Westinghouse Research and Development Center, who was responsible for the construction of the equipment and for much of the testing. In addition, M. G. Fey and T. Meyer (Westinghouse Power Circuit Breaker Division) and F. J. Harvey and D. F. Ciliberti (Westinghouse Research and Development Center) provided continued advice and discussion.

M. G. Down
Materials Chemistry

J. E. Bauerle
Materials Chemistry

A. R. Keeton
Materials Chemistry

Approved: F. G. Arcella, Manager
Materials Chemistry

33

9.0 REFERENCES

1. C. Orr, Spraying and Atomizing, from Particulate Technology MacMillan (New York) 1966, p. 1.

2. S. Nukiyama, Y. Tanasawa, "An Experiment on the Atomization of Liquid," Trans. Soc. Mech. Engrs. (Japan), 5, pp. 1-4 (1939).

3. H. Lubanska, J. Metals, 1979, p. 45.

4. N. Hughes, U.S. Patent Nos. 3,230,923; 3,230,924; 3,400,253 and 3,400,254.

5. R. G. Knollenburg, "The Use of Low Power Lasers in Particle Size Spectrometry," SPIE, Partical Applications of Low Power Lasers, Vol. 92, pp. 137-152 (1976).

6. R. G. Knollenburg, "The Optical Array," J. Appl. Meteor., Vol 9 1, (1970).

7. J. M. Beér, N. A. Chigier, Combustion Aerodynamics, Applied Science Publishers Ltd. (London) 1972, Chapter 2.

TABLE 1

Tests Performed at PMS

SONICORE NOZZLE

Run No.	Liquid Flow (GPM)	Mass Ratio $\left(\dfrac{Air}{Liq.}\right)$	Spectrometer
1	0.75	0.29	1D
2	0.75	0.22	1D
3	0.75	0.19	1D
4	0.75	0.14	1D
5	0.75	0.33	1D
6	0.75	0.28	2D
7	0.75	0.22	2D
8	0.75	0.19	2D
9 (without cup)	0.75	0.31	2D

SPRAYCO NOZZLE

Run No.	Liquid Flow (GPM)	Mass Ratio $\left(\dfrac{Air}{Liq.}\right)$	Spectrometer
10 (6.35 mm)	0.7	0.30	2D
11 "	0.4	0.46	2D
12 "	0.3	0.59	2D
13 "	0.7	0.24	2D
14 (6.50 mm)	0.7	0.26	1D
15 "	0.55	0.31	1D
16 (5.98 mm)	0.75	0.24	1D
17 "	0.45	0.39	1D

TABLE 2

Particle Size Analysis of Sodium Spray

(Sonicore Nozzle - Model 312T)

Size Range (µ)	Mass of Na (g)	Mass %	Cumulative Mass %
300-400	0.0865	11.24	100.00
200-300	0.1249	16.23	88.76
100-200	0.3434	44.63	72.52
50-100	0.1802	23.42	27.8﹀
<50	0.0344	4.47	4.47

Test Parameters

Sodium Flow	45 GPH
Argon Flow	50 SCFM
Argon Pressure	⌄40 PSI

Gas:Liquid Mass Ratio = 0.6
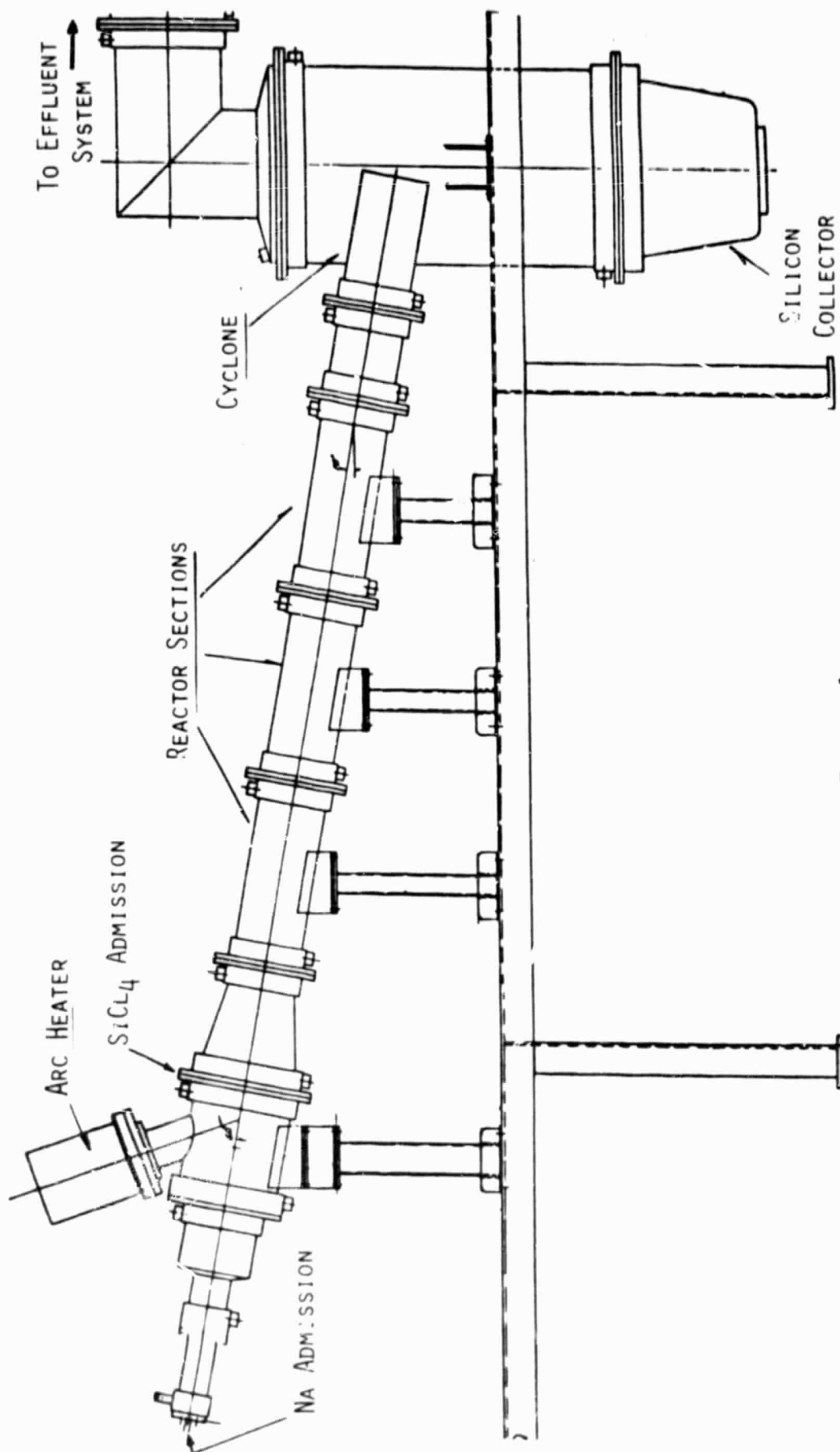
FIGURE 1

SILICON PROCESS REACTOR ASSEMBLY
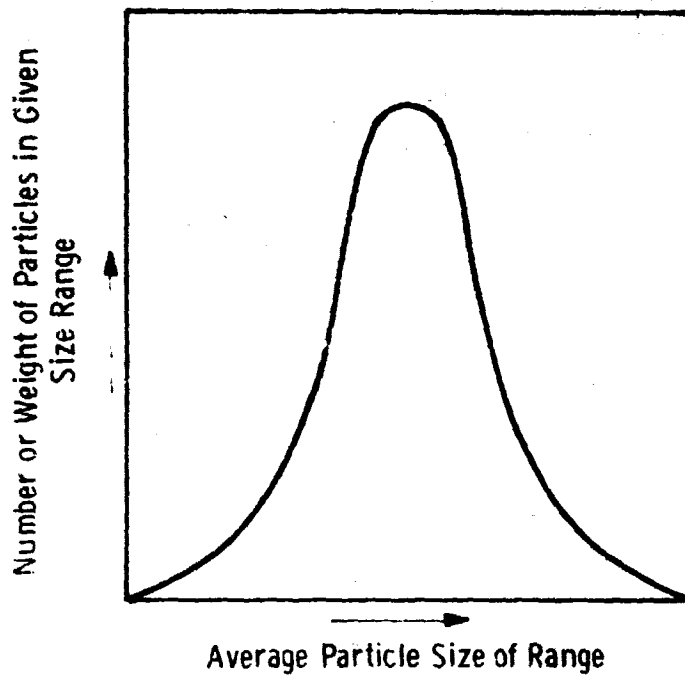
Fig. 2 — Typical frequency particle size
distribution plot
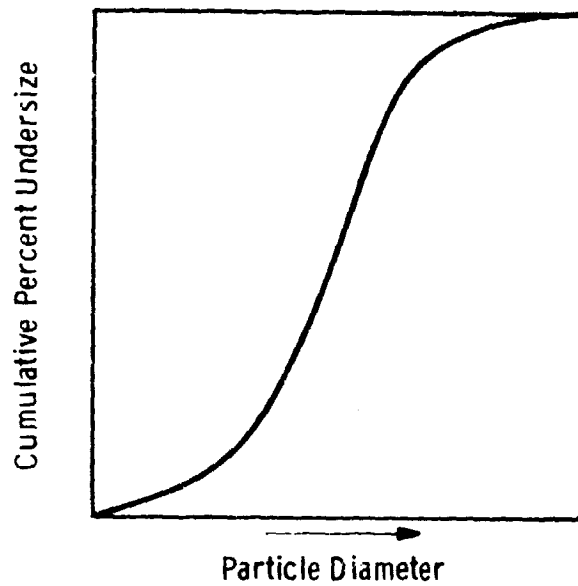
Fig. 3 — Typical cumulative particle size
distribution plot

C - 3
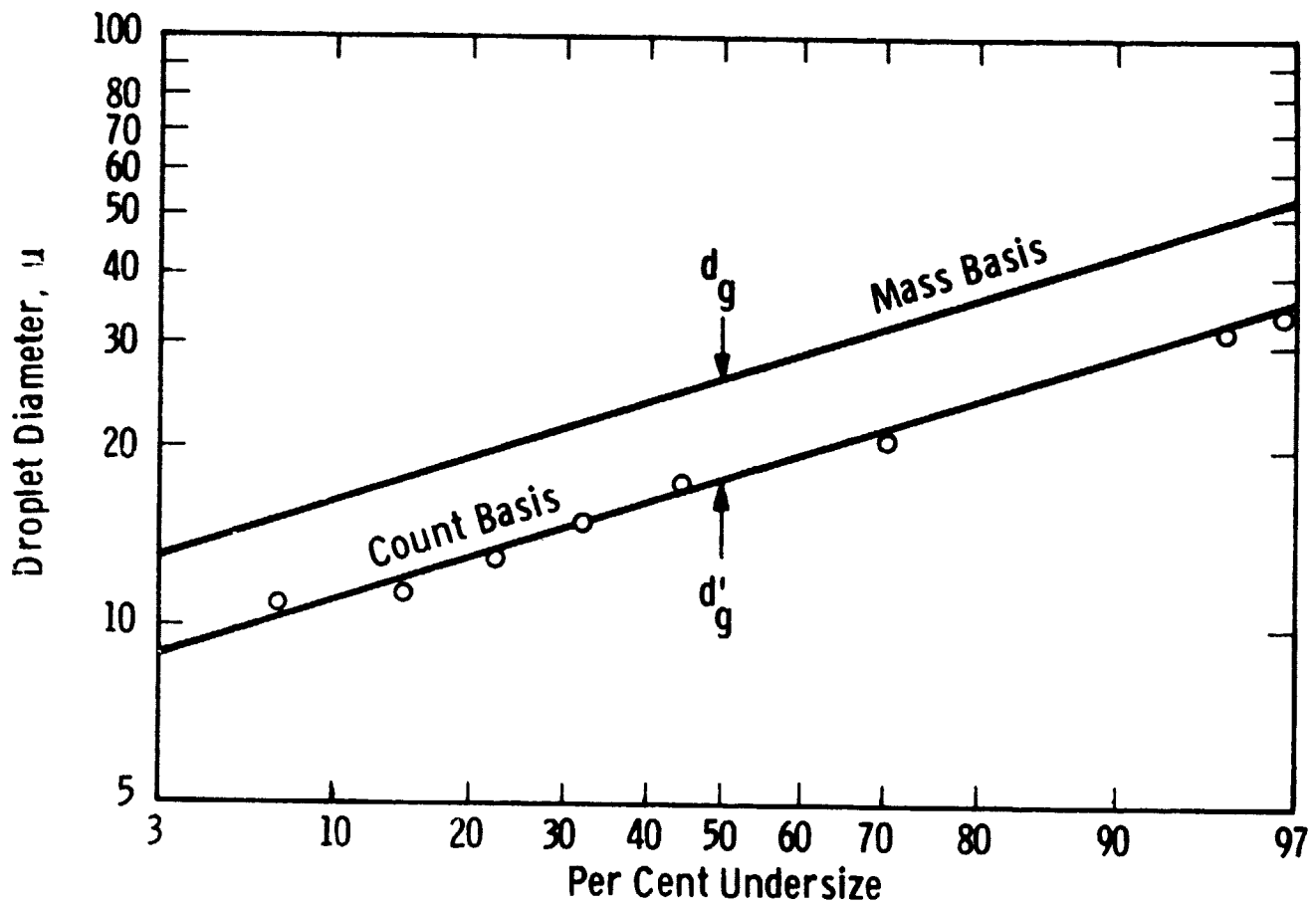
Fig. 4 — Typical log-probability plot of experimental and calculated spray-droplet data
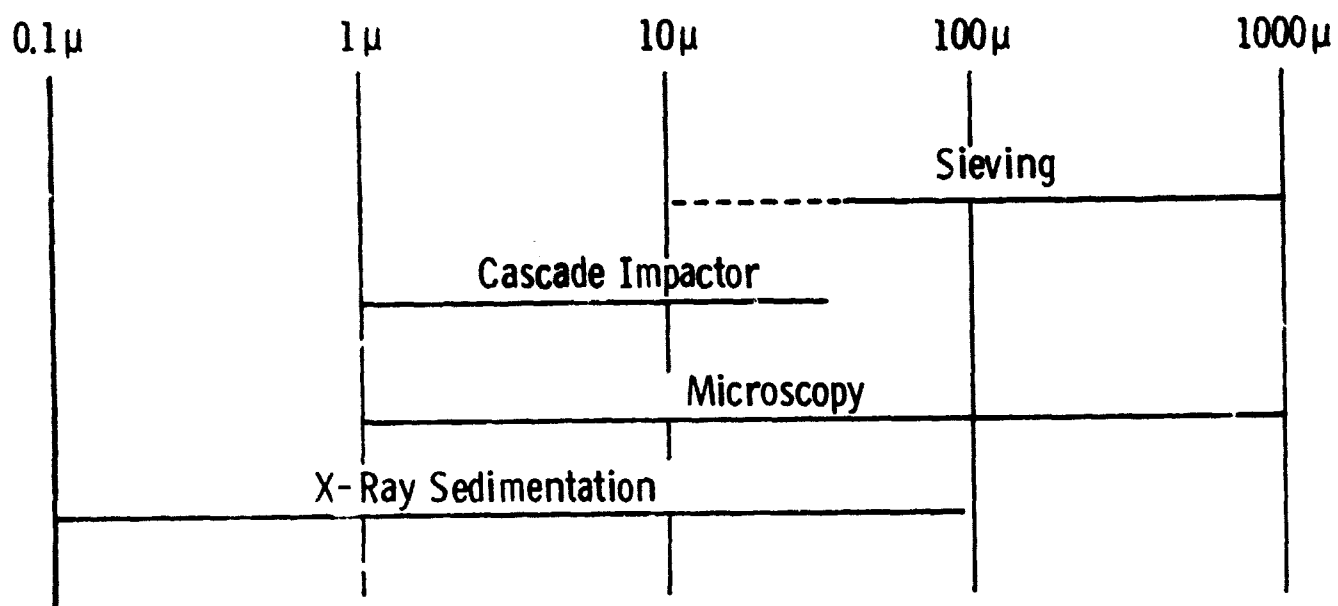
Fig. 5 — Particle size analysis ranges

1. Injection Chamber
2. Test Nozzle
3. Nozzle Holder
4. Filter
5. Ball Valve
6. Gas Circulator
7. Gas Cooler
8. View Port
9. Support Stand
10. Gas Distribution Funnel
11. Particle Collector
12. Test Fluid Supply Tank
13. View Port Sweep Gas
14. Gas Supply
15. Gas Heater
16. Emergency Pressure Relief
17. Elect. Heater
18. Gas Flowmeter
19. Liquid Flowmeter
20. 300 SCFM Absolute Filter

To Building Ventilation

Fig. 6 — Injection techniques test system
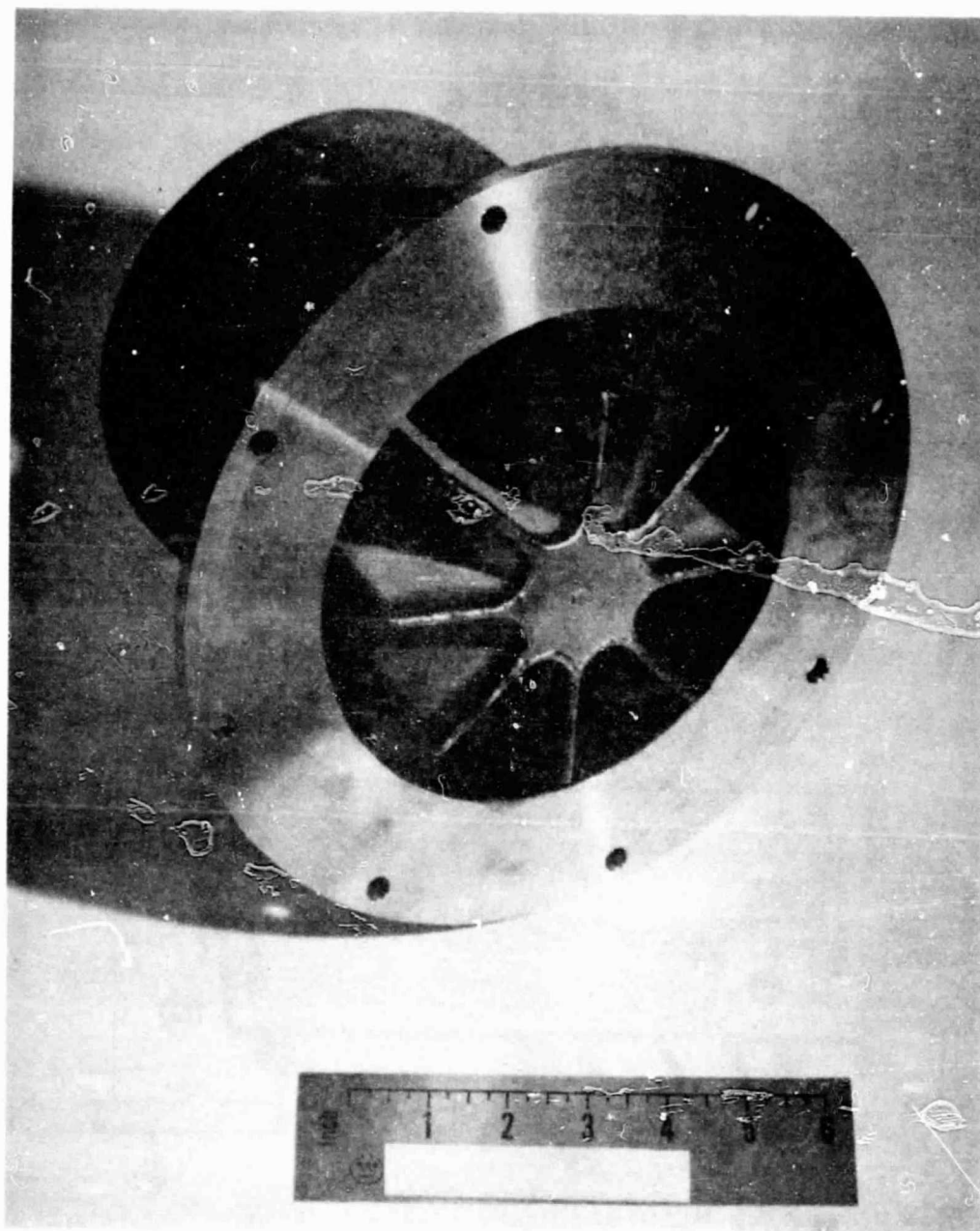
Fig. 7. Internal stainless steel filter for injection test chamber.

RM-80727
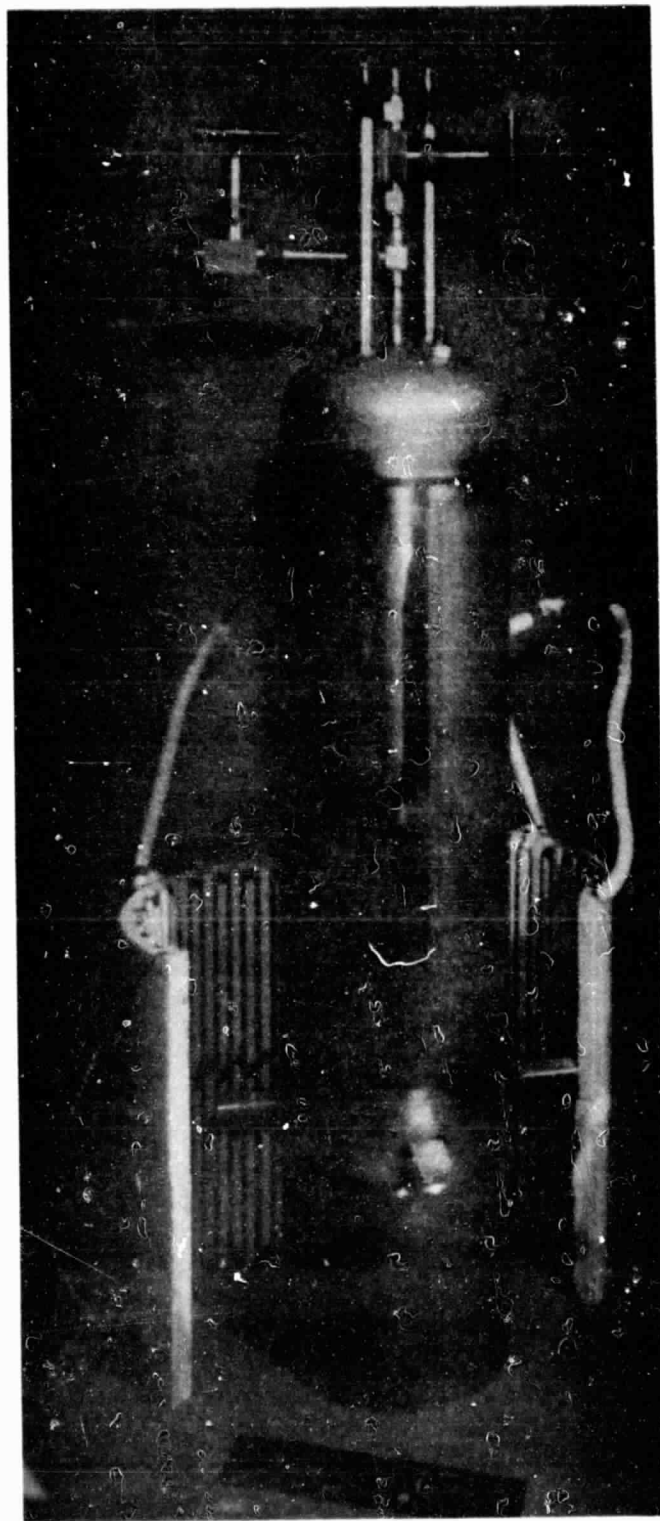
Fig. 8.   Photograph of the Sodium Storage Tank

43
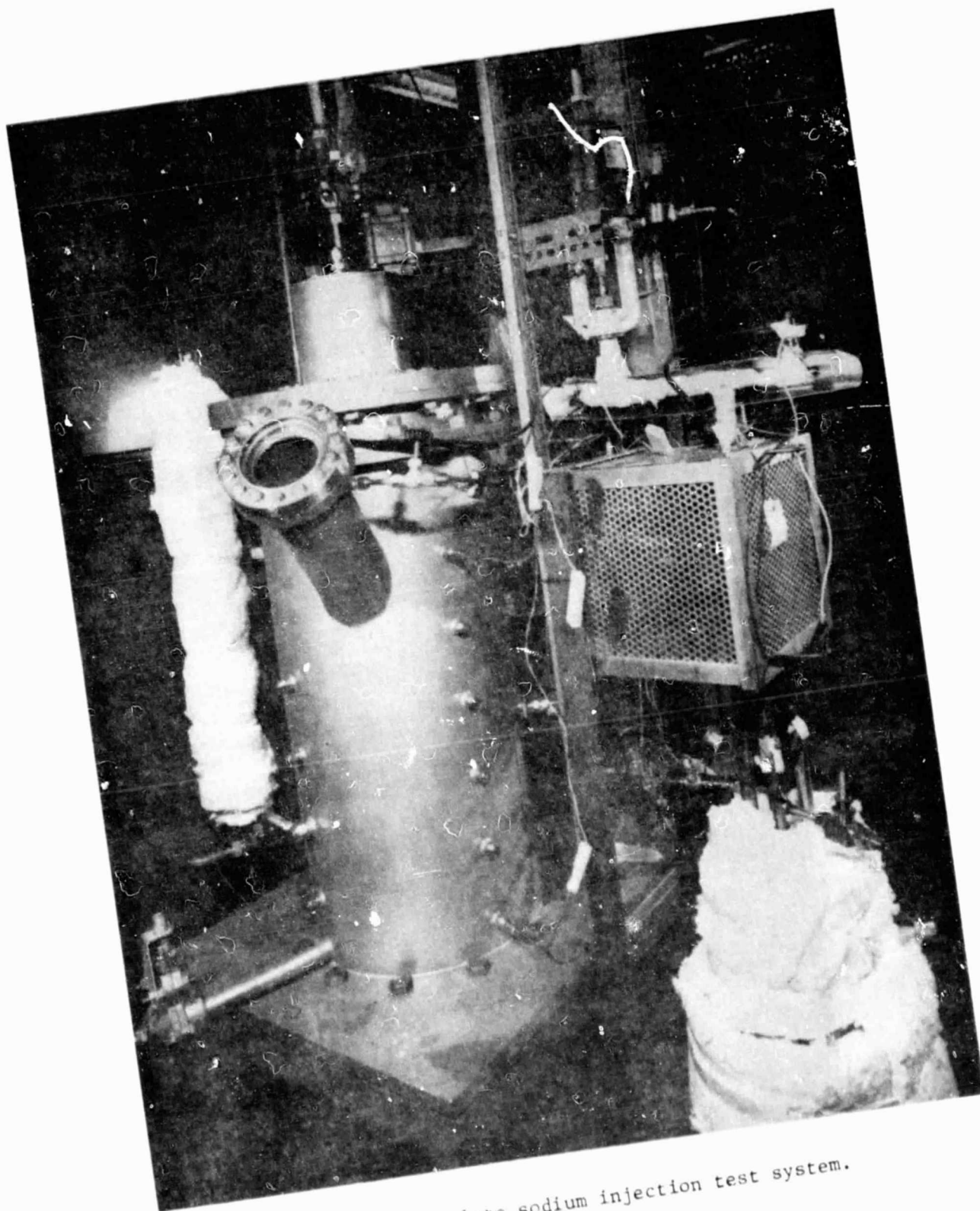
Fig. 9. Complete sodium injection test system.
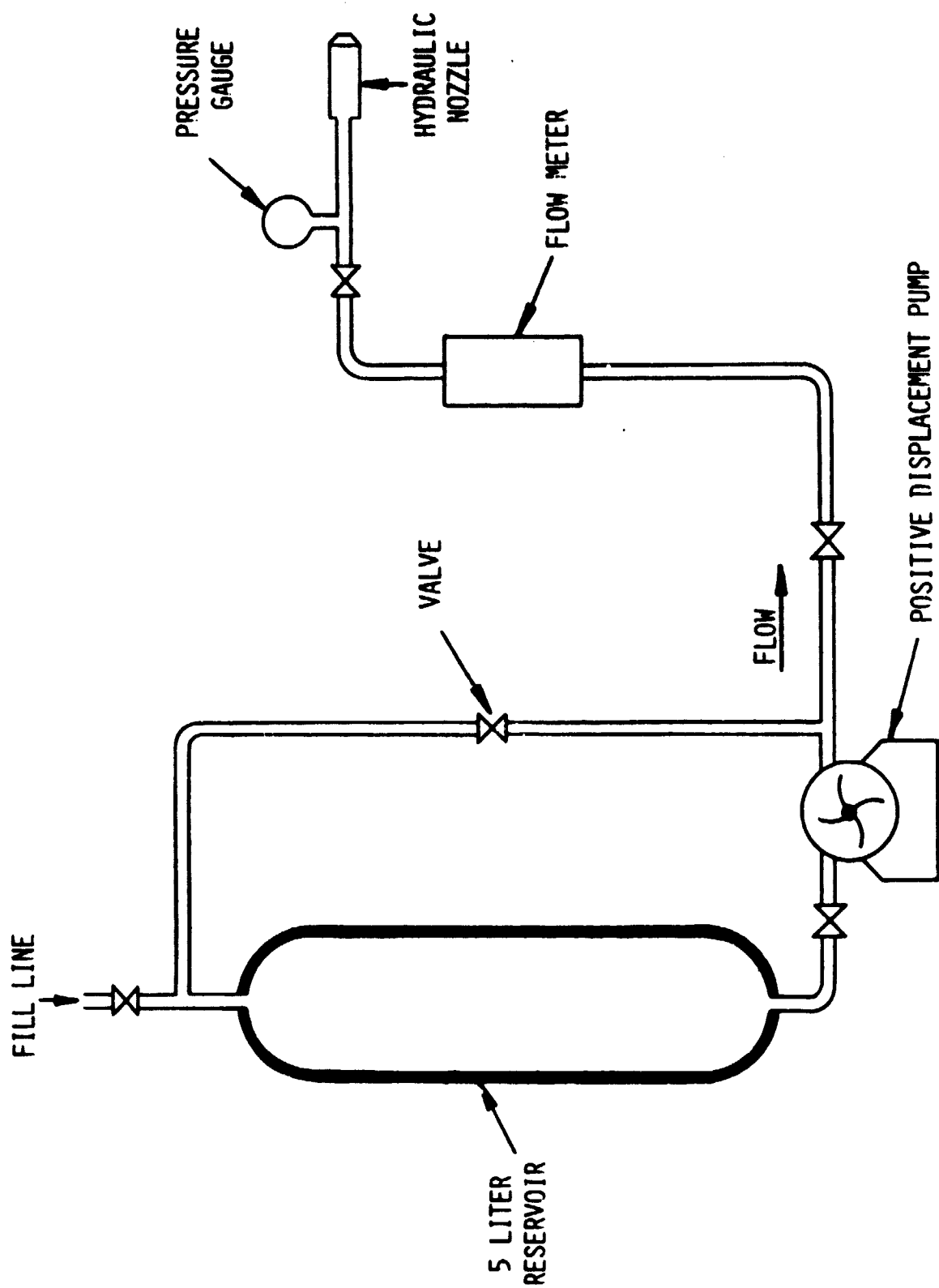
FIGURE 10. SCHEMATIC OF THE SILICON TETRACHLORIDE SUPPLY SYSTEM
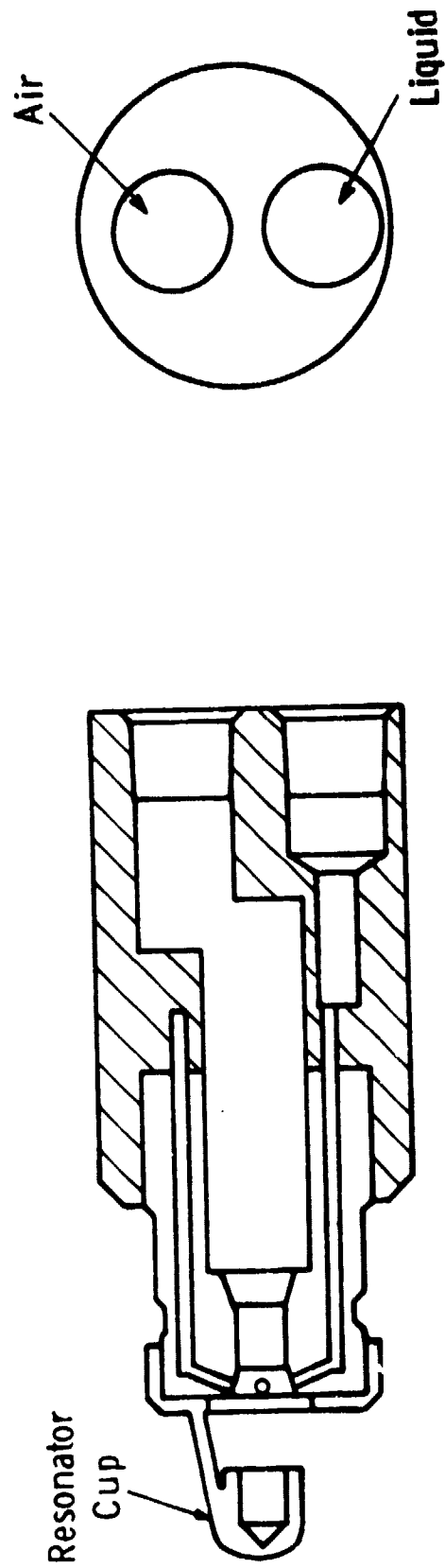
Fig. 11 – Schematic of Sonicore 312 nozzle
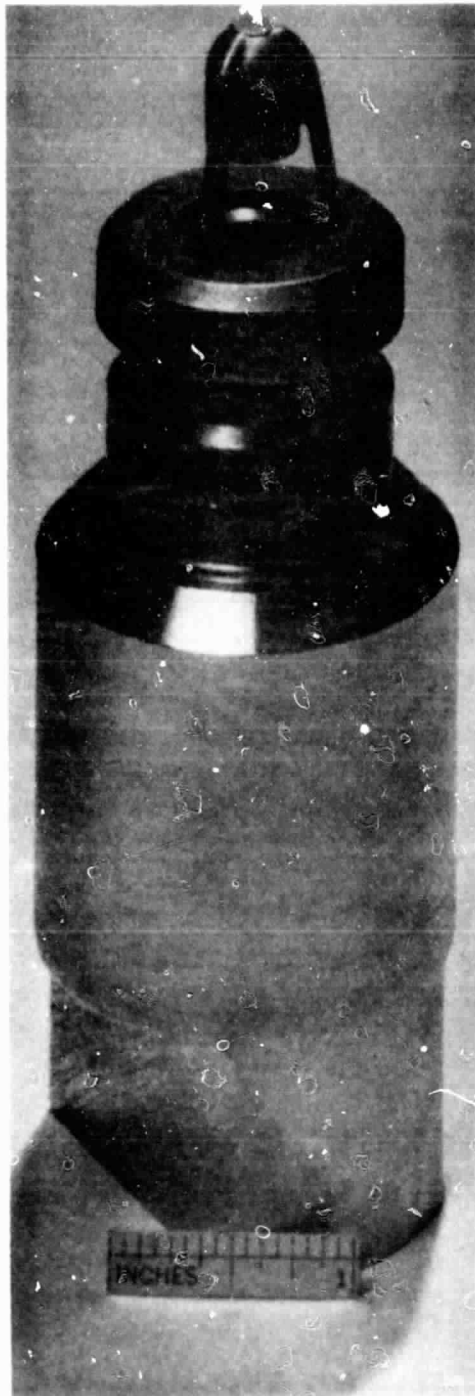
Fig. 12. Photograph of Sonicore 312T nozzle.

47
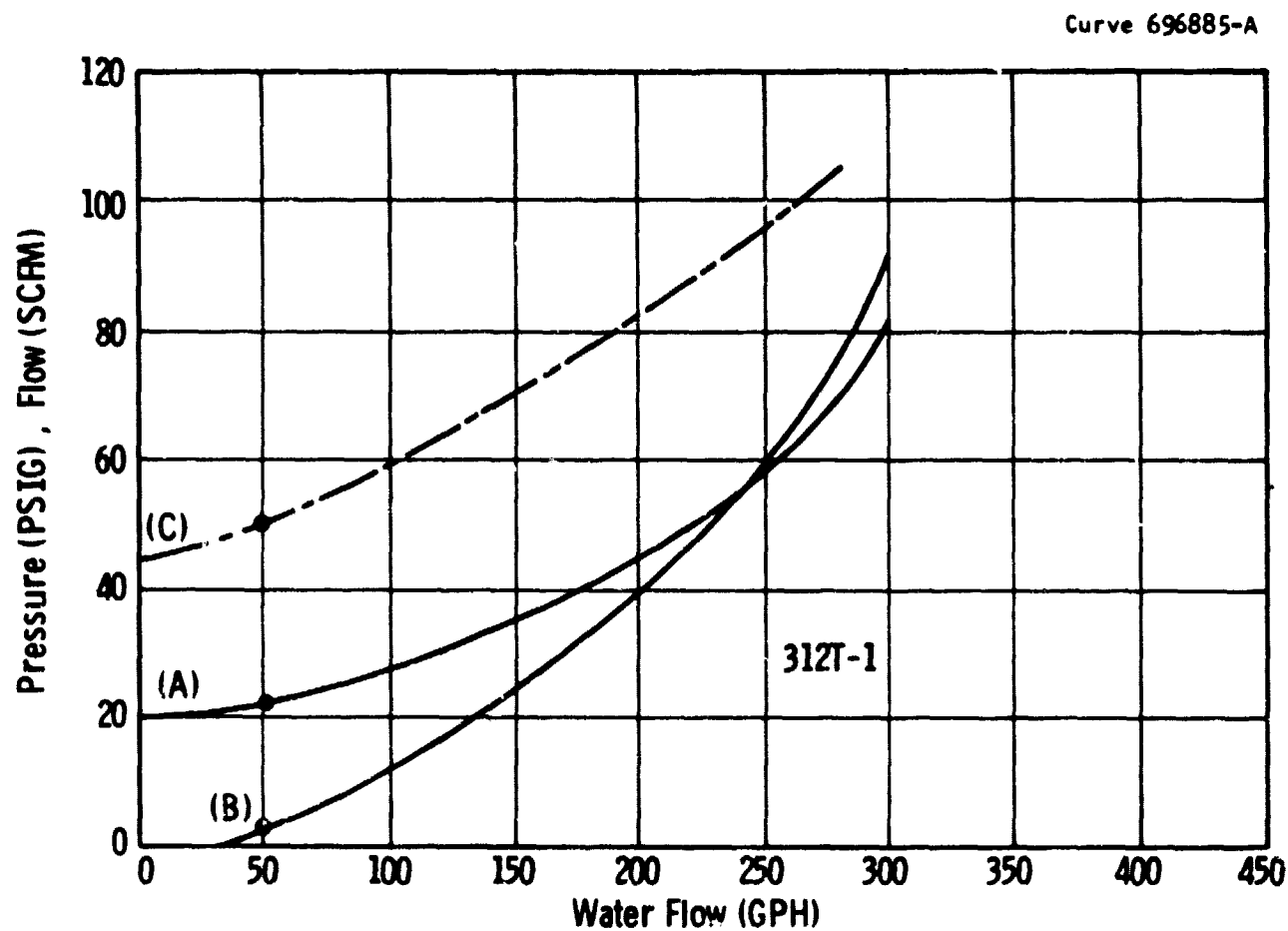
Fig.13—Operational parameters for Sonicore 312T nozzle. Water flow vs water pressure (A), Air Pressure (B), Air Flow (C)
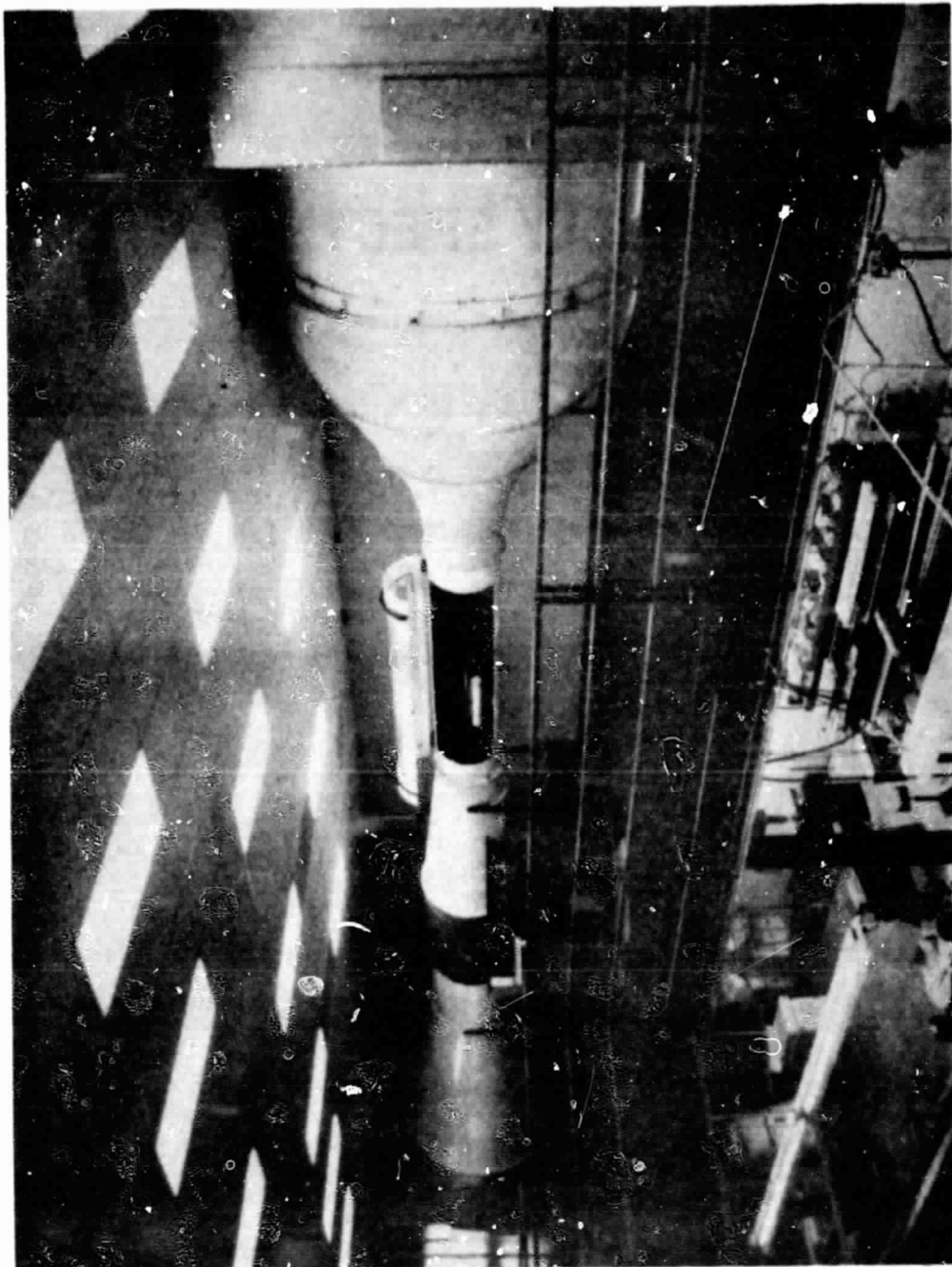
Fig. 14. Particle Size Facility at P.M.S. (Inc.), showing wind tunnel and laser spectrometers.

RM-80731

OPTICAL ARRAY SPECTROMETER
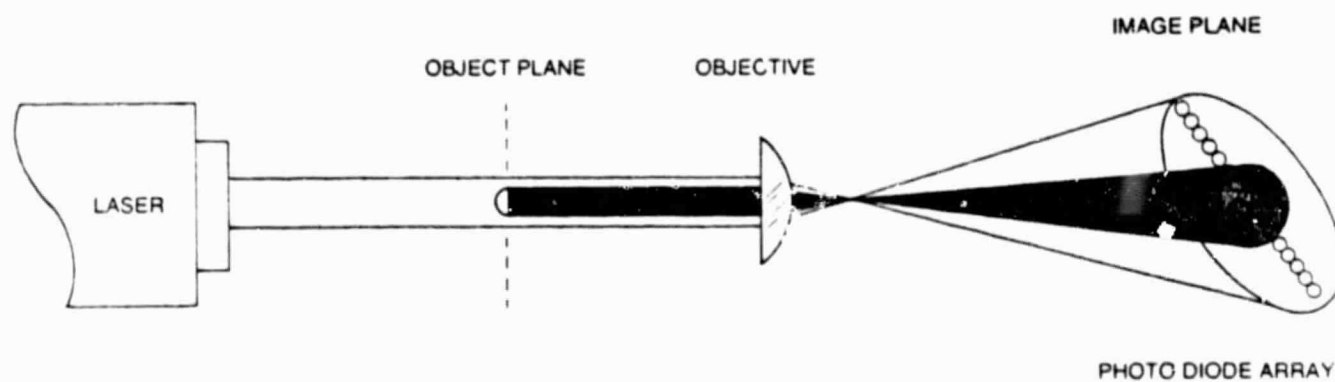
Fig. 15. Simplified optical diagram illustrating the typical collimated illumination used in the laser spectrometer.

Curve 696884-A
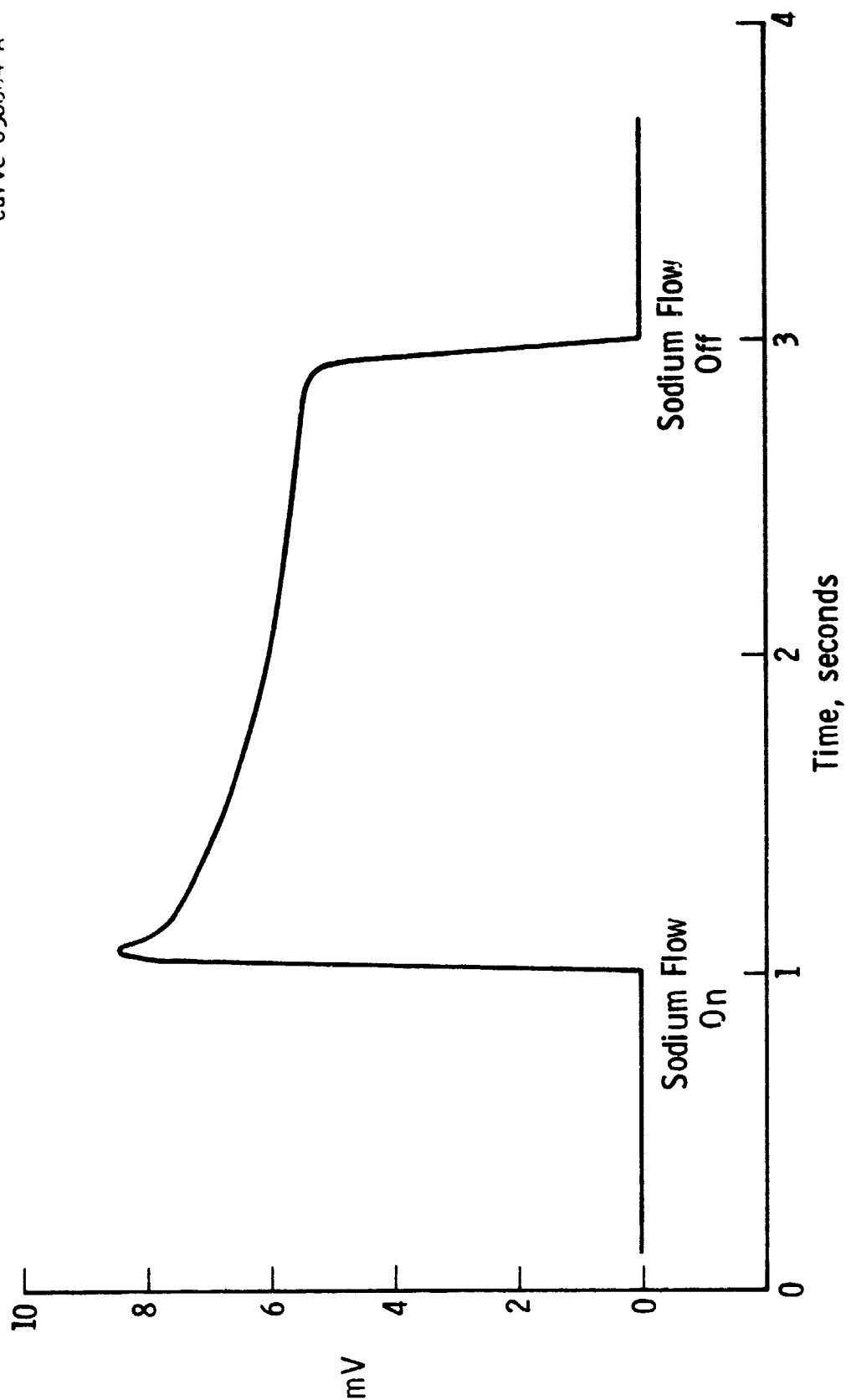
Fig.16 – Sodium flow meter output versus time – injection No.2

51

Fig. 17. Sonicore nozzle operating in air with water as the test fluid and air as the atomizing gas

52
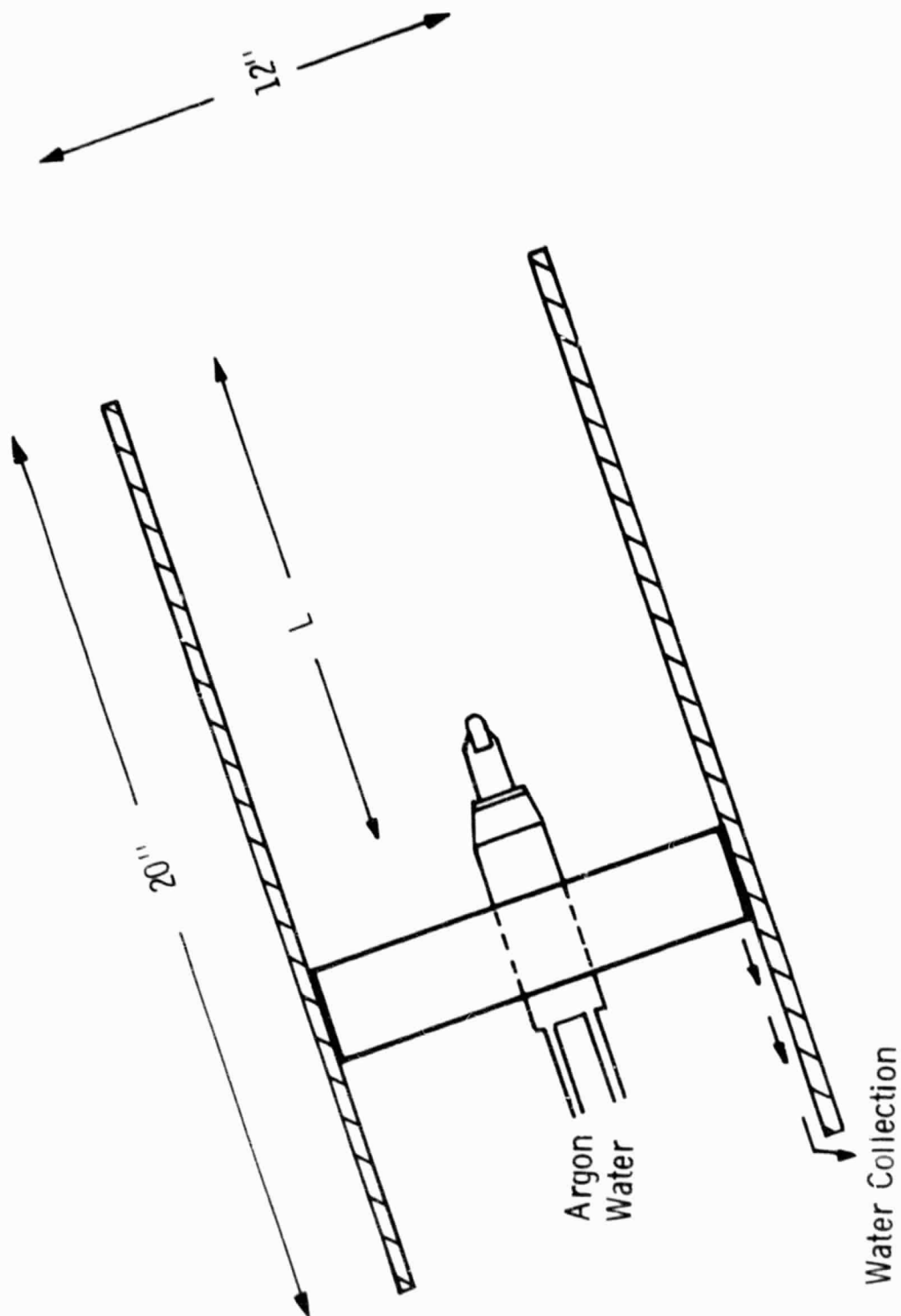
Fig.18 — Water testing shroud

Dwg. 6428A39

12"

20"

L

Argon
Water

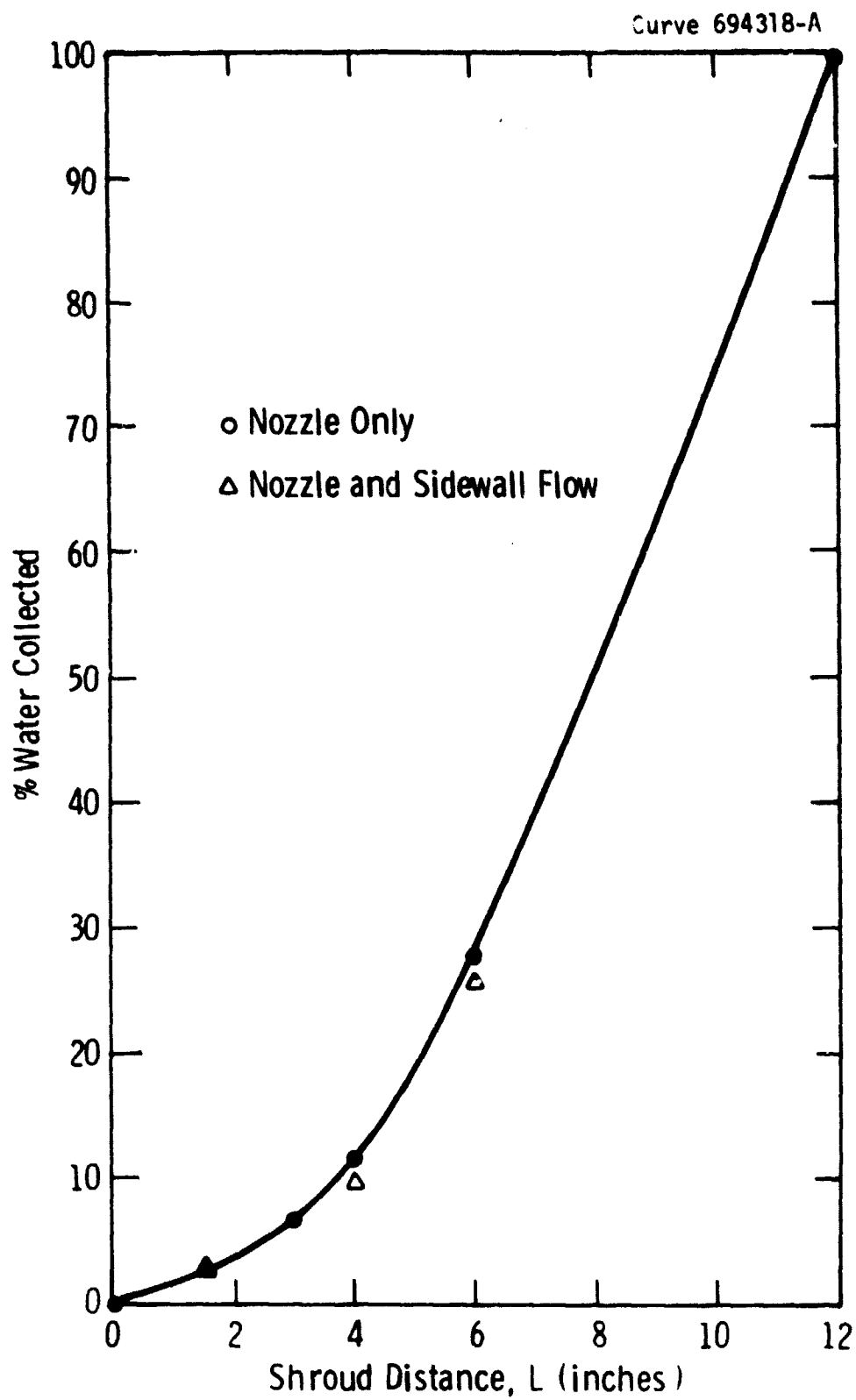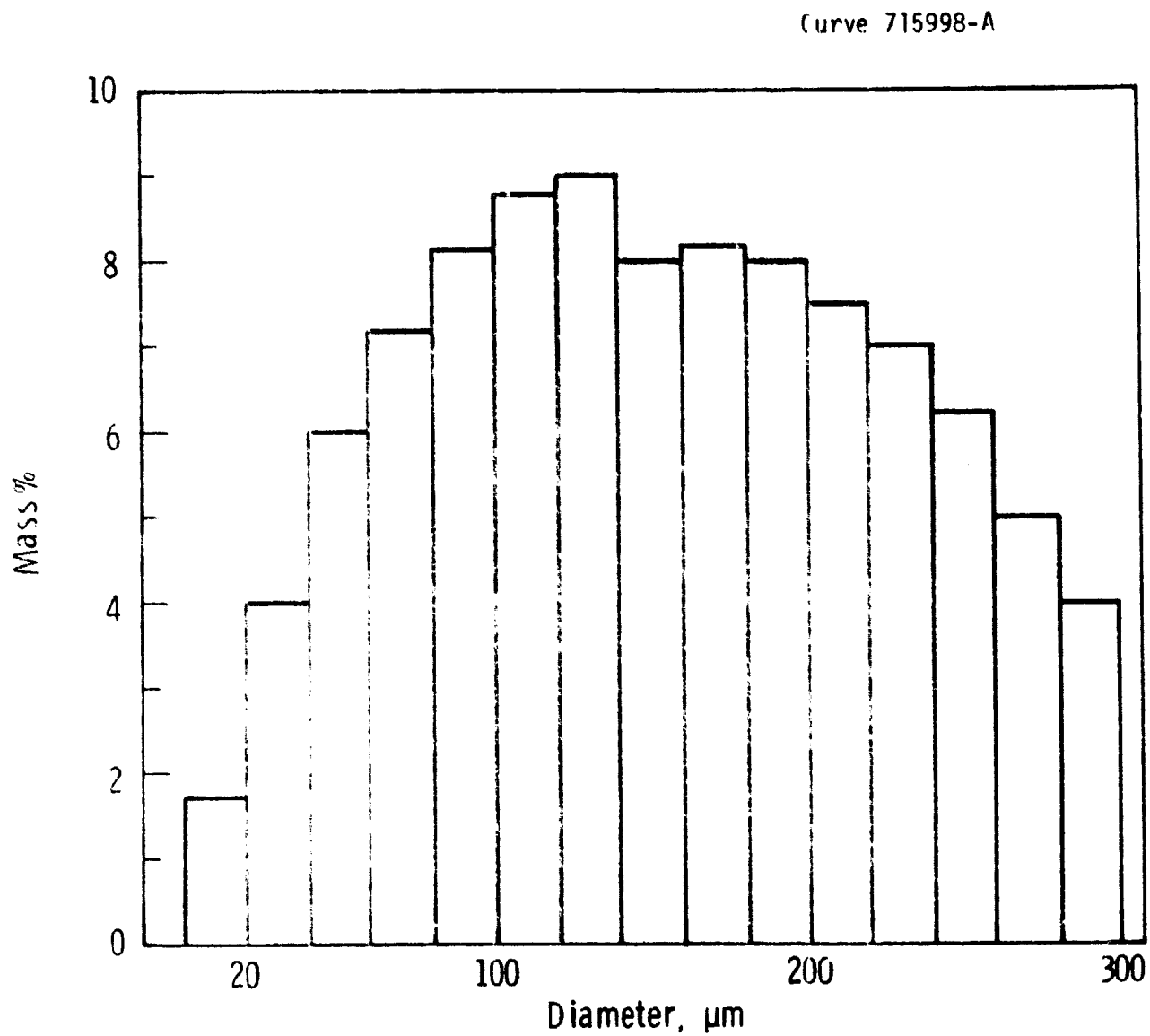Water Collection

53

Curve 694318-A

Fig. 19

Fig. 20 — Mass distribution plot for Sonicore nozzle, run #1
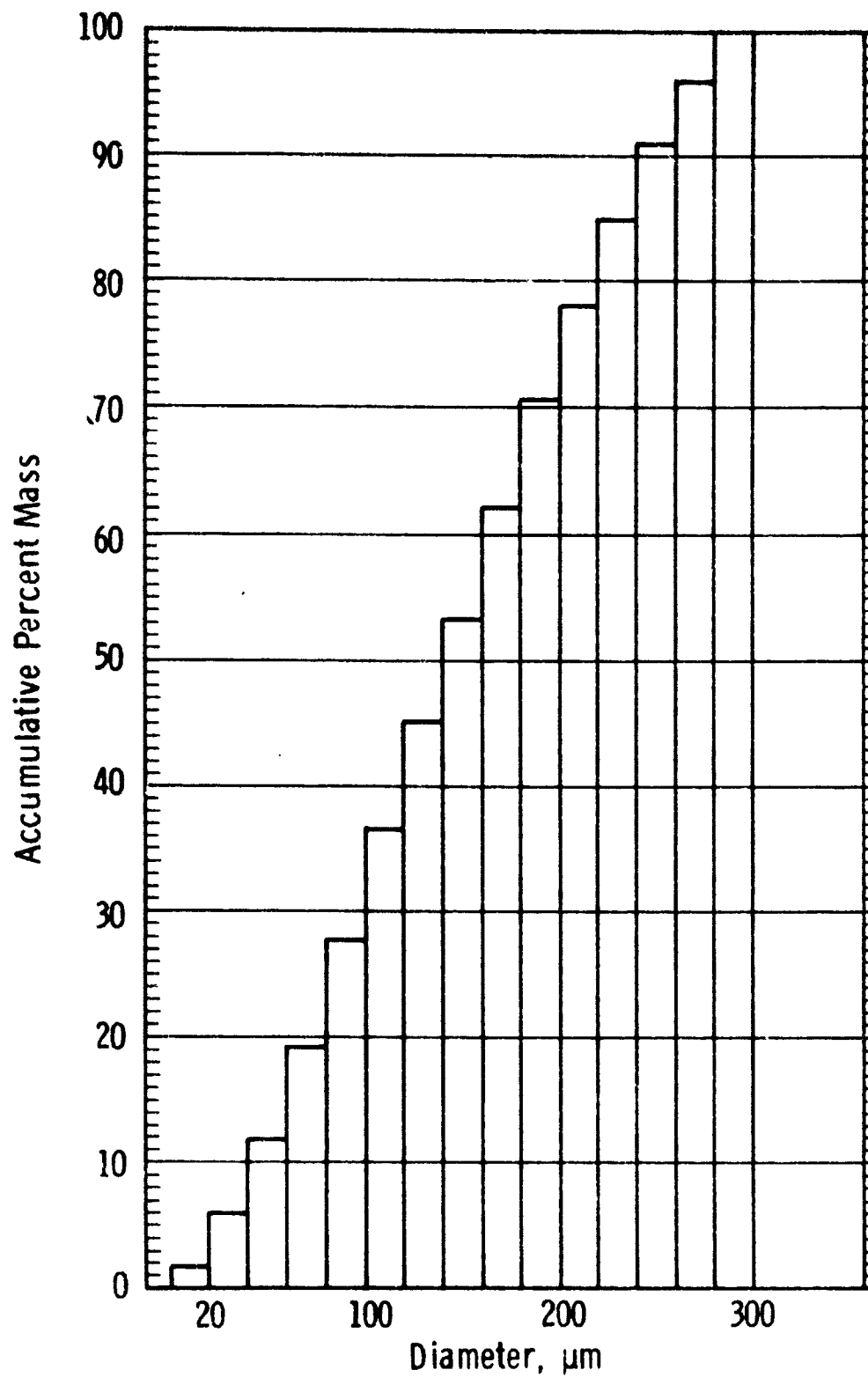
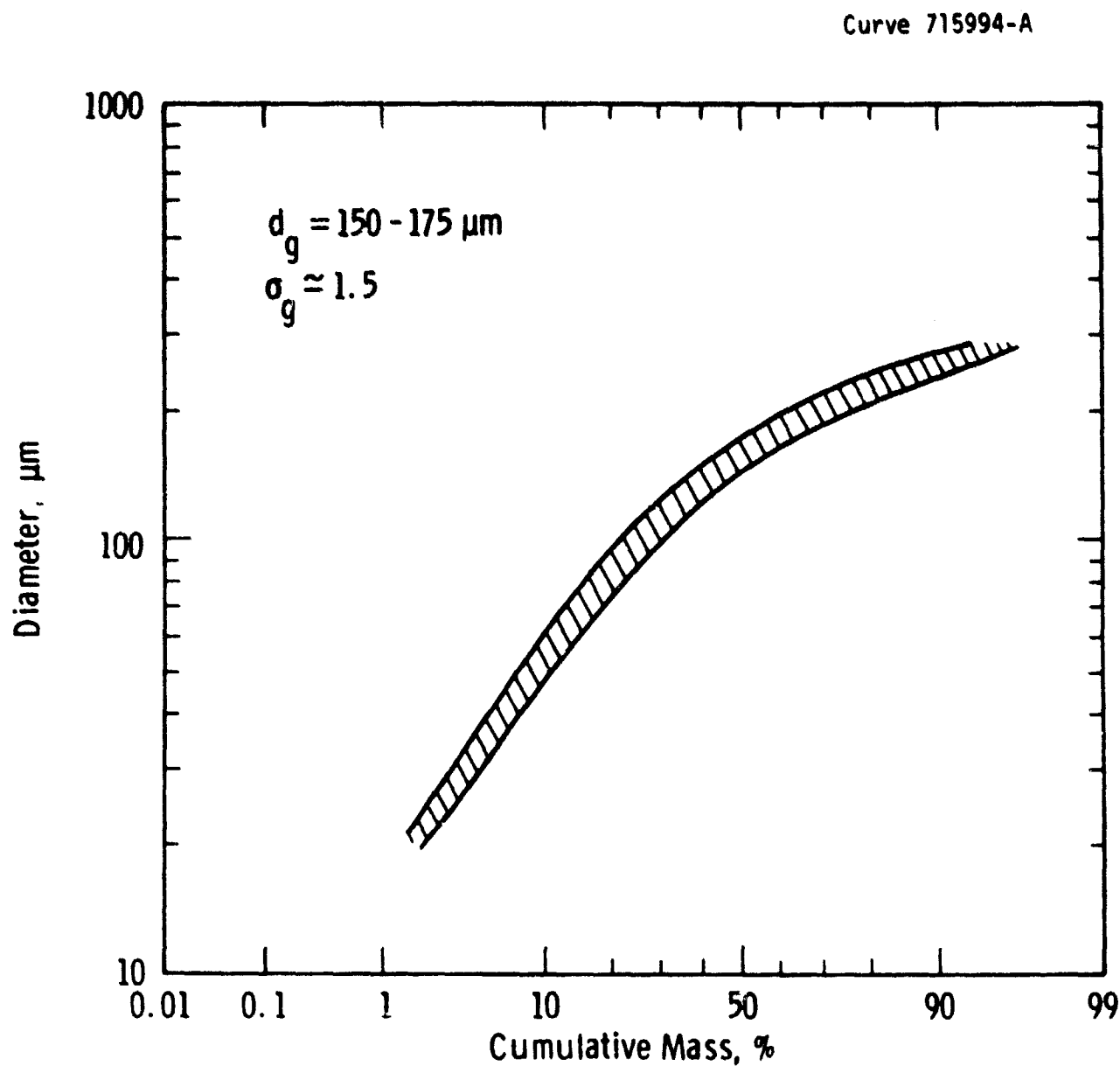Fig. 21 – Cumulative mass distribution for Sonicore nozzle, run # 1

$d_g = 150 - 175 \ \mu m$

$\sigma_g \simeq 1.5$

Fig. 22 — Log-normal distribution for Sonicore nozzle -1 D spectrometer

Fig. 23 — Log-normal distribution for Sonicore nozzle -2D spectrometer
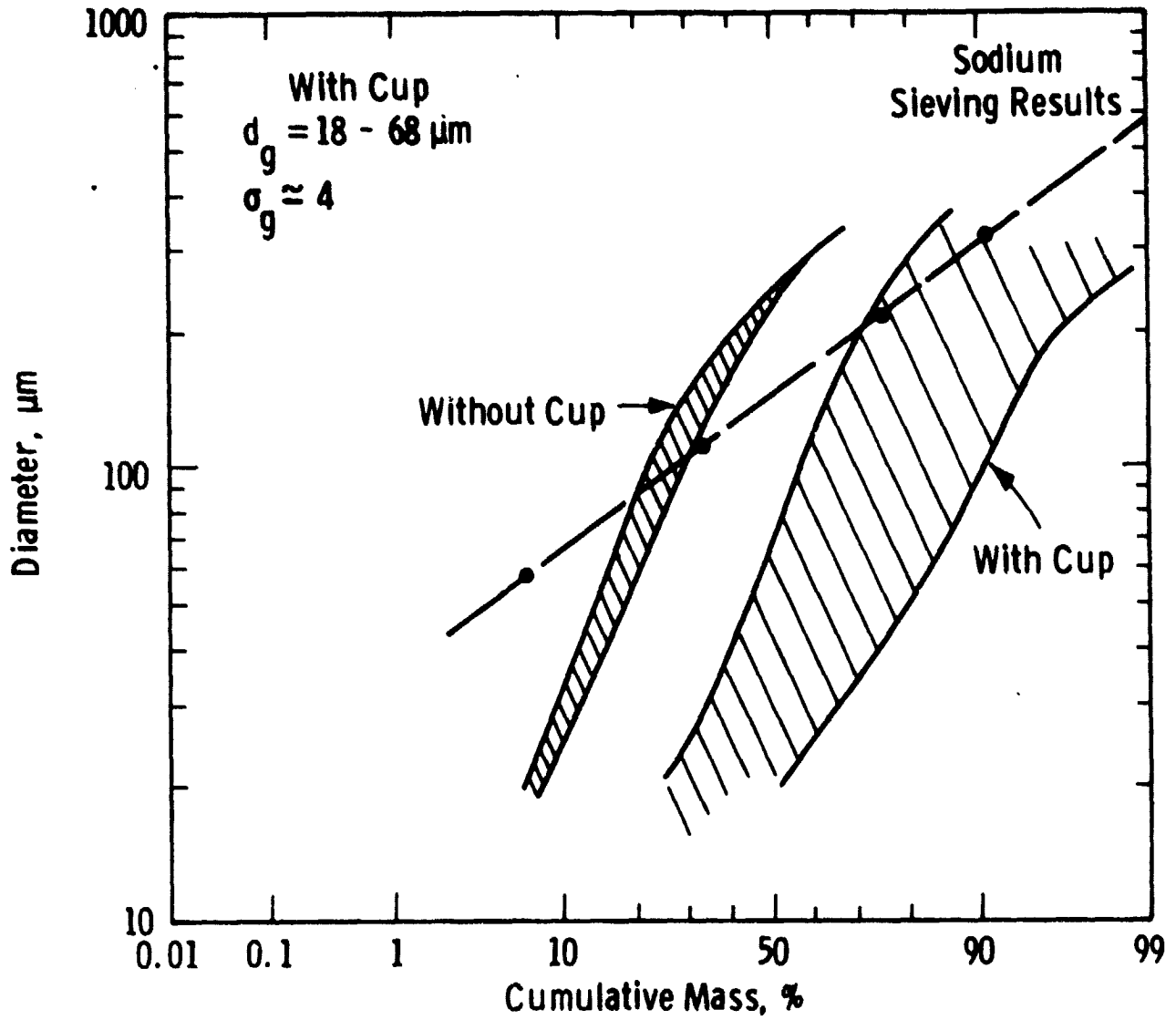
$d_g = 170 - 200 \ \mu m$

$\sigma_g \simeq 1.5$

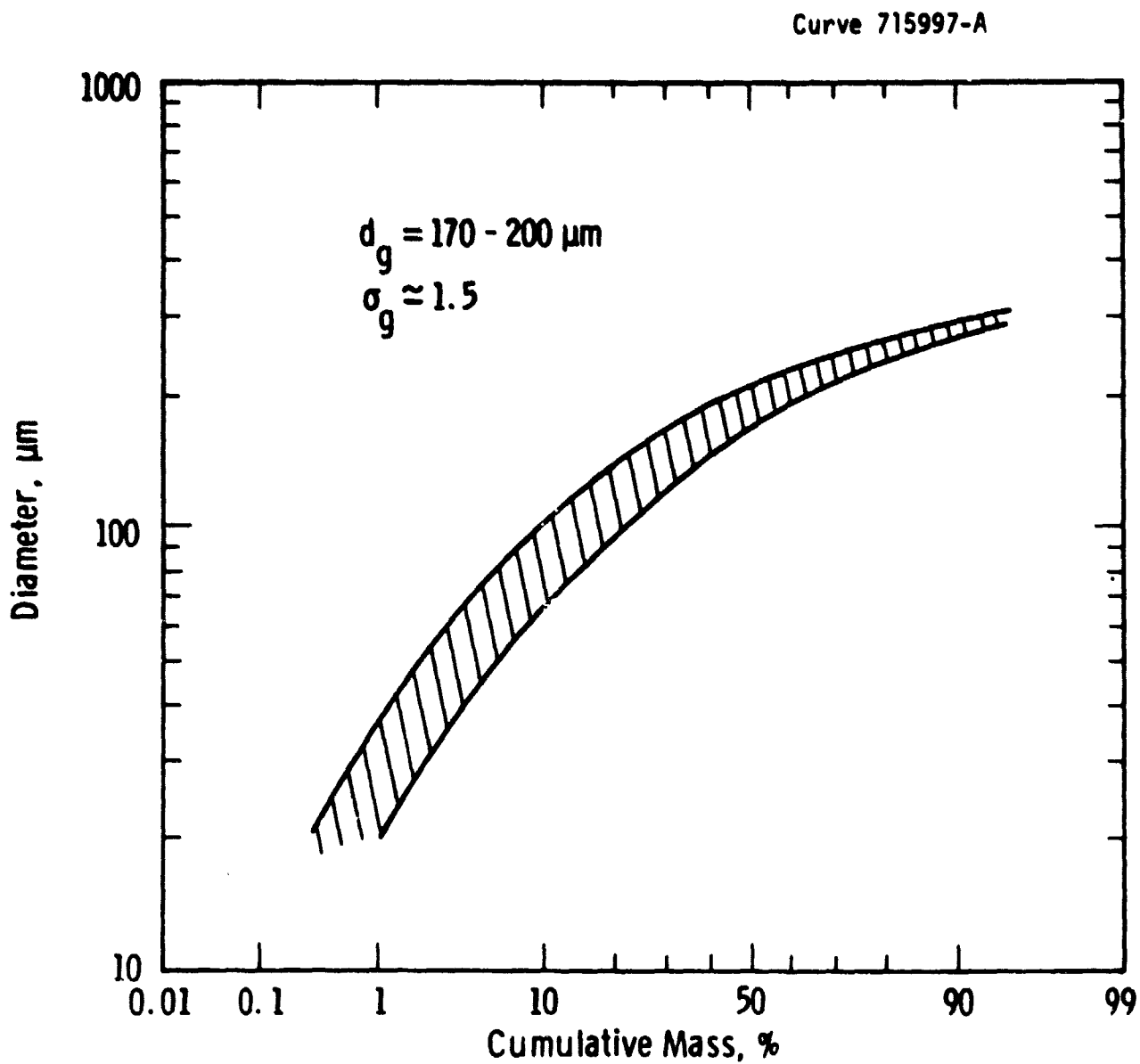Fig. 24 — Log-normal distribution for Sprayco nozzle-1D spectrometer

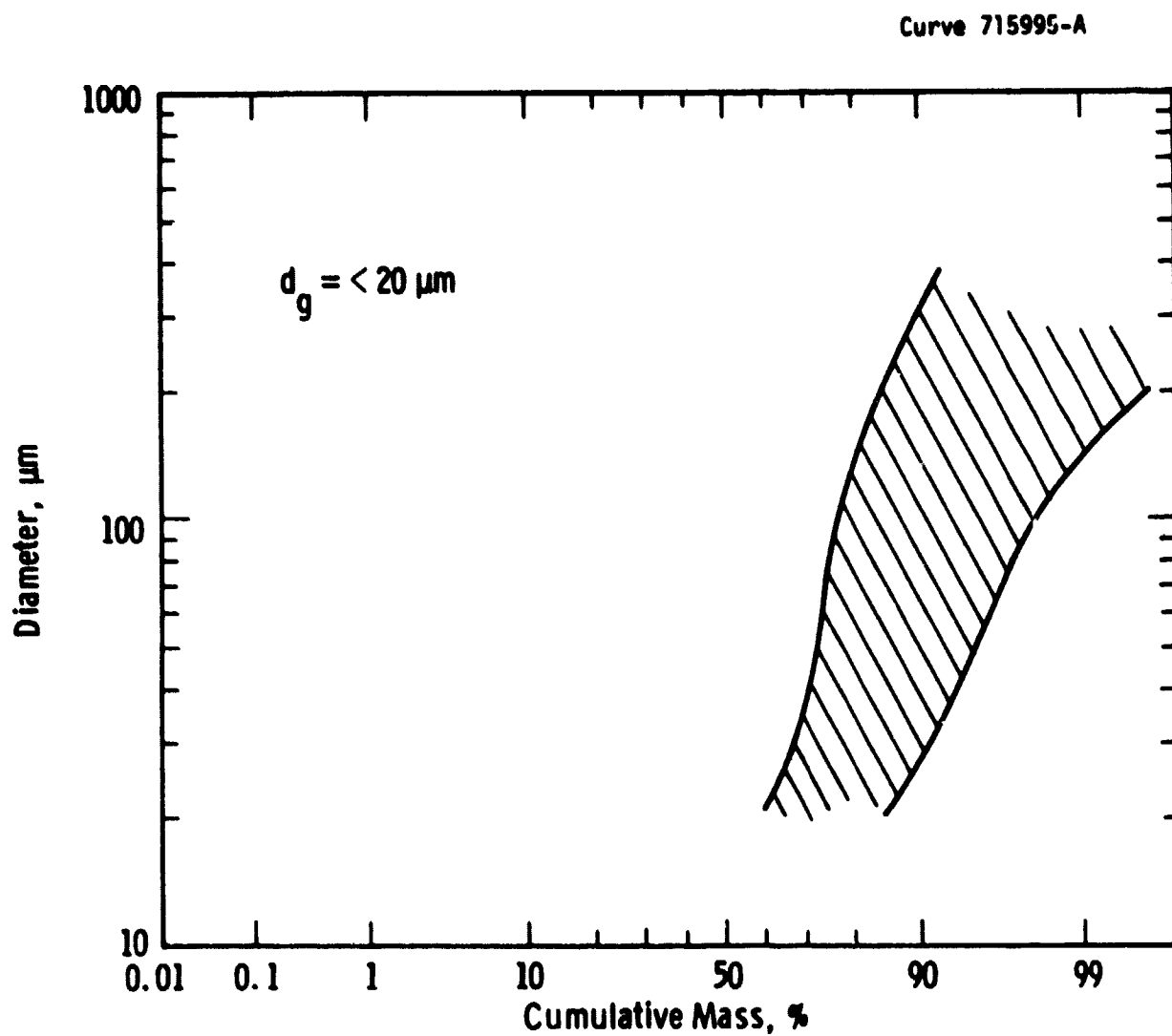Fig. 25 — Log-normal distribution for Sprayco nozzle -2 D spectrometer
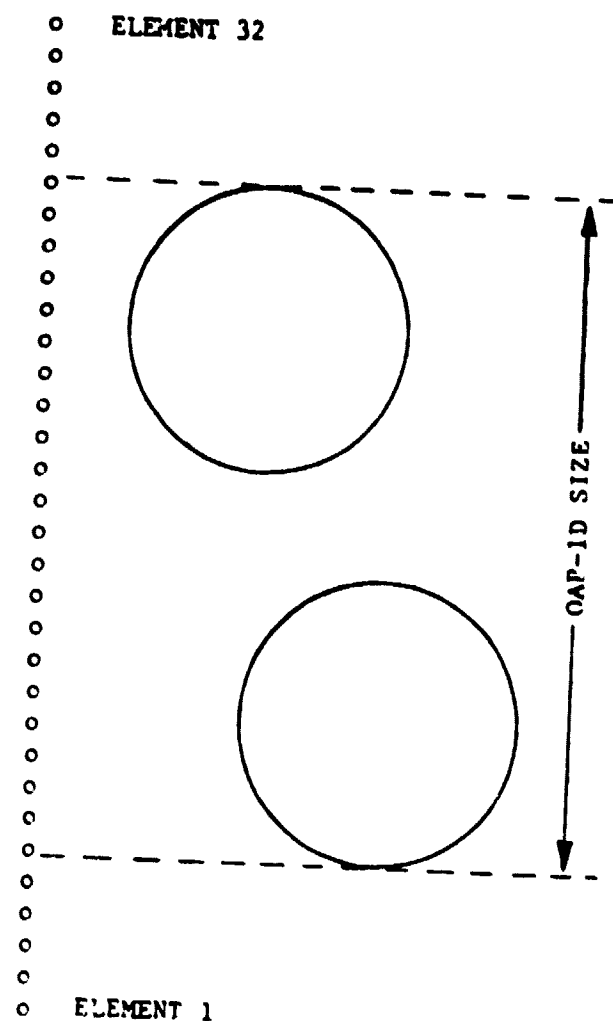
Fig. 26. 1D spectrometer coincidence error.

ELEMENT 32

ELEMENT 1

IMAGE AREA
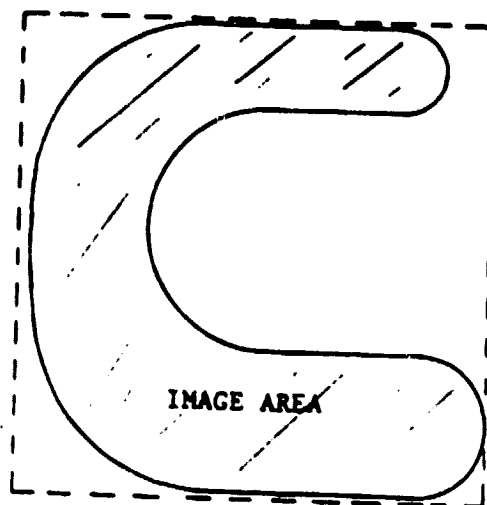
BULK AREA = X*Y
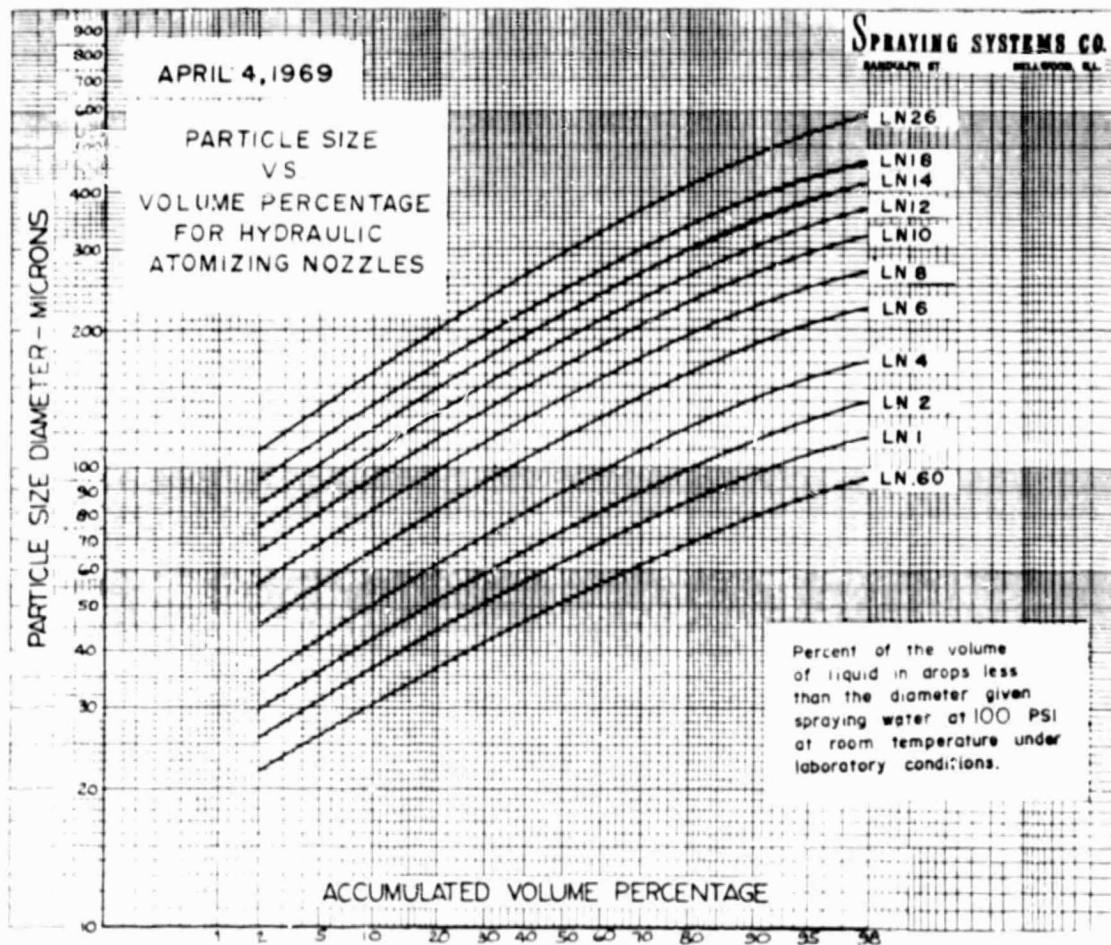
Fig. 27. 2D spectrometer bulk area algorithm.

62

Fig. 28. Particle size distribution curve for silicon tetrachloride
hydraulic atomizing nozzle (nozzle number LN6).

APPENDIX D

REDUCTANT SELECTION FOR THE
WESTINGHOUSE SILICON PROCESS

REDUCTANT SELECTION

The equilibrium composition of products resulting from high temperature reactions in multicomponent, multiphase systems can be obtained at a specified temperature, pressure, and for an initial set of reactants by solving the complex equilibria. The conditions of maximum yield of any desired product can be obtained by performing such calculations as a function of temperature, pressure, and molar feed rates of reactants. For the arc heater reduction of $SiCl_4$ to product Si, four candidate reductants (H_2, Na, Mg, and Zn) were considered initially. Calculations of the thermodynamic yield and, consequently, the material and energy requirement was performed to compare the candidate reductants and to provide a reductant selection basis. These equilibria analyses were performed using a computer program based on both the equilibrium constant and free energy minimization techniques (1).

Table 1 lists the results of the equilibria analyses for the candidate reductants including the materials requirement, arc heater energy requirement, and the calculated yield. At these higher temperatures zinc is a poor reductant. Molten handling of ultra pur magnesium is not state-of-the-art technology and solid feeding of particulate is not desirable. In addition, purity of commercially available magnesium is considered to be inconsistent with the S. G. silicon purity requirements. Finally, hydrogen requires significant energy for the reduction process. Based on the results shown in Table 1 in addition to considerations for material costs, reductant purity, and state-of-the-art technology, the sodium reductant was selected (2).

REFERENCES:

1. M. G. Fey, et al, Quarterly Report, ERDA/JPL 954589-76/1, Aug.-Oct., 1976.

2. M. G. Fey, et al, Quarterly Report, ERDA/JPL 954589-76/2, Nov.-Dec., 1976.

Table 1

SUMMARY OF THEORETICAL MATERIALS AND ENERGY REQUIREMENT

Reductant	Arc Heater Gas*	Temperature °K	Reductant Reqt. (lbs/lb Si)	Arc Heater Energy Reqt. (kW-hr (t)/lb Si)	Silicon Yield (moles/mole)
H_2	H_2	2200	5.29	26	0.339
Na	67% H_2-33% Ar	2000	3.33	3.90	0.979
Mg	67% H_2-33% Ar	2000	1.77	2.68	0.95
Zn	67% H_2-33% Ar	1800	685.0	234.0	0.3

*1 Atm Total Pressure

APPENDIX E

PROCESS ANALYSIS AND ECONOMICS

PROCESS ANALYSIS AND ECONOMICS

Recycle Process For Silicon Production

As illustrated in Figure 1, the arc heater process for silicon production has been analyzed based upon a continuous (recycle) operating mode. In this integrated system, the reactor for silicon production is augmented by the additional unit operations for $SiCl_4$ production (chlorination), $SiCl_4$ purification (distillation), NaCl electrolysis to produce Na and Cl_2 for reuse in the process, and a gas recycle system for the arc heater gases. This is the preliminary system design that was evaluated and costed for the process economic analysis in order to predict an estimated silicon product cost.

The subsystems that are interfaced with the plasma reactor/ separator for silicon production (i.e., sodium feed system, $SiCl_4$ feed system, arc heaters, arc heater gas system, and the effluent handling system) have been discussed and pictorially depicted previously (1, 2, 3).

$SiCl_4$ Production

Individual flowsheets were prepared for each of the unit operations and were combined to form the recycle process as shown in Figure 1 (2). The process for $SiCl_4$ production is based on commercial information. In this process, purchased silicon carbide (SiC) is reacted with gaseous chlorine (obtained from the NaCl electrolysis cells) to produce the raw $SiCl_4$. Descriptions of reactant feed rates, process equipment and vessels were similarly obtained. This information was used to determine equipment and vessel sizes. In addition, vendors were contacted to obtain price information for the $SiCl_4$ production equipment that was used in the economic analysis.
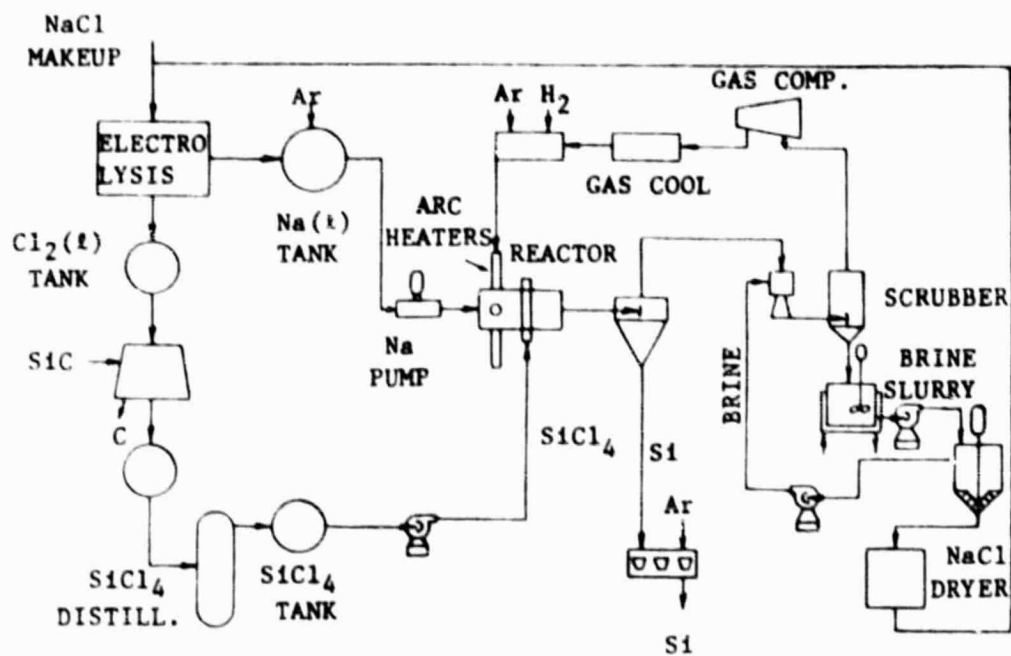
FIG. 1 - RECYCLE PROCESS FOR SILICON PRODUCTION

SiCl₄ Purification

The SiCl$_4$ that is produced in the chlorinator will require purification to remove undesirable impurities. An analysis was conducted to develop a preliminary design and flowsheet for SiCl$_4$ purification via distillation (4). The purification unit consists basically of two distillation columns plus auxiliary equipment (e.g., pumps, condensers, accumulators, reboilers, and holding tanks). This flowsheet is based on a study which enables the removal of both p- and n-type impurities from the SiCl$_4$ in addition to the undesirable metals (Ti, V, Fe), thus yielding a very versatile system design. Based on an analysis of the SiCl$_4$ purification process, the following product impurity levels are expected: boron: 1 ppb; phosphorus: 2 ppb; titanium: <1 ppb; vanadium: <1 ppb; iron: <1 ppb; and SiCl$_4$: remainder.

The engineering analysis for SiCl$_4$ purification provided design information on utility requirements and purchased equipment costs necessary for the economic analysis.

NaCl Electrolysis System

Since the reaction coproduct, NaCl, can be separated into its elemental constituents, Na and Cl$_2$, via the electrolysis of NaCl, the unit operation of NaCl electrolysis is beneficial to the system design. By producing Na and Cl$_2$ within the overall silicon production process, the need to purchase raw materials or reactant is minimized. The Na that is produced is recycled back to the arc heater-reactor for the SiCl$_4$ reduction and the Cl$_2$ is compressed and stored for subsequent use in the chlorination of SiC to produce the SiCl$_4$ reactant. Information on NaCl electrolysis was obtained from available technical literature (5-9). and confirmed via discussion with commercial sodium producers.

Actual equipment costs for the components of the electrolysis system were not available from the above sources. However, the fixed capital for a constructed NaCl electrolysis plant was available in the literature and was used for the process economic evaluation (9).

Process Economics

In order to assemble the process economics for 3000 MT/year of silicon, the purchased equipment costs for the various subsystems and unit operations were required (2). Each of the subsystems was costed and the total of the purchased equipment costs was adjusted to January, 1975 dollars via the Marshall and Steven's cost index (10). January, 1975, is the reference year for cost data according to LSA Project requirements.

After the purchased equipment costs were totalized, an estimation of fixed capital was determined. Table 1 presents the estimation of

TABLE 1

ESTIMATION OF FIXED CAPITAL*   3000 MT Si/yr (Recycle)

CONDENSATION REACTION MODE

Purchased Equipment (PE)	100%	$ 3660.0 K
Install Purch. Equip.	43%	1573.8
Instrumentation & Control	13.5%	494.1
Building with Services	23.5%	860.1
Yard Improvements	11.5%	420.9
Service Facilities, Installed	5%	2013.0
Land	6%	219.6
Engr. and Supervision	32.5%	1189.5
Construction Expense	37.5%	1372.5
Contractor's Fee	19%	695.4

Subtotal $12498.9 K

Electrolysis Plant (Total Fixed Capital)*   6629.0

19127.9

Contingency (30%)   5738.4

1975 Dollars   FIXED CAPITAL $24866.3 K

1980 DOLLARS $34800 K

fixed capital (1975 dollars) for the 3000 MT/year case based on the recycle process and the condensation reaction mode. The total fixed capital associated with the NaCl electrolysis was factored in as a single item in the estimation of fixed capital for the silicon process plant. The format and percentages of purchased equipment costs (PE) recommended for cost comparisons as developed for the LSA Project are presented in Table 2 (11, 12). The fixed capital for the plant to produce 3000 MT Si/year was estimated to be $24.9 million (1975 dollars).

Based on the fixed capital, a determination was made to estimate the product cost (without profit) in 1975 dollars. Table 2 presents a summary of the product cost estimation for a 3000 MT/year plant. As stated before, the format and percentages used to compile product costs were taken from references (11) and (12). The cost data used for utility costs (i.e., electricity, gas, steam, cooling water, etc.) were also based on recommended values (11, 12). The result of the product cost analysis represents a silicon product cost (without profit) of $9.42/kg Si (1975 dollars) which meets the 1986 DOE cost goal of $10/kg Si. In addition, a sensitivity analysis was performed to assess the effect of changes in the various cost items upon resultant silicon product cost. As shown in Figure 2. the cost items of labor, raw materials, arc heater utilities, and fixed capital contingency were varied by ± 10% of the nominal value. The resultant curves were plotted for the silicon product cost (1975 dollars) to indicate the variation in product cost resulting from changes in the above cost items. It can be seen that 10% variations in any one of these factors cause less than 2% variation in the estimated product cost.

TABLE 2

ESTIMATION OF PRODUCT COSTS   3000 MT Si/YR (RECYCLE)

CONDENSATION REACTION MODE

FIXED CAPITAL: $24,866,270 (1975 DOLLARS)
$34,812,780* (1980 Dollars)

|		$/KG SI	
1. DIRECT MANUF. COST			
	A. RAW MATERIALS	1.40	
	B. DIRECT OPERAT. LABOR (10 AT $5.90 M-HR)	.22	
	C. UTILITIES ($.03/KW-HR)	2.84	
	D. SUPERVISION & CLERICAL (15% OF 1B)	.03	
	E. MAINT. & REPAIR (10% OF FIXED CAPITAL)	.83	
	F. OPERATING SUPPLIES (20% OF 1E)	.17	
	G. LAB CHARGES (15% OF 1B)	.03	
	H. PATENTS & ROYALTIES (3% OF PRODUCT COST)	.28	
		5.80 (8.12)*	
2. INDIRECT MANUF. COSTS			
	A. DEPRECIATION (10% OF FIXED CAPITAL)	.83	
	B. LOCAL TAXES (2% OF FIXED CAPITAL)	.17	
	C. INSURANCE (1% OF FIXED CAPITAL)	.08	
	D. INTEREST (8% OF FIXED CAPITAL)	.66	
		1.74 (2.44)*	
3. PLANT OVERHEAD (60% OF 1B + 1D + 1E)		.65	(.91)*
4. TOTAL MANUF. COST (1 + 2 + 3)		8.19	(11.47)*
5. GENERAL EXPENSES			
	A. ADMINISTRATION (6% MANUF. COST)	.49	
	B. DISTRIBUTION & SALES (6% MANUF. COST)	.49	
	C. RESEARCH & DEVEL. (3% MANUF. COST)	.25	
		1.23 (1.72)*	
6. TOTAL COST OF PRODUCT, 4 + 5 (WITHOUT PROFIT)		$9.42/KG SI (13.19)*	
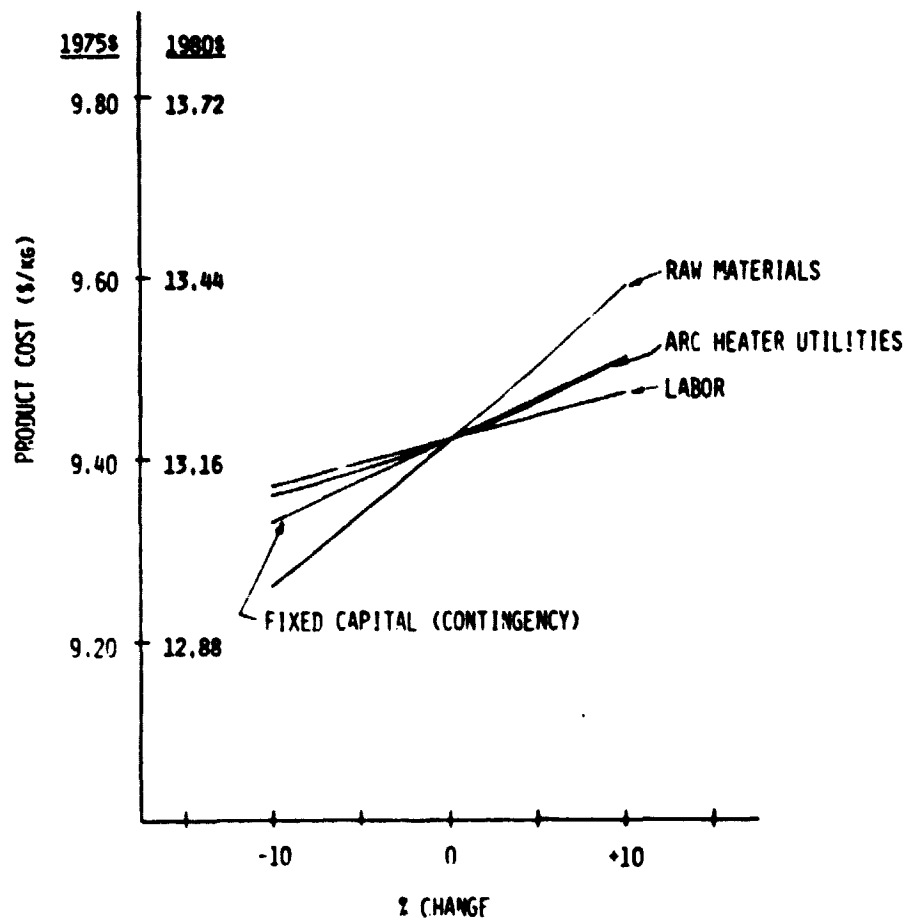
FIGURE 2 -- SILICON PRODUCT COST SENSITIVITY

REFERENCES

1. M. G. Fey, et al, Qtr. Rep., ERDA/JPL 954589-76/2, Nov.-Dec., 1976.

2. M. G. Fey, et al, Qtr. Rep., DOE/JPL 954589-77/4, Oct.-Dec., 1977.

3. M. G. Fey, et al, Qtr. Rep., DOE/JPL 954589-78/1, Jan.-Mar., 1978.

4. "Preliminary Process Design for Purification of $SiCl_4$ by Distillation", CYM Engineering Report, Beaumont, Texas.

5. Faith, Keyes, and Clark, Industrial Chemicals, John Wiley & Sons, N.Y., 1966, pp 698-701.

6. C. A. Hampel, Ed. The Encyclopedia of Electrochemistry, Huntington, N.Y., 1972.

7. M. Sittig, "Sodium, Its Manufacture, Properties and Uses", Reinhold, N.Y., 1956.

8. M. S. Peters, K. D. Timmerhaus, Plant Design and Economics for Chemical Engineers, McGraw-Hill Book Co., N.Y., 1968, p 133.

9. T. Nakamura, Y. Fukuchi, "Tekkosha's New Metallic Sodium Process" J. of Metals, Aug., 1972, pp 25-27.

10. C. L. Yaws, et al, Qtr. Rep., ERDA/JPL 954343-76/1, Sept., 1976.

11. C. L. Yaws, et al, Qtr. Rep., DOE/JPL 954343-77/3, Sept., 1977.

12. C. L. Yaws, et al, Qtr. Rep., DOE/JPL 954343-77/4, Dec., 1977.

APPENDIX F

SYSTEM PURITY ANALYSIS

SYSTEM PURITY ANALYSIS

The system purity analysis was a project subtask conducted to predict impurity concentrations in the liquid silicon product based on initial amounts in the feedstock materials (sodium and $SiCl_4$).

A thermodynamic method, which was based on a modification of the complex equilibria calculations that were carried out in the Si-H-Cl-Na system in Phase I of this study,[1] was used to establish the impurity correlations. In those previous calculations it was assumed that there was no solubility in the liquid silicon. If this assumption is relaxed, then the amount of a dissolved species in the liquid silicon can be calculated as a function of the initial amounts in the feedstocks, provided the activity coefficient of that species in liquid silicon is known. Because of the dilute solutions involved, binary activity data were assumed to apply to the multi-component liquid phase. The calculations were carried out using an existing Westinghouse computer program called CHEMEQ, which is based on the free energy minimization technique for solving complex equilibria.

In addition to modifying the CHEMEQ program, input data for the activity coefficients of the various impurities evaluated were required. The appropriate activity coefficients were obtained from either the literature or calculated based on best available data.[2]

The impurities evaluated during this study included the following based on either a sodium reduction or a hydrogen reduction process: Al, B, Cr, Cu, Fe, Mn, Mo, P, Ti, V and Zr. These elements were selected for evaluation due to their known deleterious effects (which are concentration dependent) on the performance of solar grade silicon.

A summary of representative results for all impurities analyzed is given in Table 1, in terms of the percent of feedstock impurity that is present in the liquid silicon. These values represent the maximum amount of impurity possible in the molten silicon since the analysis was based on the equilibrium condition. Under actual process condition, the amount of impurity that is present may be considerably less due to kinetic factors. For arc heater reduction by sodium, the results indicate that purity levels should substantially improve with respect to P and Al, moderately so for Mn, and not at all for B, Cr, Cu, Fe, Mo, Ti, V and Zr. In the case of hydrogen reduction, there is essentially complete impurity removal for Al, Mn, and P, significant removal for B, Ti and Zr and little or no removal for Cr, Fe, Mo and V.

TABLE 1
SUMMARY OF TYPICAL RESULTS FOR ALL
IMPURITIES ANALYZED

Impurity*	Percent of Initial Impurity in Liquid Silicon	
	Na Reduction**	H_2 Reduction***
Aluminum	19	0.2
Boron	100	52
Chromium	100	81
Copper	100	92
Iron	99	94
Manganese	71	0.7
Molybdenum	100	100
Phosphorus	1	0.3
Titanium	100	35
Vanadium	100	100
Zirconium	100	14

---

*Initial amount is 1×10^{-4} g-atm for all impurities.

**Initial conditions: 1900°K; 4.0 mols Na, 1 mol $SiCl_4$, 0.66 mol Ar, 2.65 mols H_2

***Initial conditions: 2200°K; 25 mols H_2, 1 mol $SiCl_4$

References

1. M. G. Fey, et al, Quarterly Report, ERDA/JPL 954589-76/2,
    November-December, 1976.

2. M. G. Fey, et al, Quarterly Report, ERDA/JPL 954589-77/3,
    July-September, 1977.

APPENDIX G

REACTION DEMONSTRATION

REACTION DEMONSTRATION EXPERIMENTS

The objective of this task was to determine the nature and extent of the high temperature reaction between sodium vapor and silicon tetrachloride vapor utilizing laboratory apparatus under conditions similar to that originally planned for the experimental verification testing. Following the Product Separation Study, the test plans were changed to operate the reactor under the condensation mode. The direct applicability of the reaction demonstration test results were therefore minimal. The laboratory experiments were conducted at the similar temperature, pressure, reactant concentration, and residence time range as the verification testing. The earlier ranges for these test variables were: (1) temperature, 1800-2000°K; (2) reactant concentrations, 40-45% sodium, 45-50% arc heater gas (80% H_2 - 20% Ar), 10-11% $SiCl_4$; (3) residence time, ~ 0.1 second.

The design of a laboratory-scale experimental system was conducted and the principal components of the system consisted of (1) a silicon carbide, glow bar furnace with a maximum temperature capability of 1925°K, (2) a silicon tetrachloride generator with associated flow train, (3) a sodium vapor generator with associated flow train, and (4) a product collector (see Figure 1). Heat transfer and residence time calculations were carried out to determine the reaction chamber size and the range of reactant flow rates.

The extent of reaction was measured by two techniques. A cooled probe was placed in the gas stream immediately downstream from the reaction zone in order to trap the condensable reaction products as well as any sodium that had not reacted. The deposit was weighed and chemically analyzed after each experiment. On this basis, the fractional conversion is determined by a mass balance. In addition, the exhaust gas was sampled and the concentration of silicon chlorides determined to yield a calculated fractional conversion.

Following successful assembly and installation of the test apparatus, difficulties were experienced with the sodium vapor generator (boiler) which was designed to inject vaporized sodium into the reaction tube. These difficulties were in the areas of vapor flow blockage and material compatibility. A number of sodium vapor injection techniques were evaluated. Finally, it was decided to utilize a sodium injector system consisting of a precharged sodium vaporizer with an Ar/H_2 sweep gas. Sodium vapor pressure versus temperature data was used to control the concentration of the sodium vapor with the flow rate of Ar/H_2 gas effecting the sodium vapor flow. The $SiCl_4$ system for vapor injection performed well based on the original design.

Six full scale tests based on the modified design of sodium injection were attempted. A persistent problem that arose was the sporadic breakage of the alumina reaction tubes. During these tests, the tube wall temperature was in the range of 1450-1550°C, and the failure of the
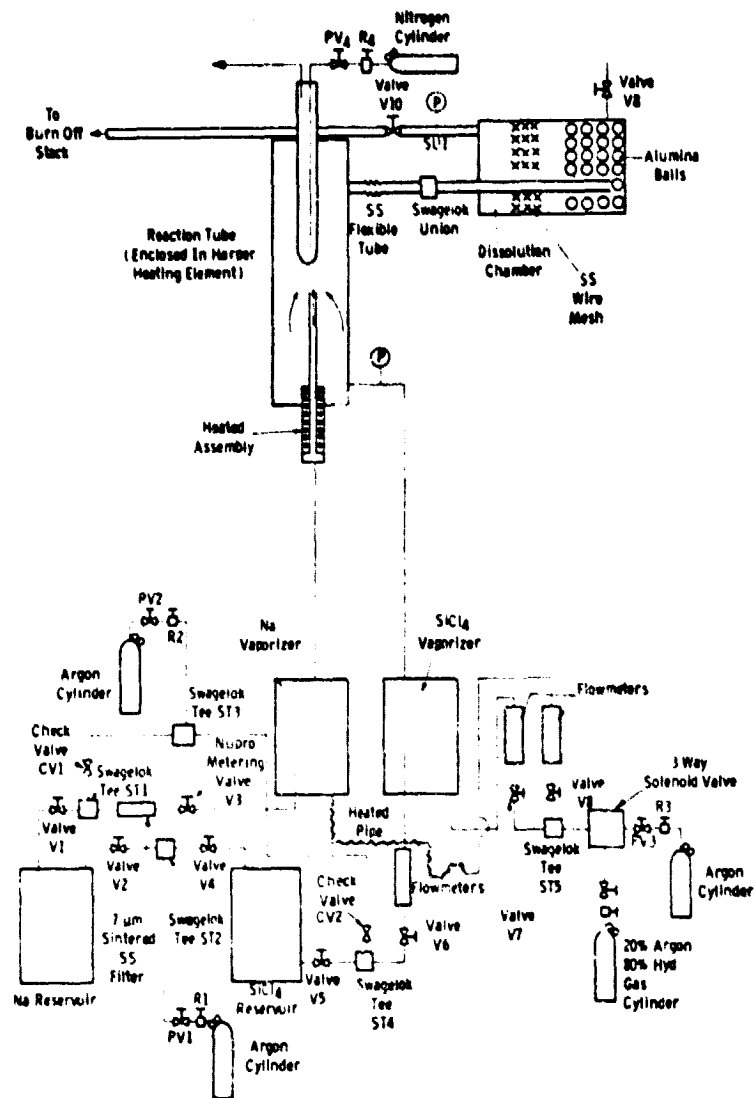
Figure 1 - Schematic of the Test System for Reaction Demonstration Experiments

alumina tubes was attributed to their poor thermal shock resistance.
Due to its superior resistance to thermal shock, a mullite reaction tube
was used for the fourth test. A most dramatic failure of this tube
occurred. The breakage of the inner sodium conveying tube splattered
hot (300°C) sodium aerosol onto the walls of the mullite tube, and the
subsequent destructive reaction between the sodium and the glass in the
mullite caused virtual disintegration of the mullite tube. Despite the
inadequate thermal shock resistance, high quality alumina tubes (e.g.,
McDanels 998 and Coors AD 998) proved more suitable candidates and a
decision was made to continue using these tubes, but employing lower
tube wall temperatures to prevent tube breakage.

In the sixth test, a lower tube wall temperature was used (1300°C).
While tube failure was prevented, 10 minutes after the run was commenced
a greatly increased bubbling and turbulence was detected in the effluent
gas scrubber and this was due to failure of the cold finger condenser.
On reducing the nitrogen flow for cooling the cold finger, the intense
bubbling in the scrubber ceased.

Figure 2 shows photographs of the broken cold finger condenser.
Three characteristic condenser deposits were identified. Closest to the
end plate was a 2.5 cms long region composed of a fine yellow-brown
powder. Adjoining this region was a 3 cms long more flaky deposit.
Closest to the reaction zone was a silver-grey metallic coating approx-
imately 6 cms in length. Samples of these deposits were analyzed by
EDAX and have shown the expected peaks for silicon, sodium, and chlorine.
The EDAX method indicated that the mass ratios in all of the deposits
were approximately stoichiometric. The agreement was particularly good
for the silver-grey metallic coating. Since the excess silicon tetra-
chloride could not have condensed out at the prevalent high reaction
tube temperature and was, therefore, swept out with the Ar purge, the
formation of elemental silicon and sodium chloride was clearly suggested
by the quantitative results.

Figure 2 -- Photographs Of The Cold Finger Condenser Showing
Deposition Of The Reaction Products

-4-